DEVELOPMENT OF PVA AND PMMA BASED COMPOSITES WITH IMPROVED FIRE RESISTANCE FOR CHEMICAL SENSING, ENERGY STORAGE AND ANTIBACTERIAL APPLICATIONS

Thesis submitted to

Cochin University of Science and Technology

in partial fulfilment of the requirements

for the award of the degree of

Doctor of Philosophy

ANJU V. P.

Department of Polymer Science and Rubber Technology

Cochin University of Science and Technology

Kochi- 682 022, Kerala, India

December 2017

Development of PVA and PMMA based Composites with Improved Fire Resistance for Chemical Sensing, Energy Storage and Antibacterial Applications

Ph. D Thesis

Author

Anju V. P.
Research Schoolar
Department of Polymer Science and Rubber Technology
Cochin University of Science and Technology
Cochin- 682 022, Kerala, India
E-mail: anjuvp09@gmail.com

Supervising guide

Dr. Sunil K. Narayanankutty
Professor
Department of Polymer Science and Rubber Technology
Cochin University of Science and Technology
Cochin- 682 022, Kerala, India
E-mail: sncusat@gmail.com

Department of Polymer Science and Rubber Technology
Cochin University of Science and Technology
Cochin- 682 022, Kerala, India

December 2017

Department of Polymer Science and Rubber Technology
Cochin University of Science and Technology
Cochin- 682 022, Kerala, India

Dr. Sunil K. Narayanankutty
Professor
Email: sunil@cusat.ac.in

22/12/2017

Certificate

This is to certify that the thesis entitled **"Development of PVA and PMMA based Composites with Improved Fire Resistance for Chemical Sensing, Energy Storage and Antibacterial Applications"** is an authentic record of research work carried out by **Anju V. P.** under my supervision and guidance in the Department of Polymer Science and Rubber Technology, Cochin University of Science and Technology, Cochin-22. No part of the work reported in this thesis has been presented for any other degree from any other institution. All the relevant corrections and modifications suggested by the audience during the pre-synopsis seminar and recommended by the Doctoral committee have been incorporated in the thesis.

Prof. Sunil K. Narayanankutty
(Supervising Guide)

Declaration

I hereby declare that the thesis entitled **"Development of PVA and PMMA based Composites with Improved Fire Resistance for Chemical Sensing, Energy Storage and Antibacterial Applications"** is the bonafide work carried out by me under the supervision of **Prof. Sunil K. Narayanankutty** Department of Polymer Science and Rubber Technology, Cochin University of Science and Technology, Cochin-22 and has never been included in any other thesis submitted previously for the award of any degree.

Cochin – 22
22/12/2017

Anju V. P.

Dedicated to...

My dear Achamma,
Achan, Amma, Ettan &
Aami Mol

Acknowledgements

The work presented in this thesis would not have been possible without my close association with many people who were always there when I needed them the most. I would like to thank a number of people who have contributed to the final result in many different ways:

To commence with, I pay my obeisance to GOD, the almighty who have bestowed upon me good health, courage, inspiration, enthusiasm and the light. After GOD, I express my sincere and deepest gratitude to my supervisor Prof. (Dr.) Sunil K. Narayanankutty, Professor, Department of Polymer Science and Rubber Technology, for the guidance, motivation, making critical suggestions and freedom throughout my research work. His expertise, invaluable guidance, constant encouragement, affectionate attitude, understanding, patience and healthy criticism added considerably to my experience. Without his continual inspiration, it would have not been possible to complete this study.

I owe my special thanks to Prof. (Dr.) Honey John, Head and Prof. (Dr.) Thomas Kurian, former Head, Department of Polymer Science and Rubber Technology for providing necessary laboratory facilities.

I take this opportunity to express my deep sense of gratitude and respectful regards to Dr. Rani Joseph, Dr. C.P. Raghunathan Nair, Dr. Sailaja G.S., Dr. Jayalatha G., Dr. Jyothish Kumar, Dr. Jinu Jacob, Dr. Prasanth Krishna, Miss Abhitha K. for valuable suggestions and concise comments on some of the research papers of the thesis.

I offer my sincere thanks to Prof. T. I. Johnson, ret. Prof., head of the Dept.of Chemistry, Christ College, for his moral support when I quit Ph.D from IITM. He has been a source of strength, and directed me to join with Sunil Sir.

I am highly thankful to Dr. P. Mohanan, and his student M. Manoj, Department of electronics for his indispensable help during microwave studies. I owe my sincere gratitude to Dr. K. Rajeev Kumar, professor, Department of Instrumentation for his valuable suggestions that have been very helpful for the fabrication of capaciotrs. I am grateful to Prof. M. K.Jayaraj of Dept. of Physics, CUSAT and his students Jesna for helping with electrode coating.

My heartfelt thanks to my fellow lab mates, dhanya chechi, neethu chehi, venu sir, gean sir, sobha teacher, Julie chechi, neena chechies, bhavya chechi shadiyechi, jisha chechi, remya, bhagyesh chetttan, renju chehi, reshmi chehi, Sunitha chechi, denny teacher, sreedevi teacher, sona chechi, sreejesh chettan, murali chettan, Rohith chettan, jolly sir, bindu teacher, abhilashettan for always being there and bearing with me the good and bad times during my wonderful days of Ph.D. I sincerely admire the contribution of all my lab mates sumitha, aswin chettan, sneha, siru, athul, liz, anu, bhashi, Nisha, meera, sona, divya, shinu, rahna, asha, jesna, irthaza, praseetha, neethu, shinci, aswathy for extending their unstinted support, sympathetic attitude and unfailing help during the course of entire study.

I sincerely express my gratitude to Anish chettan, who helped me to do analysis without getting any delay, at NCL pune.

I sincerely express my gratitude from the core of my heart to Sherin chechi without her help I won't be able to capacitance measurements.

During the course of my work, I had the pleasure of working with several project students, athira, lakshmi, meetha, mridula and alka. Their assistance during the presented work is gratefully acknowledged.

Convey my heartfelt thanks to the staff, Sophisticated Test and Instrumentation Centre, STIC, CUSAT for helping me complete the analysis results on time. The office team of PS&IRT has helped me to cruise through the official hurdles. I express my sincere thanks to all of them

My very special thanks go to my dearest husband, best friend Jithesh P R, my ettan who encouraged me to pursue with my studies by doing a Ph. D in this field. I am thankful to him for being so understanding and for putting up with me through the toughest moments of my life. This work was not possible without his constant support and scientific help. I dedicate this Ph.D thesis to my lovely aami mol who is the pride and joy of life. I appreciate all your patience and support during amma`s Ph.D studies.

I acknowledge University Grants Commission (UGC) Government of India, for providing me with the necessary funding and fellowship to pursue research at CUSAT.

I feel a deep sense of gratitude to my late grandmother chandrika who formed part of my vision and taught me the good things that really matter in life. The happy memory of my achamma still provides persistent inspiration for my journey in this life.

Last, but not least, I would like to dedicate this thesis to my family, my achan, amma, Chinju, mother in law, father in law and all the family members who supported me and helped me throughout my life and during this study. I dedicate this work to you all. Mom, dad I do not know how to thank you enough for providing me with the opportunity to be where I am today.

Anju V. P.

Preface

Intrinsically conducting polymers find various applications in the field of electronics, electromechanical devices, electroluminescence and sensors. Widely known intrinsically conducting polymers are polypyrrole, polyacetylene, polythiophene, polyaniline, polyparaphenylene, polyparaphenylene vinylene, and their derivatives. Owing to the environmental stability, excellent conductivity and facile synthesis, polyaniline based composites have developed fast. The conducting composites are widely used in electronic packaging as die attach adhesives, sensors, solder replacements, conductive coatings, chemical sensors, electromagnetic fields etc. Many factors such as diameter, structure, concentration of the fillers and polymers influence the conductivity of the composites. The composites are characterized by the percolation threshold at which dramatic increase of conductivity occurs. Hence much attention has been given to the preparation of the composites with low percolation threshold.

Conducting polymer composites can be prepared by the addition of conducting polymers or conducting fibers in to an otherwise non-conducting polymer. To improve the performance or extend the functions of conducting polymer based devices, the conducting polymers have to be modified. Recently composites of polyaniline with carbon nanotubes have been developed. The π- bonds present in the carbon nanotubes facilitate the formation of extended charge transfer between carbon nanotubes and polyaniline and improve conductivity. Composites based on carbonaceous materials and polyaniline in appropriate stochiometric combinations have been proven to be efficient. Combination of outstanding conducting properties of the carbonaceous materials and conducting polymers is growing interest in nanotechnology. Moreover, among the aforementioned carbon materials, carbon nanotube (CNT) is comparatively expensive and

graphene is difficult to prepare. Carbon nanofiber (CNF) is an alternative choice which is readily available and cheaper than CNT. Besides, CNF has a unique one-dimensional structure, excellent electrical, thermal and mechanical properties. Although PANI/CNF composites have been studied extensively, work on the development of sensors, antibacterial agents and fire retardants based on this system is in the nascent state.

The present study primarily involves the development of conducting polymer composites based on conducting fibers and non-conducting fibers. Composites were developed by using conducting carbon nanofiber and non-conducting cellulose fiber. Cellulose was isolated from coir fibers by the modification of a known method. The isolated cellulose was refined in to three different sizes- macro, micro and nano sizes. The isolated fibers were characterized by different techniques all of which confirmed uniform fibrillation and the size distribution in the successive ranges. Polyaniline was coated on the surface of cellulose and carbon nanofibers by the in-situ polymerization of aniline in acid medium. The properties of polyaniline greatly depend on the nature of the dopant used, monomer to oxidant ratio, purity of monomer, polymerization time and temperature etc. But among the variable conditions, the nature of the dopant used for the synthesis plays critical role.

Polyvinyl alcohol (PVA) and poly(methylmethacrylate) (PMMA) are two important thermoplastic polymers, known for their chemical resistance and physical properties. Polyvinyl alcohol, a semi crystalline synthetic polymer, has been extensively investigated as a host for different nano-fillers and for electrolyte applications. Although a number of studies on PVA systems have been reported already, the dielectric properties of PVA systems are not well explored. PMMA is a transparent thermoplastic polymer widely used as the substitute for inorganic glass, because of their good impact strength, light weight and easy processing conditions. It finds as a suitable material in biomedical applications also.

PMMA based bone cement has been found to be very efficient for the anchoring of artificial joints. Our aim is to develop composites, which can find various application in different areas. Due to the better compatibility and ease of processing compared to other thermoplastics, PVA and PMMA selected for further study.

Excellent dielectric properties and electrical conductivity of the composites lead us to explore the EMI shielding property. Moreover, it opened up the use in high charge storage capacitors. Potential of the composite as a sensor for humidity and ammonia was evaluated. Furthermore, the antibacterial properties of PMMA based composite was evaluated.

Summary of the thesis:

The thesis is divided into 8 chapters.

A brief introduction to the focus of the study is presented in **Chapter 1**. The significance of conducting polymers, carbon based fibers, natural fibers and thermoplastics are presented. Need for the development of sensors and capacitors is also presented. Scope and objectives of the present work are discussed towards end of this chapter.

Chapter 2 of the thesis gives a detailed description of the materials used and the methods employed for the present study.

Chapter 3 of the thesis reports studies on the effect of dopant on the properties of PANI/CNF composites.

Chapter 4 deals with the synthesis, characterization and properties of PVA based composites. The chapter isdivided into **part A** and **part B**. **Part A** focuses on development of PANI/Cellulose/PVA composites. **Part B** describes the development of PANI/CNF/PVA composites.

In part A, the isolation of cellulose from coir fibers by chemical and mechanical treatments is given. The effect of cellulose fiber size on

the properties of the composite is evaluated. Electrical, dielectric, thermal, mechanical and water absorption are studied.

In part B describes the synthesis, characterization and properties of PANI/CNF/PVA composites.

Chapter 5 describes the development of PMMA based composites. The chapter is divided in to three parts. The first part deals with the preparation of composite by using cellulose fiber in three different sizes. The second part deals with polyaniline coated CNF/PMMA composite. The third part describes the improvement in the mechanical properties of the composite by the incorporation of cellulose and silane coupling agent.

Part A deals with the synthesis and properties of three series of PANI/Cellulose/PMMA composites containing fibers in three size ranges ie. macro, micro and nano.

Part B describes the development of PANI/CNF/PMMA composites. The electrical, dielectric, thermal and mechanical properties arediscussed.

Part C presents the enhanced the mechanical as well as thermal properties of PMMA/Cellulose composite by the incorporation of silane coupling agent. The effect of silane coupling agent, bis (3-triethoxysilylpropyl tetrasulphide), on the properties of the composite is compared with PMMA/Cellulose composite.

Chapter 6 reports the applications of the prepared composites. The chapter is divided in to three parts.

Part A presents the microwave dielectric properties and EMI shielding of the composite. Comparison of dielectric and EMI shielding properties between cellulose and CNF composites of PVA is presented in the chapter.

Part B deals with the antimicrobial activity of PANI/CNF/PMMA composites. The effect of size and surface area on the antimicrobial activity is presented.

Part C reports the fire-resistant property of the carbon nanofiber incorporated PVA and PMMA composites. The chemical changes involved during the heat treatment is also discussed in this chapter.

Chapter 7 reports the development of devices based on the properties of the composites. This chapter is divided in to **Part A**, **Part B** and **Part C**.

Part A describes the development of humidity sensors using PVA based composites. A comparative study on the sensing mechanism of PANI/CNF/PVA and PANI/Cellulose/PVA composites is also presented.

Part B deals with the ammonia sensing properties of the PANI/CNF/PVA and PANI/Cellulose/PVA composites.

Part C describes the fabrication of thin film capacitor with PANI/CNF/PVA as dielectric layer. Circuit application of the fabricated capacitor is also presented in this part.

Chapter 8 presents the summary and conclusion and future outlook of the study.

Contents

Part B

Development of electrically conducting composites based on CNF and polyvinyl alcohol

Part B

Development of electrically conducting composites based on carbon nanofiber and poly(methyl methacrylate)

Part C

Impact of bis –(3-triethoxysilylpropyl)tetrasulphide on the properties of PMMA/Cellulose composite

Part B

Effect of dopants on the antimicrobial activity of PANI/CNF/PMMA composites

Part C

Highly flame-resistant composites based on nanofibers/polyaniline/polyvinyl alcohol composite

List of Abbreviations and Symbols

APS	Ammonium persulphate
AC	Alternating Current
ASTM	American Society for Testing of Materials
BET	Brunauer–Emmett–Teller
BJH	Barrett-Joyner-Halenda
BIS	Bureau of Indian Standards
CCVD	Catalytic Chemical Vapour Deposition
CNF	Carbon nanofiber
CNTs	Carbon nanotubes
CSA	Camphor Sulfonic Acid
DC	Direct Current
DLS	Dynamic Light Scattering
DMA	Dynamic Mechanical Analysis
DTG	Differential Thermogravimetry
EB	Elongation at Break
EEA	European Environment Agency
ESCA	Electron Spectroscopy for Chemical Analysis
EMI	Electromagnetic Interference
FESEM	Field Emission Scanning Electron Microscopy
FTIR	Fourier Transform Infra-Red
GHz	Giga Hertz
HPV	High Production Volume
HR-TEM	High Resolution Transmission Electron Microscope
IUPAC	International Union of Pure and Applied Chemistry
ICP	Intrinsically Conducting Polymer
LOI	Limiting Oxygen Index
MAS	Magic Angle Spinning
MIC	Minimum Inhibitory Concentration
MMA	Methyl Methacrylate
MS	Mass spectrometry
MTCC	Microbial Type Culture Collection
MWS	Maxwell Wagner Sillar
NFC	Nano Fibrillated Cellulose
NSA	Naphthalene Sulphonic Acid
PANI	Polyaniline
PC	Poly carbonate
PCS	Photon Correlation Spectroscopy

PMMA	Poly(methyl methacrylate)
PPV	Poly phenylene vinylene
PPy	Polypyrrole
PTh	Poly thiophene
PVA	Polyvinyl alcohol
PVC	Polyvinyl chloride
PS	Poly styrene
RADAR	RAdio Detection And Ranging
RAM	Radar Absorbing Material
RH	Relative Humidity
SE	Shielding Efficiency
SEM	Scanning Electron Microscopy
TEM	Transmission Electron Microscope
TESPT/Si69	Triethoxy silyl propyl tetrasulphide
TGA	Thermogravimetric analysis
TMS	Tetramethylsilane
TSA	Toluene sulfonic acid
UTM	Universal Testing Machine
UV-Vis	Ultraviolet Visible
XPS	X ray Photoelectron Spectroscopy
XRD	X-ray diffraction
A	Arrhenius constant/Area /Absorptivity
Å	Angstrom
c	Velocity of light
C	Capacitance
dB	Decibel
f	Frequency
h	Hour
I	Current
J	Heating coefficient
min	Minutes
MPa	Mega Pascal
nm	Nanometer
N/mm	Newton/millimetre
ppm	Parts per million
R	Reflectivity
RH	Relative Humidity
M	Molar
g	Gram
T	Absolute temperature / Transmissivity

Tg	Glass transition temperature
V	Voltage
σ	Conductivity
dΩ	Complex frequency shift
E*	Complex modulus
E”	Loss modulus
E’	Storage modulus
^{o}C	Degree Celsius
d	Interlayer space
D	Particle size
E	Electric field
f	Frequency
αf	Filler specific constant/Absorption coefficient
β	Full width at half maximum
2θ	Diffraction angle
n	Order of reflection
Hz	Hertz
ε’	Real part of complex permittivity
ε”	Imaginary part of complex permittivity
K	Kelvin/Resistance
L	Length
%	Percentage
Q	Quality factor
s	Seconds
S	Siemen
δf	Skin depth
Vc	Volume of the cavity
Vs	Volume of the sample
Wt	Weight of the sample after t
W0	Weight of sample before swelling
λ	Wave length of light

.....ꕥ.....

Chapter 1

INTRODUCTION

Contents

1.1 Nanocomposites

Composites are the combination of two or more materials, among them one is of reinforcing and it is implanted in another material which is called as matrix. Nanocomposites are the composites in that not less than one of the phases is of nanometre scale. The field of nanoscience is one of the most popular areas of the current research and it has changed the face of research in polymer chemistry. The addition of nanoparticles to a continuous phase or matrix have lead significant improvement in the properties of the composite. Thus, these materials have emerged as suitable alternatives to overthrown the drawbacks of macro and micro composites. This is due to the extremely high surface to volume ratio of nanoparticles which can change the properties of the composite compared to the bulk particles. Compared to the traditional fillers, nanomaterials are

found to be effective even at low filler loading. Huge amount of material is needed for the similar improvement in the bulk composites. It is the most effectiveness of nanocomposites in that the quantity of nanoparticles will be between 0.5 to 5 % by weight. In case of traditional polymer composites, the addition of high filler content reduces the optical clarity, poor toughness, and makes high melt viscosity for the composites.

Numerous diverse topics are present in the area of nanocomposites such as composite reinforcement, electrical conductivity, flame retardancy, thermal stability, optical clarity, cosmetic applications, bactericidal properties etc. At the nanoscale the properties will be more size dependent than at the macro or micro level. Consequently, the surface chemistry of the nano-reinforcement governs polymer nanocomposite's properties. Novel properties of the composite originate from the appropriate combination of the nanomaterials by suitable methods.

The polymers are considered as electrical insulators, based on that they have widespread use in electrical and electronic fields. Though, the conductivity can be imparted to the insulating materials by blending the polymers with conducting particles like carbon based materials and conducting polymers [1]. Hence the conductivity increases to the range in between the metallic conductors and insulating materials [2,3]. The electrical conductivity of these composites determines their specific applications. So, these materials can be used as floor heating elements, in electronic equipments, for electromagnetic shielding, and for the dissipation of static energy etc. [4-7]. In addition to that recent studies have shown that the conducting composites are best used as sensing materials [8,9]. In

contrast to metallic conductors, the polymeric conductive composites are light weight, ease of shaping and possess wide range of electrical conductivity [10].

Conducting polymer based composites are widely studied in both in fundamental research and in various application fields [11]. The conducting polymers can interact synergically with other organic or inorganic materials to provide the conductive backbone, improved electrical conductivity and plastic property[12-15].

1.2 Conducting polymers

Polymers, due to their light weight, ease of fabrication and low cost, have replaced metal based materials in several areas. The discovery of Alan J. Heeger, Alan G. MacDiarmid and H. Shirakawa shown that the conjugated polymers can exhibit semiconducting behaviour. They discovered that conductivity can imparted to polyacetylene by the process called doping. The presence of alternating single and double bonds in conjugated polymers make the electrons to delocalize throughout the polymer chain[16,17]. In absence of extended π-conjugation the mobile charges are not developed in the polymer chain, hence the material is not conducting.

Variety of conducting polymers are known these days. Polyacetylene is one of the simplest molecular chain which has got significant attraction. But due to the poor processability and environmental concerns lead adverse effect on the development of this polymer. Other conducting polymers are polyaniline (PANI), polypyorrle (PPy), polythiophene (PTh), polyphenylene vinylenes (PPV). Among these conducing polymers, polyaniline has shown

potential for different applications. Moreover, it possesses excellent environmental stability, biocompatibility, ease of synthesis, high redox stability and unusual doping-dedoping chemistry [18,19]. Polyaniline possesses alternating benzene and imine rings, where the nitrogen atom exists as SP^2 or SP^3 hybridized state. According to the neutral intrinsic redox states, polyaniline is categorized in to four classes, which is given in the figure 1.1. Leucoemeraldine is fully reduced form appeared pale brown. Partially oxidised form is emeraldine, which possesses green colour. This is the only conducting form of polyaniline containing both oxidised iminium and amine nitrogen atoms in equal amounts. Protonated emeraldine or nigraniline is 75 % oxidized with blue or violet colour. Pernigraniline is fully oxidised form which appears in black colour.

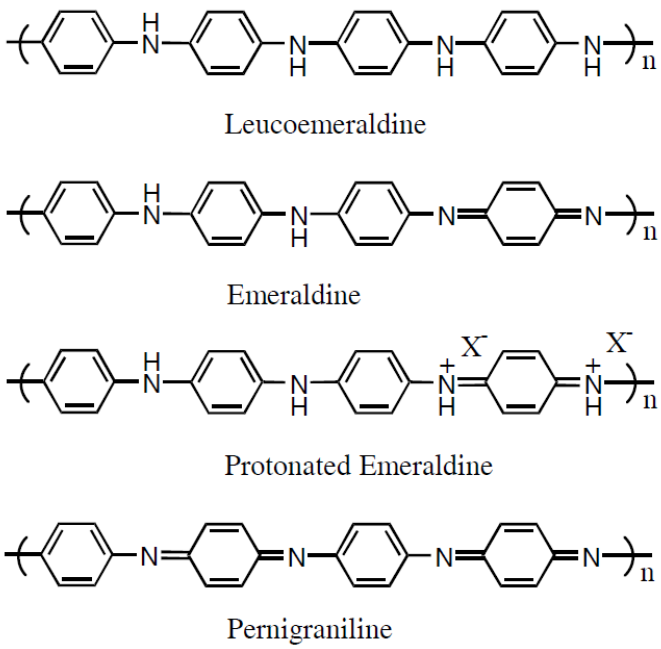

Figure 1.1: Different forms of polyaniline

Doping of leucoemeraldine base with protonic acid produces positive charge on the nitrogen atom of polymer backbone. The negative counter ion is not chemically bonded to the polymer chain, instead it is attached to the backbone by the electrostatic interaction. Doping causes changes in the electronic structure, crystallinity, solubility and produces high electrical conductivity [20,21]. The conducting mechanism of polyaniline can be understood from the exchange of positive charge on the imine and amine nitrogen atoms of the polymer chain. The properties of leucoemeraldine can be tuned by varying the dopant. Commonly used doping agents are mineral acids like HCl, H_2SO_4, H_3PO_4 and organic acids such as toluene sulfonic acid, naphthalene sulfonic acid, camphor sulfonic acid etc. The dopant anions such as chloride, sulfonate, phosphate, toluene sulfonates, naphthalene sulfonate and camphor sulfonate etc. strongly influence the electrical properties of polyaniline.

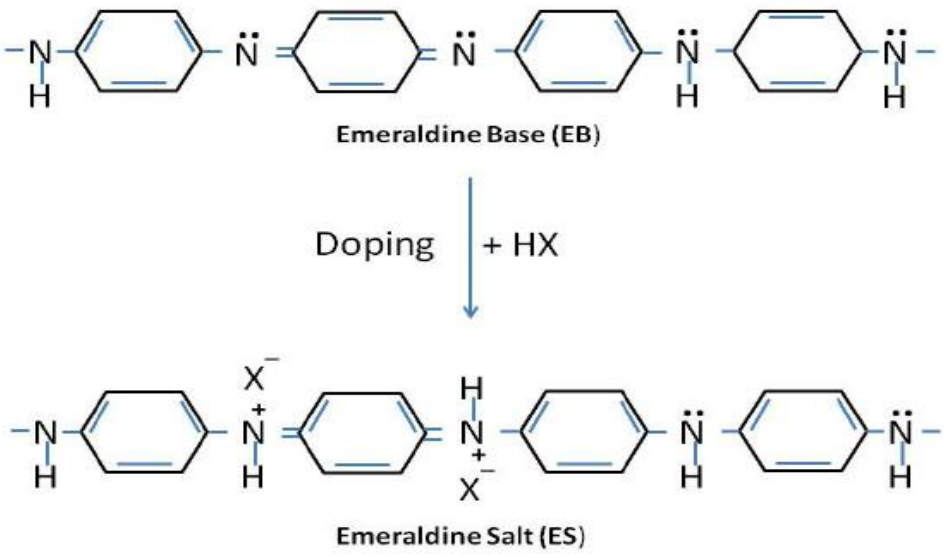

Figure 1.2: Protonation of emeraldine base to emeraldine salt

The dopant molecules can be de-doped from polyaniline reversibly owing to their non-redox and physical interaction. As discussed above the emeraldine salt is formed by the doping of emeraldine base, which results positive charge on the surface of nitrogen atoms and the anions are surrounding it. So, these anions are attached electrostatically to the polymer chain [22]. Thus, the synthesis of conductive form of polyaniline takes place in presence of a doping acid and oxidizing agent [23]. The most common oxidizing agent is ammonium peroxodisulfate (APS).

1.2.1 Polymerization of aniline

The polymerization mechanism is similar in both oxidation method and in electrochemical synthesis.

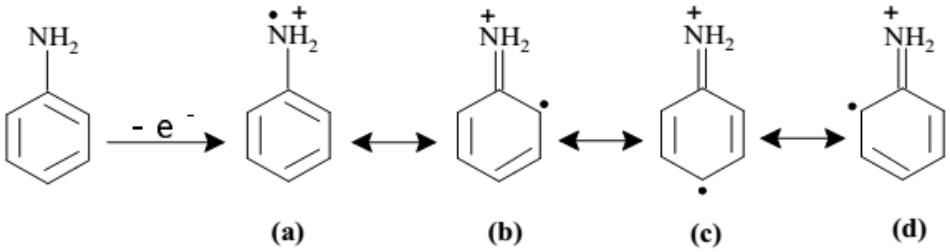

Figure 1.3: Aniline free radical formation and resonance stabilization

By the removal of an electron from the nitrogen atom of aniline free radical is formed. Then the free radical is resonance stabilized. After that the radical forms dimer by the head to tail reaction between radical cation in acid medium. The dimer formed is again oxidized resulting in the formation of new dimer.

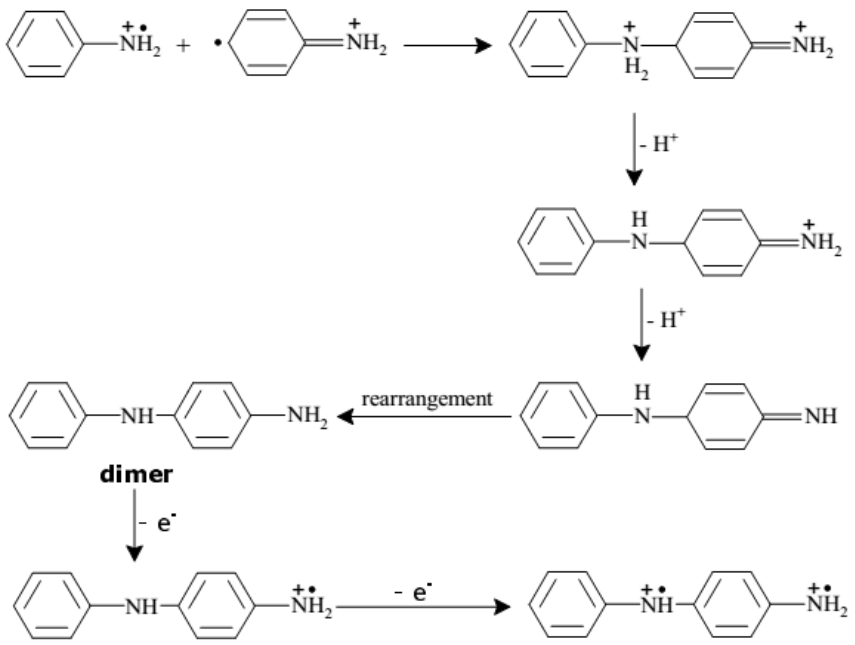

Figure 1.4: Radical cation dimer formation of aniline

The new radical dimer formed reacts with monomer radicals or the dimers yielding trimers or tetramers respectively. This step continues resulting in the formation of polymers.

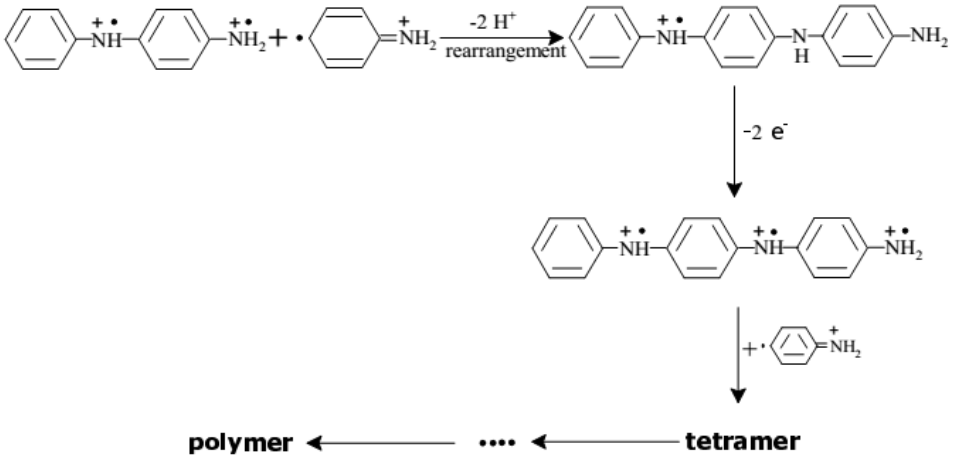

Figure 1.5: Polymerization of aniline

Conducting polymer composites can be prepared by the addition of conducting polymers or conducting fibers in to an otherwise non-conducting polymer. To improve the performance or extend the functions of conducting polymer based devices, the conducting polymers have to be modified. In recent years remarkable research efforts have been made to develop nanoscale polyaniline/carbon based material using various approaches [24,25]. The π-bonds present in the carbon nanotubes facilitate the formation of extended charge transfer between carbon nanotubes and polyaniline by introducing more conductivity to the composite. Therefore, composites based on carbonaceous materials and polyaniline on appropriate stochiometric combination have been proven to be efficient [26-29]. The synergistic combination of outstanding conducting properties of the carbonaceous materials and conducting polymers is an ongoing interest in nanotechnology. Moreover, among the aforementioned carbon materials, carbon nanotubes (CNT) are comparatively expensive and the preparation of graphene is a complex process. Carbon nanofibers (CNF) are alternative choice of materials, which are readily available and cheaper than CNTs. Besides, CNFs have attracted great interest in recent years due its unique one-dimensional structure, excellent electrical, thermal and mechanical properties [30-34]. Therefore, interest in the development of composites based on CNF and PANI is growing recently. Although PANI/CNF composites have been studied extensively, work on the development of sensors, antibacterial agents, fire retardants based on this composite is in the nascent state.

Conducting polymer composites can be developed based on conducting and non-conducting fibers. The combination of polyaniline with various carbonaceous materials has been proved to be attractive to increase the

electrical conductivity as well as mechanical properties. On the other hand, non-conducting materials can be rendered electrically conducting by the modification with electrically conducting polymer. However, addition of non-conducting fibers may reduce the conductivity and hence deteriorate the electrical properties of the composite. Among variety of renewable materials for the preparation of polymer composites cellulose fibers certainly constitute significant role. The properties of the fibers can be modified with polyaniline. Here we are discussing about the two nanofibers, carbon nanofiber and cellulose fibers.

1.3 Carbon nanofibers

The development in the field of nanotechnology has influenced carbon based materials remarkably. In recent years research in the area of vapor grown carbon nanofibers has been increased after the discovery of carbon nanotubes. Vapor grown carbon nanofibers can be synthesized in the diameter range of 15 to 100 nm. Carbon nanofibers can be produced by passing carbon feedstock over nanosized metal particles at elevated temperature [35-39], which is similar to the synthesis of carbon nanotube. While, the geometry of carbon nanofiber is different from that of carbon nanotube. Carbon nanofibers are formed by regularly packing arrangement of truncated conical or planar layers along the filament length [40-43]. This structural peculiarity provides high electrically conducting active side edges on both inner and outer surfaces of the fiber. It presents the opportunity of these materials to use as potential catalysts, for the reinforcement of the polymer composites etc. Carbon nanofibers have high specific surface area, flexibility, and super strength because of their nanosized diameter. Hence

these fibers can be used in the electrode materials of energy storage devices, hybrid-type filler in carbon fiber reinforced plastics and bone tissue scaffold.

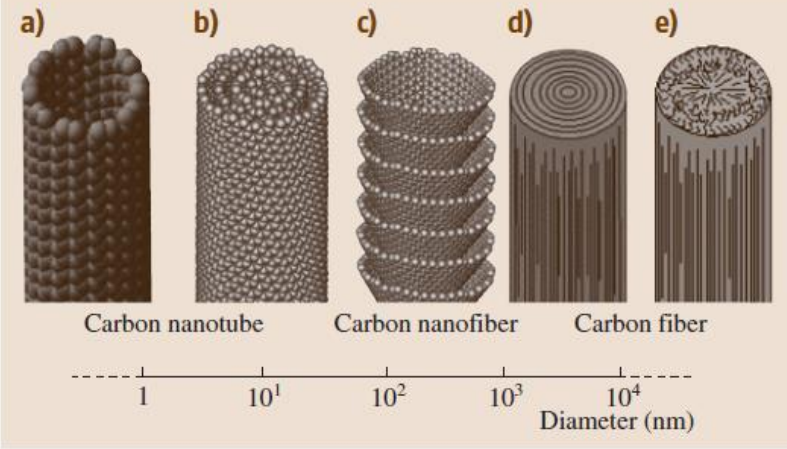

Figure 1.6: Comparison of diameter dimensions on a log scale of several carbon fibers

1.3.1 Structure

Carbon nanofibers are sp^2 hybridised linear discontinuous fibers with aspect ratio higher than 100 [44]. Carbon nanofibers consist of graphitic cylinders of diameter 1-100 nm. Graphitic planes of CNF are not always arranged along the axis. Depending on the angle of graphene layers, it can be classified as stacked and cup stacked arrangements [45]. In the stacked arrangements, the graphene layers will be perpendicular to the fiber axis. While in the cup stacked CNF, the layers are arranged at an angle between parallel and perpendicular to the fiber axis. Carbon nanofiber can be synthesized mainly by two methods. Catalytic chemical vapor deposition growth and electrospinning technique. Catalytic chemical vapor deposition technique can be used for the preparation of two types of carbon nanofibers. They are cup stacked carbon nanofiber and platelet carbon

nanofiber. Cup stacked nanofiber or conical nanofiber is first developed by Ge and Sattler [46]. Figure1.7 shows the formation of cup stacked carbon nanofiber by the CVD process.

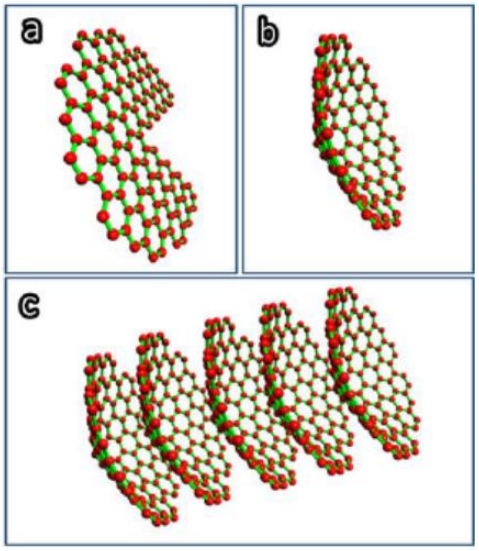

Figure 1.7: Representation of the formation of cup stacked CNF

1.3.2 Synthesis of carbon nanofiber

In the catalytic vapor deposition method, a metal catalyst is used. The catalyst should be capable of dissolving carbon, forming corresponding metal carbide. Generally, the metals used as catalyst are iron, cobalt, nickel, molybdenum, and vanadium. The carbon sources are carbon monoxide, synthesis gas, methane, ethene, ethyne in the temperature between 700 to 1200 K [47]. Carbon is dissolved in presence of metal, deposits on the metal surface as graphitic carbon [48]. The structure of the as produced fibers is determined by the shape of catalysed metal particle. The size of the metal is usually in the range of 10-100 nm which determines the outer

diameter of CNF [49]. The angle of arrangement of the graphene layers affects the properties of CNF [50,51]. The figure 1.8 illustrates the process of catalytic metal deposition. The plasma enhanced CCVD produces CNF at comparatively low temperature of about less than 650 ºC [52].

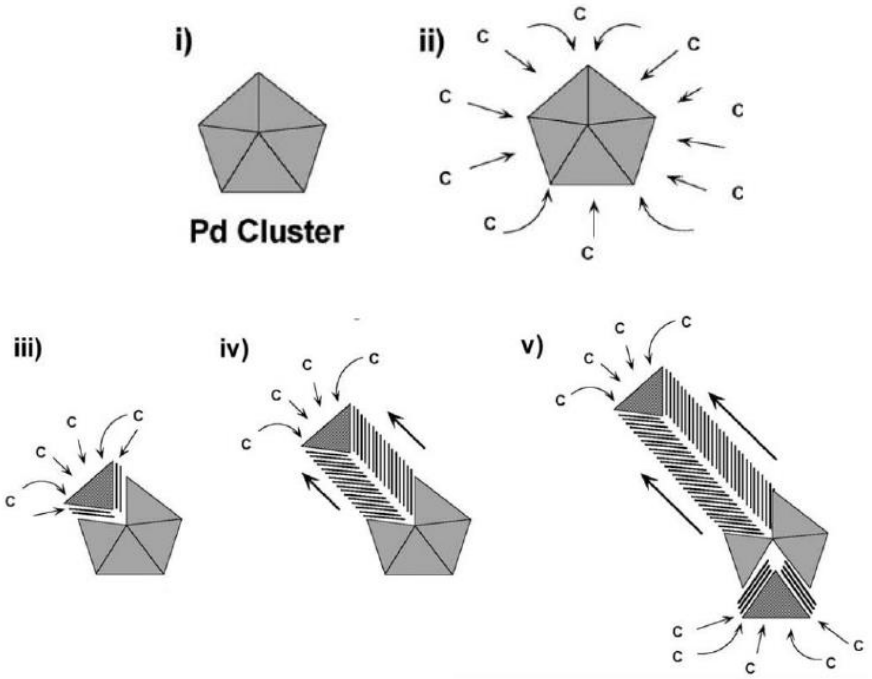

Figure 1.8: Illustration of the chemical vapor deposition growth mechanism of cup attacked carbon nanofibers.

In electrospinning, fine tip needle syringe is used, by the application of high voltage, the solution is spurt out from the needle to the target material. With increasing the surface tension to prevent the breaking of solution droplets, the fiber like particles will be deposited on the target material.

CNF based composites are capable of reversibly changing the electrical properties with the change in the external conditions. Li et al.

discovered CNF/polyacrylate composite as gas sensors based on the vapor detection of the gas [53]. Whereas another CNF based composite is capable of sensing toxic gases like NH_3 and HCl by one step vapor deposition polymerization method [54]. In addition to that carbon-based nanomaterials have arose up as novel antimicrobial agents because of their high surface area to volume ratio and unique applications [55-57].

1.4 Cellulose

Conventional composites consisting of steel, aluminum and iron etc. are not readily disposable, causing adverse environmental effects. In order to overcome these hazardous composites, the focus is on the development of natural composites. For that natural fibers are used as the filler material in composites. Cellulose is the most abundant biopolymer on earth, and it is present in animals and plants. Cellulose has been extracted from various resources such as pineapple [58], corncob [59], soy hulls [60] hemp fibers [61], rice husk [62] etc. While the coconut waste was studied extensively owing to the conscious of agricultural wastes. The hydroxyl groups of cellulose are connected to adjacent molecules forming intermolecular hydrogen bonding. The hydrogen bonding is the reason behind the strength of cellulose molecules. It causes the molecules to form bundles of cellulose chains which make the cellulose chains stiff. The hydrogen bonding also makes the molecule insoluble and it is resistant to most of the chemicals owing to the less number of available hydroxyl groups. In the cell walls of the fiber, cellulose micro fibril bundles exist, which is surrounded by lignin and hemicellulose forming a multi-layered structure of cellulose with lignin and hemicellulose. To

extract cellulose into micro and nano fibrils it is necessary to remove lignin and hemicellulose from the fiber. Many efforts have been made recently by means of chemical and mechanical treatments to extract cellulose in to nano range [63]. Chemical treatments include alkali treatment, acid treatment, bleaching etc. Mechanical treatments like grinding, homogenisation, ultrasonication or else the combination of these processes breaks down the macro fibers in to micro and nano level.

Figure 1.9: Picture of coir fiber

Natural cellulose is synthesized mostly in plants. Coir is the fruit of coconut tree, which is cultivated widely in India, especially in Kerala. Coir is the lignocellulosic fiber obtained from the mesocarp of coconut. The main constituents of these fibers are lignin, cellulose, hemicellulose, pectin and some amount of wax. The major content of coir is lignin, it is approximately 40 to 45 %. Then comes cellulose of about 30-42 %. Cellulose extraction from coir fibers will result in the production of high quantity nanofibers [64]. The chemical composition of coir is given in the table 1.1.

Table 1.1: Chemical composition of coir fiber

Cellulose	32–43 %
Lignin	40–45 %
Hemi-cellulose	0.15–0.25 %
Pectins and related compounds	3–4 %
Moisture content	8 %

1.4.1 Structure of cellulose

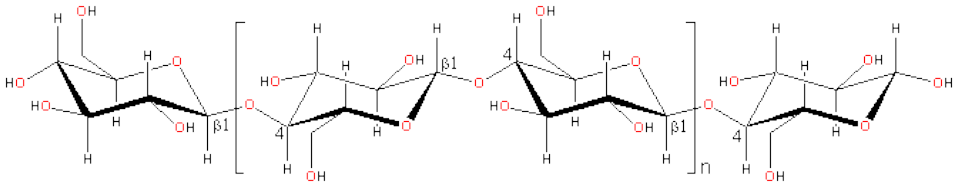

Figure 1.10: Molecular structure of cellulose

Cellulose is linear polysaccharide polymer composed of D-glucose units linked by β-1,4 glycoside bonds. The polymer chains are associated with bundles of fibrils known as microfibrillar aggregates. Natural cellulose is made up of cellulose I which is a metastable state, in which cellulose strands are parallel to each other without intermolecular hydrogen bonding. Cellulose exists as six different polymorphs, I, II, III_I, III_{II}, V_I and IV_{II}. Both I_α and I_β are present in cellulose I, in variable proportions according to their origin. Cellulose extracted from algae and bacteria contains high amount of I_α cellulose, $I_\beta$cellulose is more when it is extracted from higher plants. Meta stable I_α can be converted in to the more stable amorphous form I_β by thermodynamically through the process called annealing.

1.4.2 Extraction of cellulose

The fiber consists of cellulose bundles linked together by cementing materials like hemicellulose, lignin, wax and oils. Hemicellulose is a polysaccharide molecule, possessing extensive branching, lower molecular mass with a degree of polymerization about 50-200. Lignin is a class of natural organic polymer and it is an important constituent in the formation of cell walls. It is randomly branched polyphenol, composed of three different phenyl propane units. Ligin and hemicellulose present in the cell wall function as binder between the cells resulting the composite structure with excellent strength and elasticity [65].

Herrick et al. [66] and Turbak et al. [67] described the method to produce microfibrillated cellulose from natural sources. The wood pulp suspensions were homogenized by the means of mechanical homogenizer. High pressure homogenization is the process which consist of passing the cellulosic slurry through a small nozzle under extremely high pressures. Grinding is one of the other methods to produce nanofibrillated cellulose from its macro form. During grinding the hydrogen bonds break resulting in the individualization of pulp in to the nanometre scale [68]. High intensity ultrasonication is also employed for the production of nanocellulose, in which the oscillating power is used to isolate cellulose fibrils by hydrodynamic forces of ultrasound [69].

In addition to the mechanical treatments, the fibers are subjected to different chemical treatments including alkali treatment, acid treatment and bleaching. Alkalization is common technique used to remove hemicellulose, fats and waxes present in the fiber. It defibrillates the

external cellulose microfibrils and eposes short length crystallites. Moreover, it destroys the hydrogen bonding interaction between the cellulose molecules resulting in the increased surface roughness. After the successive acid and alkali treatments, bleaching was performed. It was carried out for the complete removal of the remaining cementing materials from the coir fiber.

Cellulose is a naturally occurring fiber that can be refined to macro, micro and nano size regimes by employing appropriate processing techniques. Conductivity can be imparted to these fibers by depositing a fine layer of known conjugated polymers on the surface [70]. Combination of these fibers with an appropriate polymeric matrix will result in composites with good dielectric properties and anisotropic mechanical properties. Nanoparticles in polymer matrix influence the structural, optical and electrical properties which can be effectively tuned for applications such as charge storage capacitors, electromagnetic shielding etc. [71].

1.5 Thermoplastic polymers

Based on the permanence of the plastics, it is classified mainly in to two. Thermoplastics and thermosetting plastics. Thermoplastic polymers can be moulded by heating and becomes hard when it is cooled. It becomes again soft while heating and can be remoulded in to different shapes without effecting its properties. Whereas thermosetting polymers cannot be remoulded. This is because of the chemical bonds between the polymer chains, which will lead to the formation of highly cross-linked structures. In thermoplastic materials, the polymers are connected by the

Vander walls forces which forms the linear or branched structures. Polyvinylchloride (PVC), Polymethylmethacrylate (PMMA), Polystyrene (PS), Poly(vinyl alcohol) (PVA) etc. are examples of thermoplastic polymers. Thermoplastic polymers are of low cost, light weight and possess better fatigue properties, hence these materials can replace metals with considerable weight savings. The thermoplastic components are easy to manufacture in high volumes with precision. These materials are highly recyclable, possess high impact resistance. So, in the study I have employed thermoplastic materials poly(vinyl alcohol) and polymethylmethacrylate for the preparation of the conducting composites.

1.5.1 Poly(vinyl alcohol) (PVA)

Poly(vinyl alcohol) is synthesised by the hydrolysis of polyvinyl acetate [72]. It is benign to living tissues, harmless, and nontoxic. Because of its use in cross-linked products and nanofillers, the chemistry related to this polymer has become attractive [73-75]. It is water soluble crystalline polymer has the ability to form excellent films. The solubility of PVA in water is governed by its intrinsic properties, it requires temperature of about 100 ^{o}C. The degree of hydrolysis varies depending on the molecular weight, elemental composition and crystal structure [76,77].

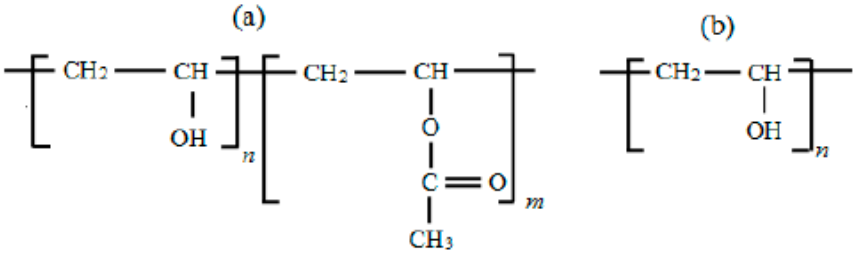

Figure 1.11: Different structures possible for poly(vinyl alcohol)

Depending on the degree of hydrolysis, two types of structures are possible for poly(vinyl alcohol). Figure 1.11a represents the partially reduced form and 1.11b shows the fully reduced form of poly(vinyl alcohol). The molecular weight of the polymer changes with the polymerization conditions. The elimination of acetate groups can take place either in acidic condition or in the basic medium. So, the molecular weight depends on the degree of hydrolysis and the length of vinyl acetate polymer [78]. PVA exhibits similarity to the human tissues, it can absorb protein molecules, and results with minimum cell adhesion, without any toxicity. It makes this polymer suitable for biomedical applications. Furthermore, poly(vinyl alcohol) responds well to humidity owing to the large number of hydroxyl groups present that can interact through hydrogen bonds indicating the efficiency of the material as potential humidity sensor. Moreover, it is an eco-friendly polymer, by the absorption of water molecules it swells indicating the chain altering of PVA by the absorbed water molecules. PVA has been extensively investigated as a host for different nano-fillers and for electrolyte applications. Presence of hydroxyl groups of PVA make it a self-charring material. The fire retardancy can be improved by the incorporation of various organic and inorganic fillers. So, the high flexibility and polar nature of PVA makes ideal host for intrinsically conducting polymers. Poly(vinyl alcohol) with hydroxy functional backbone offers good film forming property. Moreover, environmental kindly and flexibility of PVA molecules account for its EMI shielding applications. So, the high flexibility and polar nature of PVA makes ideal host for intrinsically conducting polymers.

1.5.2 Poly(methyl methacrylate) (PMMA)

Poly(methyl methacrylate) (PMMA) is one of the promising polymeric materials with desirable properties such as good weatherability, exceptional optical clarity and dimensional stability. PMMA is synthetic thermoplastic polymer formed by the block, emulsion or suspension polymerization of methyl methacrylate (MMA). It is highly transparent polymer; hence it is used as light weight and shatter resistant replacement for regular glasses.

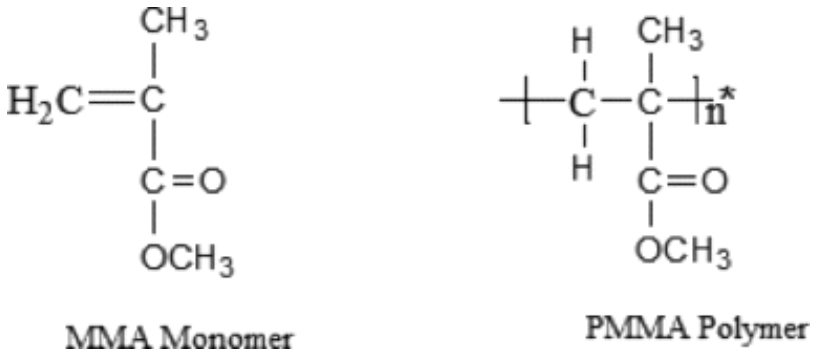

Figure 1.12: Structures of methyl methacrylate and polymethyl methacrylate

PMMA is classified in to three categories with respect to its tacticity, that is depending on the way of pendant methacrylate groups are arranged along the polymer backbone [79]. Isotactic (mm) is when the adjacent monomer groups were added in the meso diad mode, and the ester groups on the successive asymmetric carbons are projected on the same side of the polymer chain. Syndiotactic (rr) is when the monomer groups were added in the racemic diad mode, and the ester groups on the successive asymmetric carbons are projected in a regular alternation on both sides of the plane in the polymer chain. Atactic (mr) is another

racemic diad mode, but the ester groups on the successive asymmetric carbons are projected randomly on both sides of the plane in the polymer chain as shown in Figure 1.13 [80,81].

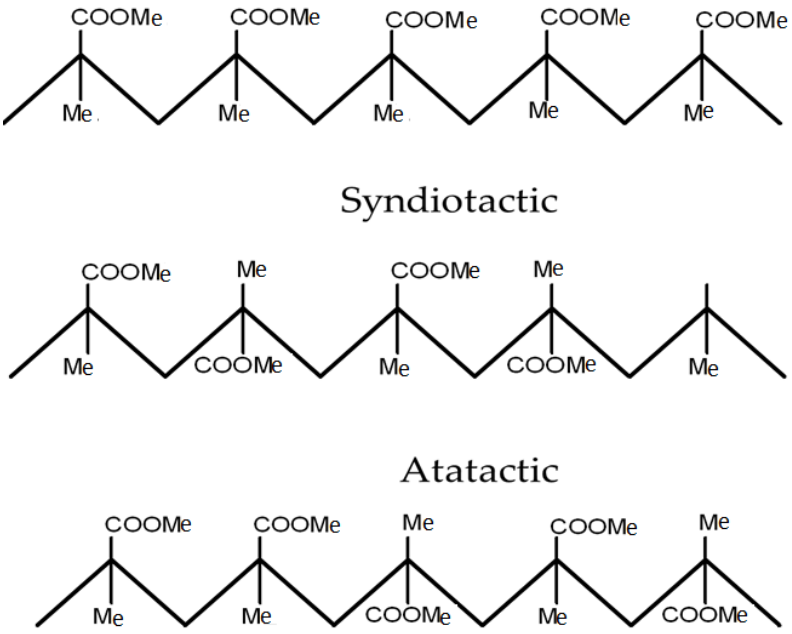

Figure 1.13: Different kinds of PMMA structures

Free radical polymerization using peroxide and azo compounds yields the formation of atactic polymer. PMMA can also synthesized by the anionic polymerization, which yields the formation of isotactic and syndiotactic polymers. Isotactic and syndiotactic forms are more crystalline in nature and are stronger and more resistant to solvents.

PMMA is an economical alternative to polycarbonate (PC) when high toughness and impact strength is not required. It exhibits low moisture and water absorbing capacity. PMMA is a combustion material, it burns even after the removal of the flame. The products eliminated in

thermal destruction possess intoxicating effect. PMMA based composites were prepared by injection moulding technique and it have excellent film forming property also. High injection pressures are needed for moulding due to its poor flow characteristics.

PMMA can be used for making contact lenses, because of its good degree of compatibility with human tissue. High stiffness and the biocompatible nature of PMMA makes this suitable for bone substitute applications [82,83]. PMMA based bone cement has been found to be very efficient for the anchoring of artificial joints. During the implantation, it is at high risk of infection. In order to avoid the infection, suitable antibacterial drugs can be coated on the surface of PMMA. So PMMA based composites can be used as bone cement with low infection rate. Hence the PMMA based composites has been the areas of numerous research works, focusing on the improvement of strength and durability [84-87].

1.6 Properties of conducting polymer composites

1.6.1 Dielectric permittivity and loss factor

The real part of permittivity is related to the capacitance of a material and its ability to store energy [88]. Dielectric material stores current without conducting to a substantial amount. The charge storage is due to the polarization in an electric field by the dipoles where surface develops a net positive charge and the opposite surface develops a net negative charge. The imaginary part is known as the loss factor (ε") and represents the energy loss of the external electric field when applied to the test material.

When the dielectric material is placed inside a DC electric field mainly four types polarizations occurs; electronic polarisation, ionic polarization, orientation polarization and space charge polarization. By the application of an electric field, the positively charged nucleus moves in one direction and the surrounding electron cloud distorts in opposite direction. As a result, the centre of electron cloud is not coinciding with the centre of nucleus, which will cause the development of a net dipole moment inside the material. This kind of polarization is possible in all types of materials, due to the presence of nucleus and electron cloud. The developed dipole moment is proportional to the magnitude of the applied electric field.

The ionic polarisation occurs when the molecules possessing ionic structure comprising of cations and anions. The cations and anions are held together by an ionic bond; hence these ion pairs will possess net dipole moment before the application of electric field, but the total may be zero. But after the application of the field, the materials exhibit spontaneous polarization it will alter the net polarization. This is called ionic polarization.

Orientation polarisation occurs in molecules possessing permanent dipole moments. In absence of field, the dipoles will be arranged randomly owing to the thermal motion of the material. By the application of an electric field, the dipoles will be aligned with the field as a result the dipoles will not cancel each other causing a net dipole moment for the material. It occurs in a frequency range of 10^6 Hz to 10^{10} Hz.

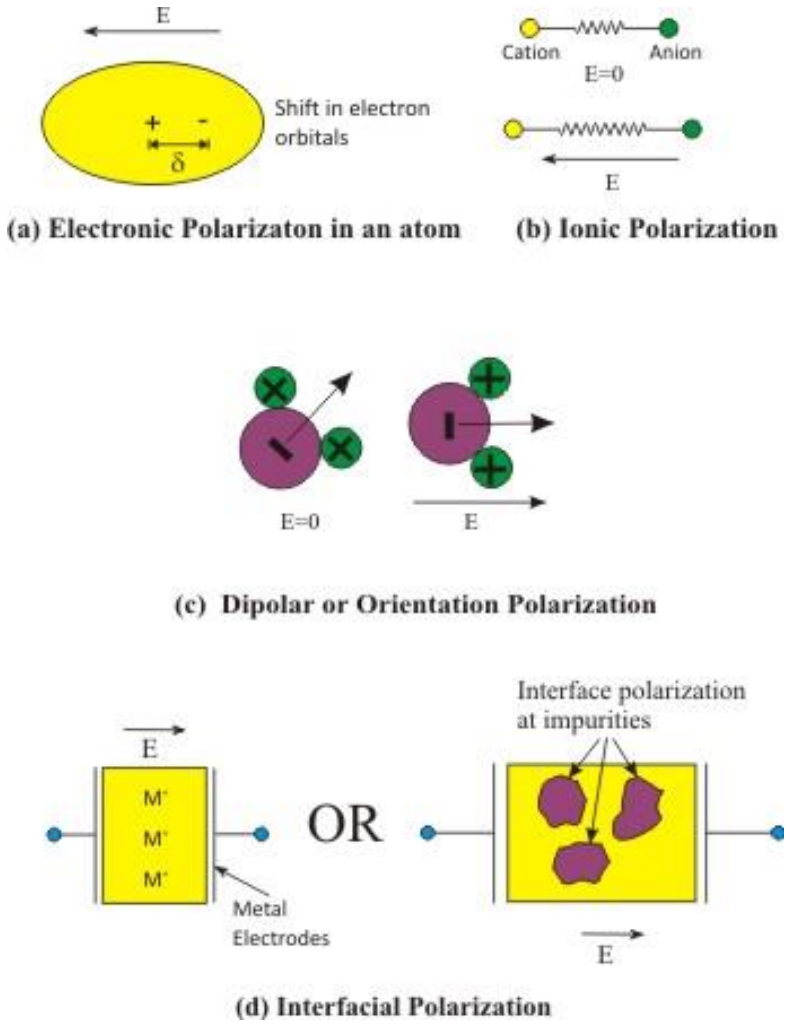

Figure1.14: Schematic representation of polarization mechanisms

Space charge or interfacial polarization involves limited movement of charges resulting in alignment of charge dipoles under applied field. This usually happens at the grain boundaries or any other interface such as electrode-material interface.

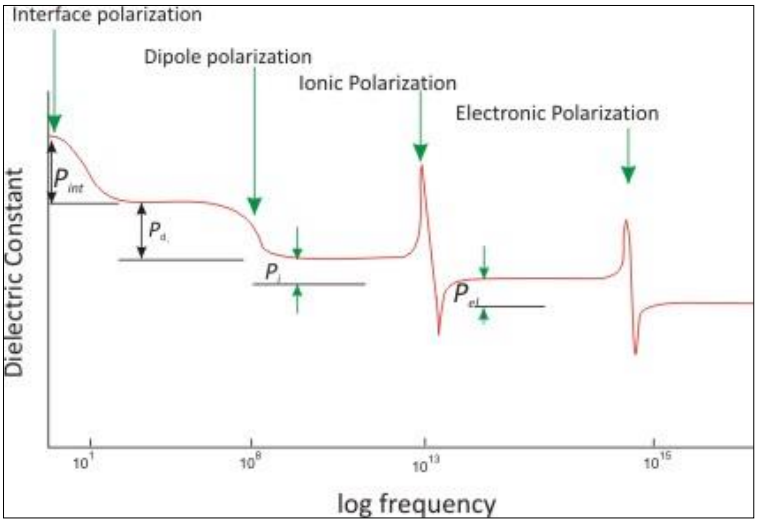

Figure 1.15: Plot of dielectric constant with frequency showing different polarization mechanisms

By the switching of the field, the polarised molecules also switch in order to align with the generated field. There is a time gap for the switching of the polarized molecules with the alteration of the field. As a result, different polarization mechanism takes different relaxation times with the frequency of the applied field, the frequency dependence is governed by the resonance phenomena. Figure 1.15 shows the plot of dielectric constant with the frequency; the peaks represent the resonant phenomena of the material. Atomic or electronic polarization is the fastest polarization mechanism, and it exists in the frequency range of 10^{13}-10^{15} Hz. Ionic polarization occurs between 10^{9}-10^{13} Hz; dipolar polarization is caused by the movement of dipoles and it occurs below 10^{9} Hz. Interfacial or space charge polarization occurs at low frequencies of about 10 Hz.

Dielectric spectroscopy is very informative technique to determine the molecular motions and structural relaxations in materials with permanent

dipole moments [89,90]. Knowing the real and imaginary permittivity, the AC conductivity can be determined. Determination of AC conductivity provides the information about the application of the materials and it gives an idea about the mechanism of conduction [91].

1.6.2 Microwave properties of the conducting polymers

Microwaves are the high frequency radio waves having wide range of applications, including radar, communication and cooking. Mostly it is used in communication systems to transfer the information such as voice, video and data. It constitutes a small portion of electromagnetic system from 300 MHz to 300 GHz. Conducting polymers are found to be very efficient as microwave absorbers and it is ideal materials for effective welding of plastics [92]. Material characterization is important for the proper selection of a material for various applications. The vital applications of microwaves are electrostatic dissipation, microwave absorption and electromagnetic interference shielding.

The high data transfer rate of microwave radiations increased the number of communication devices operating in the microwave region. In order to reduce the electromagnetic pollution, conducting and magnetic microwave absorbing materials are widely being used [93-101]. Owing to the flexibility and light weight of polymeric materials, they are preferred over sintered bodies. Hence the conducting polymeric composites replace the metals in industrial areas. Numerous microwave absorbing materials based on conducting polymers have been developed in the recent years [102,103]. Rimili et al. developed the polyaniline based highly conducting materials suitable for microwave absorbing in the X and S bands [104].

1.6.3 Electromagnetic Interference shielding

Electromagnetic interference occurs when a sensitive device receives electromagnetic radiation which is emitted by other electric or electronic devices. Consequently, the received device will malfunction and it will lead to the wastage of energy and cause economic loss [105-107]. Electromagnetic radiation can also enter into the human body. As a result, it causes to vibrate the molecules and produces heat inside the body. The heat produced is not easy to get dissipated and lead to the weakening of vein network.

Due to the advancement in the communication technology which in turn lead adverse effect in the electromagnetic radiation pollution. Consequently, there is an urge to protect the environment as well as the sensitive circuits from microwave radiations. Electromagnetic interference shielding denotes either reflection or absorption of electromagnetic radiation by a material. The EMI shielding properties of a material depends primarily on three factors. The foremost requirement is that, the material should possess high electrical conductivity and it should have good magnetic properties. High aspect ratio is the second condition, which will help to form continuous conductive network. The filler molecules must be properly dispersed in the matrix, which will lead to form good adhesion with the matrix [108].

Shielding can be performed in two ways, either by means of a shield, the emitted radiation from electric circuits can be prevented or shield the radiation outside the boundaries of the product. In both cases, the shield act as the barrier for electromagnetic radiation.

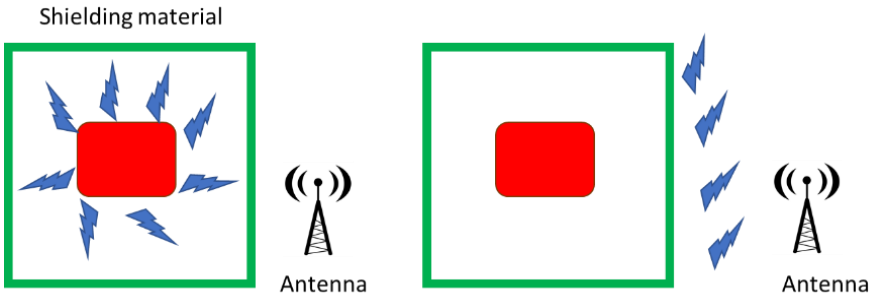

Figure 1.16: Illustration of the use of a shielded enclosure **(a)** radiation from an electrical circuit under operation **(b)** to eliminate radiation from the external source

The shielding effectiveness of a material depends on EMI attenuation, frequency, distance between the shield and the source, nature and thickness of the shielding material. It is generally expressed in decibel (dB). The total shielding efficiency of the material is the combination of absorption, reflection and multiple internal reflections [109-112].

$$SE=SE_A+SE_R+SE_M$$

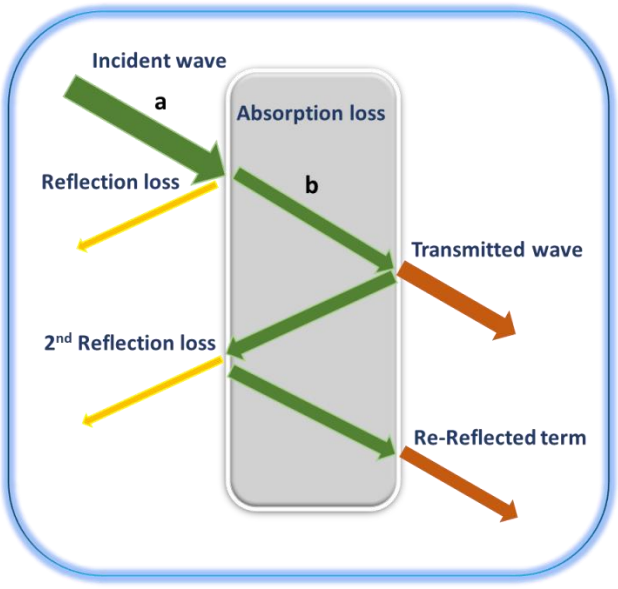

Figure 1.17: Schematic representation of EMI shielding mechanism

Figure 1.17 represents the graphical illustration of EMI shielding mechanism, **(a)** EM wave representation **(b)** Splitting of electromagnetic wave on passing through a shield [113-114].

1.6.3.1 Conducting polymer composites for EMI shielding

Earlier metals have been used for EMI shielding primarily by the reflection of electromagnetic radiation. Though, metals possess disadvantages like high density, corrosion and rigidity. One of the ways to overcome the issues related to EMI shielding, is the use of polymer composites embedded with conducting particles [115-117]. In order to make polymers effective for shielding the conductivity should be higher than 10^{-2} S/cm. So, by using one kind of material (eg. Carbon black) higher filler loading is necessary. Carbon nanofibers are conducting materials, the conductivity can be increased by the modification with suitable conducting polymers. The synergistic effect of these two-conductive material will produce high conducting materials, with lower filler loading.

1.6.4 Antibacterial Properties

The area of antibacterial drug has found unique attention, as the pathogens get resistant to the existing drugs in vogue. Antimicrobial agents are the materials used for the treatment of diseases, inhibitory chemicals employed to kill micro-organisms or prevent their growth. Based on the application and spectrum of activity, these microorganisms are classified variously. Germicides are the materials that can kill the microorganisms. Whereas the micro biostatic agents cause the inhibition to the growth of pathogens. The germicides may show selective toxicity depending on

their spectrum of activity. They may act as viricides (killing viruses), bacteriocides (killing bacteria), algicides (killing algae) or fungicides (killing fungi).

There are two types of materials such as bactericidal and bacteriostatic. Bactericidal materials are capable of killing bacteria but not necessarily the bacterial spores. While the bacteriostatic materials are chemical species which are not killing the bacteria instead it can prevent the growth of microorganisms. Hence the reproduction and replication are also prevented. The activity of these two kinds of the chemical species can be evaluated by different ways. Serial dilution fluid media method, serial dilution solid media method, cup plate method, gradient plate method, ditch plate method etc. are the methods used to evaluate the activity of bacteriostatic materials. But mostly end point methods are used for the evaluation of bactericidal materials.

We have followed the cup plate method or agar well diffusion method [118] for the evaluation of polymer composite activity. Hence the method is describing here. The agar medium is poured in to a sterile petri dish and it is allowing to solidify. Agar surface of each plate is marked by a sterile cotton swab with the reference bacterial strain. Then the agar plate is punched with a sterile cork borer of 4 mm size and 15 μL of the sample by means of a micropipette. The plates are allowed to standby for 30 min. After that the plates are incubated at 37 °C for 48 h.

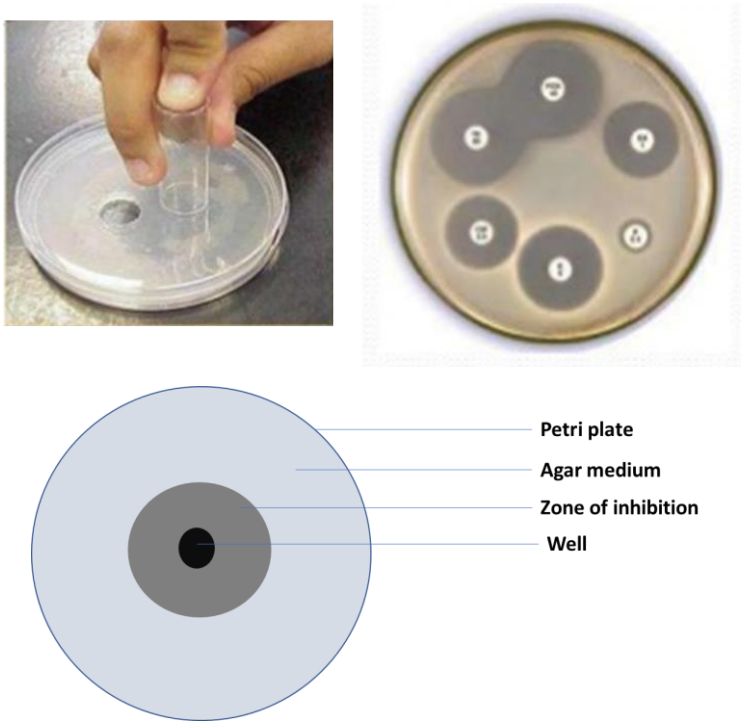

Figure 1.18: Agar well diffusion method with essential arrangement.

1.6.4.1 Mode of action

Antibacterial agents can interfere with the synthesis and function of the vital components of the microorganisms. The material can react with microorganisms differently and causes the inhibition of the growth of microorganisms.

(a) Cell-wall synthesis
(b) Protein synthesis
(c) Nucleic acid synthesis
(d) Enzymatic activity
(e) Folate metabolism or
(f) Damage cytoplasmic membrane

1.6.4.2 Minimum Inhibitory Concentration (MIC)

It is the lowest concentration of the antimicrobial agent which inhibit the growth of test microorganisms. The methods adopted to study the antibacterial activity can also be used for the determination of MIC. Lower MIC value indicates that the drug is more powerful to bacteria. MIC scores are vital in diagnostic laboratories in order to confirm resistance of microorganisms to an antimicrobial agent and also to monitor the activity of new antimicrobial agents. They are using the MIC values of the drugs to select the antibiotics to administer to patients with specific infections and to identify an effective dose of antibiotic.

1.6.5 Flame Retardancy

Burning is a chemical process occurs when oxygen reacts with another material producing adequate heat and light (exothermic reaction) to cause ignition. During the pyrolysis of the polymer, flammable gases are formed. An adequate ratio between these gases and oxygen leads to ignition of the polymer.

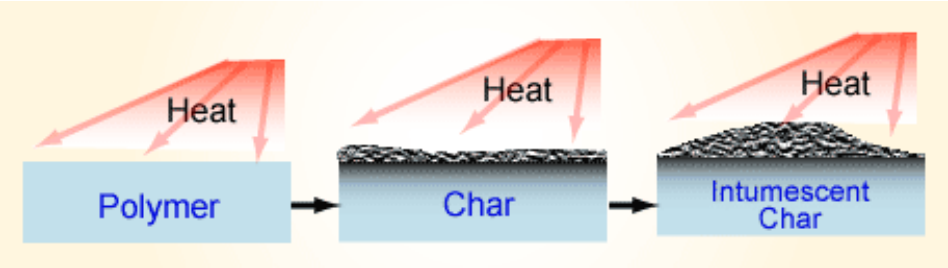

Figure 1.19: Char layer formation on the surface of the burning material

The addition of flame retardants to the polymeric system increases the LOI values of the material. That means the flame retardants can inhibit one

or more stages of the combustion process. It can be heating process, decomposition, ignition, spreading of the flame or smoke process. This depends on the nature of the polymer and flame retardant. There are two types of flame retardant processes. It can be either chemical or physical process. In chemical process, the flame retardants benefit the polymer breakdown, causes the flow of polymer which in turn reduces the effect of flame on the material. Flame retarding materials causes the formation of carbon layer on the surface of the polymer. During the heating process, the water molecules will get eliminated, creating double bonds in the polymer system. As a result, it forms carbonaceous layer on the surface by cyclising and cross linking. The process of char formation on the polymer surface is illustrated in the figure 1.19.

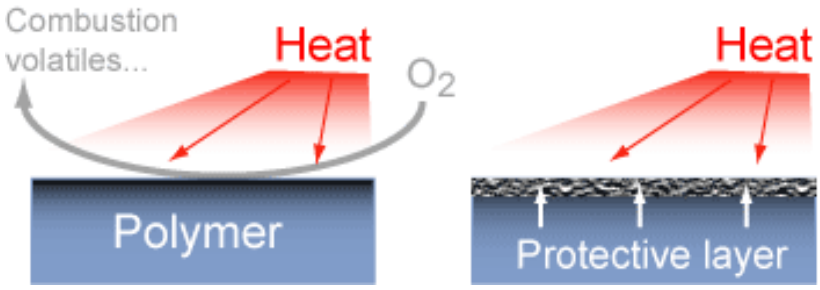

Figure 1.20: Schematic illustration of the protective layer formation inhibiting combustion and volatiles

When the flame retardant is acting physically, the heat transfer is reduced by the formation of a protective layer on the surface. It can reduce the flow of flammable gases and the degradation of the polymeric material. In other way, the flame retardant additive can degrade through an endothermal process. Which will reduce the temperature of the host material. In turn, it increases the LOI value.

Recent years scientist succeeded in the development of nanomaterial based polymer composites for the flame retardant applications. In the discovery of new fire safe materials, Kashiwagi et al. have developed unique nanocomposites consisting of CNTs or CNFs [119-122]. The improvement in the fire retardancy of these composites can be explained as the formation of protective char layer on the surface. Even after the decomposition of the polymer chain, the carbon nanofiber will be present which will lead to the formation of compact network structure. Consequently, it slows down the mass loss of polymer while burning. Moreover, Morgan et al. stated that the fire retardancy is due to the reduction in heat release rate which in turn reduces the mass loss rate [123]. Successively the use of carbon based materials for fire safety purposes is increasing in the day to day life.

1.7 Applications of conducting polymer composites

1.7.1 Sensors

Conducting polymers, such as polypyrrole, polyaniline, polythiophene and their derivatives have been used as the active layers of gas sensors since 1980s [124]. Metal oxide based sensors are commercially available these days, compared to this kind of traditional sensors the conducting polymer sensors possesses better characteristics. Metal oxide sensors require high temperatures whereas room temperature sensing is possible for polymer sensors. In addition, polymer sensors have short response and recovery times. Owing to the good mechanical properties of conducting polymer composite lead to the facile fabrication of sensors. Thus, more attention has been paid to develop polymer based composites.

1.7.1.1 Ammonia sensors

According to European Environment Agency (EEA), 10 million metric tons of ammonia are being produced per year in the areas of western Europe. So, it causes ammonia as one of the common High Production Volume(HPV) industrial chemicals. Ammonia is widely used in industrial work places including petrochemical, paper, pulp and in oil industry. It is the building block for fertilizers and pharmaceuticals. Anhydrous ammonia is used as coolant in large industrial refrigerants. In the view of environmental pollutions, it is crucial to detect and measure the accurate amount of the toxic polluted gases to evade the major health issues in the near future. Anhydrous NH_3 is such a toxic gas, high levels of NH_3 can cause irritation to eyes, skin and respiratory organs. Four types of ammonia sensors are used most commonly. They are infrared sensors, chemo sorption, electrochemical and charge carrier injection sensors. Polyaniline based sensors are examples of electrochemical sensors. Electrochemical sensors are compact, needs less power, exhibits excellent repeatability. Gas enters in to the sensing material undergoes an electrochemical reaction that causes a change in the electrical properties of the material. The difference in the resistance is related to the amount of gas absorbed in to the material. Electrochemical sensors are developed in such a way to reduce the effects of interfering contaminants, making the readings as specific as possible.

At present metal oxide semiconductors are being used for monitoring of toxic gases. Usually these sensors entail high working temperature, moderate selectivity and are expensive. Conducting polymeric materials

are widely been used as ammonia sensors because of their interesting characteristics like high sensitivity, short response time and room temperature operating [125]. Among the conducting polymers, polyaniline has extensively been investigated as gas sensing polymer due to its conducting property and chemical stability [126-128]. PANI can be synthesized by a fast and facile in-situ polymerization technique. Moreover, the size and morphology of the PANI particles can be controlled during the synthesis. It also opens up a way to industrial processing. The cost of sensor fabrication and maintenance are thus likely to be low. In the pioneering work of Chani et al. [129] the polyaniline sensors in the form of pellets responded but the response time was approximately 3-4 minutes. So, the development of novel and high-performance gas sensor with good sensitivity, stability and response remains a challenge.

1.7.1.2 Humidity sensors

Humidity sensors are used for the detection of relative humidity in various atmospherics. Humidity sensing has also become essential for weather prediction, historic preservation, environmental studies and mobile electronics etc. [130-132]. There are many domestic applications like intelligent control of living environment, cooking control in microwave ovens etc. [133]. Humidity sensing is measured as the variation of electrical conductivity or the variation of the capacitance value. Normally used units for humidity measurements are relative humidity (RH), Dew/Frost point (D/F PT) and Parts Per Million (PPM) [134]. Relative humidity is a function of temperature; hence it is a relative measurement. Relative humidity is expressed as percentage. Dew point is the temperature above

which the water vapor condenses to form liquid water. However, frost point is the temperature at which the water vapor condenses to form ice. Both dew point and frost point are independent of temperature, thus it is absolute humidity measurement. Parts Per Million (PPM) represents the water vapor content by volume fraction. Among the various humidity measurements relative humidity is commonly used although this measurement unit is relative.

Based on the method of measurements there can be resistive type humidity sensors and capacitive type humidity sensors or thermal sensors. Resistive type humidity sensors measure the resistance of the material with the alteration of humidity. In capacitive type humidity sensors, the material is placed in between two electrodes. The change in capacitance with respect to the atmospheric humidity levels are measured. In thermal sensors, two sensing materials are used. The materials will conduct electricity based on the humidity of the surrounding atmosphere. Among the two sensing materials one is encased in dry nitrogen while the other measures the ambient air. The difference between the two sensing materials measures the relative humidity.

Polymers are carbon hydride compounds or their derivatives. Functional groups are attached to the back bone of polymer chain, the properties of the polymer are determined by the functional groups and its basic backbones structure. Polymeric humidity sensors are widely studied in applied industry [135-136]. Porous polymeric structures are mostly used as humidity sensors. The micropores function as the sites for water absorption. During the recent years polymeric sensors have been developed

based on quaternary ammonium salts, sulfonate compounds, and based on polymers containing phosphonium atoms [137-142].

1.7.2 Capacitor

It is a two-terminal electrical device which has the ability to store electrical energy in an electrical field. Basically, a capacitor consists of two or more parallel conductive metal plates which are separated either by air or by means of an insulating material. The size and shape of the capacitor is based on the application. The consecutive plates can be square, rectangle, cylindrical or spherical.

When DC voltage is applied on a capacitor, the charge accumulation taking place on the metal plates. There are two kinds of electrical charge, one is positive in the form of protons and the negative charge in the form of electrons. So, by the application of voltage, positive charges accumulate on one plate thus some negative charges accumulate on the other plate. Same number of positive and negative charges will be formed on two parallel plates of the capacitor, as a result the total charge of the plates will be neutral. But by the separation of charges, a potential difference will be created, consequently the capacitor will not conduct electricity. Charging current of a capacitor is the flow of electrons to the metal conductive plates. The flow of electrons stops only when the voltage across the plates becomes equal to the applied voltage.

Many types of capacitors are available in the market. Among them the parallel plate capacitor is the simplest form, consisting of two metalized plates which are parallel to each other. The capacitance of the

capacitor depends on the surface area of the plates and the distance between the plates. The energy of the electron is stored as the electrical charge. Thus, the area of the plates is directly related to the capacitance value. As the area increases more and more electrons can store energy. Whereas the distance between the plates is inversely proportional to the capacitor performance for a given voltage.

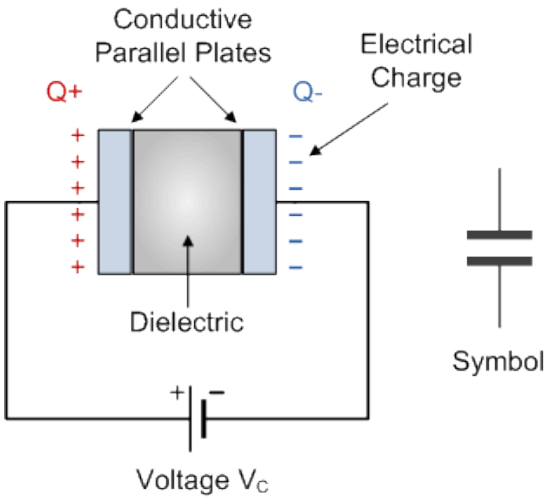

Figure1.21: Schematic representation of the capacitor

The equation for the capacitance of a parallel plate capacitor is given as:

$$C=\varepsilon*\frac{A}{d}$$

where ε represents the absolute permittivity of the dielectric material being used. The permittivity of a vacuum, ε_o has the value of $8.84x10^{-12}$ Farads per metre. A is the conductive plate area, d is the distance between the plates.

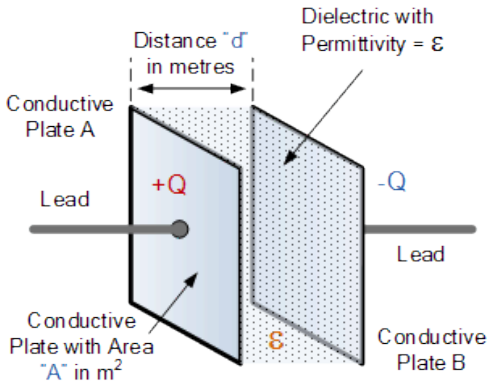

Figure 1.22 Representation of parallel plate capacitor.

Usually the conductive plates of the capacitor are separated by an insulating material. Apart from the area and the distance between the plates, another factor determining the capacitance of a capacitor is the permittivity of the insulating medium. Polymer composites are good choice for the use of insulating material inside a capacitor. Materials possessing high dielectric constant can store more energy and it can serve as a good insulating medium. Hence this kind of materials have a great potential in power energy storage applications. Polymer materials with embedded high K nanoparticle fillers have replaced the conventional polymer composites with excellent characteristics [143-147]. Moreover, nano materials are preferred over the bulk materials, because they can form thinner dielectric films with higher capacitance density [148-149].

1.8 Scope and objectives of the work

The current work involves development of conducting polymer composites based on conducting fibers and non-conducting fibers. Accordingly conducting carbon nanofiber and non-conducting cellulose fiber were selected. Cellulose was isolated from coir fibers by the

modification of a known method. The isolated cellulose was refined into three different sizes- macro, micro and nano sizes. The isolated fibers were characterized by different techniques all of which supported uniform fibrillation and the size distribution in the successive ranges. Polyaniline was coated on the surface of cellulose and carbon nanofibers by the in-situ polymerization of aniline in acid medium. The properties of polyaniline greatly depend on the nature of the dopant used, monomer to oxidant ratio, purity of monomer, polymerization time and temperature etc. But among the variable conditions, the nature of the dopant used for the synthesis plays critical role.

PVA and PMMA based composites were prepared by the solution casting method. Polyaniline modified cellulose and carbon nanofiber are incorporated separately in to both PVA and PMMA polymer matrices. The electrical, dielectric, thermal and mechanical properties of the as prepared composites were studied in detail. Significant improvement in the properties was observed for PVA based composites than that of PMMA composites. Characterization of the composites suggested that this improvement is due to the extensive hydrogen bonding present in PVA composites. The properties of the composite were related to the evenness of the fibrous fillers distributed in the polymer matrix. CNF/PANI composites yielded higher electrical and dielectric properties owing to the π-π interaction between the π orbitals of CNF and the quinoid rings of PANI. PANI/Cellulose composites exhibited low conductivity and dielectric properties than PANI/CNF composites. Among three different sizes of cellulose fibres excellent electric and dielectric properties were obtained for nanocomposites with low

percolation threshold. It can be due to the effective conductive network formed in case of nanocomposite. As the aspect ratio of the filler becomes high, fiber–fiber contact increases which results in effective network formation at lower filler concentrations.

The relatively inferior properties of PMMA/Cellulose composite were thought to be due to the weak interaction between the hydrophilic cellulose and the hydrophobic PMMA. The compatibility of cellulose and PMMA was improved by the addition of Bis–(3-triethoxysilylpropyl)tetrasulphide (Si69). Drastic increase of mechanical properties was observed for silane coupled composite than PMMA/Cellulose composite. The composites were characterized and found that the interactions in PMMA/Cellulose/Si69 composite were mainly chemical in nature. The result proved that Si69 is compactable to both PMMA and cellulose and can be used as an effective coupling agent for PMMA/Cellulose system.

Excellent dielectric properties and electrical conductivity of the composites lead us to explore the EMI shielding property of the composites. The advancement in the communication technology lead increased radiation pollution. Consequently, there is an urge to protect the environment as well as the sensitive circuits from microwave radiations. PANI/CNF/PVA composite exhibited good EMI shielding with very low thickness.

The redox properties of polyaniline have opened up new avenues in biological field, such as immobilization platform for tissue growth, biosensors, controlled drug delivery systems and neural probes etc. The antibacterial activity of polyaniline has significant effect on hydrophilicity, molecular weight and the electrostatic attraction between PANI and bacteria.

The dopant molecule is one of the key factors that affects these properties. In view of growing importance to antibacterial drugs I have studied the effect of dopant on the antibacterial properties of PANI/CNF/PMMA nanocomposite.

Carbon nanofibers are source of electrical conductivity, improves EMI shielding and mechanical properties of the composite. In addition, it can act as good flame retardant. Hence the flame retardant properties of polyaniline coated carbon nanofibers in PVA and PMMA matrices were studied. Large amounts of hydroxyl groups available in PVA make it a self-charring material and the charring can be improved further by proper compounding. Therefore, LOI values of PANI/CNF/PVA and PANI/CNF/PMMA nanocomposites were evaluated for investigating their flame retardant property. Both composites exhibited higher LOI values than pure polymers and increased with increasing PANI/CNF content. The flame retardant efficiency of PVA composite was significantly higher than PMMA composite. The high flame retardancy of PANI/CNF/PVA composite is due to the good dispersion of PANI/CNF in PVA matrix and the high surface area of the carbon nanofibers. The improvement is also ascribed to the synergistic effect of polyaniline and carbon nanofiber in self-charring PVA matrix.

Number of studies have indicated that poly(vinyl alcohol) is sensitive to moisture and can interact with water molecules through hydrogen bonding. Moreover, it is an eco-friendly polymer. By the absorption of water molecules, it swells. Humidity sensing has become essential for weather prediction, historic preservation, environmental

studies and mobile electronics etc. At the same time, it is crucial to detect and measure the accurate amount of the toxic polluted gases like ammonia to evade the major health issues in the near future. Our challenge was to develop humidity and gas sensor using the same material with good sensitivity, stability and response. PVA is water absorbing material, the absorbing capacity was improved by the incorporation of PANI/CNF or PANI/Cellulose in to the matrix. The absorbed water molecules bring variation in AC capacitance. When polyaniline is exposed to ammonia gas, protonation/deprotonation reactions take place resulting in changes in the electrical resistance. The difference in the sensing performance was studied by the incorporation of carbon nanofiber and nanofibrillated cellulose (NFC). It is worth noticing that the properties of the composite were changed by the incorporation of different nanofibers. The addition of CNF resulted better sensing properties.

The composites with high dielectric constant materials opened up many applications in the area of high charge storage capacitors, gate dielectrics, electroactive materials etc. PANI/CNF/PVA composite exhibited high dielectric constant with low dielectric loss. Hence it can be used as insulating material in parallel plate capacitors. Combination of conducting polymers with carbonaceous materials have developed as effective combination for the fabrication of efficient charge storage capacitors. The variation of capacitance and dissipation factor was measured against frequency. Very high capacitance with low dissipation factor was obtained for the thin film capacitor.

Specific Objectives

- To develop conducting thin films and composites based on non-conducting polymeric matrices and conducting fillers.
- To study the electrical, dielectric, thermal and mechanical properties of the composites developed.
- To study the potential of the conducting composites prepared as anti-bacterial and fire-retardant material.
- To develop thin, easily foldable materials with enhanced EMI shieling applications.
- To design devices for sensing humidity and ammonia.

References

[1] M. Narkis, M. Zilberman, A. Siegmann, Polym Adv Technol 1997, 8, 525

[2] R. M. Scarisbrick, J Phys D: Appl Phys 1973, 6, 2098

[3] E. Frydman, UK Patent 1948, 604695, 8

[4] T. Fujitani Osaka, K. Matsuoka Tondabayashi US4258100, 1981

[5] R. H. Norman Conductive rubbers and plastics. Elsevier Publishing Company Limited, Amsterdam, 1970, 224

[6] A. Y. Xiao, Q. K. Tong, A. C. Savoca, H. Van Oosten IEEE Trans Compon Pack Technol 2001, 24, 445

[7] S. K. De, J. R. White Short fibre-polymer composites. Woodhead Publishing Limited, Cambridge England, 1996, 182 , ISBN 978-1-85573-220-9

[8] X. Wang, D. D. L. Chung Sensor Actuator A 1998, 71, 208

[9] L. Flandin, Y. Brechet, J. Y. Cavaille Compos Sci Technol. 2001, 61, 895

[10] R. H. Norman Conductive rubbers and plastics. Elsevier Publishing Company Limited, Amsterdam, 1970, 3

[11] S. Sivakkumar, R. Saraswathi, J. Power Sources, 2004, 137, 322

[12] Y.-H. Huang, J. B. Goodenough, Chem. Mater., 2008, 20, 7237

[13] L. Shao, J.-W. Jeon, J. L. Lutkenhaus, Chem. Mater.,2011, 24, 181

[14] Y. E. Miao, W. Fan, D. Chen, T. Liu, ACS Appl. Mater. Interfaces, 2013, 5, 4423

[15] G. Liu, S. Xun, N. Vukmirovic, X. Song, P. Olalde-Velasco, H. Zheng, V. S. Battaglia, L. Wang, W. Yang, Adv.Mater., 2011, 23, 4679.

[16] W. Brutting, Physics of organic semiconductors, KGaA, Weinheim, Wiley-VCH Verlag GmBH &Co, 2005

[17] T. A. Skotheim, Handbook of conducting polymers, CRC Press, 1998

[18] Y. G. Wang, H. Q. Li, Y. Y. Xia, Adv. Mater. 2006, 18, 2619

[19] Z. F. Li, H. Zhang, Q. Liu, L. Sun, L. Stanciu, J. Xie, ACS Appl. Mater. Interfaces 2013, 5, 2685

[20] A. Pron, P. Rannou, Prog. Polym. Sci. 2002, 27, 135

[21] S. Srivastavaa, S. S. Sharmaa, S. Agarwala, S. Kumara, M. Singha, Y. K. Vijaya, Synth. Met. 2010, 160, 529

[22] E. Kang, K. Neoh, K. Tan, Prog.polym.Sci. 1998, 23, 277

[23] F. Lux, polymer, 1994, 35, 2915

[24] W. K. Maser, Mater. Sci. Eng. 2003, 23, 87

[25] S. Bhadra, D. Khastgir, N. K. Sinha, J. H. Lee Prog. Polym. Sci. 2009, 34, 783

[26] M. Ertas, R. M. Walczak, R. K. Das, A. G. Rinzler, J. R. Reynolds, Chem. Mater. 2012, 24, 433

[27] D. W. Wang, F. Li, J. P. Zhao, W. C. Ren, Z. G. Chen, J. Tan, Z. S. Wu, I. Gentle, G. Q. Lu, H. M. Cheng, ACS Nano 2009, 3, 1745

[28] E. Frackowiak, V. Khomenko, K. Jurewicz, K. Lota, F. Beguin, J. Power Sources 2006, 153, 413

[29] K. Zhang, L. L. Zhang, X. S. Zhao, J. Wu, Chem. Mater. 2010, 22, 1392

[30] Q. Cheng, J. Tang, J. Ma, H. Zhang, N. Shinya, L. C. Qin, J. Phys. Chem. C 2011, 115, 23584

[31] R. Sengupta, M. Bhattacharya, A. K. Bhowmick, Prog. Polym. Sci. 2011, 36, 638

[32] N. Roy, R. Sengupta, A. K. Bhowmick, Prog. Polym. Sci. 2012, 37, 781

[33] Y. K. Choi, K. Sugimoto, S. M. Song, Y. Ohkoshi, Endo, M. Carbon 2005, 43, 2199

[34] J. Jang, J. Bae, M. Choi, S. H. Yoon, Carbon 2005, 43, 2730

[35] M. S. Dresselhaus, G. Dresselhaus, K. Sugihara, I. L. Spain, H. A. Goldberg: Graphite Fiber and Filaments (Springer, Berlin Heidelberg 1988)

[36] A. Oberlin, M. Endo, T. Koyama, J. Cryst. Growth 1976, 32, 335

[37] R. T. K. Baker, Carbon 1989, 27, 315

[38] G.G. Tibbetts, J. Cryst. Growth 1984, 66, 632

[39] N. M. Rodriguez, J. Mater. Res. 1993, 8, 3233

[40] N. M. Rodriguez, A. Chambers, R. T. K. Baker, Langmuir 1995,11, 3862

[41] M. Endo, Y. A. Kim, T. Fukai, T. Hayashi, K. Oshida, M. Terrones, T. Yanagisawa, S. Higaki, M. S. Dresselhaus, Appl. Phys. Lett. 2002, 80, 1267

[42] S. H. Yoon, C. W. Park, H. J. Yang, Y. Korai, I. Mochida, R. T. K. Baker, N. M. Rodriguez, Carbon 2004,

[43] S. H. Yoon, S. Lim, Y. Song, Y. Ota, W. M. Qiao, A. Tanaka, I. Mochida, Carbon 2004, 42, 1723, ISBN 978-3-642-20595-8.

[44] Y. A. Kim, T. Hayashi, M. Endo, M. S. Dresselhaus, Carbon nanofibers. In: R. Vajtai (Ed.), Springer handbook of nanomaterials Berlin: Springer, 2013, 1500

[45] K. B. K. Teo, C. Singh, W. I. Milne, Catalytic synthesis of carbon nanotubes and nanofibers. In: H. S. Nalwa (Ed.), Encyclopedia of nanoscience and nanotechnology, Stevenson Ranch, CA, USA: American Scientific Publishers, 2003, 665

[46] M. Ge, K. Sattler, Observation of fullerene cones. Chem. Phys. Lett. 1994, 220, 192

[47] K. P. De Jong, J. W. Geus, Catal. Rev. 2000, 42, 481

[48] Y. A. Kim, T. Hayashi, M. Endo, M. S. Dresselhaus, Carbon nanofibers. In Springer Handbook of Nanomaterials; Vajtai, R., Ed.; Springer: Berlin/Heidelberg, Germany, 2013; 233, ISBN 978-3-642-20594-1

[49] H. Terrones, T. Hayashi, M. Muñoz-Navia, M. Terrones, Y. A. Kim, N. Grobert, Chemical Physics Letters, 2001, 343, 241

[50] C. Y. Wei, D. Srivastava, Applied Physics Letters, 2004, 85, 2208

[51] J. Gu, F. Sansoz, Carbon, 2014, 66, 523

[52] A. V. Melechko, V. I. Merkulov, T. E. McKnight, M. A. Guillorn, K. L. Klein, D. H. Lowndes, Journal of Applied Physics, 2005, 97, 041301

[53] L. Li, J. Li, C. M. Lukehart, Sens. Actuators B Chem. 2008, 130, 783

[54] J. Jang, J. Bae, Sens. Actuators B Chem. 2007, 122, 7

[55] G. Jia, H. Wang, L. Yan, X. Wang, R. Pie, T. Yan, Y. Zhao, X. Guo, Environmental Science and Technology 2005, 39, 1378

[56] L. Dong, A. Henderson, C. Field, Journal of Nanotechnology, 2012, 1, 2012

[57] S. Liu, L. Wei, L. Hao, N. Fang, M. W. Chang, R. Xu, Y. Yang, Y. Chen, ACS Nano 2009, 3, 3891

[58] L. M. Costa, G. M. Olyveira, B. M. Cherian, A. L. Leao, S. F. Souza, M. Ferreira Indus.Crops Prod, 2013, 41, 198.

[59] H. A. Silverio, W. P. Flauzino Neto, N. O. Dantas, D. Pasquini, Indus. Crops Prod, 2013, 44, 427

[60] W. P. Neto, H. A. Silverio, N. O. Dantas, D. Pasquinia, Indus.Crops Prod, 2013, 42, 480

[61] D. Dai, M. Fan, P. Collins, Indus. Crops Prod, 2013, 44, 192

[62] N. Johar, I. A. Ahmad, Indus. Crops Prod, 2012, 37, 93

[63] Y. Fan, T. Saito, A. Polymer, 2009, 77, 832

[64] J. I. M. AlVera A. Alvarez, V. P. C. Analia Vazquez, Cellulose, 2008 15, 149

[65] J. C. Cintil, M. Lovely, Sabu Thomas, Reviews on Advanced Material Science, 2014, 37, 20

[66] F.W. Herrick, R. L Casebier, J. K. Hamilton, Journal of Applied Polymer Science, Applied polymer Symposium,1983, 37, 797

[67] A. F. Turbak, F. W. Snyder, K. R Sandberg, Journal of Applied Polymer Science, 1983, 37, 815

[68] H. P. S. Abdul Khalil, Y. Davoudpour, Md. Nazrul Islam, M. Asniza, K. Sudesh, Rudi Dungani, M. Jawaid, Carbohydrate Polymers, 2014, 99, 649

[69] N. F. Adriana, M. P. Denis, D. Dan, U. P. B. Scientific Bulletin, Series B, 2011, 2, 73

[70] C. Merlini, G. M. O. Barra, D. P. Schmitz, S. D. A. S. Ramoa, A. Silveira, T. M. Araujo, A. Pegoretti, Polymer Testing 2014, 38,18

[71] P. Barber, S. Balasubramanian, Y. Anguchamy, S. Gong, A. Wibowo, H. Gao, H. J. Ploehn, H. C. Z. Loye, Materials, 2009, 2, 1697

[72] M. T. Razzak, D. Darwis, S. Zainuddin, Radiat. Phys. Chem. 2001, 62, 107

[73] K. Qiu, A. N. Netravali, J. Polym. Environ. 2013, 21, 658

[74] K. Qiu, A. N. Netravali, Compos. Sci. Technol.2012, 72, 1588

[75] K. Qiu, A. N Netravali, Polym. Compos. 2013, 34, 799

[76] M. T. Albdiry, B. F. Yousif, Mater. Des. 2013, 48, 68

[77] N. A. Peppas, E. W. Merrill, J. Biomed. Mater. Res.1977,11, 423

[78] C. C. Demerlis, D. R. Schoneker, Food Chem. Toxicol. 2003, 41, 319

[79] J. A. Brydson, Plastics Materials, Butterworths, 1999, 398

[80] R. C. Chen Chuanfu, F. Xi, Chinese Journal of Polymer Science. 1995, 13, 91

[81] J. E. Mark, Physical Properties of Polymers Handbook, 2nd ed.; Springer: NY, 2007, 3, ISBN 978-0-387-69002-5.

[82] K. Goto, M. Hashimoto, H. Takadama, J. Tamura, S. Fujibayashiand K. Kawanabe, J. Mater. Sci. Mater. Med. 2008, 19, 1009

[83] A. Boger, A. Bisig, M. Bohner, P. Heini and E. Schneider, J. Biomater. Sci. Polym. Ed. 2008, 19 ,1125

[84] Z. M. Li, Carbon 2005, 43, 2397

[85] B. Marrs, R. Andrews, T. Rantell, D. Pienkowski, J. Biomed. Mater. Res. 2006, 77A, 269

[86] Z. M. Dang, J. K. Yuan, J. W. Zha, T. Zhou, S. T. Li, G. H. Hu, Prog. Mater. Sci. 2012, 57, 660

[87] J. N. Coleman, U. Khan, Y. K. Gun'ko, Adv. Mater. 2006, 18, 689

[88] C. Talens, M. Castro-Giraldez, P. J. Fito, LWT-Food Sci. Technol. 2016, 66, 622

[89] N. G. Mc Crum, B. E. Read, G. Williams Anelastic and dielectric effects in polymeric solids. Wiley, New York: Dover, 1967.

[90] P. Avakian, H. W. Starkweather Jr., W. G. Kampert. In: Cheng SZG, editor, Dielectric analysis of polymers, Handbook of thermal analysis and calorimetry, New York: Elsevier, 2002, 3, 147

[91] C. G. Koops, Phys Rev. 1951,83, 121

[92] J. R. Ellis. In: Skotheim TA, editor. Handbook of conducting polymers, New York; Marcel Dekker Inc, 1986, 1, 489

[93] O. Hashimoto, Technologies & Applications of Wave Absorber II, CMC, Tokyo, 2003

[94] Y. Naito, K. Suetake, IEEE Trans Microwave Theory Tech. 1971, 19, 65

[95] O. Hashimoto, Introduction to Wave Absorber, Morikita Publication, Tokyo, 1997.

[96] D. Y. Kim, Y. C. Chung, T. W. Kang, H. C. Kim, IEEE Trans. Magn. 1996, 32, 555

[97] M. Matsumoto, Y. Miyata, J. Magn. Soc. Jpn. 1998, 22, 885

[98] Y. Naito, Electromagnetic Wave Absorber, Ohmsha, Tokyo, 1987

[99] A. Saito, M. Ogawa, K. Tsutsui, H. Endo, S. Yahagi, Mater. Jpn. 1999, 38, 46

[100] S. Yoshida, M. Sato, E. Sugawara, Y. Shimada, J. Appl. Phys. 1999, 85, 4636

[101] T. Maeda, S. Sugimoto, T. Kagotani, D. Book, K. Inomata, H. Ota, Y. Houjou, Mater. Trans. JIM 2001, 42, 446

[102] Y. Duan, S. Liu, Bin Wen, H. Guan, G. Wang, Journal of Composite Materials, 2006, 40, 1841

[103] F. Roselena, M. Inacio Martin, P. Marco-A De, C. R. Mirabel, Journal of Applied Polymer Science, 2001, 83, 1568

[104] H. Rmili, J. L. Miane, H. Zangar and T. E. olinga, Eur. Phys. J Appl. Phys., 2005, 29, 65

[105] J. L. N. Violette, D. R. J. White, M. F. Violette. Electromagnetic compatibility handbook. New York, NY: Van Nostrand Reinhold Company, 1987, ISBN 978-94-017-7144-3.

[106] C. W. Lou, Y. C. Yang, C. M. Lin, Adv Mater Res, 2011, 239, 1994

[107] R. P Clayton. Introduction to electromagnetic compatibility. New Jersey: John Wiley & Sons, Inc., 1992,633

[108] M. S. Han, Y. K. Lee, H. S. Lee, C. H Yun, W. N Kim, Chem. Eng. Sci., (in press).

[109] C. R. Paul. Electromagnetics for Engineers, Wiley, Hoboken, NJ. 2004.

[110] H. W. Ott. Noise Reduction Techniques in Electronic Systems, 2nd ed New York: John Wiley & Sons. 1988

[111] R. B. Schulz, V. C Plantz, D. R. Brush. IEEE Trans Electromagn Compat EMC. 1988, 30, 187

[112] S. A. Schelkunoff, Electromagnetic Waves, Van Nostrand, NJ. 1943.

[113] B. Reddy, InTech, 2011

[114] X. C. Tong, CRC Press, 2008

[115] K. Y. Park, S. E. Lee, C. G. Kim, J. H. Han, Compos. Struct. 2007, 81,401

[116] Y. Huang, N. Li, Y. Ma, F. Du, F. Li, X. He, X. Lin, H. Gao, Y. Chen, Carbon 2007, 45, 1614

[117] J. S. Im, J. G. Kim, Y. S. Lee, Carbon 2009, 47, 2640

[118] C. Olga, C. Marta, P. Aida, M. Olga, Rio de Janeiro 2001, 96, 583

[119] T. Kashiwagi, F. Du, K.I. Winey, K.M. Groth, J.R. Shields, S.P. Bellayer, Polymer, 2005, 46, 471-481

[120] T. Kashiwagi, F. Du, J. F. Douglas, K. I. Winey, R. H. Harris, J. R. Shields, Nat Mater, 2005,4, 928

[121] B. H. Cipiriano, T. Kashiwagi, S. R. Raghavan, Y. Yang, E. A. Grulke, K. Yamamoto, Polymer, 2007, 48, 6086

[122] T. Kashiwagi, M. Mu, K. Winey, B. Cipriano, S. R. Raghavan, S. Pack, Polymer, 2008, 49, 4358

[123] A. B. Morgan, W. D. Liu, Fire Mater, 2011, 35, 43

[124] C. Nylabder, M. Armgrath, Proceedings of the International Meeting on Chemical sensors, Fukuoka, Japan, 1983, 203

[125] C. Nylander, M. Armgarth, Proc. Int. Meet. Chem. Sens. 1983, 203

[126] H. J. Sharma, D. V. Jamkar, S. B. Kondawar, Proc. Mater. Sci. 2015, 10, 186

[127] C. Steffens, M.L. Corazza, E. Franceschi, F. Castilhos, P.S. Herrmann, J.V. Oliveira, Sens. Actuators B 2012, 171, 627

[128] H. Xu, D. Ju, W. Li, H. Gong, J. Zhang, J. Wang, B. Cao, Sens. Actuators B 2016, 224, 654

[129] M. T. S. Chani, K. S. Karimov, F. A. Khalid, Solid State Sci. 2013, 18, 78

[130] W. Xuan, X. He, J. Chen, W. Wang, X. Wang, Y. Xu, et al., Nanoscale 2015, 7, 7430

[131] Y. Sakai, Y. Sadaoka, M. Matsuguchi, Sens. Actuators B 1996, 35, 85.

[132] Y. Sakai, Y. Sadaoka, M. Matsuguchi, Y. Kanakura, M. J. Tamura, Electrochem. Soc. 1991, 138, 2474.

[133] E. Traversa, Sens. Actuators B 1995, 23, 135 http://www.iceweb.com.au/ Analyzer/humidity_sensors.html (2005)

[134] Y. Sakai, Y. Sadaoka, M. Matsuguchi, Sens. Actuators B 1996, 35,85

[135] L. G. Wade, Jr., Organic Chemistry, Prentice Hall, NJ, 2001

[136] S. Tsuchitani, T. Sugawara, N. Kinjo, S. Ohara, Sens. Actuators 1988, 15, 378

[137] K. L. Rauen, D. A. Smith, W. R. Heineman, Sens. Actuators B 1993, 17, 61

[138] M. S. Gong, J. S. Park, M. H. Lee, H. W. Rhee, Sens. Actuators B 2002, 86, 160

[139] K. Ogura, H. Shiigi, M. Nakayama, J. Electrochem. Soc. 1996 ,143, 292

[140] C. W. Lee, H. W. Rhee, M. S. Gong, Synth. Metals 1999, 106, 177

[141] M. Yang, Y. Li, X. Zhan, M. Ling, J. Appl. Polym. Sci. 1999, 74, 2010

[142] N. R. R. Royan, A. B. Sulong, J. Sahari, and H. Suherman, Journal of Nanomaterials, 2013, 2013, 717459.

[143] D. G. D. Mauro, A. I. Grimaldi, V. L. Ferrara, Journal of Sensors, 2009, 2009, 7032060

[144] L. Zhang, J. Zhu, W. Zhou, J. Wang, and Y. Wang, Energy, 2012, 39, 294

[145] H. Cong, M. Radosz, B. F. Towler, Y. Shen, Separation and Purification Technology, 2007, 55, 281

[146] L. W. Tang, H. Y. Chien, T. S. Yeong, C. Y. An, W. J. Li, C. Z. Hua, European Polymer Journal, 2011, 46, 634

[147] M. F. Frechette, M. L. Trudeau, H. D. Alamdari, S. Boily, IEEE Transactions on Dielectrics and Electrical Insulation, 2004, 11, 808

[148] J. Lu, K. S. Moon, B.-K. Kim, C. P. Wong, Polymer, 2007, 48, 1510

.....ൠ.....

Chapter 2

MATERIALS AND EXPERIMENTAL METHODS

Contents

This chapter deals with the materials used, preparation of composites and the characterization techniques adopted in the present investigations.

2.1 Materials

Poly(methyl methacrylate)

Thermoplastic Poly(methyl methacrylate) (PMMA), was supplied by Plaskolite West (Compton, CA, USA).

Grade	PERSPEXVR CP-61
Density	1.18 g/cm^3
The specific gravity	1.12

Poly(vinyl alcohol)

Poly(vinyl alcohol) (hot) was obtained from Research lab fine chem. Industries.

Molecular weight	17000 g/mol

Carbon nanofibers

Carbon nanofiber of 95% purity was purchased from Pyrograf Products, Inc., USA.

Grade	Pyrograf III PR 19
N_2 Surface area	20-30 m^2/g
Diameter	70-90 nm
Length	30-50 μm.

2.2 Chemicals

Aniline

Aniline was obtained from Electrochem private Ltd., Mumbai. It was double-distilled before use.

Ammonium peroxodisulphate

Ammonium peroxodisulphate (APS) was obtained from S.D. Fine Chem, Mumbai, India

Molecular weight	228.2 g/mol

Sodium hydroxide

Sodium hydroxide was supplied by Nice Chemicals Ltd., Mumbai.

Molecular weight	40 g/mol

Sodium chlorite

Assay	80 %

Sodium chlorite was obtained from Loba chemicals.

Silane coupling agent (Si 69)

The coupling agent, TESPT used was Si 69, obtained from B. P. Chemicals, Mumbai.

Calcium chloride

Calcium chloride was obtained from Merck Specialties Private Ltd., Mumbai, India.

Molecular weight	110.98 g/mol

Camphor sulphonic acid

Camphor sulphonic acid was procured from Merck Specialties Pvt. Ltd., Mumbai, India.

Toluene sulphonic acid

Toluene sulphonic acid was procured from Merck Specialties Pvt. Ltd., Mumbai, India.

Hydrochloric acid

Hydrochloric acid was obtained from Merck Specialities Pvt. Ltd., Mumbai.

Glacial Acetic acid

Assay	≥ 99.0 %
Non-volatile substances	≤ 0.01 %

Acetic acid was supplied by Merck Specialities Pvt. Ltd., Mumbai.

Sulphuric acid

Assay (H_2SO_4)	95-98 %
Residue on ignition	≤ 0.005 %

Sulphuric acid was supplied by Merck Specialities Pvt. Ltd., Mumbai.

Phosphoric acid

Assay (H_3PO_4)	95-98 %
Molecular weight	93.13
Boiling point	182-185 ^oC

Phosphoric acid was supplied by Spectrochem Pvt. Ltd., Mumbai.

Ammonia gas

Ammonia gas (1%) was procured from Baruka gas Pvt. Ltd. Bangalore, India.

Bacterial cultures

Bacterial cultures were purchased from Microbial Type Culture Collection (MTCC) and gene bank, Institute for Microbial Technology, Chandigarh, India. Microbial culture media ingredients such as peptone, yeast extract, NaCl, agar and potato dextrose agar were obtained from Himedia Laboratories Pvt. Ltd.

2.3 Experimental methods

2.3.1 Preparation of test specimen

The PMMA/Cellulose/Si69 composites were injection moulded in DSM Explore, Micro 12 cc injection moulding machine at 190 °C for 8 minutes, to prepare test samples for impact, tensile, and flexural testing according to the relevant ASTM standards. The samples were moulded at identical conditions and the properties were taken as the average of five samples.

Figure 2.1: DSM Micro 12 cc Injection moulding machine

2.4 Characterization techniques

A detailed account of the characterization techniques employed in elucidating the various sample properties is being portrayed.

2.4.1 Morphology studies

The morphology and microstructure of the samples were investigated using the following microscopic techniques.

2.4.1.1 Scanning Electron Microscopy (SEM)

Scanning electron microscopy is very powerful technique to get information about the topography, morphology and the structural information of the materials. In this technique the electrons are thermionically emitted from tungsten or lanthanum hexaboride cathode. The emitted electrons are accelerated towards the anode. These focussed beam of high energy electrons are scanned across the specimen and can generate a variety of signals at the surface. It consists of secondary electrons of low energy, back scattered electrons of high energy, diffracted back scattered electrons and X-rays. The signals are monitored by detectors and magnified.

SEM observations of the samples reported in the present study were examined using a JEOL Model JSM.6390 LV scanning electron microscope. Prior to analysis, the samples were mounted on a metallic stub and an ultrathin coating of electrically conducting material was deposited by vacuum sputter coating. It is used to prevent the accumulation of static electric fields at the specimen due to the electron irradiation during imaging. The samples were gold coated before the analysis to make it

conductive. A major advantage of SEM is that bulk samples can also be directly studied.

2.4.1.2 Field Emission Scanning Electron Microscopy (FESEM)

The structure of nanocellulose was studied using Hitachi SU6600 Variable Pressure Field Emission Scanning Electron Microscope (FESEM). It is a better tool for imaging compared to conventional SEM. In this technique a field emission gun provides very narrow probing with high and low energies. It can provide improved special resolution, slight sample damage and charging. An accelerating voltage of 20 kV was used in the microscope.

2.4.1.3 High Resolution Transmission Electron Microscopy (HRTEM)

Direct imaging of individual nanoparticles with high resolution is made possible using transmission electron microscopy. It uses a beam of electrons accelerated with high voltage. When these electrons are allowed to pass through thin materials, it get scattered. So, the thickness of the material should be less than 200 nm. The sample can be magnified about 100-100,000 times. It can provide more useful information about the crystalline materials than the amorphous samples. TEM analysis was performed for carbonaceous materials using JEOL 300 KV HRTEM microscope with an accelerating voltage of 200 kV. The topographic information obtained by TEM in the vicinity of atomic resolution can be utilized for structural characterization and identification of various phases of mesoporous materials, *viz*., hexagonal, cubic or lamellar [1].

2.4.2 Spectroscopy

2.4.2.1 Raman Spectroscopy

Raman spectroscopic measurements of the samples were carried out on Bruker RFS27 R spectrometer using Nd: YAG laser with a 100 mW operating at 1064 nm in the range of 200-3000 cm^{-1}.

Raman spectroscopy measures the vibrational modes of a material like infrared spectroscopy. Raman spectroscopy is based on the scattered light whereas the infrared spectroscopy measures the absorption of photons. Raman spectroscopy is one of the most powerful technique for the analysis and identification of molecular structure. The G band, located near 1600 cm^{-1}, could be used to determine the orientation of the carbonaceous materials in a composite by measuring the Raman spectra at angles 0-90 º. It also helps to determine the type of the material whether metallic or semiconducting. If the material is semiconducting, the peak around 1600 cm^{-1} will be broad and it becomes narrower when it is metallic [2]. The presence of D band near the 1300 cm^{-1} is due to the defects within the graphitic structure. The intensity of the peak is directly related to the defects present in the structure. High intense D band indicates more defective structure and low intense band shows that the structure is further perfect.

2.4.2.2 Fourier Transform Infrared Spectroscopy (FTIR)

Infrared spectroscopy is the common form of vibrational spectroscopy and it depends on the excitation vibrations of molecules by the absorption of photons. Absorption of an infrared photon occurs only if the dipole moment changes during the vibration. The intensity of the absorption

peak is proportional to the change in the dipole moment. A variety of IR techniques have been used to attain information on the surface chemistry of different solids. IR spectroscopy exploits the fact that molecules have specific frequencies at which they rotate or vibrate corresponding to discrete energy levels. FTIR aims at determining the molecular structure by detecting the characteristic vibrational frequencies of molecules. The infrared radiation is allowed to pass through the material, then some of the radiation will get absorbed and some will get transmitted. All molecules have specific frequencies at which they rotate or vibrate corresponding to discrete energy levels. As the different functional groups absorb at their unique characteristic frequencies, the resulting spectrum representing the molecular absorption and transmission, is the molecular fingerprint of the sample [3].

Fourier transform infrared spectra of the samples were recorded on Thermo Nicolet, Avatar 370 model.

2.4.2.3 Ultra Violet - Visible (UV–Vis) Spectroscopy

The absorption of light by a material in the ultraviolet (l0 - 420 nm) and visible region (420-700 nm) is measured by a spectrometer. The absorption of the light in this region is solely dependent on the nature of the functional groups present in the molecules. When a molecule is exposed to light energy which matches the energy difference between the possible electronic transition within the molecule. Hence a fraction of light energy will be absorbed by the molecule and it will be excited to the higher energy orbital. There can be various possible transitions which are σ-σ*, n-σ*, π-π* and n-π* depending on the sample under analysis.

Among these transitions n-π* transition requires minimum energy; hence it occurs at longer wavelengths. A spectrometer records the degree of absorption by the material at different wavelengths and the resulting plot of absorbance versus wavelength is known as a spectrum. The significant features of the spectrum are λ_{max} and ε_{max}. Where the λ_{max} is the wavelength at which maximum abortion taking place, and ε_{max} is the intensity of maximum absorption. By analysing the UV-Vis absorption spectra of materials, it is possible to estimate the absorption coefficient α, direct and indirect band-gap energies and the density of states.

2.4.2.4 Solid state Nuclear Magnetic Resonance Spectroscopy

Nuclear magnetic resonance spectroscopy provides information on the interaction of nucleus with an external field. The chemical shift is measured relative to the reference compound and it is expressed in hertz or ppm. The interaction of nuclear spins with externally applied magnetic fields is described as spin Hamiltonian H.

$$H = HZ + HCS + HQ + HD + HJ \quad \text{.....2.1}$$

where *HZ* is a Hamiltonian, which describes the interaction of the nuclear spin with the external field *Bo* (Zeeman Interaction). The chemical shift Hamiltonian *HCS* gives information on the local environment of a nucleus. The chemical shift is measured relative to that of a reference compound (TMS in case of 29Si NMR) and is expressed in Hertz or in ppm with respect to the resonance frequency of the reference compound. *HQ* describes the quadrupolar interaction of the nucleus with the surrounding electric field gradient. *HD* describes the dipolar interaction

with other nuclei, while *HJ* describes the interaction with other nuclei through *J*-coupling.

Magic angle spinning (MAS) NMR spectra for ^{29}Si and ^{13}C nuclei were recorded on BRUKER DSX300 spectrometer at 7.05T (resonance frequencies 59.595 MHz, rotor rate 10000 Hz, external reference of $Si(OCH_3)_4$ and 75.43 MHz, rotor rate 10000 Hz). Chemical and structural information is obtainable from the high-resolution NMR spectroscopy [4-6]. Moreover, Magic Angle Spinning solid state NMR technique allows high spectral resolution as that of liquids [7].

2.4.2.5 Mass Spectrometry (MS)

Mass spectrometer characterizes substances by identifying and measuring the intensity of molecular fragment ions of different mass-to-charge ratio (m/z). The incoming gas molecules are first ionized by the ion source. The positive molecular ion and fragment ions formed are then separated according to their m/z value by a combination of magnetic and electrostatic fields. A mass spectrum is recorded by scanning the field strength so that ions of increasing m/z ratio arrive at the detector. The combination of mass spectrometer with thermogravimetric analyser provides information about the nature of gaseous reaction products formed in TGA. TGA-MS gives the key idea of mass ions and fragments. It is possible to analyse each segment individually for further understanding of the material composition. In TGA coupled gas analysers, a part of the gas evolved from the sample is sucked into the mass spectrometer. The sensitivity of the sample is very high, hence only about 1 % effluent gas is needed.

The composites were analysed by TGA coupled mass spectrometer. The evolved gas during heating was analysed by MKS Cirrus 2 instrument, which was connected to Q50 thermogravimetric analyser, TA instrument.

2.4.2.6 X-ray Photoelectron Spectroscopy (XPS)

X-ray Photoelectron Spectroscopy (XPS), also known as Electron Spectroscopy for Chemical Analysis (ESCA), is an analysis technique used to obtain chemical information about the surfaces of solid materials. The sample is placed in an ultrahigh vacuum environment and exposed to a low-energy, monochromatic x-ray source. When x-ray is incident on the sample, the core level electrons get ejected. The energy of the photoemitted core electron is characteristic of the binding energy and the element from which it was emitted. Energy analysis of the emitted photoelectrons is the primary data used for XPS. The ejection of core electron from the sample reasons an outer electron fills the core hole. The energy of this transition is balanced by the emission of an Auger electron or a characteristic x-ray. Analysis of Auger electrons can be used in XPS, in addition to emitted photoelectrons. The photoelectrons and Auger electrons emitted from the sample are detected by an electron energy analyser and their energy is determined as a function of their velocity entering the detector. By counting the number of photoelectrons and Auger electrons as a function of their energy, a spectrum representing the surface composition is obtained. The energy corresponding to each peak is characteristic of an element present in the sampled volume. The area under a peak in the spectrum is a measure of the relative amount of the

element represented by that peak. The peak shape and precise position indicates the chemical state for the element.

2.4.3 X-ray diffraction analysis (XRD)

X-ray diffraction (XRD) is a powerful non-destructive technique to provide more in-depth information about crystalline compounds. It provides information on crystal structure, phase, preferred crystal orientation (texture), and other structural parameters, including identification and quantification of crystalline phases. X-ray diffraction peaks are formed by constructive interference of a monochromatic beam of X-rays diffracted at specific angles from each set of lattice planes in a sample. The diffracted x-rays are detected, processed and counted [8]. For an incident ray, at an angle θ, according to Bragg's equation, path difference is given by,

$$n\lambda = 2d \sin \theta \quad \text{.....2.2}$$

Where, n is an integer, d is the distance between atomic layers in the crystal, λ is the wavelength, and θ is the angle of incidence.

The peak intensities are determined by the distribution of atoms within the lattice. The X-ray powder diffraction measurement was performed using a Bruker D2 phaser X-ray Powder Diffractometer equipped with Cu Kα radiation. The diffraction intensities of the samples were recorded for a range of 5-80 °(2θ). The crystallite size was calculated by using the Scherrer equation,

$$L_{h,k,l} = K\lambda/b\cos\theta \quad \text{.....2.3}$$

where, K = 0.94.

2.4.4 Brunauer-Emmett -Teller (BET) surface area analysis

The specific surface area, total pore volume and average pore diameter of the samples were measured by N_2 adsorption-desorption methods using a Autosorb 1C Quantachrome USA. Prior to analysis the samples were activated at 150 °C for 4 h under vacuum and then the adsorption-desorption was conducted by passing nitrogen into the sample. The BET method was used to calculate the total surface area at relative pressures of P/Po = 0.65–0.45 and to determine the total pore volume and average pore diameter at a relative pressure of P/Po = 0.99.

The BET equation can be represented as:

$$p/V(po-p) = 1/cVm + [(c-1)/cVm]\,(p/po) \quad \ldots\ldots 2.4$$

where p is adsorption equilibrium pressure, po is saturation vapor pressure of the adsorbate at the experimental temperature, V is volume of N_2 adsorbed at pressure p, Vm is volume of adsorbate required for monolayer coverage and c, a constant that is related to the heat of adsorption and liquefaction [9]. Numerous computational methods are available to calculate the pore size distribution of mesoporous sample. Among them Barrett-Joyner-Halenda (BJH) model is the most popular model, which is applied here to the adsorption branch of isotherm.

2.4.5 Dynamic Light Scattering (DLS)

The particle size of cellulose and polyaniline coated carbon nanofibers were determined by Microtrac Nanotrac wave using dynamic light scattering (DLS) method. This technique is also known as Photon Correlation Spectroscopy (PCS). Particle size was calculated by measuring the changes

in the intensity of light scattered from the mixture. The sample is irradiated by a laser beam and photon detector detects the fluctuations of scattered light at a known scattering angle θ by a fast photon detector. For particle size distribution, the water suspended nanofibril particles were diluted appropriately and analysed.

2.4.6 Zeta potential measurement

Zeta potential was measured using Zetasizer 2000 system (Malvern Instruments Ltd., Worcestershire, UK). The instrument was equipped with a photon correlation spectroscopic system. Zeta potential is the potential difference across the phase boundaries between the solid and liquid. Zeta potential analysis indicates the extend of electrochemical equilibrium on interfaces. It is dependent on the nature of both liquid and on the properties of the surface. It plays an important role in the theory of aggregative stability-DLVO theory [10,11]. Higher zeta potential value indicates higher stability of the system. The presence of surface charge develops an electrostatic filed which can affect the ions in the bulk of the liquid.

The measurement of zeta potential involves the determination of the rate at which the charged particle moves in response to an electric field. The particles having a particular zeta potential moves to the opposite charged electrode. The rate of movement is proportional to the value of zeta potential. The speed is measured by the Laser Doppler Anemometer.

2.4.7 DC conductivity measurements

DC conductivity of the composites were measured by a standard two-probe electrode using a Keithley 2400 source-measure unit in dry air at ambient temperature. The circle shaped sample was kept in between two copper electrodes and the resistance of the sample was directly read out from the instrument. Knowing the thickness and area of the sample, the conductivity was measured using the equation

$$\sigma = \frac{1}{R} * \frac{L}{A} \quad \text{.....2.5}$$

where L is the thickness of the material, R is the resistance and A is the cross-sectional area of the sample.

Temperature variation of DC conductivity was measured using standard four probe methods employing Keithley as per the standard procedure ASTM F 43-99. The powdered samples were compressed into pellets of 13 mm diameter and about 1-2 mm thick disk using a hydraulic press operated at a pressure of 200 MPa. To understand the stability of the sample at higher temperatures, the pelleted samples were subjected to heating. The temperature was increased from 30 ^{o}C to 110 ^{o}C. The DC conductivity variation was measured at every 5 ^{o}C intervals.

2.4.8 Dielectric properties

2.4.8.1 Impedance Analyser

The dielectric properties of the samples were measured out at frequencies ranging from 40 Hz to 30 MHz using an impedance analyser, Agilent E 4980 A Precision LCR Meter. Disc shaped samples having

diameter of 10 mm were used for the measurements. The sample was placed in between two parallel metallic plates. The field between the plates passes through the material, hence the material is polarized.

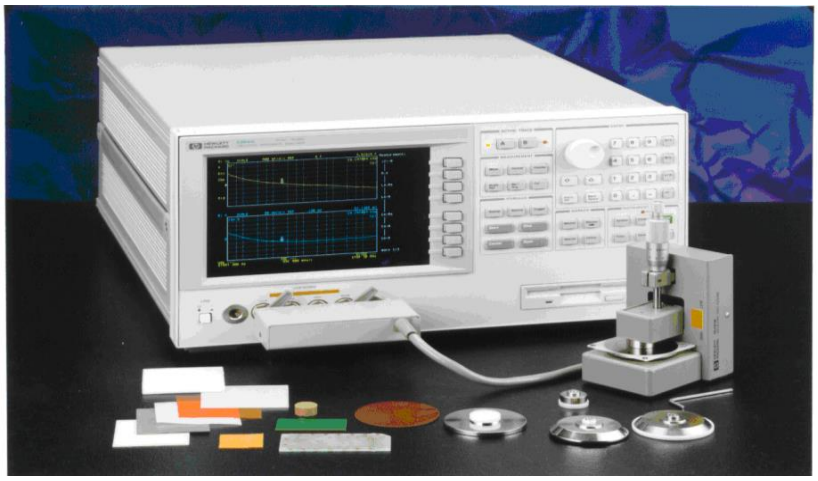

Figure 2.2: Impedance analyser and parallel plate capacitor fixture set up

The capacitance of a sample parallel plate capacitor is given by

$$C=\varepsilon A/d \quad \text{.....2.6}$$

Where A is the area of the plates, d is the separation between the plates and ε is the permittivity of the medium. When a parallel plate capacitor with a dielectric in between is charged, then the capacitance, *C* is given by

$$C= \varepsilon_o \varepsilon_r A/d \quad \text{.....2.7}$$

Where, ε_o is the permittivity of free space and ε_r is the dielectric constant of the material between the plates. Permittivity is calculated knowing the area of the plate and the thickness of sample.

$$\varepsilon_r = C\, d/\varepsilon_o A \quad \text{.....2.7}$$

In most analyzers the calculation is automated, making this a convenient technique for accurately measuring the permittivity of sheet materials at low frequencies. The extend of polarization is measured as dielectric constant of the material. Permittivity is a physical quantity that describes the ability of a material to store energy or it is the materials ability to permit an electric field. The energy can be exchanged between the field and the material in a lossless manner. So, this stored energy can be represented as the permittivity of the medium. On the other hand, energy may be permanently lost from the electric field and it can be absorbed by the material in the form of heat. This energy loss is represented as imaginary part of permittivity.

2.4.8.2 Impedance analyser for capacitance measurement

Figure 2.3: Wayne Kerr 6510B impedance analyser

The Wayne Kerr 6510B Precision Impedance Analyzer provides precise and fast testing of devices at frequencies up to 10 MHz. The accuracy of the instrument is ±0.05 %. The accuracy and versatility make the precision analysers the ideal choice for many different tasks and applications including passive component design, dielectric material characterisation and manufacturing test.

2.4.9 Measurement of microwave properties

The microwave properties of the conducting composites were studied using ZVB20 vector network analyser. The microwave characteristics were measured in the X band frequency region (8-12 GHz). The image of the cavity resonator is shown in the figure 2.5. The cavity resonators are constructed using brass or copper wave-guides. The inner walls of each cavity were silvered to reduce the wall losses. Both the resonators were of transmission type. The dimensions of the X band waveguide are 34.5 cm ×7.2 cm ×3.4 cm.

Figure 2.4: Vector network analyser

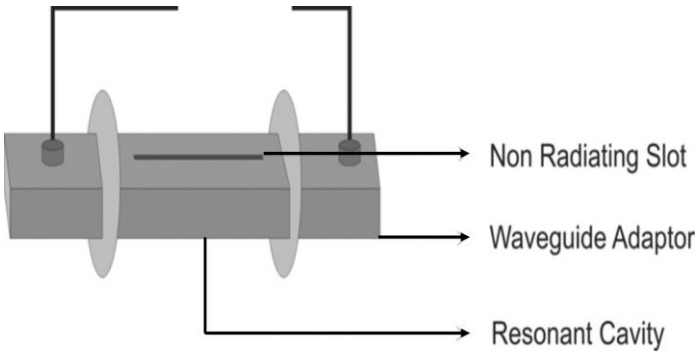

Figure 2.5: X band wave guide cavity resonator

2.4.9.1 Theory of microwave

The introduction of a dielectric material into resonance cavity produces a field. The field perturbation due to the presence of a material is given by Kupfer et al. [12].

$$-(d\Omega/\Omega) = \frac{[(\varepsilon*-1)\int E.E0*dV]}{2\int_{Vc} |E0|2\ dV} \quad \text{.....2.8}$$

where dΩ is the complex frequency shift; V_c and V_s are the volumes of the cavity and the sample, respectively. E and E0 are the perturbed and unperturbed fields in the cavity, respectively; and ε* is the relative complex permittivity of the sample material.

$$\varepsilon^* = \varepsilon' - j\varepsilon'' \quad \text{.....2.9}$$

here ε' is the real part of permittivity and ε" is the imaginary part.

Complex frequency shift is associated to the quality factor by the equation

$$(d\Omega/\Omega) \approx (dw/w) + j/2\ [(1/Q_s)-(1/Q_0)] \quad \text{.....2.10}$$

Q_s is the quality factor of the cavity with the sample material and Q_0 is the quality factor without sample.

Quality factor Q can be calculated from the resonant frequency f.

$$Q=f/\Delta f \quad \text{.....2.11}$$

Where Δf is the corresponding 3 dB band width of resonant frequency. Assuming that $E=E_0$

$$E0 = E_{omax} \sin(\Pi x/a) \sin(\Pi pz/d),\ p = 1, 2, 3 \text{ etc} \quad \text{.....2.12}$$

E_{omax} is the peak value of E0, 'a' is the broader dimension and 'd' is the length of the wave guide resonator.

From the equations 2.8 and 2.10 the real and imaginary permittivity can be calculated as

$$\varepsilon' = 1 + \frac{(f0 - fs)Vc}{2fs\ Vs} \quad \text{.....2.13}$$

$$\varepsilon'' = \left(\frac{Vc}{4Vs}\right)\left[\frac{(Q0 - Qs)}{Q0Qs}\right] \quad \text{.....2.14}$$

The heating efficiency can be compared by means of a heating coefficient: J, which is defined as [13,14]

$$J = \frac{1}{\varepsilon' \tan\delta} \quad \text{.....2.15}$$

The absorption of electromagnetic waves when it passes through the medium is given by the absorption coefficient (αf), is defined as

$$\alpha_f = \frac{\varepsilon'' f}{nc} \quad \text{.....2.16}$$

where $n = (\varepsilon'^2 + \varepsilon''^2)^{1/2}$ and c is the velocity of light

The skin depth of a material can be calculated from the absorption coefficient. It is the inverse of absorption coefficient and can be defined as the effective distance of penetration of an electromagnetic wave into the material. The penetration depth of a material can be expressed as

$$\delta_f = \frac{1}{\alpha f} \quad \text{.....2.17}$$

2.4.9.2 Method of measurement

Initially the resonance frequency f_0 and the quality factor Q_0 of the cavity in the unperturbed condition was measured. Then the rectangular shape sample was inserted into the cavity and positioned at the maximum electric field. Resonance frequency fs and the quality factor with sample is measured. Knowing the frequency and quality factor with and without sample, the permittivity was calculated.

By the application of a dielectric material in to the cavity, the resonance frequencies of the cavity are perturbed at the position of maximum electric filed. At the position of maximum electric field, the contribution from the magnetic field is minimum [15,16]. By the insertion of a sample into the cavity, the overall geometric configuration of electromagnetic field is changed. Hence by measuring the perturbation of the sample, the dielectric constant, dielectric loss, penetration depth, heating coefficient and AC conductivity can be determined.

2.4.10 Electromagnetic interference shielding

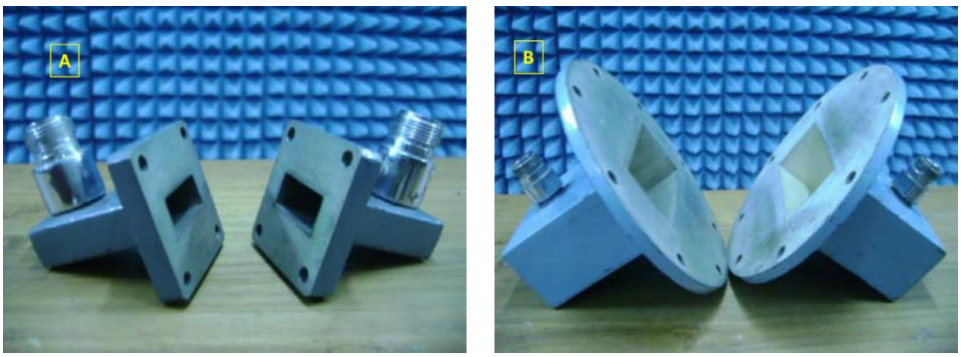

Figure 2.6: (a) X band wave-guide (b) S band wave-guide

EMI shielding measurements were carried out in S (2-4 GHz) band and X (8-12 GHz) band frequencies using wave-guides coupled to a ZVB20 vector network analyser. The wave-guides were of dimensions 2.3 cm× 1 cm× 13.5 cm for X band and 7.2 cm× 3.4 cm× 35.2 cm for S band. The images of both X and S band wave guides are shown in the figure 2.5. The two test port cables of the vector network analyser are connected to the wave guides via co-axial adapters. The sample was placed between two sections of the wave guide and the transmission loss was determined. It gives the shielding efficiency of the material. The rectangular samples of 0.5-0.09 mm thickness were inserted into rectangular sample holder which matches the internal dimensions of X-band and S-band waveguides. Scatter parameters (S-parameters), were used to calculate shielding parameters in a two-port EMI shielding setup. The S parameters are represented as S_{xy}. The first number in the suffix refers to the port where the output was measured and the second number refers to where the signal originated from. Hence S11 is the reflected signal and S21 is the transmitted signal. Hence it can be defined as

$|S_{11}|$: Reflected voltage magnitude divided by the incident voltage magnitude in port 1

$|S_{12}|$: Transmitted voltage magnitude from port 2 to port 1 divided by incident voltage magnitude in port 2

Shielding efficiency of the sample can be calculated from S21. Knowing reflectivity (R) and transmissivity (T), absorptivity (A) can be calculated using the relation

$$A=1-T-R \quad \text{.....2.18}$$

2.4.11 Mechanical properties

2.4.11.1 Tensile Analysis

Tensile properties of the composites were studied using a Shimadzu Universal Testing Machine (model AG-I) with a load cell of 10 kN capacity according to ASTM D638. The rectangular shape samples were used for thin films, whereas the specimens were dump bell shaped for injection moulded samples. The gauge length between the jaws was adjusted to 40 mm before the measurements. All the measurements were carried out at a cross speed of 50 mm/min at room temperature. A minimum of four samples were tested and the average value was reported.

The ability of a material to resist breaking under tensile stress is an important property of elastomers. The force per unit area needed to break the material is known as tensile strength. Tensile modulus gives the ratio of stress to elastic strain in tension. The elongation at break is the percentage increase in length that occurs before it breaks under tension. The materials possessing high tensile strength and elongation are applicable to many areas.

2.4.11.2 Flexural properties

The flexural test determines the force needed to bend a beam under three-point loading conditions. Flexural modulus gives an indication about the stiffness of the material. Flexural properties were determined by three-point loading system employing UTM (Shimadzu AG-1) with a load cell capacity according to ASTM D 79. The flexural properties were measured using rectangular shaped samples at a crosshead speed of 5mm/min. A minimum of four samples were tested for each composite and the average results were recorded.

The flexural strength is given by

$$S = 3PL/2bd^2 \quad \text{.....2.19}$$

Where S = f1exural strength, P = maximum load at the moment of break, b = width of the specimen, L= length of the span and d = the thickness of the specimen.

The flexural modulus was calculated from the slope of initial portion of the flexural stress strain curve.

2.4.11.3 Impact strength

The impact strength is the measure of the ability of a material to absorb shock and impact energy without undergoing breaking. The impact strength is calculated as the ratio of impact absorption to test specimen cross-section. The area under the stress-strain curve is directly related to the material toughness. More the impact strength of the material, more will be the toughness and vice versa.

Impact strength was measured using unnotched samples according to ASTM D 4812-99 on a Ceast Resil Impact analyser (Junior) using a hammer of 4 J at a striking rate of 3.96 m/s. The sample was placed vertically at the base of the instrument. A pendulum swings on its track and strikes the sample. The energy lost as the pendulum continuous on its path is measured from the distance of follow through. The impact energy is directly read from the machine.

Impact strength = Impact energy (J)/Thickness (m)……2.20

2.4.11.4 Dynamic Mechanical Analysis (DMA)

Dynamic mechanical analysis measures the mechanical properties of materials as function of time, temperature and frequency. It works by applying a sinusoidal deformation to samples of known geometry. The samples are subjected to either controlled stress or controlled strain, as a result it undergoes certain amount of deformation. DMA measures stiffness and damping of the material and these are expressed as modulus and tan δ. The dynamic mechanical thermal analysis was conducted with a dual cantilever clamp on a dynamic mechanical analyser (Model Q 800, TA instruments) using rectangular test specimens of 60 mm, 4 mm and 2 mm. The tests were carried out by temperature sweep (temperature ramp from 40 °C to 120 °C at 3 °C/min) method at a constant frequency of 1 Hz to get the dynamic storage modulus and loss modulus of the samples. Tan δ was calculated as the ratio of loss modulus to storage modulus.

Storage modulus of a material represents the amount of stored energy in the system, the loss modulus measures the energy dissipated as heat. The storage modulus represents the elastic part while the loss modulus represents the viscous portion. For viscoelastic materials, the modulus is a complex quantity.

$E^* = E' + I\,E''$ 2.21

E' = storage modulus corresponding to the elastic response and it is a measure of stiffness

E" = loss modulus corresponding to the plastic response it is measure of dissipation of energy as heat

E"/E'= tan δ, used for the determination of glass transition temperature.

2.4.12 Thermal properties

2.4.12.1 Thermogravimetric analysis (TGA)

Thermogravimetric analysis is a type of thermal analytical technique in which weight change of a material is monitored as a function of temperature or as a function of time. This method is used to understand the changes in physical and chemical properties of a material with controlled change in temperature or time in a controlled atmosphere. The sample placed in a high precision balance called thermo balance which is kept inside an electrically heated furnace. Results are displayed by plotting mass change versus temperature or time and are known as thermo gravimetric curves.

Thermogravimetric analysis of samples was performed on Q50 thermogravimetric analyser, TA instrument. 5-8 mg of samples were heated with programmed heating rate of 20 ^{o}C/min from room temperature to 700 ^{o}C under nitrogen, air and oxygen atmospheres.

2.4.12.2 Differential Scanning Calorimetry (DSC)

DSC is a thermo analytical technique in which the difference in the amount of heat required to increase the temperature of a sample and reference is measured as a function of temperature. This method is adopted to study the thermal transitions. The increase of temperature will be different for sample and the reference material. Usually this technique is used to study the thermal transitions like phase changes, crystallization, melting, glass transitions of a material as a function of temperature [17]. If the sample is undergoing any chemical transitions, it may yield or release heat compared to the reference material to maintain both sample

and reference at the same temperature. The quantity of heat flow to the material depends on the process whether it is exothermic or endothermic. The heat flow to the material is measured as a function of time or temperature. The materials, as they undergo changes in chemical and physical properties, which are detected by transducers, which changes into electrical signals that are collected and analysed to give thermograms. The melting and crystallization parameter, such as melting point (Tm), heat of fusion (ΔHf), temperature of crystallization (Tc) and hat of crystallization (ΔHc) were used for the comparison of composites.

DSC measurements were carried out using Mettler Toledo DSC 822 instrument. Tests were performed under air, oxygen and nitrogen atmospheres at a flow rate of 20 mL/min. The heating was done room temperature to 300 °C and at a heating rate of 7 °C/min and followed by cooling at 10 °C/min.

2.4.13 Limiting oxygen index

The limiting oxygen index (LOI) or oxygen index (OI) is a method for evaluating the relative flammability of polymeric compounds. LOI is the minimum concentration of oxygen in an oxygen–nitrogen atmosphere which is required to support the burning of a vertically mounted specimen. The oxygen index was usually expressed as

$$\text{Oxygen index} = \frac{[O2]}{[O2]+[N2]} * 100 \quad \text{.....2.22}$$

This method is used for quality assurance purposes and indicates the flammability of a material. Material with high LOI value that is greater

than 21 indicates less flammability of the sample. The flame retardancy of all the composites was evaluated by the test of LOI using an oxygen index instrument (Dynisco, Alpha Technologies, USA) following ASTM D 2863. The photograph of the experimental setup for the LOI analysis is given below.

Figure 2.7: Set up for LOI measurement

2.4.14 Water absorption measurement

The water absorption measurement was performed for PVA based composites. The moisture sensitivity of the samples was measured according to the standard ASTM D 570 – 98. The disc shaped specimens were used and it was immersed in a sealed bath of distilled water (100 % humidity) at room temperature to study the effects of fibre treatments on the water uptake of composites. All the samples were placed in the oven at 60 °C for 24 h before the water immersion. The samples were immersed in

the sealed water bath for long period to reach the equilibrium. The initial weight of the sample was recorded and the amount of water absorption was analysed by weighing the sample at certain time intervals (30 min). When the samples were taken out from water at certain time interval, the wet surface of the sample was quickly dried and weighted. The percentage of water absorption was calculated using the following equation [18]

$$Mt\ (\%) = \frac{wt - wo}{wo} * 100 \quad \text{.....2.23}$$

Wt. is the weight of the sample at time t, Wo is the initial weight of the sample.

References

[1] J. M. Thomas, O. Terasaki, P. L. Gai, W. Zhou, J. Gonzalez-Calbet, Acc. Chem.Res. 2001, 34, 583

[2] C. A. Cooper, R. J. Young, M. Halsall, Composites Part A, 2001, 32, 401

[3] Banwell, McCash, Fundamentals of Molecular Spectroscopy, Tata McGraw Hill Publishing Company Ltd., 4th edn., New Delhi,1995.

[4] G. Engelhardt, D. Michel, John Wiley and Sons Ltd., Chichester, 1987

[5] A. Fyfe, G. C. Gobbi, J. Klinowski, J. M. Thomas, S. Ramdas, Nature 1982, 296, 530

[6] G. Engelhardt in: Handbook of Heterogeneous Catalysis, Vol. 2, Eds: G. Ertl, H.Knozinger, J. Weitkamp, Wiley-VCH, Weinheim, 1997, 525

[7] M. Mehring, High Resolution NMR Spectroscopy in Solids, Springer-Verlag,Berlin, 1976

[8] B. D. Cullity, S. R. Stock, Elements of X-ray Diffraction, Prentice Hall, New Jersey, 2001.

[9] S. Brunauer, P. H. Emmett, E. Teller, J. Am. Chem. Soc. 1938, 60, 309.

[10] E. J. W. Verwey, J. Th. G. Overbeek, Elsevier 1948

[11] B. V. Derjaguin, L. Landau, Acta Phys. Chim, USSR, 1941, 14, 733

[12] K. Kupfer, A. Kraszewski, R. Knoochel, In Sensors Update, Wiley- VCH, Germany, 2000, 186

[13] C. C. Ku, R. Liepins, Hansen Publishers, Munich, 1987, 92

[14] T.A. Ezquerra, F. Kremmer, Wegner, Progress in electromagnetic research Elsevier, New York, 1992, 6

[15] B. Meng, J. Booske, R. Cooper, IEEE Transactions on Microwave Theory and Techniques. 1995,437

[16] M. Santra, K. U. Limaye, IEEE Transactions on Microwave Theory and Techniques. 2005, 53.

[17] P. W. Zhu, G. P. Zhang, J. Y. Yu, G. Dai, Journal of Applied Polymer Science, 2004, 91,431

[18] J. K. Kim, C. Hu, R. Woo, M. L. Sham, Compos. Sci. Technol., 2005, 65, 805

.....ꕥ.....

Chapter 3

EFFECT OF DOPANT ON THE PROPERTIES OF PANI/CNF COMPOSITES

Contents

Electrically conducting nanocomposites of polyaniline with carbon based fibers were synthesized using five different dopant acids. The morphological, electrical, dielectric and thermal properties of pure PANI and PANI/CNF composites were studied. The composites were characterized by X-ray diffraction, FTIR spectroscopy, BET surface area analysis, DLS measurements, SEM and TEM microscopic techniques. Scanning electron micrographs and surface area analysis showed that phosphoric acid doped composite had the smallest average size and highest surface area among other four composites. High electrical and dielectric properties were obtained for all PANI/CNF composites. Higher conductivity and thermal stability of DC conductivity were obtained for toluene sulfonic acid doped composite. Further, thermogravimetric analysis showed good thermal stability for organic acid doped composites.

3.1 Introduction

Intrinsically conducting polymers find various applications in the field of electronics, electromechanical devices, electroluminescence and sensors [1,2]. Widely known intrinsically conducting polymers are polypyrrole, polyacetylene, polythiophene, polyaniline, polyparaphenylene, polyparaphenylene vinylene, and their derivatives [3]. Owing to the environmental stability, excellent conductivity and facile synthesis, polyaniline based composites have developed fast. The properties of polyaniline greatly depend on the nature of the dopant used, monomer to oxidant ratio, purity of monomer, polymerization time and temperature etc. [4,5]. But among the variable conditions, the nature of the dopant used for the synthesis plays critical role in determining the properties of PANI and its composites [6,7]. The use of doping molecules improves the conductivity as well as the solubility of PANI [8-11]. Generally, inorganic acids are used for the doping of polyaniline. But the resultant products are of low solubility in common solvents [12,13]. Some organic acids like camphor sulfonic acid (CSA), toluene sulfonic acid (TSA), naphthalene sulfonic acid (NSA) are also used as dopants. Sulfonic acid group present in these acids protonate aniline during the polymerization. Polyaniline can be tuned to either conducting or insulating form by controlling the doping and de-doping processes. Moreover, it can be made semiconducting or conducting form by controlling the quantity of the doping ion. Doping process creates defects like solitons, polarons and bipolarons in the polymer chains. Electron hoping is one mechanism by which the polymer is rendered conductive.

Recently researchers have developed composites of polyaniline with carbon fibers [14-16]. The π-bonds present in the carbon fibers facilitate extended charge transfer process between carbon fibers and polyaniline thereby increasing the conductivity. In this chapter carbon nanofiber and polyaniline are used to prepare conductive composite. The effect of dopant was studied keeping all other parameters similar. The polyaniline was synthesized by the in-situ polymerization of aniline in presence of five different doping agents. The dopants used are hydrochloric acid, sulfuric acid, phosphoric acid, camphor sulfonic acid and toluene sulfonic acid. The electrical, dielectric and thermal properties are also presented.

3.2 Experimental

3.2.1 In situ polymerization of aniline

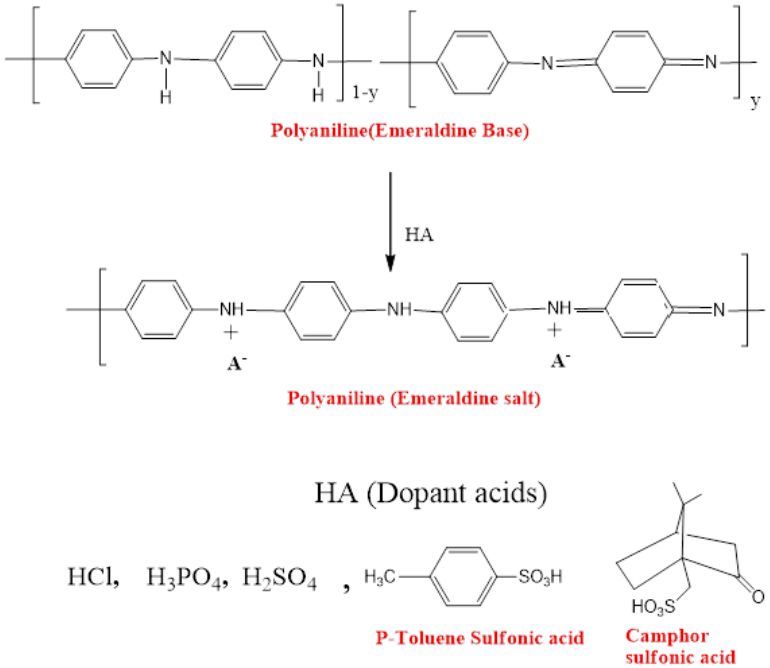

Figure 3.1: Schematic representation of synthesis of polyaniline by different dopants

5 g of aniline was dispersed in 100 mL of 1 M HCl by sonication for 1h. Then 6.25 g of ammonium persulfate dissolved in 100 mL 1 M HCl solution and it was slowly added in to the aniline/acid solution which is kept under constant magnetic stirring. The polymerization reaction was continued for 24 h at 0-4 ^{o}C. The product was filtered, washed repeatedly with distilled water and acetone, dried at 80 ^{o}C for 24 h. The monomer/oxidant ratio was kept as 1:1.5.

3.2.2 In situ polymerization of aniline/carbon nanofiber composite

PANI/CNF composites were prepared by the in situ oxidative polymerization of aniline in presence of dopant acid, APS and carbon nanofiber. 3 g of carbon nanofibers were dispersed in 1 M acid dopant by sonication for 2 h. 5 g of aniline monomers were added in to the cold solution of CNF in dopant acid. The solution was stirred for half an hour at 0-4 ^{o}C. The APS/acid solution was added slowly to the aniline/acid medium. Drop-wise addition was carried out using pipette over a period of 1.5 h. During this time, aniline oligomers were absorbed on to the CNF and the polymerization was continued on the fiber surface. It resulted in the uniform coating of polyaniline on the CNF surface. The reaction mixture was stirred for 4-5 h at low temperature. After that it was kept undisturbed for further growth. The formed polymer composite was vacuum filtered using distilled water and finally washed with acetone.

The graphitization of CNF takes place during its preparation at high temperatures. This results in the deposition of crystalline, pyrolytic carbon at the outer edges of CNF. Hence the outer surface of CNF is mostly unreactive. Therefore, the polyaniline will not undergo any chemical

reaction with CNF. Instead, the aniline oligomers will get absorbed on to the fiber surface and grow as the polymerization proceeds. Many reports are available in the literature regarding the uniform coating of PANI on various substrates [17,18].

3.3 Results and Discussion

3.3.1 Characterization of PANI/CNF composites

3.3.1.1 Scanning Electron Microscopy

PANI-HCl/CNF

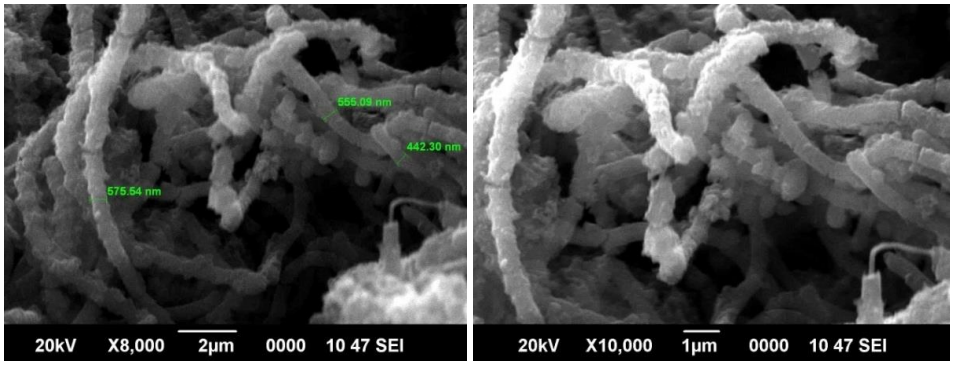

PANI-H_2SO_4/CNF

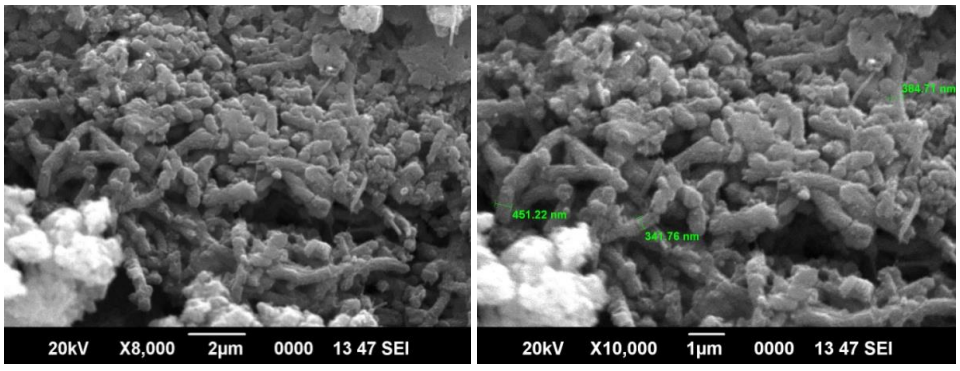

***Figure 3.2**: Continued….*

PANI-H_3PO_4/CNF

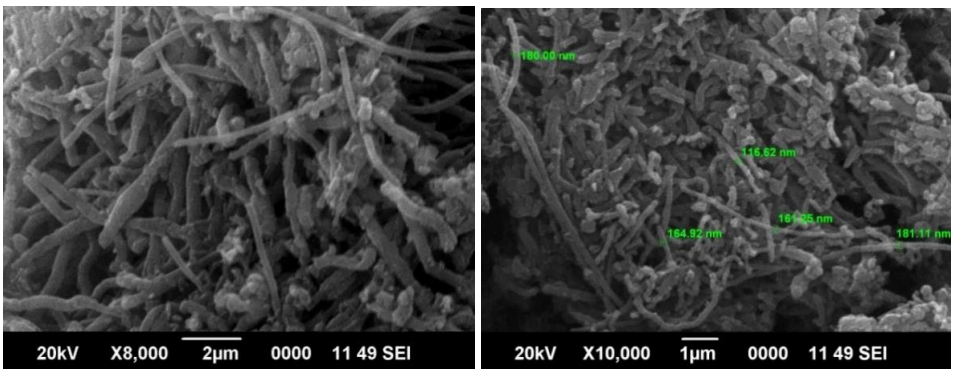

PANI-CSA/CNF

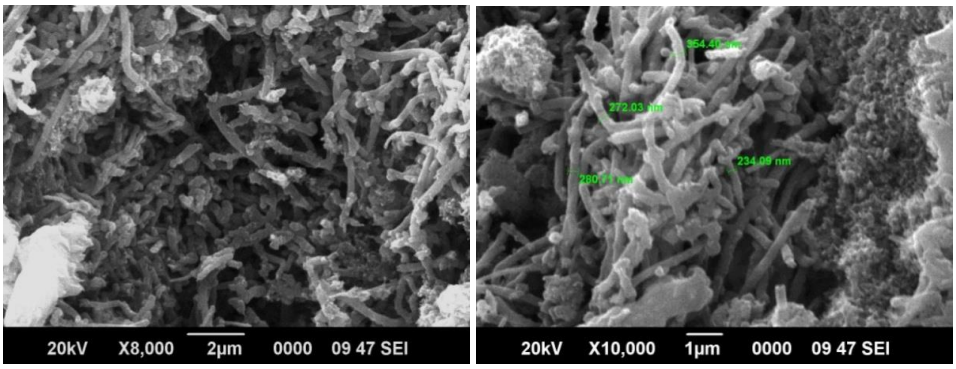

PANI-TSA/CNF

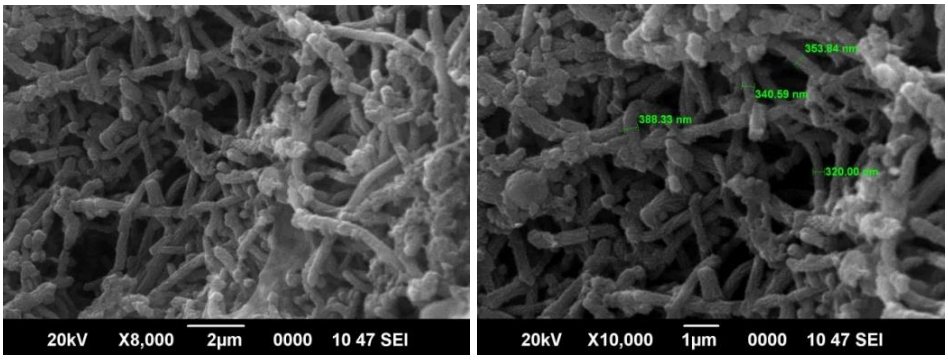

Figure 3.2: SEM micrographs of PANI/CNF composites

PANI/CNF composites are characterized by scanning electron microscopy. SEM images (Figure 3.2) reveal good coating of polyaniline on carbon nanofiber surface for all the composites. The diameter of CNF is about 90 nm. While the modification of CNF with polyaniline increases the diameter to an average of 340 nm. It provides a strong evidence for the coating of PANI on the surface of CNF. The degree of coating is different for various dopant molecules. Among different doping agents phosphoric acid doped PANI/CNF composite exhibits much lower diameter, approximately 152 nm, i.e. half of the diameter of other PANI/CNF composites.

3.3.1.2 DLS measurements

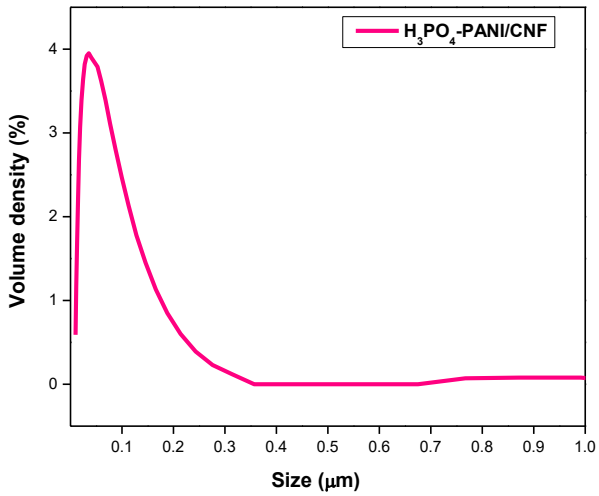

Figure 3.3: particle size distribution from DLS spectra

The particle size of phosphoric acid doped PANI/CNF composite is confirmed by the dynamic light scattering method by measuring the random changes in the intensity of light scattered. The particles were dispersed in DMSO solvent and the analysis was carried out at ambient

temperature. The size distribution of PANI/CNF particles is shown in the figure 3.3. The data reveals lower size compared to the size obtained from SEM micrographs. The DLS measurement shows that most of the particles fall in the range of 90-100 nm. This value is lesser than the value obtained from SEM images. An average diameter obtained from SEM micrographs is about 152 nm.

3.3.1.3 XRD analysis

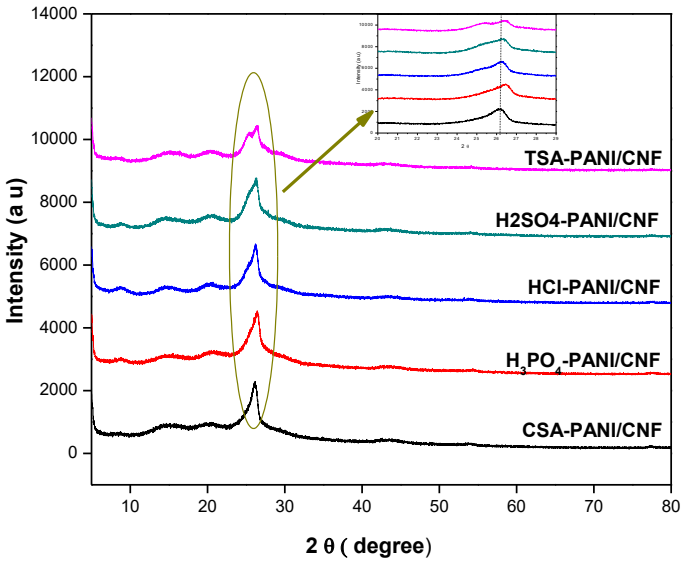

Figure 3.4: X-ray diffraction pattern of PANI/CNF composites

X-ray diffractograms of PANI/CNF composites are represented in figure 3.4. The characteristic peaks of both PANI and CNF are obtained. Broad diffraction peaks in between 2θ of 10° and 20° indicates the partial crystallinity of PANI structures. These peaks can be attributed to the periodicity of parallel and perpendicular rings of polyaniline chain. Since polyaniline chain is composed of repetitive quinoid and benzenoid rings it

results in low crystallinity of PANI chains. An intense peak centered on 26.4 ° is indicating the (002) graphitic plane of CNF in the composite.

The small peaks obtained at higher 2θ values represent (100), (101) and (004) planes of the CNF. The inset shows the zoomed version of the sharp peak. It shows that the peak is slightly shifted to lower 2θ values with respect to CNF. The crystallinity of CNF is retained regardless of the introduction of PANI. A marginal shift can be observed for the peak of CNF. The peak obtained for CSA-PANI/CNF, H_2SO_4-PANI /CNF, HCl-PANI/CNF, H_3PO_4-PANI/CNF, TSA- PANI/CNF composites are at 26.13 °, 26.25 °, 26.34 °, 26.39 ° and 26.34 ° respectively. Slight shift of the peak centered at 26.4 ° is observed. The peak is shifted to lower 2θ values with various dopants. The shift in the peak position implies that the dopants effect the ordering of the graphitic planes and hence the crystallinity.

Further, the d-spacing was calculated from the (002) peaks of CNF, CSA-PANI/CNF, H_2SO_4-PANI /CNF, HCl-PANI/CNF, H_3PO_4-PANI/CNF, TSA- PANI/CNF composites are respectively 3.37, 3.40, 3.39, 3.38 and 3.37 A^o. The increased d-spacing is related to the lower graphitic ordering of the samples, implying slight distortion in the CNF matrix [19,20].

3.3.1.4 FTIR spectroscopy

The FTIR spectra of PANI/CNF (figure 3.5) prepared using various dopants show peaks in the range 3400-3200 cm^{-1} corresponding to the N-H stretching vibrations. The C-H vibrations are observed at 2900 cm^{-1}.

The peaks around 1550-1600 cm^{-1} and 1390 cm^{-1} correspond to the signatures of PANI backbone stretching vibrations of quinoid and benzenoid rings [21,22]. The peaks at 1330 cm^{-1} are due to the strong aromatic C-N stretching vibrations present in polyaniline [23,24].

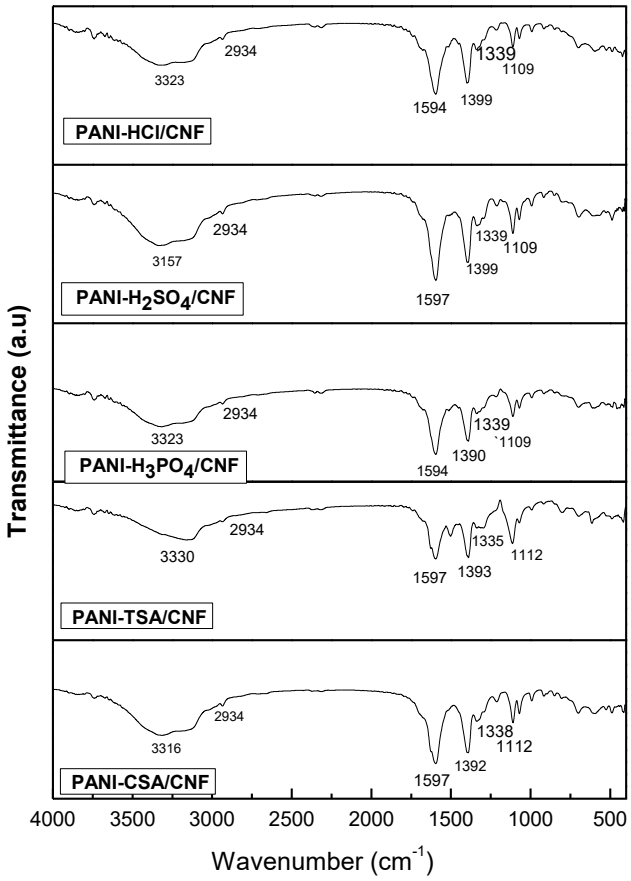

Figure 3.5: FTIR spectrum of PANI/CNF composites

Aromatic C-H in plane deformation leads to peak around 1110 cm^{-1}. 1,4-disubstituted aniline exhibits peaks due to the out of plane bending mode of aromatic C-H groups at around 800 cm^{-1} [25]. The stretching and bending vibrations present around 1600-500 cm^{-1} are slightly shifted upon the change in the dopant. It is due to the different anion present around the nitrogen atom of polyaniline. The interaction of dopant anion in polyaniline can be observed from the variation of N-H stretching frequency. The position of stretching band is very sensitive to the hydrogen bonding interaction and electron density variation which is based on the interaction between electron donor and acceptor molecules present in the composite. The oxidation degree of polyaniline is calculated from the relative intensity ratios of the quinoid and benzenoid rings. The ratio of intensity of the composites is in the range of 1-1.2, indicating the presence of more quinoid rings in the structure. Resonance stabilized hybrid orbitals of quinoid rings enables charge transport between the rings results in the high conductivity of the composites.

Table 3.1: Observed IR frequencies of the composites

Composite	C-H in plane (cm^{-1})	C-N Stretching (cm^{-1})	Benzenoid and Quinoid rings (cm^{-1})			C-H Stretching (cm^{-1})	N-H Stretching (cm^{-1})
PANI-HCl/CNF	1109	1339	1399	1514	1594	2934	3323
PANI-H_2SO_4/CNF	1112	1335	1399	1504	1594	2934	3157
PANI-H_3PO_4/CNF	1109	1339	1390	1514	1594	2934	3323
PANI-CSA/CNF	1112	1335	1393	1511	1597	2934	3316
PANI-TSA/CNF	1112	1338	1392	1511	1594	2934	3330

3.3.1.5 UV Vis Spectroscopy

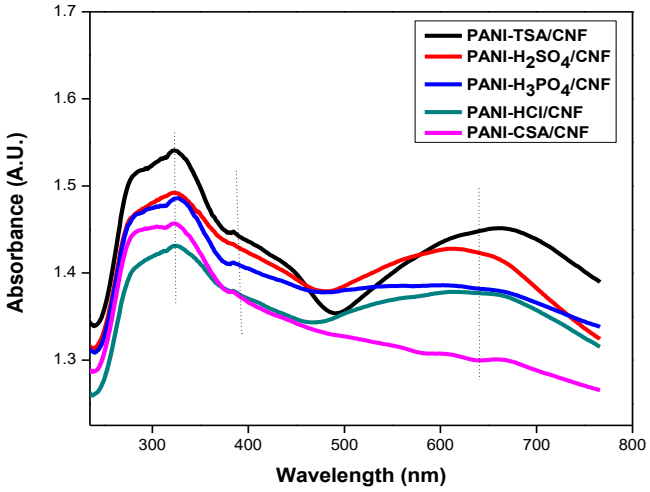

Figure 3.6: UV- Vis spectra of PANI/CNF composites

Figure 3.6 shows the UV-Vis absorption spectra of a series of acid doped PANI/CNF composites. Two prominent absoprtion peaks are obtained at 318 nm and a broad peak in the range of 600-700 nm. The peak in the vicinity of 322 nm can be assigned to the π-π^* transition of the benzene rings of the polyaniline backbone and the bands at 400 nm and 640 nm indicate the polaron-π^* transition and π-polaron transiton respectively [26-28]. The peak at 322 nm is slighty shifted to higher wavelengths for organic acid doped composties than the mineral acids. This can be attributed to the extended conjugation between CNF and PANI. Hence these systems need comparatively lower energy for π-π^* transitions. The band at 640 nm is red shifted for TSA doped PANI/CNF composite. Accordingly TSA-PANI/CNF composite is expected to show good DC conductivity. The presence of bands in the higher wavelength confirms the polaron band formation in the band gap of polyaniline by the acid doping. But very low intense band is observed for CSA doped composite due to the

decrease in localized defect states in the polaron band. This will end up in the low DC conductivity for the CSA doped composites.

3.3.1.6 Brunauer-Emmett -Teller (BET) surface area analysis

In order to obtain additional evidence for the size variation of PANI coated CNF fibers the surface area and porosity of composites were measured by nitrogen sorption experiments at 77.3 K. The nitrogen adsorption/desorption isotherms of PANI/CNF composites are shown in the figure 3.7. The isotherms can be characterized as type IV following the International Union of Pure and Applied Chemistry (IUPAC) classification. All composites have low surface area compared to pristine CNF owing to the presence of polyaniline on the surface of CNF. The surface area obtained for the CNF is about 45 m^2/g while it is reduced to 33-14 m^2/g range for PANI/CNF composites. The surface area is found to vary with different doping agents. The highest surface area is obtained for H_3PO_4 doped PANI/CNF composites. Apart from this, H_3PO_4 composite exhibited lowest pore diameter of about 15.25 nm. The pore diameter of the PANI/CNF fibres are distributed in the mesoporous region at 10-35 nm. H_3PO_4-PANI composite shows the highest N_2 absorption at P/P0=1. The fundamental parameters such as the nitrogen absorption at P/P0=1, surface area, and pore diameter obtained from N_2 adsorption/desorption study are summarised in table 3.2.

Table 3.2: Surface area and pore size data from the N_2 sorption isotherms

composite	V (N_2) [mmol/g]	Surface area (BET) [m^2/g]	Pore diameter (nm)
PANI-HCl/CNF	2.79	26.35	16.85
PANI-H_2SO_4/CNF	2.02	16.69	18.85
PANI-H_3P0_4/CNF	3.65	33.34	15.25
PANI-CSA/CNF	1.72	18.95	17.52
PANI-TSA/CNF	1.95	14.02	20.51

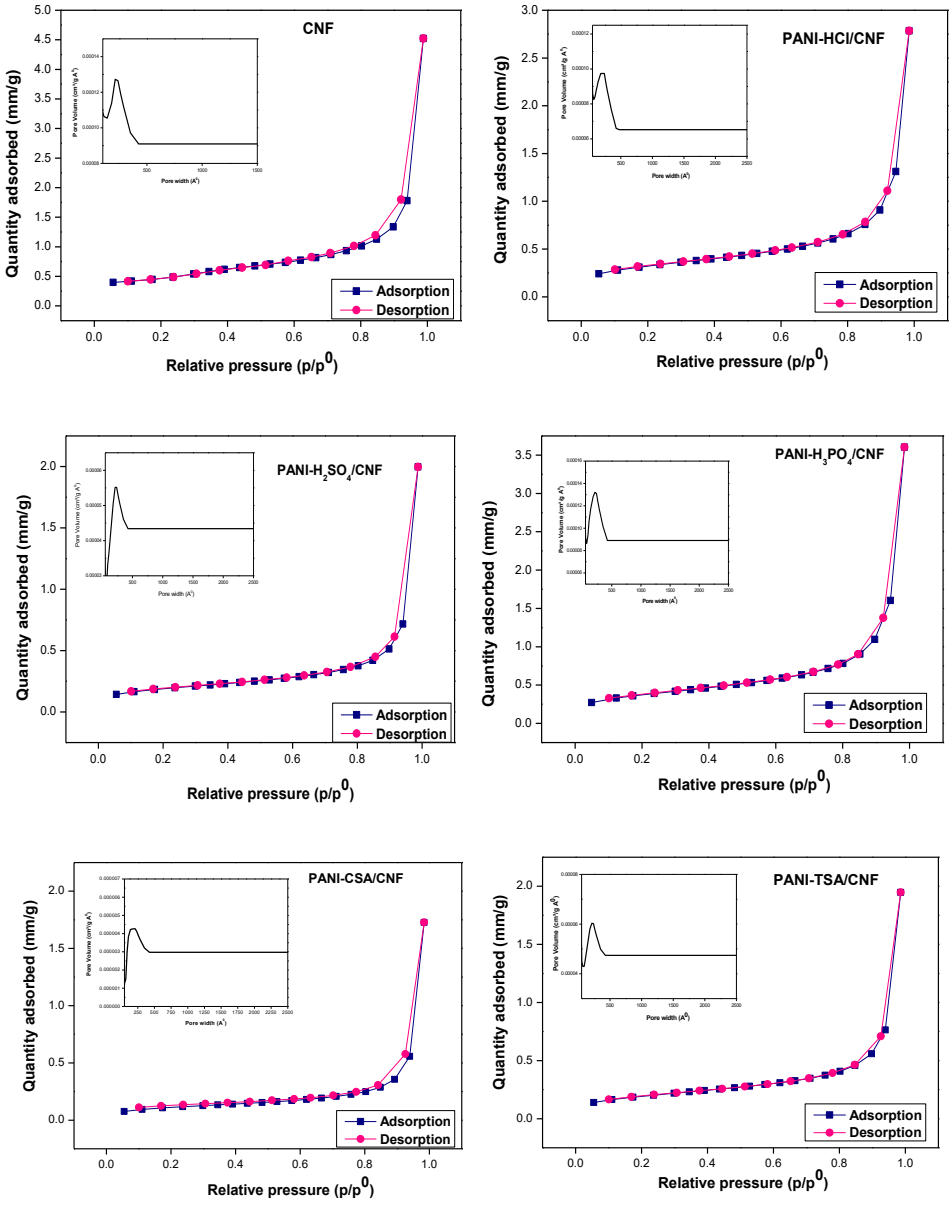

Figure 3.7: N_2 adsorption-desorption curves of the composites

3.3.2 Properties of PANI/CNF composites

3.3.2.1 Electrical properties

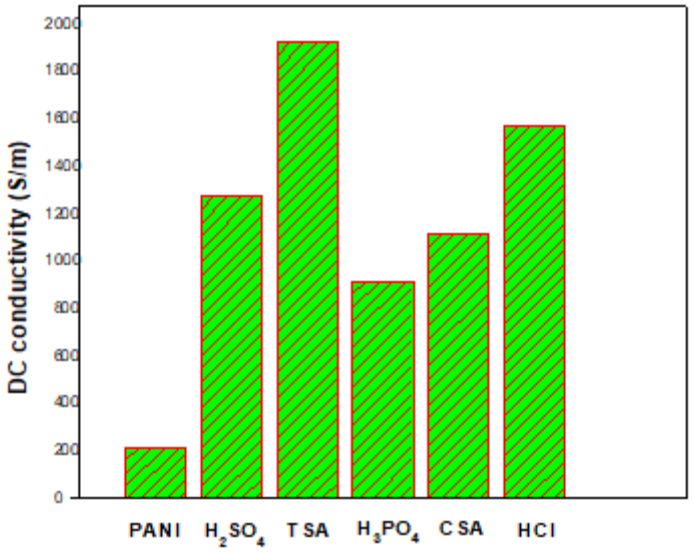

Figure 3.8: DC conductivity of pure PANI and PANI/CNF composites

The DC conductivity of PANI and its composites were measured and the values are given in the table 3.3. Compared to polyaniline, PANI/CNF composites show more conductivity due to the electron donor acceptor interaction between CNF and PANI. CNF is comparatively electron accepting molecule, whereas PANI is relatively electron donating molecule [29]. By the coating of PANI on CNF π-π^* interaction between the quinoid rings of PANI and the surface of CNF is facilitated. The extended π bond formation is evident from the UV-Vis spectrum of the composites. Intense band is obtained at higher wavelength indicating polaron formation and hence enhanced conductivity. Among the composites, the highest conductivity is observed for TSA doped PANI/CNF composite. The dopants with sulfonate counter ion is capable of forming hydrogen bonds

resulting in enhanced DC conductivity [30]. But in contrast to TSA doping CSA doping results in lower conductivity. This can be ascribed to the larger size of camphor sulfonic acid which will not be able to diffuse in to the polymer backbone as easily as the comparatively smaller tosyl group [31]. The large size of the amorphous particles formed in the case of CSA doped PANI composite also influences the mobility of the charge carriers and hence the conductivity.

Table 3.3: DC conductivity values of the samples

Sample	Conductivity (S/cm)
PANI	2.18
PANI-H_2SO_4/CNF	12.73
PANI-TSA/CNF	19.23
PANI-H_3PO_4/CNF	9.16
PANI-CSA/CNF	11.16
PANI-HCl/CNF	15.73

3.3.2.2 Thermal dependence of DC conductivity

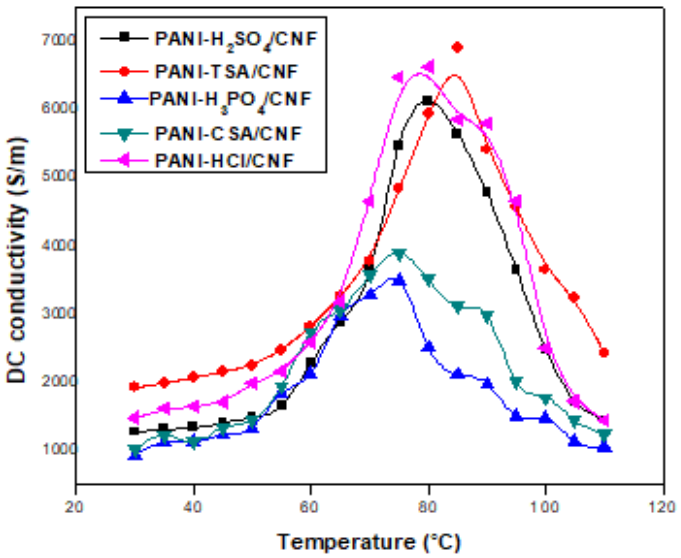

Figure 3.9: Variation of DC conductivity with temperature

The thermal stability of conductivity of the composite is important for high temperature applications. In order to enhance the life span of the devices and to withstand high temperatures it is necessary to know the thermal stability of the device. A detailed analysis of thermal ageing of the composites is carried out by repeatedly measuring the DC conductivity with increasing temperature from 30 ^{o}C to 110 ^{o}C was carried out. The conductivity was measured at every 5 ^{o}C.

The variation of DC conductivity with temperature is plotted in figure 3.9. The electrical conductivity increases with temperature up to around 70-90 ^{o}C for various composites. Beyond this temperature the conductivity drops drastically for all the composites. The increase of electrical conductivity is different for different doping agents. High conductivity is achieved for TSA and HCl doped composites whereas the conductivity is low for CSA and H_3PO_4 doped composites. At higher temperatures, imperfections occur in the polymer chain due to the dislocations of ions hence defects are formed in the composite. As a result, the conductivity is reduced causing discontinuity of the conduction pathways of PANI. Polyaniline chains consist a conducting and nonconducting parts, in which the protonated entities describes the conducting phase whereas the non-conducting phase is formed by the structural defects. Pioneer work of Rannoue et al. [32] suggested that the decrease of conductivity at high temperature was due to the chemical reactions occurring in polyaniline. The chemical changes usually occur at high temperatures but the temperature range we have adopted in the current study is of 30 ^{o}C to 110 ^{o}C. So, here slow aerial oxidation and decomposition reactions are taking place. Compared to PANI the thermal stability of PANI/CNF composites is

improved. PANI/CNF composites are stabilized by the π-π interaction between the π orbitals of CNF and the quinoid rings of PANI. Even beyond 110 ^{o}C the composites exhibit conductivity, it is due to strong interaction of PANI and CNF which is not disturbed by heating. PANI-TSA/CNF composite shows the highest conductivity at elevated temperature owing to the extended interaction by the presence of tosyl group in the composite.

3.3.2.3 Dielectric properties

3.3.2.3.1 Dielectric constant

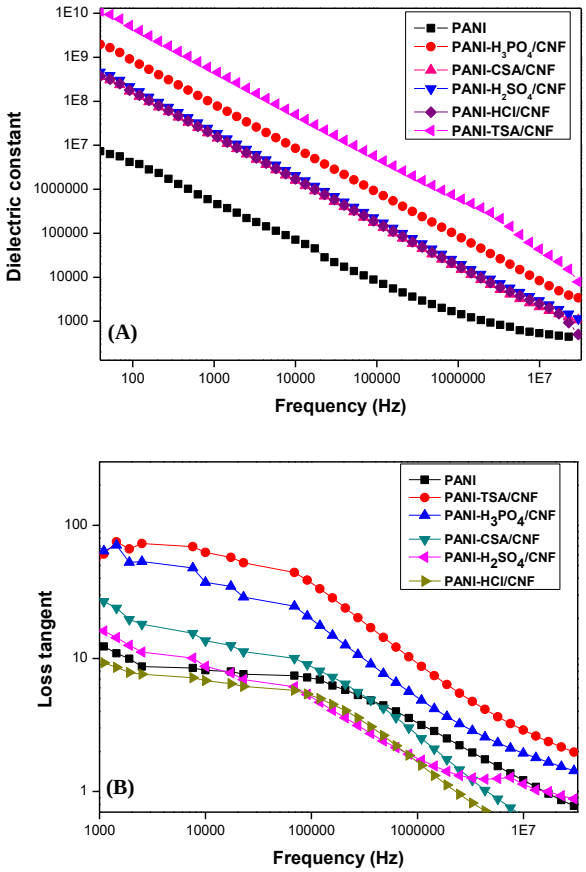

Figure 3.10: Variation of A) dielectric constant and B) tan d with frequency of PANI/CNF composites

To further comprehend the effect of dopant, the dielectric properties of PANI/CNF composites were compared. Figure 3.10A shows the variation of dielectric constant with the applied frequency for a range of 40 Hz to 30 MHz. For all PANI/CNF composites the dielectric constant decreases with increase of frequency. A linear decrease of dielectric constant is seen in the frequency range of 40 Hz to 1×10^6 Hz. But beyond 1 MHz decrease becomes slower. The high dependency at low frequency region can be attributed to the interfacial polarization i.e. Maxwell−Wagner−Sillars (MWS) polarization [33,34].

It is worth noting that large improvement of dielectric constant is observed for TSA doped PANI/CNF composite. TSA doped composites has attained a value of 5×10^7 at 10000 Hz which is about 245 times greater than other PANI/CNF composites. The large increase can be ascribed to the high electron withdrawing nature of toluene sulfonic acid than the other acid dopants. The tosyl group is comparatively more electron withdrawing than others. Presence of electron withdrawing groups will strengthen the interfacial polarization in molecules.

3.3.2.3.2 Loss tangent

The dissipation factors of composites as a function of frequency is plotted in figure 3.10B. The dissipation factors of the composites decrease with the applied frequency. At high frequencies the loss tangent is found to be low as the orientation polarization due to chain motion of polymer becomes out of phase with the rapidly oscillating electric field. Composites which exhibit large dielectric constant also show high loss tangent which can be related to the leakage current. High dielectric constant is obtained

for PANI-TSA/CNF composite. While PANI-CSA/CNF, PANI-HCl/CNF and PANI-H_2SO_4/CNF composites exhibited more or less similar dielectric constant value. But when comparing the tan δ values of these three composites, remarkable reduction in the loss factor is observed for PANI-HCl/CNF composite. That means, it can store energy same as that of CSA and H_2SO_4 doped composites. But less energy is dissipated as heat for HCl composite. Dielectric properties show that HCl doped PANI/CNF composites are effective with good dielectric constant and optimum dissipation factor. TSA and H_3PO_4 doped composites are good enough to store charges but the loss factors for those composites are also high.

3.3.2.3.3 AC conductivity

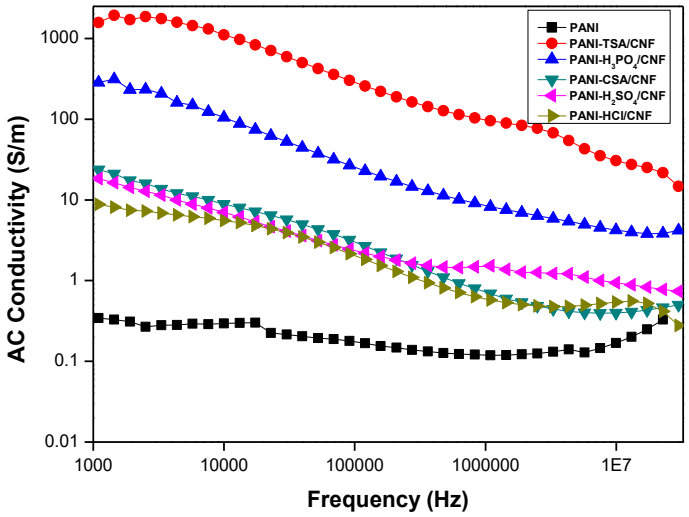

Figure 3.11: Plot of AC conductivity with frequency

A common feature of all amorphous semiconductors including polymer nanocomposites is that AC conductivity increases with frequency

according to the following equation. $\sigma = 2\pi f\varepsilon^{*}\varepsilon_0 \tan\delta$. That means AC conductivity is directly related to the dielectric constant and dielectric loss of the material and the frequency of applied field. Unlike other polymer composites, PANI/CNF composites exhibit remarkable reduction in the dielectric constant with increase of frequency. Hence the rate of decrease of dielectric constant is more than the rate of increase of frequency. So, the net effect is the reduction in AC conductivity with frequency.

3.3.2.4 Thermogravimetric analysis

To understand the effect of dopant on the thermal properties of the composite thermogravimetric analysis was carried out (figure 3.12). Three major weight losses are detected for PANI/CNF composites. The first weight loss occurs at temperature below 100 ^{o}C which can be attributed to the loss of water molecules from the composites. The second loss appears around 270 ^{o}C, owing to the loss of counter anions of the dopant acids.

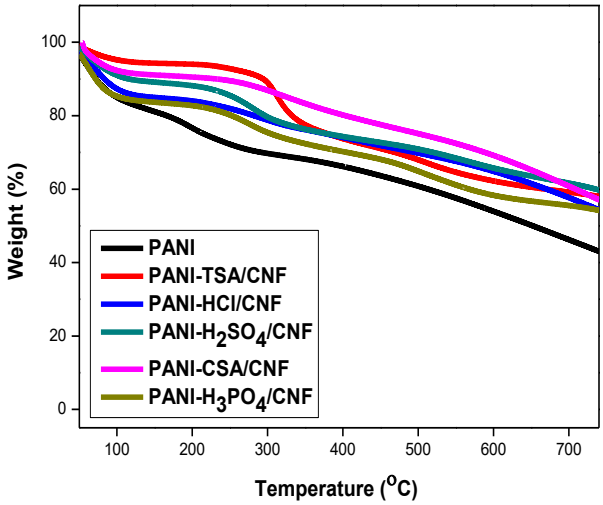

Figure 3.12: Thermogravimetric curves of PANI and PANI/CNF composites

The second weight loss temperature varies with the nature of the dopant used. The major weight loss occurs in a wide range of temperatures, between 350-500 ^{o}C related to the oxidative decomposition of PANI chains. In all the composites good charred residue can be observed due to the presence of stable CNF molecules.

An improvement in thermal stability can be achieved for PANI/CNF composites than pure PANI. Moreover, the stability of the dopant molecules is enhanced. The loss of dopant appears at around 270 ^{o}C. The dopant molecules are more confined to the compact and well aligned CNF fibers. Hence stabilizing interactions are taking place between the dopant molecules and carbon nanofibers. A shift is observed for the major degradation peak of PANI. The results suggest presence of strong interaction between PANI and CNF. The extent of interaction varies with the dopant ion used. High thermal stability is observed for organic acid doped composites.

3.4 Conclusion

Conducting PANI/CNF composites were synthesized in presence of five different dopant acids. High electrical conductivities and dielectric constants were observed for all PANI/CNF composites. However better conductivity and thermal stability of DC conductivity were observed for organic toluene sulfonic acid dopant. It can be attributed to the better electron transfer in the system as evidenced from UV -Vis analysis. SEM images and BET analysis showed low particle size and high surface area for H_3PO_4 doped composite. Further, thermogravimetric analysis showed good thermal stability for organic acid doped composites. Better electrical

and dielectric properties were obtained for PANI/CNF composites than that of pure PANI. Hydrochloric acid doping resulted in moderate conductivity and thermal properties. Moreover, it yielded good dielectric constant with low loss tangent. So, concerning the dielectric properties, low cost and ease of preparation we have adopted HCl doping for further studies.

References

[1] W. J. Feast, J. Tsibouklis, K. L. Pouwer, L. Groenendaal, E. W. Meijer, Polymer, 1996, 37, 5017

[2] A. A. Syed, M. K. Dinesan, Talanta, 1991, 38, 815

[3] S. M. Park, H. J. Lee, Bull Korean Chem.Soc., 2005, 26, 697

[4] M. T. Cortes, E. V. Sierra, Polym. Bull., 2006, 56, 37

[5] A. Pron, F. Genoud, C. Menardo, M. Nechtschein, Synth. Met., 1988, 24, 193

[6] V. G. Kulkarni, L. D. Campbell, W. R. Mathew, Synth. Met., 1989, 30, 321

[7] P. K. Kahol, K. K. Satheesh Kumar, S. Geetha, D. C. Trivedi, Synth. Met., 2003, 139, 191

[8] S. Yang, W. Chen, K. You, Synth. Met., 1997, 87, 77.

[9] Y. Li, Y. Cao, Z. Xue, Synth. Met., 1987, 20, 141.

[10] K. Shannon, J. Fernandez, Chem. Soc. Chem. Commun.,1994, 643.

[11] K. Tazou, R. Gregory, Synth. Met., 1993, 53, 365

[12] S. Sinha, S. Bhadra, D. Khastgir, J. Appl. Polym. Sci., 2009, 112, 3135

[13] K, Levon, K. H. Ho, W. Y. Zheng, J. Laakso, T. Karna, T. Taka, J. E. Osterholm Polymer, 1995, 36, 2733

[14] S. Bhadra, D. Khastgir, N. K. Sinha, J. H. Lee, Prog. Polym. Sci., 2009, 34, 783

[15] W. K. Maser Mater. Sci., Eng., 2003, 23, 87

[16] M. Cochet, W. K. Maser, A. M. Benito, M. A. Callejas, M. T. Martinez, J. Benoit, J. Schreiber, O. Chauvet, Chem. Commun., 2001, 16, 1450

[17] M. Paligova, J. Vil_ca´kova,´ P. Sa´ha, V. Kr˘esa´lek, J. Stejskal, O. Quadrat, Physica A, 2004, 335,421

[18] H. Dong, S. Prasad, V. Nayme, Jr. E. J. Wayne, Chem Mater, 2004, 16, 371

[19] Y. Li, J. Wang, X. Li, J. Liu, D. Geng, J. Yang, R. Li, X. Sun, Electrochem. Commun., 2011, 13, 668.

[20] S. Lim, S. H. Yoon, I. Mochida, D. H. Jung, Langmuir, 2009, 25, 8268.

[21] H. S. O. Chan, S. C. Ng, W. S. Sim, S. H. Seow, K. L. Tan, B. T. G. Tan, Macromolecules, 1993, 26, 144

[22] Y. Guo, Y. Zhou, Eur. Poly. J., 43, 2007, 2292

[23] I. Sedenkove, M. Trchova, N. V. Blinova, J. Stejskal, Thin Solid Films, 2006, 515, 1640

[24] N. Kuramoto, E. M. Genies, Synth. Met., 1995, 68, 191

[25] L. Zhang, Electrochim. Acta, 2007, 52, 6969

[26] Y. Fu, R. A. Weiss, Synth. Met., 1997, 84, 103

[27] S. Koul, R. Chandra, S. K. Dhawan, Polymer, 2000, 41, 9305

[28] P. Ghosh, S. K. Siddhanta, K. S. Samir, S. RejaulHaque, A. Chakrabarti Synth. Met., 2001, 123, 83

[29] H. Zengin Adv. Mater, 2002, 14, 1480

[30] A. R. Hopkins, P. G. Rasmussen, R. A. Basheer, Macromolecules, 1996, 29, 7838

[31] H. Mathew, V. S. Punnackal, S. Kuriakose, B. S. Kumari, A. Manuel, IJSRP, 2013, 3, 1

[32] A. Pron, P. Rannou, Progress in Polymer Science, 2002, 27, 135

[33] Z. M. Dang, L. Wang, Y. Yin, Q. Zhang, Q. Q. Lei, Adv. Mater., 2007, 19, 852

[34] He, F.; Lau, S.; Chan, H. L.; Fan, J. T. Adv. Mater., 2009, 21, 710−715.

Chapter 4

CONDUCTING POLYMER COMPOSITES BASED ON POLY(VINYL ALCOHOL)

Contents

Part A

Development of electrically conducting composites based on cellulose, polyaniline and poly(vinyl alcohol)

Cost effective, high performance dielectric composites based on poly(vinyl alcohol), cellulose fibers and polyaniline were prepared and the electrical, dielectric, thermal and mechanical properties were studied as a function of fiber content, fiber dimensions and polyaniline content. The short cellulose fibers were size-reduced to micro and nano levels prior to coating with polyaniline. Fiber surface was coated with Polyaniline by an in-situ polymerization technique in aqueous medium. The composites were prepared by solution casting method. Short cellulose fiber composites showed a dielectric constant of 2.3 x 10 ^{5} at 40 Hz. For the micro- and nano- cellulose fiber composites the dielectric constant was increased to 4.5 x 10^{5} and 1.3 x 10^{8} respectively. To gain insight into the inflection point of the dielectric data polynomial regression analysis was carried out. The loss tangent of all the composites remained at less than 1.5. Further, AC conductivity, real and imaginary electric moduli of all the composites were evaluated. PVA nanocomposite attained an AC conductivity of 3 S/m. The addition of PANI coated cellulose fiber improved the tensile strength and storage modulus for micro and nanocomposites. But due to the poor compatibility of macro fiber the mechanical properties were decreased. TGA studies showed that the thermal stability of all the composites increased with the addition of fibers. It showed that by controlling the size of the fiber used, it is possible to tune the properties to desired values over a wide range. These novel nanocomposites, combining high dielectric constant, low dielectric loss, good electrical conductivity can be effectively used in applications such as high-charge storage capacitors.

4.A.1 Introduction

Polyaniline is well-known conjugated polymer with tunable conductivity, low density compared to metals and good environmental stability [1-5]. Cellulose is one of the most abundant natural biopolymer in the world. It is a renewable, biodegradable, easy to isolate, low cost and its chemistry finds a significant role in the active field of study. It can be refined to macro, micro and nano size regimes by employing appropriate processing techniques. These fibers can be rendered conductive by depositing a fine layer of polyaniline on the surface [6]. Combination of these fibers with an appropriate polymeric matrix will result in composites with good dielectric properties and anisotropic mechanical properties. Nanoparticles in polymer matrix influence the structural, optical and electrical properties which can be effectively tuned for applications such as charge storage capacitors, electromagnetic shielding etc. [6].

Poly(vinyl alcohol), is the world largest synthetic polymer produced due to its excellent chemical resistance, physical properties and good biodegradability [7,8]. Consequently, it finds many potential applications. It is a semi crystalline thermoplastic polymer, has been extensively investigated as a host for different nano-fillers and for electrolyte applications [9-12]. Although a number of studies on PVA systems have been reported already [13-17], the dielectric properties of PVA systems are not well explored. The pioneer work of Dutta and his co-workers has established the importance of PVA- polyaniline combination [18].

Polymer composites with high dielectric permittivity and conductivity have received great scientific and technological interest due to their potential applications in high-charge capacitors, artificial muscles etc. [19-22]. Over the years many attempts have been made to improve the properties of these composites by using ceramic, metallic and organic particulate fillers. The incorporation of these materials resulted in good dielectric constant, low dielectric loss and ease of fabrication. However, in many cases these composites had relatively low dielectric constants, usually<100. So, high ceramic loading had to be used to achieve high dielectric constant. Conducting organic fibrous fillers are alternative choice because of low density and better mechanical properties.

In this chapter a novel nanocomposite system consisting of poly(vinyl alcohol) and polyaniline-coated cellulose fibres in macro, micro and nano size regimes is proposed. The mechanical, thermal, electrical and dielectric properties of the composite were studied as a function of filler loading and filler size.

4.A.2 Experimental

4.A.2.1 Isolation of cellulose from coir

Cellulose was isolated from coir fiber by the modification of the reported method [23]. Coir fibers were chopped in 4 mm size, then it was treated with 5 % NaOH solution for 5 h at 60 ^{o}C. The fibers were washed free of alkali. After that it was treated with 5 M hydrochloric acid for 12 h. And the fibers were washed well removed all the traces of acid present. Finally bleaching was carried out to remove the lignin and hemicellulose present after acid and alkali treatments. It was then treated with 20 g of

sodium hypochlorite and 5 mL of acetic acid for 3 h at 70 ^{o}C. The process was repeated with 15 g sodium hypochlorite and 3 mL acetic acid. The fiber obtained was in the micrometer size. The fibers were mechanically grinded to reduce the size and homogenized for 1 h at 14000 rpm. Fibers in three different sizes ie. macro, micro and nano were prepared.

4.A.2.2 Preparation of composites

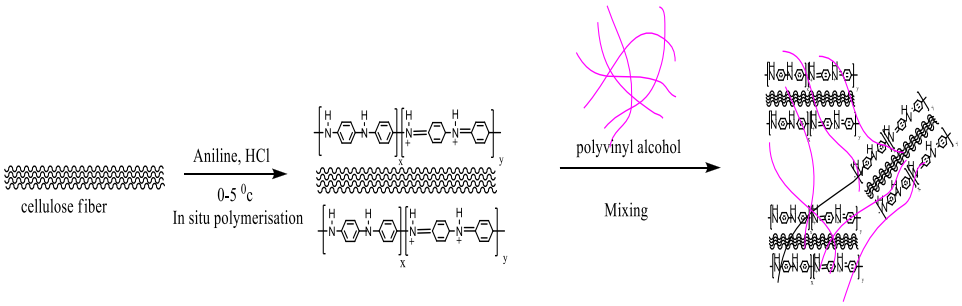

Figure 4.A.1: Schematic representation of the preparation of PANI/Cellulose/ PVA composites

The cellulose fibers thus obtained were dispersed in 100 mL of 1 M hydrochloric acid by sonication for 1 h. Then the dispersion was kept at 0-4 ^{o}C temperature followed by addition of 10 g of aniline. 12.50 g of ammonium persulfate (APS) was dissolved in 100 mL 1.25 M HCl solution and was taken in a burette. The APS/HCl was added drop-wise into the aniline-fiber solution to initiate polymerization reaction. The polyaniline-coated fibers (PANI/Cellulose) were then isolated. Different weight percentages of modified fibers were then mixed with poly(vinyl alcohol) solution in water at 90 ^{o}C followed by ultrasonication for 2 h. Films were prepared by casting and dried slowly at 70 ^{o}C for 24 h.

4.A.3 Results and discussion

4.A.3.1 Characterizations

4.A.3.1.1 Scanning Electron Microscopy & Transmission Electron Microscopy

Surface morphology of cellulose macro fiber

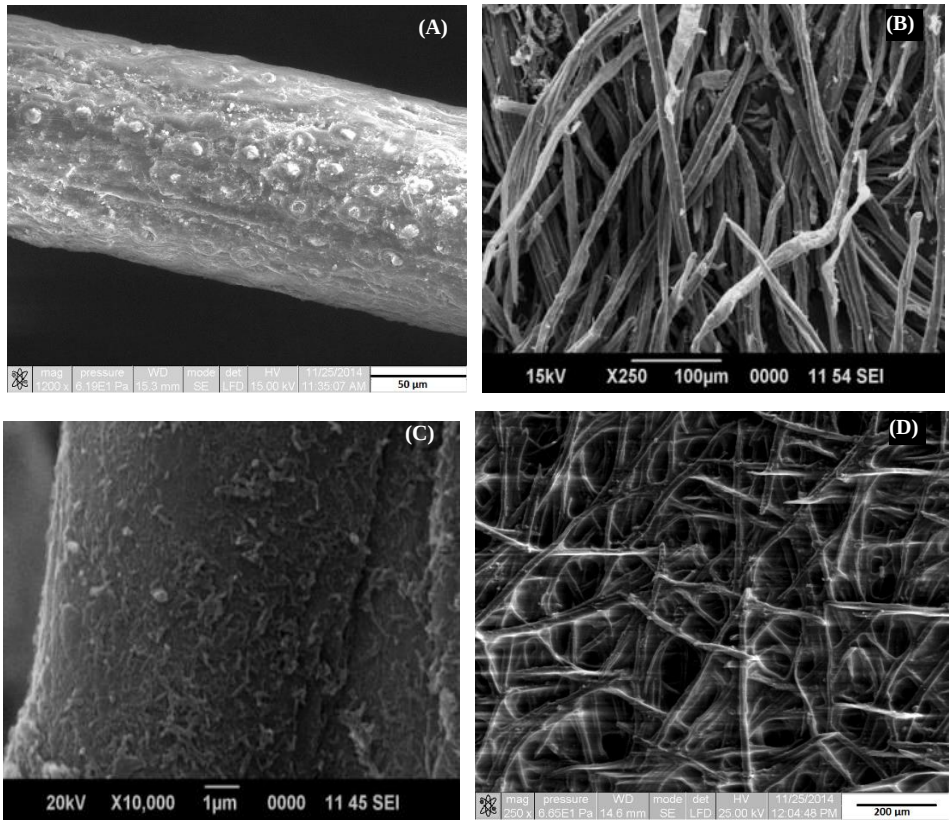

Figure 4.A.2: SEM images of A) untreated coir fiber B) treated coir fiber C) PANI coated short fiber D) short cellulose fiber in the PVA polymer matrix

Surface morphology of cellulose micro fiber

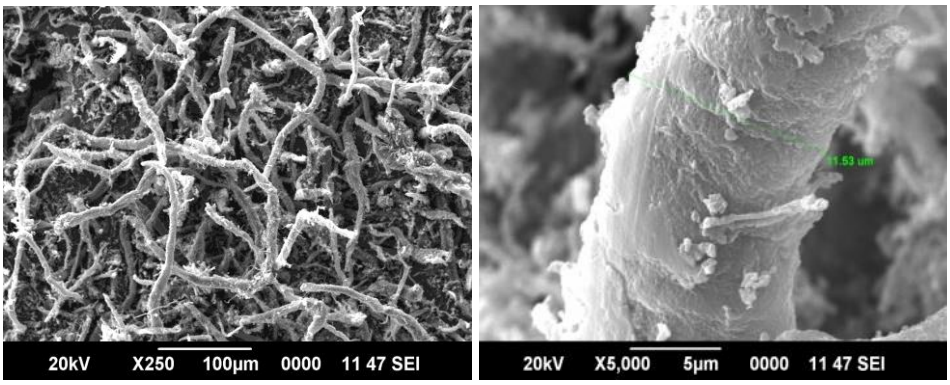

Figure 4.A.3: SEM images of PANI coated micro fiber

Surface morphology of cellulose nano fiber

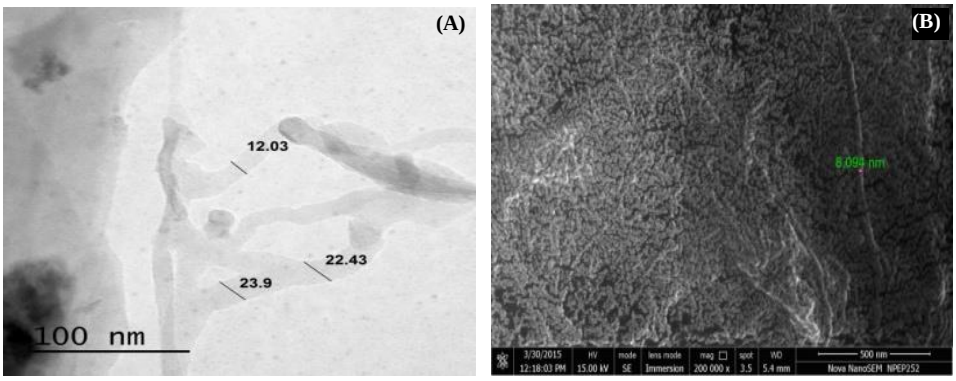

Figure 4.A.4: A) TEM and B) FESEM image of nanocellulose fiber

Figures 4.A.2A and 4.A.2B show cellulose fiber before and after chemical treatments. The surface of coir fiber (figure 4.A.2A) is not smooth. A number of nodes and irregular strips are clearly visible on the surface. The surface of untreated fiber will have pectin, lignin and other impurities. The chemical treatments will increase the amount of cellulose exposed on the fiber surface which will result an increase in the number of possible reaction sites. After chemical treatments, a

decrease in diameter is observed. The untreated coir fiber has a diameter of 0.15 mm whereas the diameter of the treated fiber is 0.08 mm. Chemical treatments also lead to the defibrillation as well as opening of fiber bundles.

Nanocellulose fibers were prepared from the micrometer sized coir fibers by the repeated chemical and mechanical treatments. Nanocellulose fiber thus obtained was characterized by ultra-high-resolution FE-SEM and TEM images. Uniform fibrillation is evident from the TEM and FE-SEM images of nanocellulose (Figure 4.A.4 A&B). After chemical treatments, the cellulose fibers get separated in to individual fibrils and the diameter of the fibers is about 10 nm. The particle size of the samples determined from the TEM images are in good agreement with the values obtained from FESEM images. From the TEM image the average size of the fiber is 15±4 nm.

Polyaniline, a conjugated conducting polymer, is coated on all three types of cellulose fibers by the in-situ polymerization of aniline. The oligomeric aniline intermediates adsorbed at the fiber substrate starts the growth of PANI chains, resulting in uniform coating of polyaniline on the surface of fibers. Polyaniline coating on the fiber surface can be confirmed from the increase in the diameter of the fiber. An increase (0.08 mm to 0.13 mm) of fiber diameter is observed after PANI coating. Scanning electron microscopy (SEM) illustrates a uniform coating of fiber with PANI (Figure 4.A.2C). The coated fiber becomes thicker as the amount of deposited PANI increases. However, PANI is not covalently bonded to the fiber. Aniline oligomers adsorbed on the surface grow in

molecular weight [24]. A number of reports on the uniform coating of conducting polymers on textiles [25-27] and carbon fibers [28] as well as on polymer nanofibers [29] are available. Conductive network formed by PANI coated cellulose fiber in the PVA matrix is apparent from the SEM image of the PANI/Cellulose/PVA composite (Figure 4.A.2D). The conductive network will help to improve the electrical conductivity of the composite. The diameter of fiber in PVA matrix is found to be 0.125 mm. This shows that PANI is not easily removed when added to PVA matrix.

4.A.3.1.2 X-ray Diffraction

Cellulose thus obtained from coir fiber was characterized by X-Ray Diffraction technique, the diffractogram (Figure. 4.A.5A) shows peaks around 2θ of 16 º, 22.5 º corresponding to the typical β- cellulose structure, for the crystallographic planes of (110) and (200) respectively. An increase in fiber crystallinity is observed after chemical treatments. This indicates the reduction of amorphous fractions of fiber and consequently enrichment of relative crystalline content.

The crystallite size was calculated by using the Scherrer equation,

$$L_{h,k,l} = K\lambda/b\cos\theta \quad \text{.....4.A.1}$$

Where, K = 0.94, size of crystallite peaks is found to be 2.89 nm, 3.61 nm for untreated and chemically treated fiber respectively. The increase in the crystallite peaks indicates that the fiber molecules are closely packed and parallel to each other. The values obtained are in accordance with the values available in literature [30].

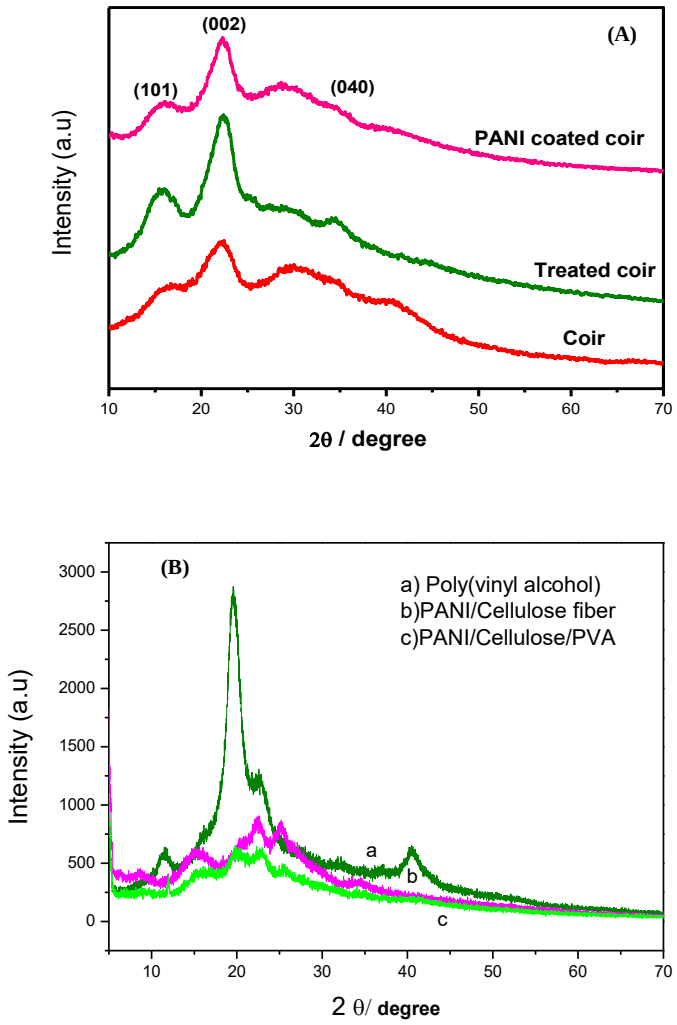

Figure 4.A.5. X-ray diffraction pattern of A) untreated coir, treated cellulose fiber and PANI coated fiber; B) PVA, PANI coated cellulose fiber and the composite.

The diffractogram of the chemically treated cellulose fiber shows improved crystallinity, as evident from the higher peak height at a 2θ of 22.5 º compared to 22.4 º of the untreated fiber. This can be ascribed to

the fact that chemical treatment removes the amorphous regions resulting more order and good alignment in the crystalline cellulose.

XRD pattern of pure PVA indicates a sharp peak at 19.6 º, typical of crystalline PVA (Fig. 4.A.5B). High degree of crystallinity of PVA can be attributed to the regularity in the molecular structure. In the case of nanocomposites, the intensity of crystalline peak of PVA is reduced and is broader. This may be due to a different thermal history of the composites and the presence of filler that interacts with the matrix chains. Similar amorphous peak has been reported in the case of hot pressed PVA molecules [31].

For crystalline polyaniline a peak at 6.7 º is expected to appear. But in this case the peak is absent indicating that the polyaniline is not ordered. I have carried out the conventional coating, this will lead to deposits more and more PANI on the fiber surface, as the distance from the fiber surface increases it is not possible to distribute the polymer chains with the same order of periodicity. So, the crystalline peak is absent in the composite.

4.A.3.1.3 BET surface area analysis

The surface area and pore diameter of all three sized PANI/Cellulose fibers were measured using N_2 adsorption-desorption experiments. Adsorption of N_2 at subcritical temperatures (BET) is the routine technique for the determination of the specific surface area of dispersed solids [32]. The adsorption isotherms obtained at 77 K is shown in the figure 4.A.6. Following the general classification of adsorption isotherms, adsorption isotherm appears to be of type IV. The variation of surface area with the particle size was studied by BET analysis.

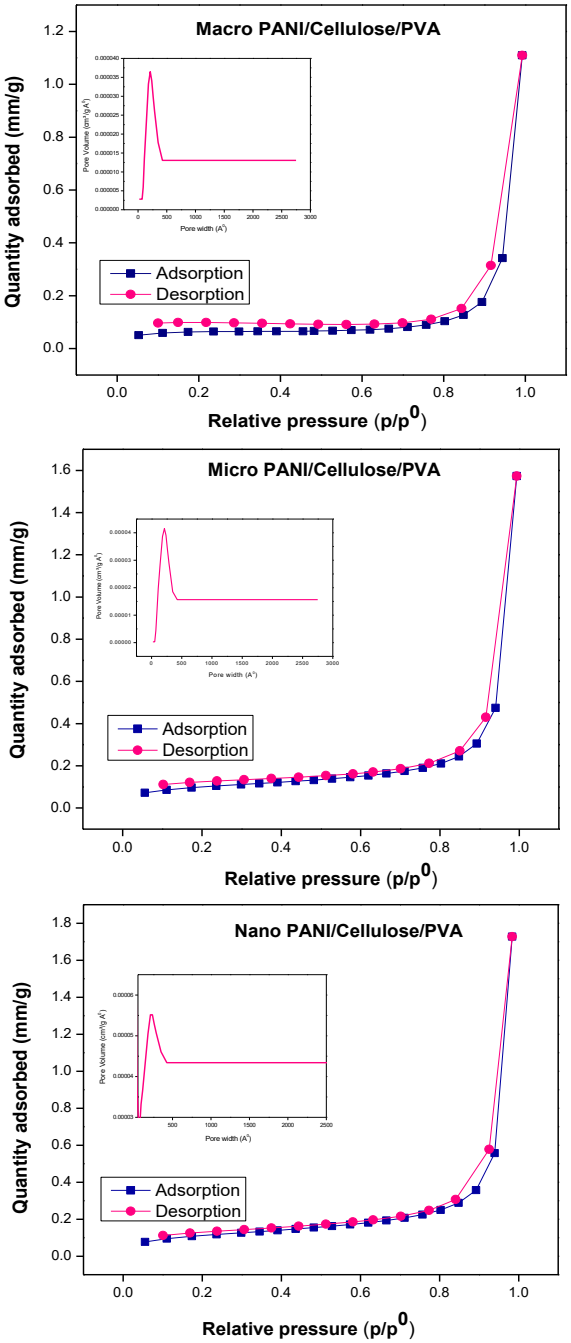

Figure 4.A.6: N_2 adsorption-desorption plots of macro, micro and nano polyaniline modified cellulose fibers

The surface area increases with the decrease of the particle size. Moreover, the surface area obtained for nano cellulose particles is not very high. It is due to the coating of polyaniline on the surface of nanocellulose particles. The coated polyaniline is of micro meter size. Macro sized PANI/Cellulose fibers have comparatively less surface area of about 6 m^2/g, whereas for micro PANI/Cellulose fibers the surface area is approximately 14 m^2/g. But higher surface area is obtained for nanofibers, of about 25 m^2/g. The surface area increases with reduction in the size of the filler. Consequently, better interaction is possible with the polymer matrix, which will enhance the properties of the nanocomposites. From the BET surface area analysis, nano composite is expected to show good mechanical, thermal and electrical properties.

4.A.3.2 Properties of the composite

4.A.3.2.1 DC conductivity

The room temperature conductivity of the composites with variation of filler loading is given in the figure 4.A.7. The conductivity of PVA is about 10^{-9} S/m. The addition of conducting PANI/Cellulose fibers in to the PVA matrix lead to a drastic increase of conductivity. The conductivity of the composite increases by 9 orders of magnitude from $1*10^{-9}$ S/m to 2.69 S/m as the nano PANI/Cellulose content increases from 10 wt.% to 50 wt.%. Nevertheless, this kind of sharp increase cannot be observed for micro and macro composites. For micro composite, the DC conductivity increases by 8 orders and for macro it is 7 orders in magnitude. Sudden shoot up appears for nanocomposite even after 5 % filler loading. This result can correspond directly to the morphological

differences between the composites. As the concentration of PANI/Cellulose in PVA increases it leads to the formation of conductive network which will produce good interconnectivity between conducting fibers. This in turn reduces the conductive resistance formed by the band gap at the interfaces. The network formation at higher filler concentration is responsible for the sharp increase of conductivity. The particle-particle contact becomes very efficient at low particle size. It is evident from the figure 4.A.7 that the percolation threshold for nano composites is much smaller than the other two composites. So, with minimum PANI/Cellulose loading the composite is able to achieve maximum conductivity.

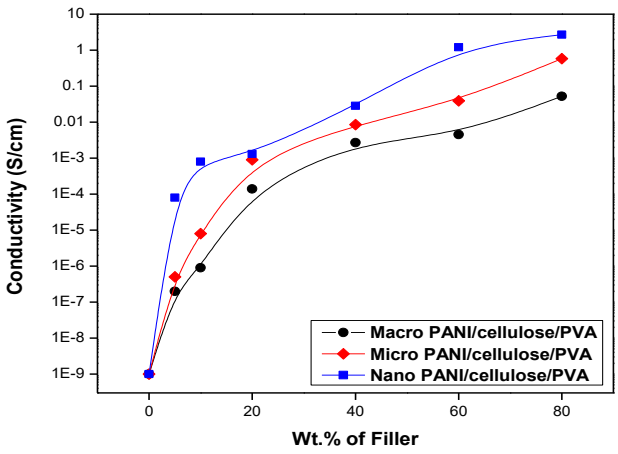

Figure 4.A.7: Variation of DC conductivity with concentration of PANI/Cellulose fiber

According to the percolation theory, percolation threshold is a mathematical concept, it is the formation of conductive network in random systems. Connected components are absent below the percolation

threshold but above that point, there exists connectivity. The high percolation threshold for macro composite is due to the increased particle size. Unlike nanocomposite minimum fiber content will not be sufficient for the formation of conductive pathways. So, it indicates that more filler loading is necessary to make macro composite conductive.

4.A.3.2.2 Dielectric properties

4.A.3.2.2.1 Dielectric permittivity

The ability of dielectric material to store energy is attributed to different types of polarizations. Figures 4.A.8A-C show the variation of dielectric permittivity with frequency of PANI-coated macro, micro and nano sized cellulose fiber/PVA composites, respectively.

For all the three composites (figure 4.A.8 A-C), the dielectric constant decreases with increasing frequency. For pure PVA the dielectric constant drops sharply until a frequency of ~ 300 Hz beyond which the it remains constant. For the macro fiber filled composites (figure 4.A.8A), a similar trend is observed with increasing frequency, though the dielectric constant values are higher. Decrease of dielectric constant with frequency is due to dielectric dispersion as a result of lag of the molecules behind the alternation of the electric field especially at higher frequency. A close look at the pattern shows that the point at which the initial higher frequency-dependence is changed, it is gradually shifted to higher frequency levels for composites with higher PANI coated fiber content.

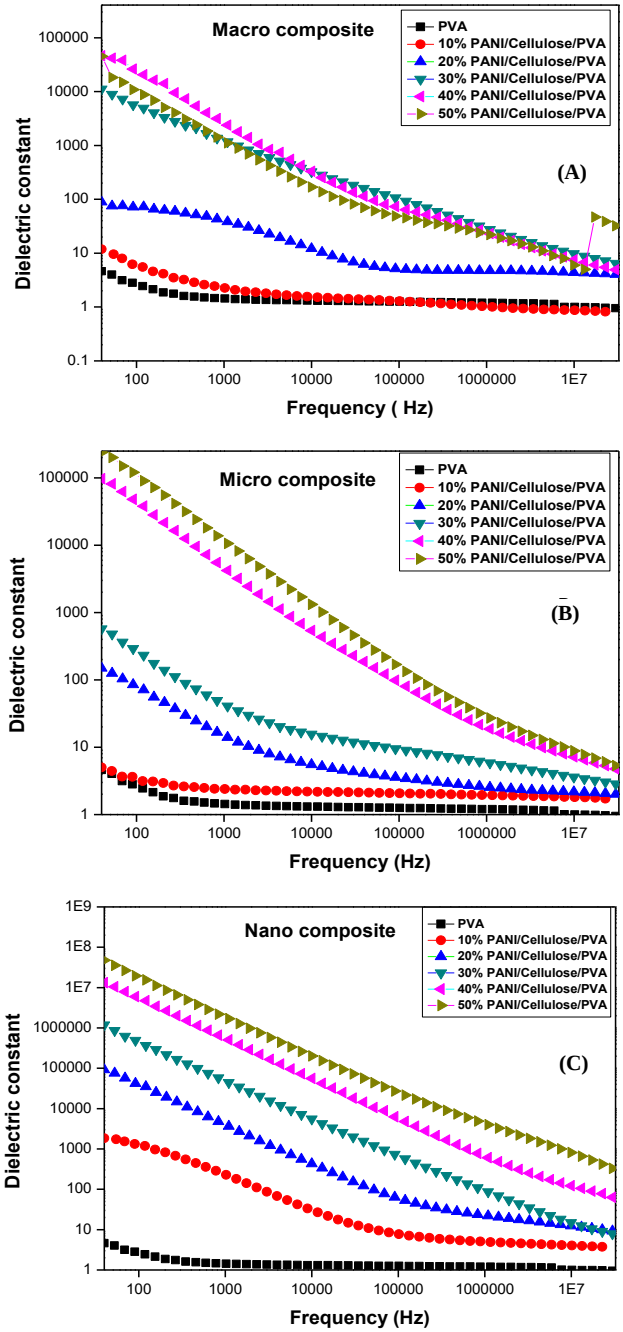

Figure 4.A.8: Dielectric constant as a function of frequency A) Macro composites B) Micro composites C) Nano composites

The dielectric behavior of polymer depends on the charge distribution and statistical thermal motion of the polar groups. Polyaniline coated cellulose fiber introduces polar groups in the matrix which will lead to increase the dielectric constant. Polyaniline is a good dielectric material; polarization of a dielectric material is contributed by electronic, ionic and orientational polarization. Electronic polarization occurs during very short interval of time (10^{-15} s); ionic polarization occurs in the range of (10^{-13}-10^{-12} s) whereas the orientational polarization requires comparatively longer time. Polyaniline noticeably enhances the electrical conductivity as well as the polarizability of the composite. Hydrochloric acid doped polyaniline contains chlorine atoms. Presence of these groups in the composites will increase interfacial polarization. Similar reports are available for electron withdrawing carboxylic acid group on CNT [33]. The higher the possibility of polarization the larger will be its dielectric constant. At low frequencies, the electric dipoles have sufficient time to align with the filed, before the field changes its direction. At high frequencies, the dipoles do not get enough time to orient with the field. In such cases the polarization arising from the charge accumulation decreases which lowers the dielectric constant [34]. High dielectric constant at low frequency range (10^2- 10^4) is due to the electrode effect and interfacial polarization [35,36].

Micro and nano size composites show a similar trend with respect to frequency and fiber content (Figures 4.A.8B &C). However, for the nanocomposites containing higher wt.% of fiber, the dielectric constant is relatively higher. The highest value, $7.5*10^7$ is achieved with 50 wt.% nanofibers. This may be associated with the higher area of PANI–coated

fiber surface for nanocomposite. This can well be explained based on the conductive network formed in the composite. At relatively low concentration of filler loading, the filler particles are too separate to allow electron transport between them. The insulating PVA polymer matrix does not have significant contribution to electrical conductivity. At higher wt.% composites the filler particles are connected to each other which will help to form conductive network in the composite. The nanocomposites also show a very sharp decrease in dielectric constant at low frequencies and become stable at higher frequencies. This variation in the nature of dielectric constant curves of macro, micro and nanocomposites can be due to the effective conductive network formed in case of nanocomposite. As the aspect ratio of the filler becomes high, fiber–fiber contact increases which results in effective network formation at lower filler concentrations. Due to large conductivity difference between the PANI/Cellulose and the insulating PVA matrix, there would be charge accumulation at their interfaces, known as Maxwell-Wagner-Sillars (MWS) effect [37-39]. The nanocellulose fibers will be aligned in the interfacial regions of the composite, so minimum quantity of filler can make an effective conductive network.

The dielectric constant is also found to be a function of the fiber content. The 50 % fiber filled sample shows the highest dielectric constant at all frequency range. There appears to be a non-linear relationship between the dielectric constant and fiber content. A cross plot at 1000 Hz prepared against fiber content is shown in figure 4.A.9. The dielectric constant of macro composite shows a sudden shoot up beyond 30 wt.% filler loading while the micro and nanocomposites show such an increase at 21 % and 9 % filler loadings, respectively. This shows that

minimum fiber content is needed for the formation of a percolative network. This point represents the threshold for the composites. The dielectric permittivity of the composites dramatically increases in the vicinity of the percolation threshold [40-42]. Beyond the percolation threshold, high dielectric constant is obtained due to the formation of microcapacitor or nanocapacitor network.

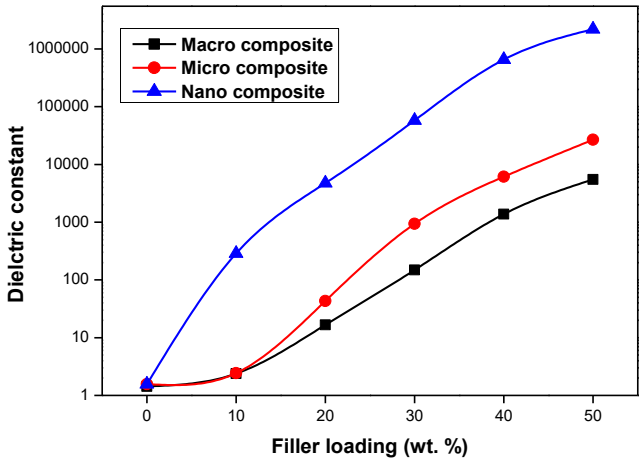

Figure 4.A.9: Dielectric constants of the composite at a frequency of 1000 Hz.

Significant change in the concavity of the dielectric curves is observed in the figures 4.A.8 A-C. These inflection points are dependent on filler content of the composites. With increase of filler loading the inflection point shifts to higher frequency. All the composites show similar trend. But for nano and micro composites the inflection points are shifted to higher frequencies than the macro composite. This shows that with decrease of size of the filler the inflection points are shifting to higher frequencies. For higher wt.% composites the inflection point cannot be obtained from the plots. In such case the inflections were

calculated using polynomial regression analysis in which the relationship between the dependent variable X (wt.% of filler) and the independent variable Y (frequency) was modeled as 3rd order (Figure 4.A.10) polynomial.

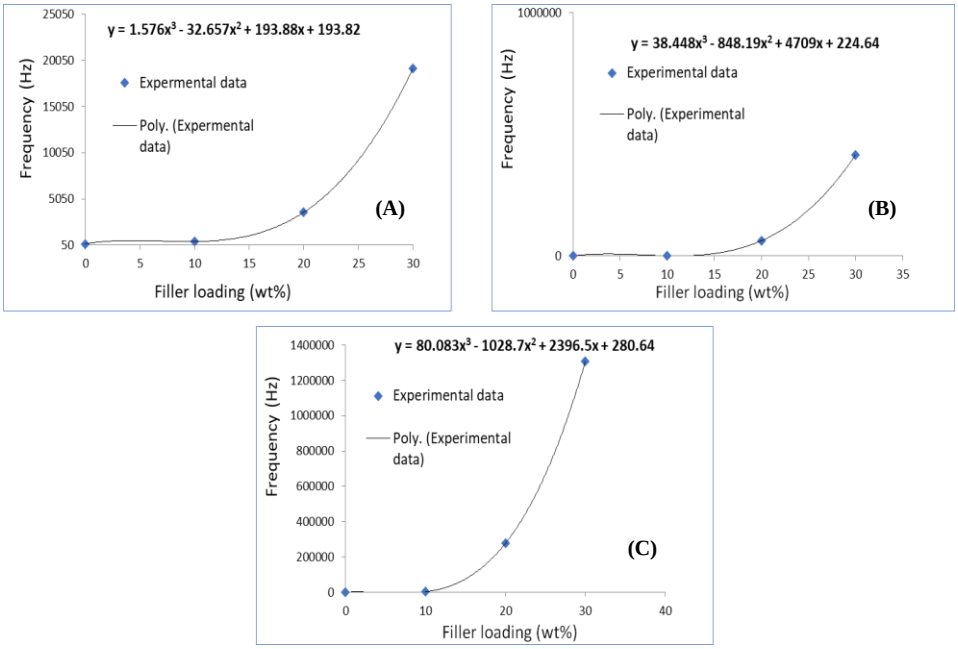

Figure 4.A.10: Polynomial regression for A) macro, B) micro and C) nano composites

The inflection frequency calculated using polynomial regression analysis for higher wt.% composites (40&50 wt.%) are given in table 4.A.1. The polynomial equations used for finding out the inflection points of macro, micro and nano composites, respectively are:

$$y = 1.576x^3 – 32.657x^2 – 193.88x + 193.82 \quad \text{.....4.A.2}$$

$$y = 38.448x^3 – 848.19x^2 + 4709x + 224.64 \quad \text{.....4.A.3}$$

$$y = 80.083x^3 – 1028.7x^2 + 2396.5x + 280.64 \quad \text{.....4.A.4}$$

For the 50 % fiber loaded macro samples the point of inflection is close to 1E4. Highest inflection frequency is obtained for 50 % nanocomposite. Maximum filler-polymer interaction is present in nanocomposite containing high filler content. This results in high inflection frequency in nanocomposite.

Table 4.A.1: Inflection points of higher wt.% composites.

Sample	**Frequency at inflection point (Hz)**	
	40 wt.% fiber	**50 wt.% fiber**
Macro composite	$1.6*10^4$	$7.3*10^4$
Micro composite	$1.2*10^6$	$3.1*10^6$
Nano composite	$3.5*10^6$	$7.5*10^7$

A comparison of dielectric constants of three composites at different frequencies is shown in Table 4.A.2. It is interesting to note that under the same filler loading the dielectric constant of PANI coated nanofiber PVA composites is much higher than that of micro and macro fiber PVA composites. Furthermore, it is found that nano PANI/Cellulose/PVA composite show a maximum of dielectric constant at very low frequency with certain PANI/Cellulose content. For nanocomposite, the highest dielectric constant is near $1.3*10^8$ at the filler content of 50 wt.%, for micro composite, it is about $4.5*10^5$ at the filler loading of 50 wt.%. As the size of the filler reduces the composite exhibits better properties. This dramatic increase in *k* is possibly due to the formation of microcapacitor or nanocapacitor networks by neighboring conducting polyaniline-cellulose fibers and the insulating PVA in between.

Table 4.A.2: Comparison of dielectric constants of three composites at different frequencies.

Frequency (Hz)	Dielectric Constant		
	Macro composite 50 %	**Micro composite 50 %**	**Nano composite 50 %**
40	$9.7*10^4$	$4.4*10^5$	$4.7*10^7$
1000	5509	26767	$2.1*10^6$
10000	541	2233	200600
30000000	4.9	28	329

4.A.3.2.2.2 Loss tangent

The dielectric permittivity and dielectric loss are related to each other by the dissipation factor tan δ.

$$\tan \delta = \varepsilon''/\varepsilon' \quad \text{.....4.A.5}$$

Figures 4.A.11A-C show the dissipation factors of macro, micro and nano PANI/Cellulose/PVA composites, respectively as function of filler content and frequency. With the increasing fiber content, the loss tangent of the composites increases and its dependence on the frequency is enhanced. At high frequencies, the loss tangent is found to be low as the orientation polarization due to chain motion of polymer becomes out of phase with the rapidly oscillating electric field. Composites which exhibit large dielectric constant also show high loss tangent which can be related to the leakage current. Leakage current will be more pronounced near the percolation threshold when there is direct contact between conductive fillers. Leakage current can be minimized by preventing the contact between conductive fillers.

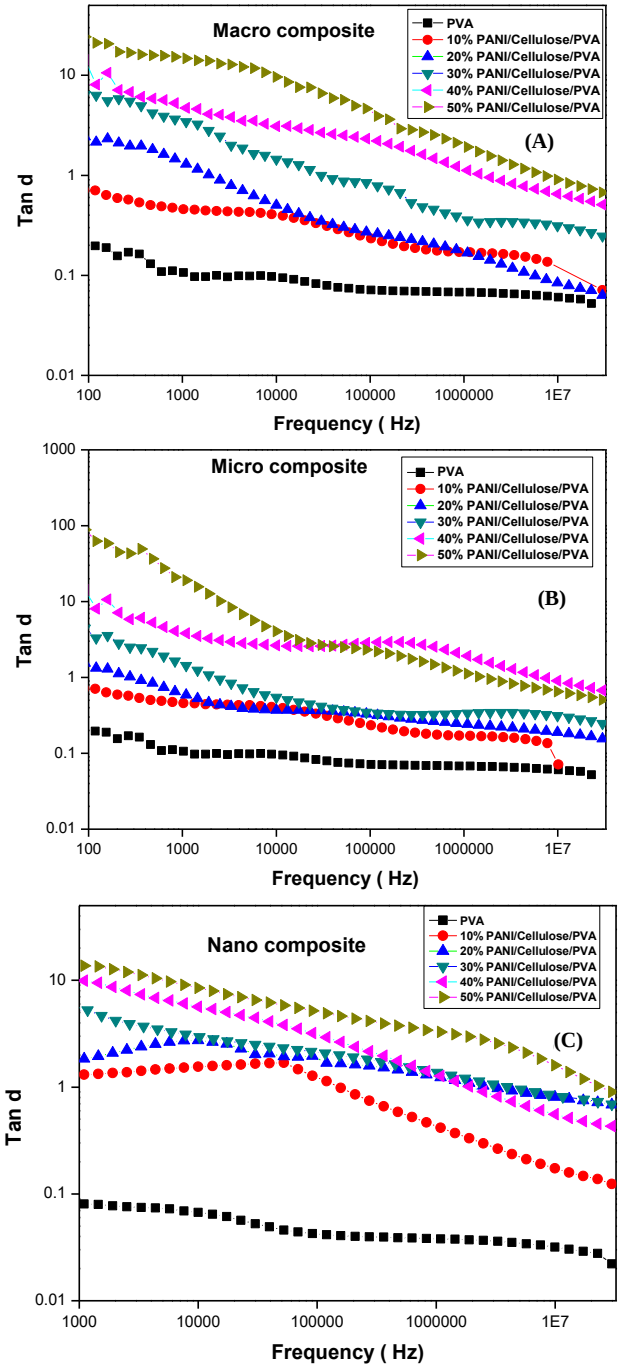

Figure 4.A.11: Dielectric loss as a function of frequency A) Macro composite, B) Micro composite, C) Nano composite

4.A.3.2.2.3 AC Conductivity

Figures 4.A.12-14 show the variation of AC conductivity of the composites containing fibers in macro, micro and nano sizes, respectively. AC conductivity was calculated from the dielectric permittivity and dielectric loss by the equation $\sigma_{AC}=2\pi f\varepsilon\varepsilon^{*}\tan\delta$, ε is the permittivity of vacuum. Conductivity of all the composites increase with increase of frequency. This can be attributed to the presence of induced surface currents created by the application of external electric filed. For nanofiber composite a linear increase of AC conductivity with frequency is observed at all fiber loadings. However, for micro and macro composites containing higher weight percentages of fiber a linear increase of AC conductivity is observed. For composites containing lower fiber concentration, a deviation from linear dependence is observed. The conductivity is found to increase with the filler loading. This increase of conductivity can be related to the good dispersion of conductive filler in the PVA matrix. A fine dispersion of conducting filler generates a conducting network, facilitating good conductivity. The dispersion of fiber in the PVA matrix is favored because of the possibility of H- bonding between the two.

Generally, AC conductivity curves have two distinct regions: a low frequency region where the graph displays a jump and a high frequency region where the graph is almost horizontal. The frequency at which such transition occurs is called hopping frequency. Such a sharp transition is not observed for higher wt.% composites in the present study.

Usually the application of conductive nano particles to an insulating polymer matrix is supposed to induce an electrical conductivity, when the volume fraction exceeds the percolation threshold. The percolation threshold is considered to be lesser for fiber-shaped fillers (high aspect ratio) than for spherical particles.

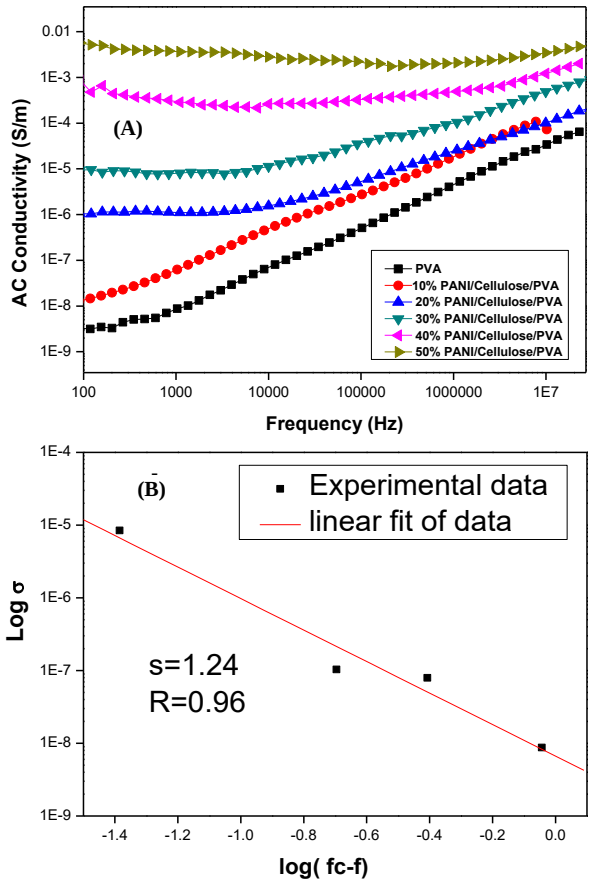

Figure 4.A.12. A) Plot of AC conductivity as a function of frequency and B) best fits of the conductivity to the equation 4.A.6 for macro composite

For the composites filled with conductive fillers, the percolation theory illustrates that the variations of dielectric constant with frequency follow a power law as the filler content approaches percolation threshold. The figures 4.A.12A, 4.A.13A, 4.A.14A illustrate the dependence of filler size on the percolation threshold. It is observed that percolation threshold has a strong dependence on size. It decreases with decrease in the size of the filler.

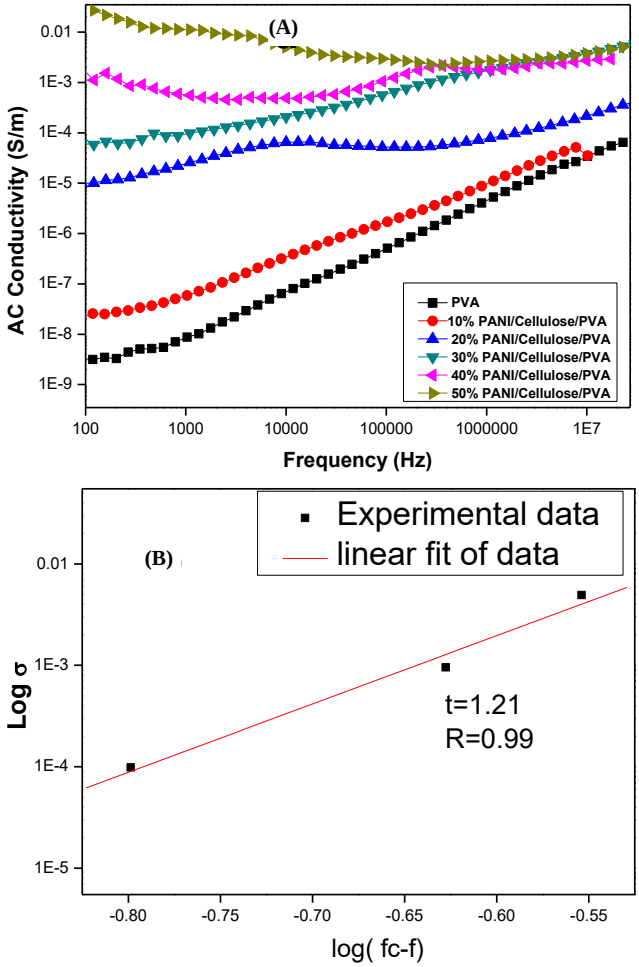

Figure 4.A.13. A) Plot of AC conductivity as a function of frequency and B) best fits of the conductivity to the equation 4.A.7 for Micro composite

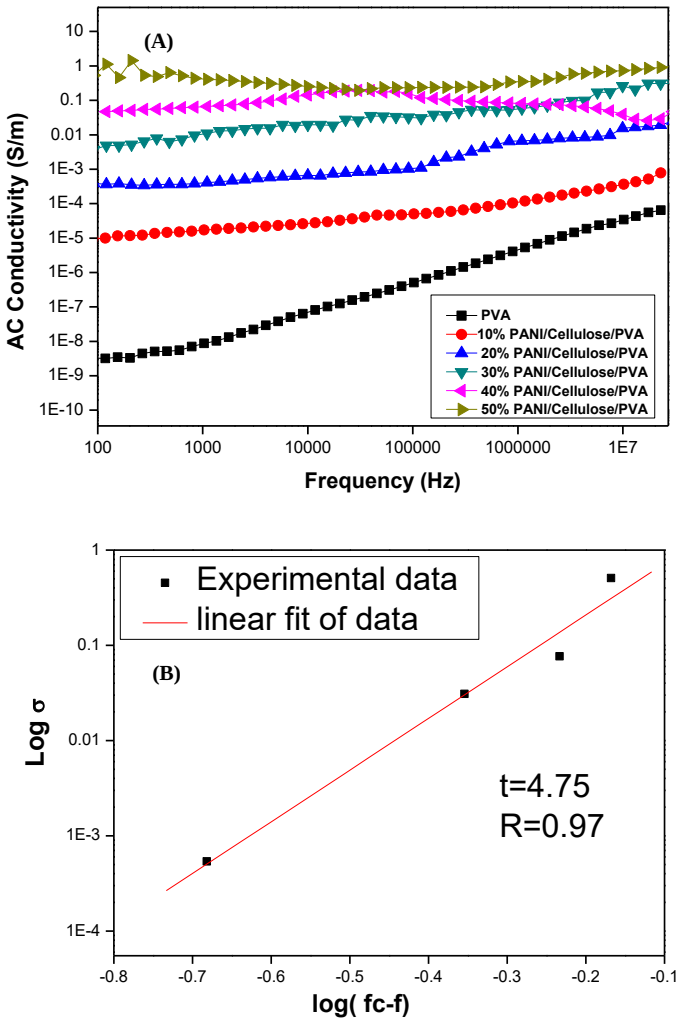

Figure 4.A.14. A) Plot of AC conductivity as a function of frequency and B) best fits of the conductivity to the equation 4.A.7 for Nano composite

In inorganic–organic conducting-polymer based composites, the critical volume fraction at the percolation threshold, *f*c, is a key parameter to study the electrical properties of these composites. It is observed that near the percolation threshold the electrical conductivity as well as dielectric permittivity of the composites increases by several orders of magnitude. The conductivity σ of the conductor- insulator composites near the percolation threshold can be predicted by the power laws in equation

$$\sigma(f_{cpani}) \alpha (f_c - f_{cpani})^{-s'} \text{-For } f_{cpani} < f_c \quad \text{.....4.A.6}$$

$$\sigma(f_{cpani}) \alpha (f_{cpani} - f_c)^{t} \text{-For } f_c < f_{cpani} \quad \text{.....4.A.7}$$

In equations 4.A.6 & 4.A.7, σ is the electrical conductivity, fcpani is the volume fraction of PANI/Cellulose and fc is the percolation threshold. s′ and t are the critical exponents in the insulating region and conducting regions respectively.

The best linear fits of the conductivity data for macro PANI/Cellulose/PVA composite to the log–log plots of the power laws for equation **1** gave *f*c = 30 %, s′=1.24 (Figure 4.A.12B). But for micro and nanocomposite the fc values, respectively, are 21 % and 9 % filler loading. The critical exponent in the conducting region i.e. t is found to be 1.21 for micro PANI/Cellulose/PVA composite and 4.75 for nanocomposite. In percolation theory, the critical exponents are considered to be universal independent of the type and properties of inclusions comprising the composite. The universal values for the critical exponent

for insulating region as well as conducting region are s_{un}≅0.8–1, t≅1.6-2, respectively [43]. Nanocomposites show more deviation from the universal value of critical exponent than that of macro and micro filler composites. The large critical exponent can be attributed by the high aspect ratio of the fiber in the nanocomposite. Similar result in the case of carbon nanotube/electroactive-polymer nanocomposites has been reported by Dang et al. [39]

4.A.3.2.2.4 Electric modulus

Electric modulus represents the real dielectric relaxation process which corresponds to relaxation of electric field in the material when the electric displacement remains constant [44]. By considering the role of polarizing cloud hopping of charge carriers the dielectric properties of the sample can be described by the complex electric modulus(M*) as follows [45,46].

$$M^* = \frac{1}{\varepsilon *} = \frac{1}{(\varepsilon' - i\varepsilon'')} = \frac{\varepsilon'}{\varepsilon'^2 + \varepsilon''^2} + \frac{\varepsilon''}{\varepsilon'^2 + \varepsilon''^2} = M' + M''$$

Where M′ and M″ are the real and imaginary parts of the electric modulus. Electric modulus formalism can suppress the electrode effect and illustrates the conductivity relaxation. The variations of real and imaginary part of the electric modulus for the sample at different frequencies are shown in the figures below. Electric modulus formalism is a good method to study the polarization process.

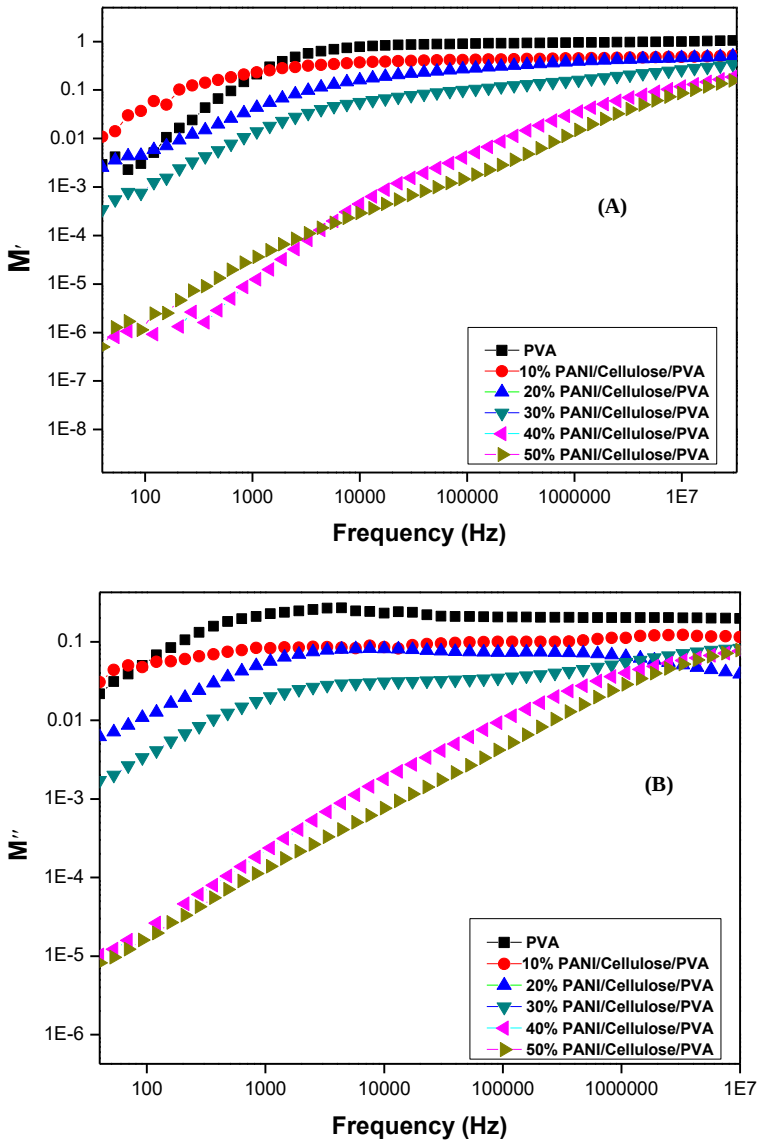

Figure 4.A.15: A) Real and B) imaginary part of electric modulus for Short composite

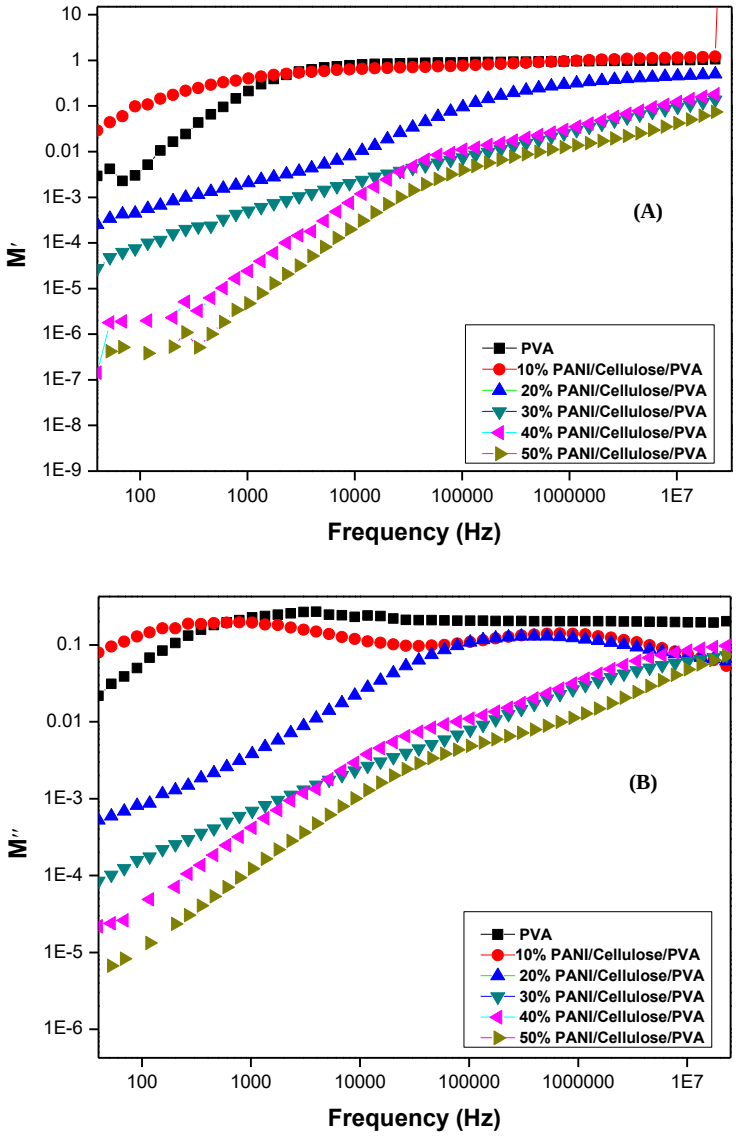

Figure 4.A.16: A) Real and B) imaginary part of electric modulus for Micro composite

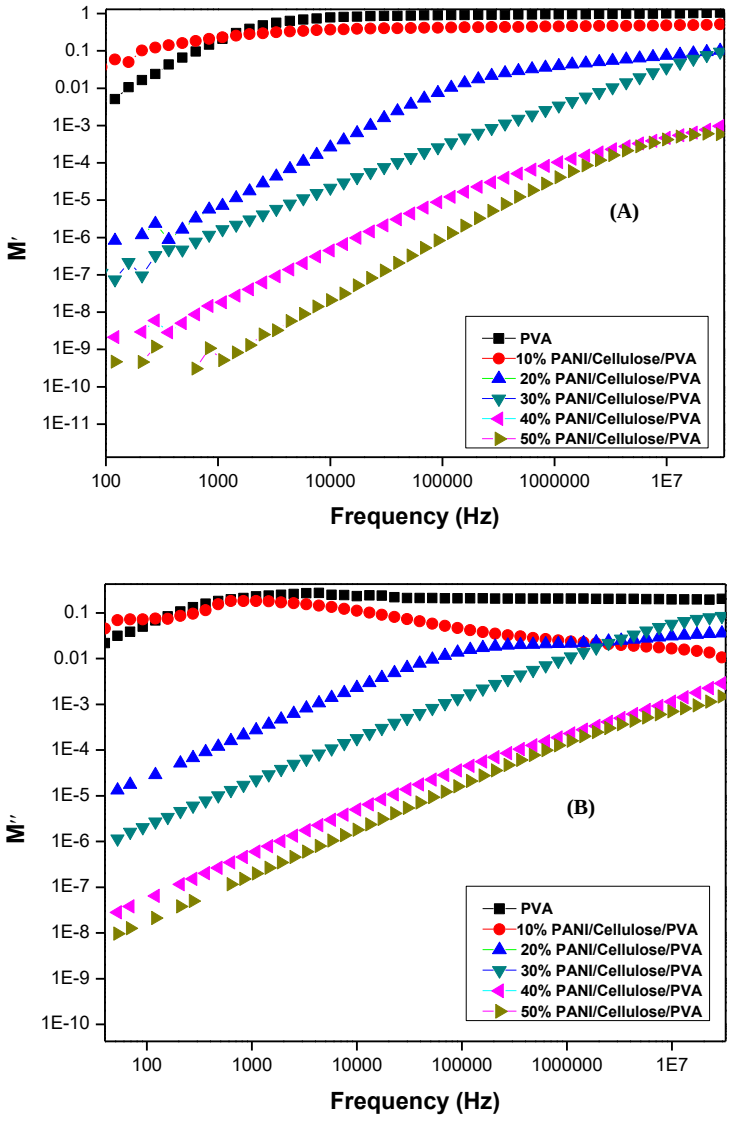

Figure 4.A.17: A) Real and B) imaginary part of electric modulus for Nano composite

Figures 4.A.15-17 show the variation of real and imaginary electric moduli of PANI/Cellulose/PVA composites containing fibers in macro, micro and nano sizes, respectively. For all composites, real and imaginary electric moduli increase with increase of frequency. Sharp increase of real electric modulus is observed at lower frequency range, while the increase becomes slow at high frequencies. With further increase of frequency M` curves for all samples attain an asymptotic value indicating a highly capacitive nature of the sample.

Small peaks can be observed for M″ plots, which is an indication of the presence of relaxation process in the composites. Normally at room temperature loss peaks will be absent. The loss peaks arise with increase of temperature. Interfacial polarization may be the origin of these loss peaks. The peak position gives the evidence of transition from long range to short range mobility with increase of frequency.

4.A.3.2.3 Thermogravimetric analysis

The degradation temperature of PVA is about 242 ^{o}C. The addition of PANI/Cellulose fibers causes a shift in the degradation temperature of PVA, it is shifted to higher temperature. The shift is dependent on the nature and morphology of the fiber used. It is evident from the figure (4.A.18) that the polyaniline coated cellulose fibers are efficient fillers for enhancing the thermal stability of PVA. The degradation temperature is further shifted to higher temperatures with the addition of micro and nano fillers. For the same concentration of the filler, the predominant increase in the degradation temperature is obtained for nanocomposite.

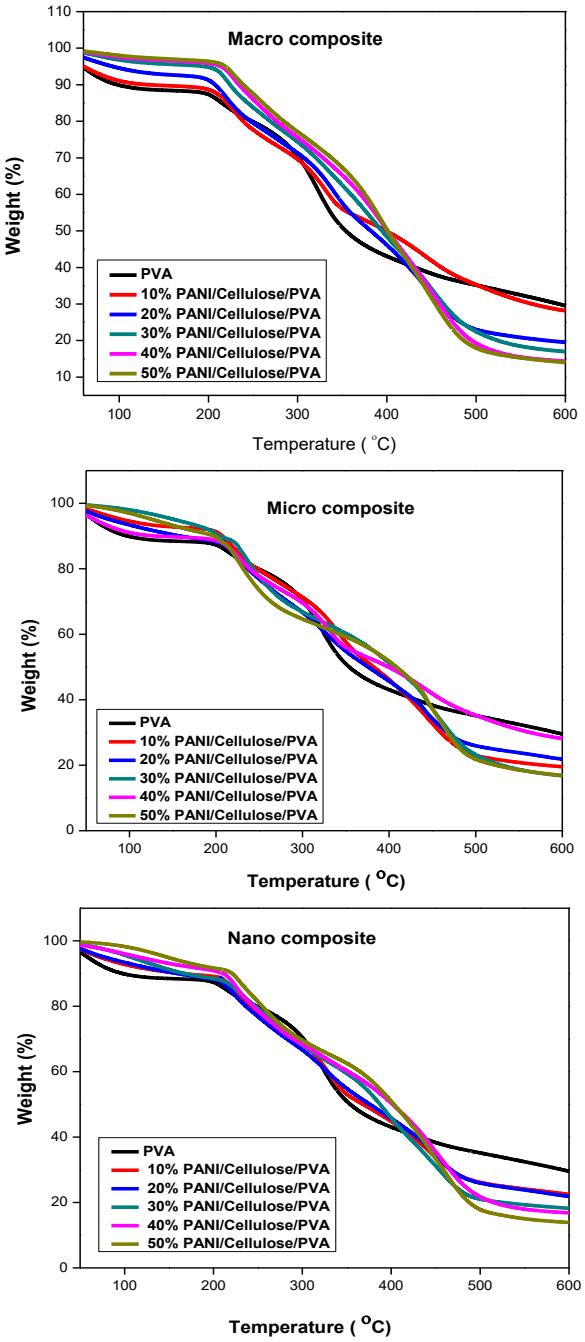

Figure 4.A.18: Thermogravimetric curves of macro composite, micro composite and nano composite

The mechanism of PVA degradation is extensively studied by various research groups [47-49]. The decomposition of PVA takes place in two steps, in the first step is the elimination of water molecules and side groups. The second step appears at higher temperature, it is the degradation of PVA backbone. The first peak appears at between 230 ºC and 320 ºC due to the elimination reactions and the second peak appears between 320 ºC and 420 ºC. A shoulder peak is observed followed by the second peak due to the chain scission and cyclisation reactions. The degradation of polyaniline occurs at 380 ºC. But due to the presence of high intense peaks of PVA, polyaniline peak is visible only for high filler concentration composites. As the concentration increases, the degradation peaks of polyaniline start to appear beyond 400 ºC. The degradation of cellulose takes place between 230 ºC to 300 ºC. While this peak is merging with the degradation peak of PVA.

4.A.3.2.4 Mechanical properties

4.A.3.2.4.1 Tensile

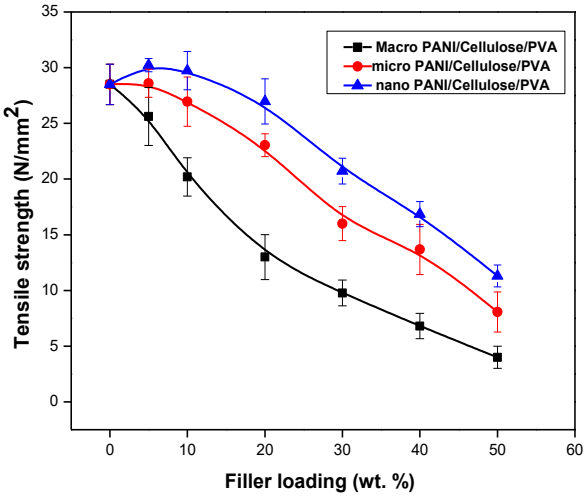

Figure 4.A.19: Variation of tensile strength with filler loading

The variation of tensile strength of the three different size composites with fiber loading is shown in figure 4.A.19. For micro and nano composites the tensile strength increases slightly up to 10 wt.% then reduces sharply. The increase of tensile strength for nanocomposite is about 6.5 % while for micro it is 2 %. But such an increase is not observed for macro composite, incorporation of macro PANI/Cellulose into PVA lead to the reduction in tensile strength. The initial increase of tensile strength for micro and nano composites is due to the reinforcing characteristics of the dispersed micro and nano cellulose fibers. Better increase in the tensile strength is observed for nanofibrillated cellulose, indicating an efficient stress transfer leading to the plastic deformation in the PVA matrix. The decrease in tensile strength at higher concentration is due to the agglomeration of cellulose fibers. The stress acting on a small part of the material surface would be much greater than the average stress applied to the test specimen in the presence of cellulose agglomerates. The reduction in the tensile strength of macro composite can be attributed to the incompatibility of macro cellulose in PVA matrix. The poor dispersion of macro sized cellulose lead to the sudden decrease of tensile strength of the composites. As the size increases the chances for the formation of voids in the composite also increases. The microstructure and the location of voids are significant. It can influence whether or not a crack emanates from voids and propagates and finally result in failure of the composites.

4.A.3.2.4.2 Dynamic Mechanical Analysis

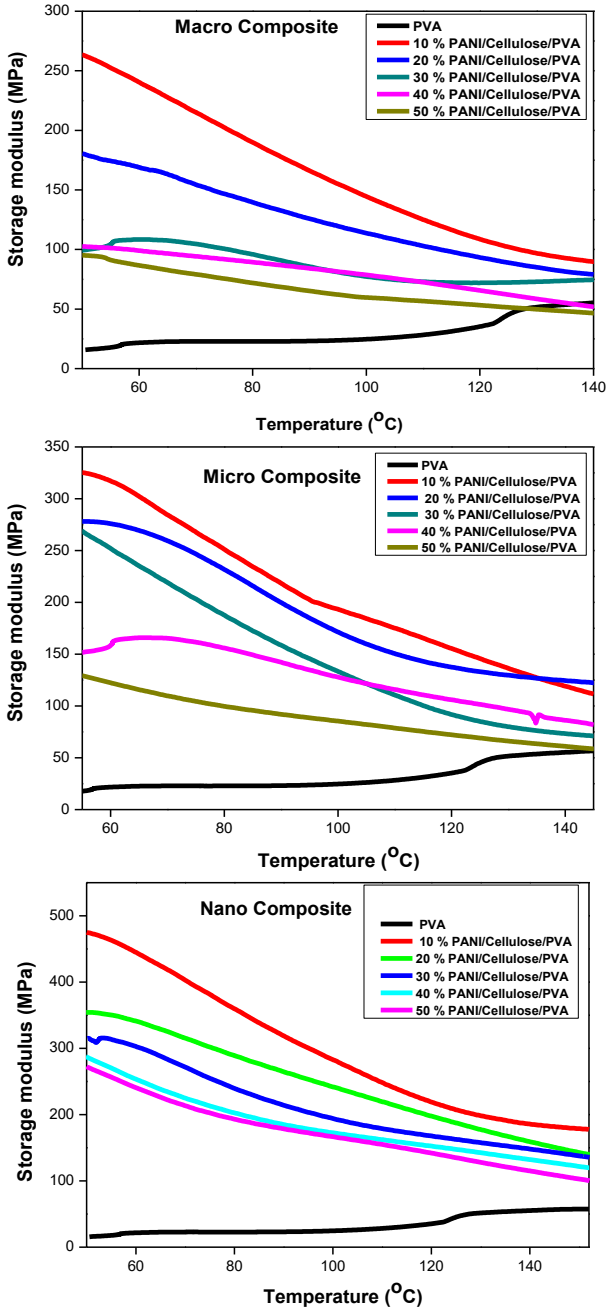

Figure 4.A.20: Plot of storage modulus against temperature for macro, micro and nano composites

The reinforcing effect of polyaniline coated cellulose on the mechanical properties of PVA was analyzed by dynamic mechanical analysis. The analysis was carried out at a fixed frequency of 1 Hz and the temperature was varied from 40 ºC to 150 ºC. The variation of storage modulus with the change of temperature is shown in the figure 4.A.20. For all the three composites, an initial increase of storage modulus is observed, after that the storage modulus decreases. Prominent increase of storage modulus is observed for nanocomposite. As the size of the filler increases the storage modulus decreases.

All the composite exhibited higher storage modulus than pure PVA. The storage modulus for pure PVA is about 15 MPa, it is increased up to 273 MPa for macro composite and to 324 MPa for micro composite. Whereas significant improvement in storage modulus is obtained for nanocomposite of about 473 MPa. It is due to the reinforcing effect of nanofillers. As the size reduces to nanometer scale better interaction is taking place between the conducting filler and the polymer matrix. It allows improved stress transfer at the matrix-filler interface. Due to the agglomeration at higher filler loading reduction in storage modulus is observed. Prominent reduction at higher filler concentration is obtained for macro composite. But for nano and micro fillers the reduction is not considerably significant. This can be ascribed to more agglomeration of the conducting fibers at high loading for macro composite. Particle-particle interaction is high for the macro sized particles. As a result, large drop of storage modulus is observed for macro composite than the micro and nano composite. In case of all the three composites, 50 % composite

exhibits the lowest storage modulus. This is due to the poor interface formed at higher loading.

4.A.3.2.5 Water absorption behavior

The specimens for water absorption were immersed in water at room temperature. Initial weight of the sample was recorded and the amount of water absorption was analyzed by weighing the sample at certain time intervals (30 min). The water absorbed at the surface was wiped out before weighing. The percentage of water absorption was calculated using the following equation [50]

$$Mt\ (\%) = \frac{wt-wo}{wo} * 100 \quad \text{.....4.A.9}$$

Wt is the weight of the sample at time t, Wo is the initial weight of the sample.

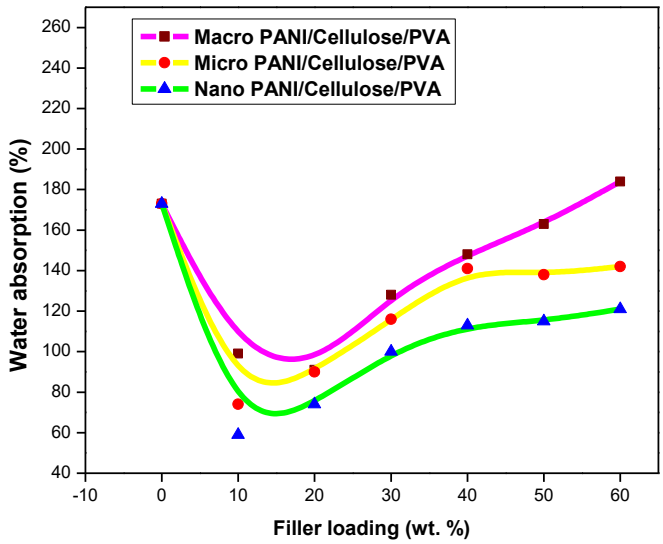

Figure 4.A.21: Comparison of water absorption behavior of the composites

PVA is known to be a water absorbing material. The addition of fibers in to the PVA molecules reduces the percentage of water absorption. A sudden decrease of water absorption is observed for the initial concentration of the composites. But as the fiber content increases the water absorbing capability also increases. This increase can be attributed to the hydrophilic nature of the fiber and the increased interfacial area between the fiber and matrix [51]. The upsurge of absorption % is more for macro composite. Since the water uptake can also takes place from the open fiber edges of the macro composites. The fibers are not well dispersed in the matrix, which will also cause increased water absorption. The high cellulose content in coir fibers results in the increased water absorption, these extra water molecules penetrate through the voids present in the composites. In turn, these voids can cause additional water intake due to the capillary action, this results in the flow of water molecules along the fiber matrix interfacial region and also causes the diffusion through the PVA matrix. This will result in the de-bonding of PANI/Cellulose and PVA in macro composite. For all the composites, the rate of water absorption is high at the early stages of the exposure, after the initial increase of water absorption becomes slow then reaches a saturation value. This is called Fickian diffusion process [52]. The initial rate of increase and the maximum water uptake increase with the more fiber addition. All the natural fibers are exhibiting similar behavior [53]. Composite failure occurs for high wt.% composites. The more the composite cracks, the more capillary and transport via micro-cracks become active [54]. All the composites exhibited high water sensitivity and reached the saturation stage only after 72 h.

4.A.4 Conclusion

Novel PANI/Cellulose/PVA composite were successfully fabricated by solution cast method. The electrical, mechanical and dielectric characteristics were investigated. Three series of PANI/Cellulose/PVA composites containing fibers in three size ranges i.e. macro, micro and nano were studied. Compared to short cellulose fiber composite, higher dielectric permittivity together with lower loss factor are achieved in nanocomposites in frequency range of 40 Hz to 30 MHz. PVA nanocomposite attained an AC conductivity of 3 S/m. For all the three composites, the real and imaginary electric moduli increase with conductivity. The addition of PANI coated cellulose fiber improved the tensile strength and storage modulus for micro and nanocomposites. But due to the poor compatibility of macro fiber the mechanical properties were decreased. TGA studies showed that the thermal stability of all the composites increased with the addition of fibers. The addition of micro and nano cellulose fibers in to PVA molecules reduced the percentage of water absorption while for the macro fibers the percentage of water intake was increased. The result obtained here is an example of how nanoscopic changes in the structure of conductive filler and the subsequent change in the interfacial polarization can affect the macroscopic properties of composites. These novel nanocomposites with high dielectric performance can find applications in high-charge storage capacitors.

Reference

[1] D. G. Li, C. Chen, W. Rao, W. H. Lu, Y. H. Xiong, J. Mater. Sci. Mater. Electron., 2014, 25, 76

[2] Z. Ye, Y. Jiang, H. Tai, N. Guo, G. Xie, Z. Yuan, J. Mater. Sci. Mater. Electron., 2015, 26, 833

[3] H. Qiu, J. Wang, S. Qi, Z. He, X. Fan, Y. Dong, J. Mater. Sci. Mater. Electron., 2015, 26, 564

[4] Y. Zhao, H. Zhao, C. Liu, Z. Cai, J. Wang, X. Fu, J. Mater. Sci. Mater. Electron., 2015, 26, 3621

[5] T. Zhou, J. W. Zha, Y. Hou, D. Wang, J. Zhao, Z. M. Dang, Appl. Mater. Interfaces, 2011, 3, 4557

[6] C. G. M. O Merlini, D. P. Barra, S. D. A. S. Schmitz, A. Ramoa, T. M. Silveira, A. P. Araujo, Polymer Testing, 2014, 38, 18

[7] D. D. Brunelli, V. C. Barboza, I. Joekes, T. D. Z. Atvars, Journal of Applied Polymer Science, 1998, 69, 645

[8] G. J. Prichard, Poly(vinyl alcohol): Basis principles and uses. Gordon and Breach, New York, 1970

[9] S. Kulanthaisami, D. Mangalaraj, S. K. Narayandass, European Polymer Journal, 1995, 31, 969

[10] B. V. S. Chandar, V. Veeravazhuthi, S. Sakthivel, D. Mangalaraj, S. K. Narayandass, Thin Solid Film, 1999, 348, 122

[11] Awadhia, S. K. Patel, S. L. Agrawal, Progress in Crystal Growth and Characterization of Materials, 2006, 52, 61

[12] R. J. Sengwa, S. Sankhla, Polymer, 2007, 48, 2737

[13] S. Roy, S. Gupta, S. Sindhu, A. Parveen, P. C. Ramamurthy, Composites, 2013, 47, 314

[14] W. E. Mahmoud, A. A. Al-Ghamdi, Polym. Int., 2010, 59, 1282

[15] D. Bhadra, J. Sannigrahi, B. K. Chaudhuri, H. Sakata, Polym. Compos., 2012, 33, 436

[16] S. Mahendia, A. K. Tomar, S. Kumar, J. Alloys Compounds, 2010, 508, 406

[17] Hassen, A. M. El Sayed, W. M. Morsi, S. El-Sayed, J. Appl. Phys., 2012, 112, 093525

[18] P. Dutta, S. Biswas, S. Kumar, Materials Research Bulletin, 2002, 37, 193

[19] T. Mirfakhrai, J. D. W. Madden, R. H. Baughman, Mater Today, 2007, 10, 30

[20] P. Brochu, Q. Pei, Macromol. Rapid Commun., 2010, 31, 10

[21] P. Barber, S. Balasubramanian, Y. Anguchamy, S. Gong, A. Wibowo, H. Gao, H. Ploehn, H. Loye, Materials, 2009, 2, 1697

[22] D. Wang, Y. Bao, J. W. Zha, J. Zhao, Z. M. Dang, G. H. Hu, Appl. Mater. Interfaces, 2012, 4, 6273

[23] P. K. Bipinbal, T. Teena, J. J. Makkolil, K. Narayanan, K. N. Sunil, Advanced Science, Engineering and Medicine, 2015, 7**,** 492

[24] J. Stejskal, I. Sapurina, Pure Appl Chem., 2005, 77, 815

[25] C. R. Martin, Handbook of Conducting Polymers. In: Skotheim TA, Elsenbaumer RL, Reynolds JR, editors. 2nd ed. New York: M Dekker, 1998, 409

[26] R. M. Karim, C. J. Lee, Y. T. Park, M. S. Lee, Synth Met., 2005, 151, 131

[27] Varesano, L. Dall'Acqua, C. Tonin, Polym. Degrad. Stab., 2005, 89, 125

[28] M. Paligova,´ J. Vil_ca´kova,´ P. Sa´ha, V. Kr˘esa´lek, J. Stejskal, O. Quadrat, Physica A, 2004, 335, 421

[29] H. Dong, S. Prasad, V. Nayme, Jr. E. J. Wayne, Chem Mater, 2004, 16, 371

[30] K. Das, D. Ray, N. R. Bandyopadhyay, S. Sengupta, J. Polym. Environ., 2010, 18, 355

[31] T. Badapanda, V. Senthil, S. Anwarb, L. S. Cavalcante, N. C. Batista, E. Longo, Current Applied Physics, 2013, 13, 1490

[32] S. Brunauer, P. H. Emmett, E. Teller, Adsorption of gases in multimolecular layers. J. Am. Chem. Soc., 1938, 60, 309

[33] Q. Li, Q. Z. Xue, X. L. Gao, Q. B. Zheng, Polymer Letters, 2009, 3, 769

[34] V. Raja, A. K. Sharma, V. V. R. Narasimha Rao, Materials Letters, 2004, 58, 3242

[35] K. P. Singh, P. N.Gupta, European Polymer Journal, 1998, 34, 1023

[36] Karmakar, A. Ghosh, Current Applied Physics, 2012, 12, 539

[37] R. Tamura, E. Lim, T. Manaka, M. Iwamotoa, J. Appl. Phys., 2006, 100, 114515

[38] Z. M. Dang, L. Wang, Y. Yin, Q. Zhang, Q. Q.Lei, Adv. Mater., 2007, 19, 852

[39] F. He, S. Lau, H. L. Chan, J. T. Fan, Adv. Mater., 2009, 21, 710

[40] L. Liu, S. Matitsine, Y. B. Gan, L. F. Chen, L. B. Kong, K. N. Rozanov, J. Appl. Phys., 2007, 101, 094106

[41] J.-K. Yuan, W.-L. Li, S.-H. Yao, Y.-Q. Lin, A. Sylvestre, J. Appl. Phys. Lett., 2011, 98, 032901

[42] Dimiev, W. Lu, K. Zeller, B. Crowgey, L. C. Kempel, J. M. Tour, Appl. Mater. Interfaces, 2011, 3, 4657

[43] W. Nan, Prog. Mater. Sci., 1993, 37, 1

[44] J. Liu, C. G. Duan, W. G. Yin, W. N. Mei, R. W. Smith, J. R. Hardy, J. Chem. Phys., 2003, 119, 2812

[45] G. M. Tsangaris, G. C. Psarras, N. Kouloumbi, Journal of Materials Science, 1998, 33, 2027

[46] S. Abdul-Jawad, A. Alnajjar, M. H. Abdallah, Applied Physics A: Materials Science and Processing, 1997, 64, 199

[47] P. Alexy, D. Bakos, G. Crkonova, Macromol. Symp., 2001, 170, 41

[48] W. Zhao, Y. Yamamoto, S. Tagawa. J Polym Sci., 1998, 36, 3089

[49] B. J. Holland, J. N. Hay. Polymer, 2001, 42, 6775

[50] J. K. Kim, C. Hu, R. Woo, M. L. Sham, Compos. Sci. Technol., 2005, 65, 805

[51] H. N. Dhakal, Z. Y. Zhang, M. O. W. Richardson, Compos. Sci. Technol., 2007, 67,1674

[52] T. P. Mohan, K. Kanny, A. Compos, Appl. Sci. Manuf., 2011, 42, 385

[53] H. N. Dhakal, Z. Y. Zhang, M. O. W. Richardson, Compos. Sci. Technol., 2007, 67,1674

[54] N. Graupner, J. Mater. Sci., 2008, 43, 5222

Part B

Development of electrically conducting composites based on CNF and poly(vinyl alcohol)

Conducting polymer composites based on carbon nanofiber, polyaniline and poly(vinyl alcohol) were prepared by solution casting method. Polyaniline was coated on the surface of carbon nanofibers by the in-situ method. The electrical, dielectric, thermal and mechanical properties of the composite was measured. Compared to cellulose based composites, PANI/CNF/PVA composites exhibited improved electrical and mechanical properties. An electrical conductivity of 0.39 S/m was achieved by 50 % PANI/CNF/PVA composite which is about times 10^{12} higher than that of pure PVA. The dielectric constant of about $4.3*10^{8}$ was obtained at 100 Hz frequency. Slight improvement in the mechanical properties was achieved for 10 wt.% composites. Higher fiber loading resulted in agglomeration hence the mechanical properties of the composite are deteriorated. Moreover, the addition of PANI/CNF into PVA matrix resulted in the drastic improvement in the thermal stability of poly(vinyl alcohol). So composites with high DC conductivity, high dielectric constant and good mechanical properties could be developed.

4.B.1 Introduction

Conducting polymers have been considered as the promising materials for capacitors, electronic devise, owing to lightweight, low cost, easy processability etc. [1,2]. Particularly polyaniline is considered as the excellent conducting polymer, due to the high conductivity in the doped state, high redox reversibility etc. Conducting polymer composites can be prepared by the addition of conducting polymers or conducting fibers in

to an otherwise non-conducting polymer. To improve the performance or extend the functions of conducting polymer based devices, the conducting polymers have to be modified. Recently some research groups have developed composites of polyaniline with carbon nanotubes [3,4]. The π-bonds present in the carbon nanotubes facilitate the formation of extended charge transfer between carbon nanotubes and polyaniline by introducing more conductivity to the composite. Therefore, composites based on carbonaceous materials and polyaniline on appropriate stochiometric combination have been proven to be efficient combination. The synergistic combination of outstanding conducting properties of the carbonaceous materials and conducting polymers is an ongoing interest in nanotechnology. Moreover, among the aforementioned carbon materials, carbon nanotubes (CNT) are comparatively expensive and the preparation of graphene is a complex process [5]. Carbon nanofibers (CNF) are alternative choice of materials, which are readily available and cheaper than CNTs. Besides, CNFs have attracted great interest in recent years due its unique one-dimensional structure, excellent electrical, thermal and mechanical properties [6-9]. Therefore, interest in the development of composites based on CNF and PANI is growing recently. Although PANI/CNF composites have been studied extensively, work on the development of sensors, antibacterial agents, fire retarding compounds is in the nascent state. On the other hand, non-conducting materials can be rendered electrically conducting by the modification with electrically conducting polymer.

During the last few years research on the vapor grown nanofiber has been attracted in many fields such as energy storage, energy conversion,

sensors, and for the composite reinforcement [10-15]. Carbon nanofibers are known by excellent mechanical properties, flammability, high electrical conductivity, extraordinary dielectric properties etc. The discovery and development of carbon nanofibers and carbon nanotubes have brought high impact on the carbon fiber industry [16]. Many reports are available in the literature about the reinforcing effect of CNF in polymeric materials [17-19]. The fiber-polymer adhesion is governed by the chemical and physical interactions taking place between the two. If the interaction is not strong enough, composite failure may occur at the interface resulting in reduced longitudinal and transverse mechanical properties. So, one of the most challenging effort of the researchers is to make a strong interface producing good mechanical properties.

The dispersion of carbon nanofiber in PVA matrix is one of the major issues. Carbon nanofibers possess a bundling nature; thus, the CNF fibers exist as small bundles in the polymer matrix. This will produce weak interface and deteriorate the properties. Surface modification of CNF can be done by the coating of polyaniline on the surface. Then CNF fibers are no longer connected to the matrix directly. Otherwise conducting polymer is connected to the polymer matrix. So, by the coating of polyaniline on the surface of carbon nanofiber will enhance the interfacial properties. In this chapter the preparation of novel composite system comprising of carbon nanofiber, polyaniline and poly(vinyl alcohol) is described. The electrical, dielectric and mechanical properties of the composite were studied as a function of fiber concentration.

4.B.2 Experimental

4.B.2.1 Preparation of the composites

3 g of CNF was dispersed in 100 mL of 1 M hydrochloric acid solution by ultrasonication for 1 h. Then the dispersion was kept at 0-4 ^{o}C temperature followed by addition of 10 g of aniline. 12.50 g of ammonium persulfate (APS) was dissolved in 100 mL 1 M HCl solution and was taken in a burette. The APS/HCl was added drop-wise into the aniline-fiber solution to initiate polymerization reaction. The polyaniline-coated fibers (PANI/CNF) were then isolated. Different weight percentages of modified fibers were then mixed with poly(vinyl alcohol) solution in water at 90 ^{o}C followed by ultrasonication for 2 h. Films were prepared by casting and dried slowly at 70 ^{o}C for 24 h.

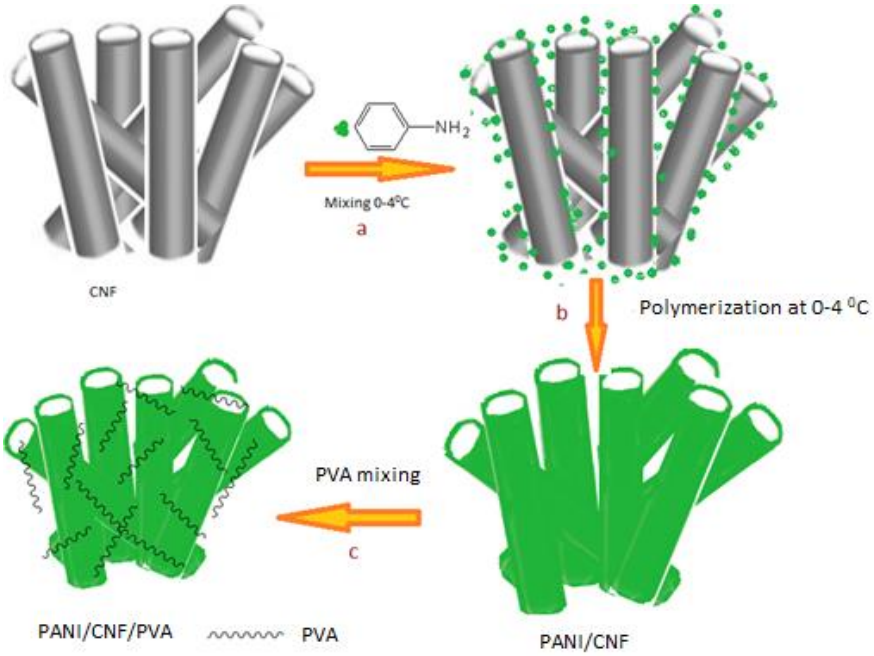

Figure 4.B.1: Schematic representation of the synthetic route for the preparation of PANI/CNF/PVA composite.

The graphitization of CNF takes place at high temperatures results in deposition of crystalline, pyrolytic carbon at the outer edges of CNF. So, the outer surface of CNF is mostly un-reactive. Hence the polyaniline will not undergo any chemical reaction with CNF; instead the aniline oligomers will get attached to the fiber surface and start growing as the reaction proceeds (step a). As the polymerization reaction was continued for 24 h at 0-4 °C a uniform coating of PANI on CNF surface is formed (step b). Many reports are available in the literature regarding the uniform coating of PANI on various substrates [20-22]. Polyaniline coated CNF fibers were added in to the solution of PVA in water (step c). Then the resulting composite mixture was solution casted in to thin films.

4.B.3 Results and discussion

4.B.3.1 Characterization of the composite

4.B.3.1.1 Transmission Electron Microscopy

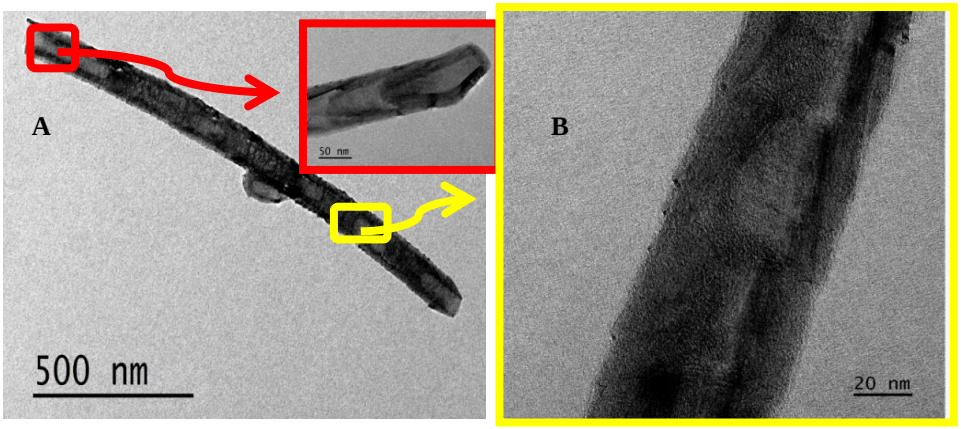

Figure 4.B.2: A) TEM image of pristine CNF; A) low magnification image shows the length of the fiber is of few micrometres, inset to 'A' shows the open tip; B) the high magnification image of CNF showing the parallel cupstcked graphitc arragemenet on the outer wall.

Figure 4.B.2 represents the HR-TEM micrographs of carbon nanofiber at different magnifications. It is evident from the image that CNF possesses huge central hollow core and it has open tips. The open tip is marked in figure 4.B.2A and the enlarged view is given as inset. Large central hollow core with highly active edge sites along the inner wall of CNF is due to the cup stacked orientation of graphene layers. The inner diameter of CNF is approximately 55 nm while the outer diameter is about 90 nm. It confirms that these materials possess high aspect ratio with length of about few micrometers and diameter of few nanometers.

4.B.3.1.2 Scanning Electron Microscopy

SEM images of the PANI/CNF fibers are shown in figure 4.B.3. It shows tubular morphology with core shell structure. Carbon nanofibers as core encapsulated by the polyaniline resulting in the core shell structure. Polymerization of aniline takes place at the surface of carbon nanofibers. So, the nanofibers act as both core and template yielding a polyaniline encapsulated structure. The smooth surface of PANI/CNF fibers indicate the formation of polyaniline chain on CNF through the homogenous nucleation. The diameter of pristine CNF is about 90 nm which is evident from the TEM images. While the modification with polyaniline increased the diameter to 490 nm. SEM micrographs reveal uniform coating of polyaniline on CNF surface and no free CNF are present in the images. So, it is believed that the polymerization is starting on the surface of CNF and it proceeds with time.

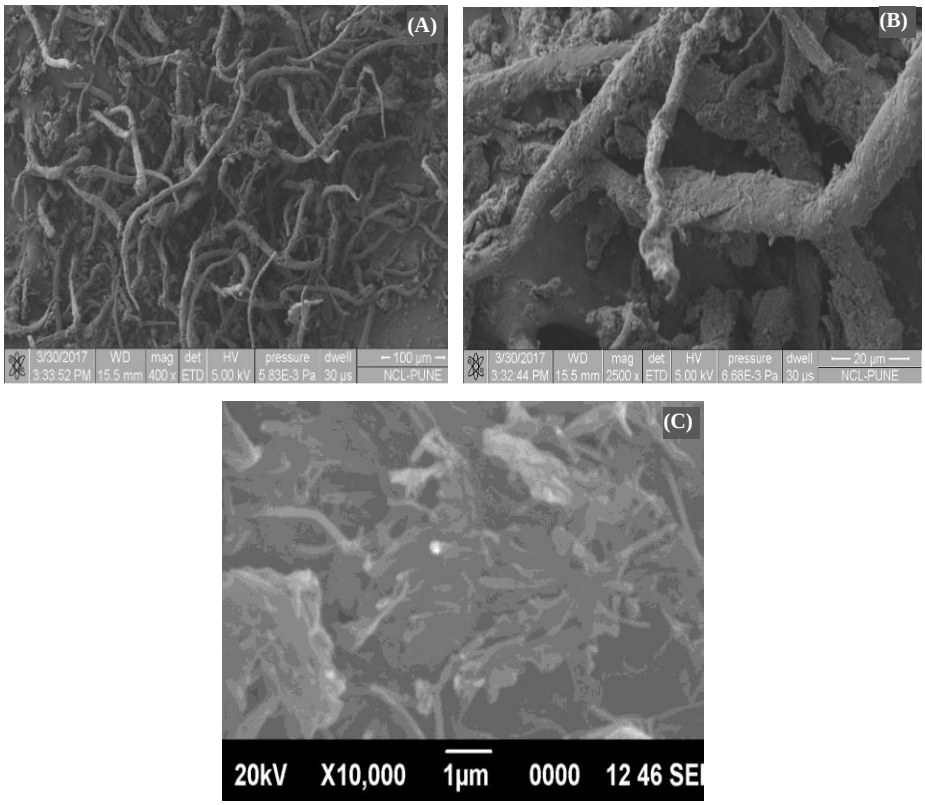

Figure 4.B.3: SEM images of A, B) PANI/CNF fibers, C) PANI/CNF/PVA composite

As shown in figure 4.B.3C, polyaniline coated CNF fibers construct a three-dimensional conductive network. The conductive network formation facilitates the electron/ion transport across the composites. The hydrogen bonding interaction between the hydroxyl groups of PVA and the counter ions of polyaniline results in the good dispersion of PANI/CNF in PVA matrix. PANI/CNF fibers makes an interconnected conducting network in which PVA molecules are entrapped. As the PANI/CNF content increases well defined conductive paths develop in the composite.

4.B.3.1.3 X-ray diffraction

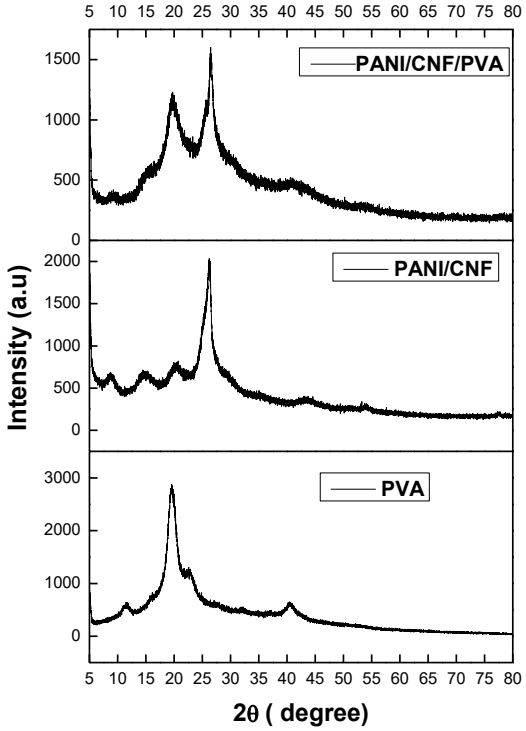

Figure 4.B.4: XRD pattern of PVA, PANI/CNF and PANI/CNF/PVA composite

XRD pattern of PVA, PANI/CNF and PANI/CNF/PVA composite is represented in the figure 4.B.4. Pure CNF exhibits a sharp peak at 2θ of 26.4 °. It can be ascribed to the (002) plane diffractions from the graphitic carbon of CNF. Less intense peaks can also be seen at higher 2θ values correspond to the (100), (101) and (004) planes of the CNF. It shows that carbon nanofibers are well preserved in the composite.

XRD pattern of pure PVA indicates a sharp peak at 19.6 °, typical of crystalline PVA. High degree of crystallinity of PVA indicates the ordered packing of molecular chains. Reduction in intensity is observed

for the crystalline peak of PVA in the composite. This may be due to a different thermal history of the composites and the presence of filler that interacts with the matrix chains. Similar amorphous peak has been reported in the case of hot pressed PVA molecules [23]. The characteristic peaks of polyaniline and CNF are also observed in the XRD pattern of the composite.

4.B.3.1.4 FTIR spectroscopy

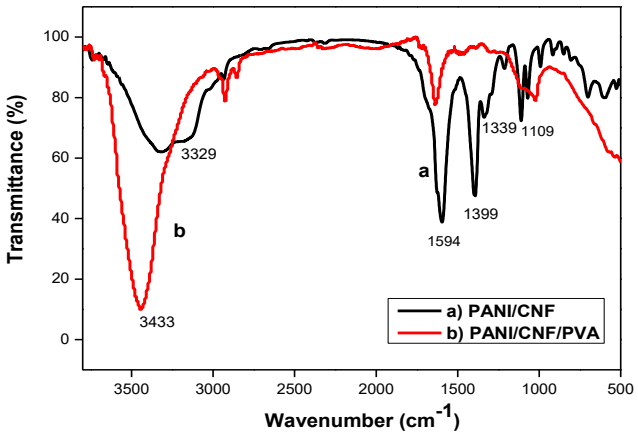

Figure 4.B.5: FTIR spectra of PANI/CNF and PANI/CNF/PVA composites

Figure 4.B.5 depicts the FTIR spectra of PANI/CNF fibers and PANI/CNF/PVA composite. All the characteristic peaks of PANI are reflected in the spectrum of PANI/CNF. The peak at 1339 cm^{-1} is due to the strong aromatic C-N stretching vibrations present in polyaniline. The peaks around 1550-1600 cm^{-1} and 1390 cm^{-1} correspond to the signatures of PANI backbone stretching vibrations of quinoid and benzenoid rings. Broad and high intense peak is observed in the spectrum of the composite. It can be ascribed to the presence of hydroxyl groups of PVA. The

nanofiber dispersion in the polymer matrix is crucial to electrical, dielectric, thermal and mechanical properties of the composite. Favorable nanofiller polymer interactions will increase better dispersion of nanofibers in the matrix which in turn enhances the properties of the composite. FTIR spectra indicates the formation of extensive hydrogen bonding in the composite. Strong hydrogen bonds are mainly formed by the hydroxyl groups of PVA and the counter ions of PANI. Hydrogen bonding interaction benefits to stabilize the dispersion of polyaniline coated carbon nanofibers in PVA matrix.

4.B.3.2 Properties of PANI/CNF/PVA composites

4.B.3.2.1 DC conductivity

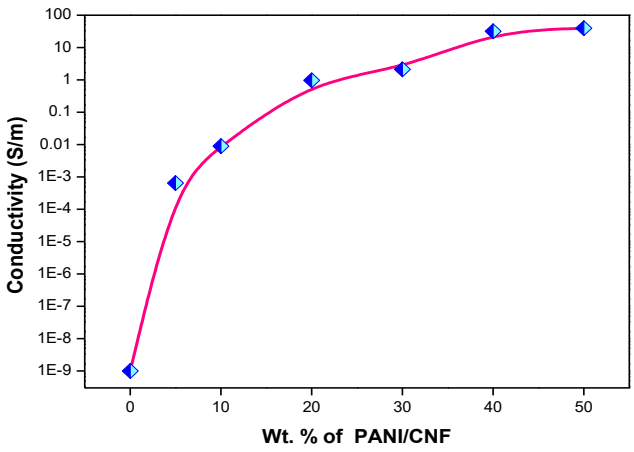

Figure 4.B.6: DC conductivity variation with wt. % of the filler

The variation of DC conductivity of the composites with PANI/CNF is shown in the figure 4.B.6. Tremendous increase of conductivity is observed upon the addition of PANI coated CNF fibers. The conductivity increases from 10^{-9} S/cm to 0.39 S/cm. This huge increase of conductivity supports

the formation of conductive network in the composite. The increase is about 10^{12} times compared to pure PVA. The addition of 5 % PANI/CNF in to PVA matrix increases the conductivity from 10^{-9} to 10^{-3} S/cm. It indicates the highly conductive nature of PANI/CNF fibers. The conductivity keeps on increasing with the addition of PANI/CNF fibers, but the rate of increases is slow. It can be explained by the percolation theory.

Percolation threshold of a material is characterized by the sudden increase of conductivity due to the formation of conductive pathway formed. The formation of conductive network can be well understood from the figure 4.B.7.

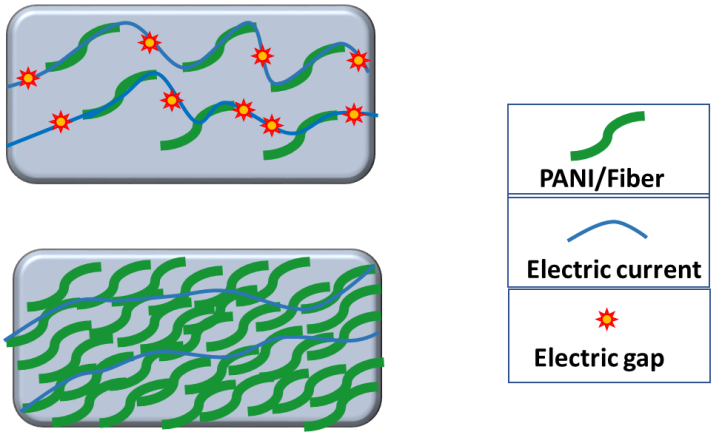

Figure 4.B.7: Schematic representation of formation of conductive network at higher fiber concentrations.

The figure 4.B.7 illustrates the conductive network formation beyond the percolation threshold. For lower wt.% composites, the conducting fibers do not touch one another. Many interfaces are formed by the conducting fiber and insulating matrix, thereby creating energy gaps between the fibres. Hence continuous conducting path is not formed in low concentration

composites. When the concentration reaches in the vicinity of percolation threshold, fibers will be in contact with each other, reducing the conductive resistance. It results in high conductivity values.

4.B.3.2.2 Dielectric properties

4.B.3.2.2.1 Dielectric constant

The dielectric constant as a function of frequency is shown in the figure 4.B.8.A. For all the composites dielectric constant decreases with increase of frequency. The rapid decrease in the dielectric constant is noticed over the frequency range 40 Hz to 10^5 Hz. It may be attributed to the tendency of dipoles in composites to orient themselves in the direction of the applied field in the low frequency range. However, at high frequency range the dipoles are not getting enough time to orient with the alternation of frequency. The polarization due to charge accumulation decreases which will decrease the value of dielectric constant [24,25].

Compared to PANI/Cellulose/PVA composite, PANI/CNF/PVA composite show high dielectric constant. The dielectric constant of 50 % PANI/Cellulose/PVA is about $7.5*10^7$ whereas under the same fiber concentration the dielectric constant is $4.3*10^8$ about for PANI/CNF/PVA composite. The increase in the dielectric constant is due to the good conductive nature of carbon nanofibers. The dielectric properties of a material are dependent upon the conductivity of the filler particles. The dielectric properties increase with the conductivity of the material. Koops et al. described the dielectric permittivity as the inverse of the square root of resistivity [26]. So accordingly, the CNF based composites shows higher permittivity than cellulose composites due to the conductivity difference.

The dielectric properties of the composites can be understood by the percolation theory and interfacial polarization effect. PANI coated carbon nanofibers are dispersed in an insulating PVA matrix. Consequently, the conducting fibers and PVA matrix can form lot of interfaces. The presence of π-orbital of CNF can provide enough domains for free moving electrons. By the application of electric field these electrons get oriented and causes the interfacial polarization. As the concentration of PANI/CNF increases in the PVA matrix, number of interfaces increases thus the interfacial polarization. As a result, dielectric polarization increases with the concentration of PANI/CNF in the composite.

Like PANI/Cellulose/PVA composites, remarkable change in the concavity of the dielectric curves are observed for PANI/CNF/PVA composite also. These inflection points are dependent on filler content of the composites. With increase of filler loading the inflection point shifts to higher frequency. For higher wt.% composites the inflection points are beyond the frequency limit studied.

The dielectric properties of the composite can be understood from the percolation theory and the interfacial polarization effect. The permittivity of composites dramatically increases in the vicinity of the percolation threshold of conductive fillers [27-30]. This kind of increase is more pronounced at higher filler concentrations (close to the percolation threshold) and lower frequency ranges. Recent studies on the dielectric properties of graphene/PVA composites illustrates the formation of strong MWS polarization between the PVA matrix and graphene nanosheets [31].

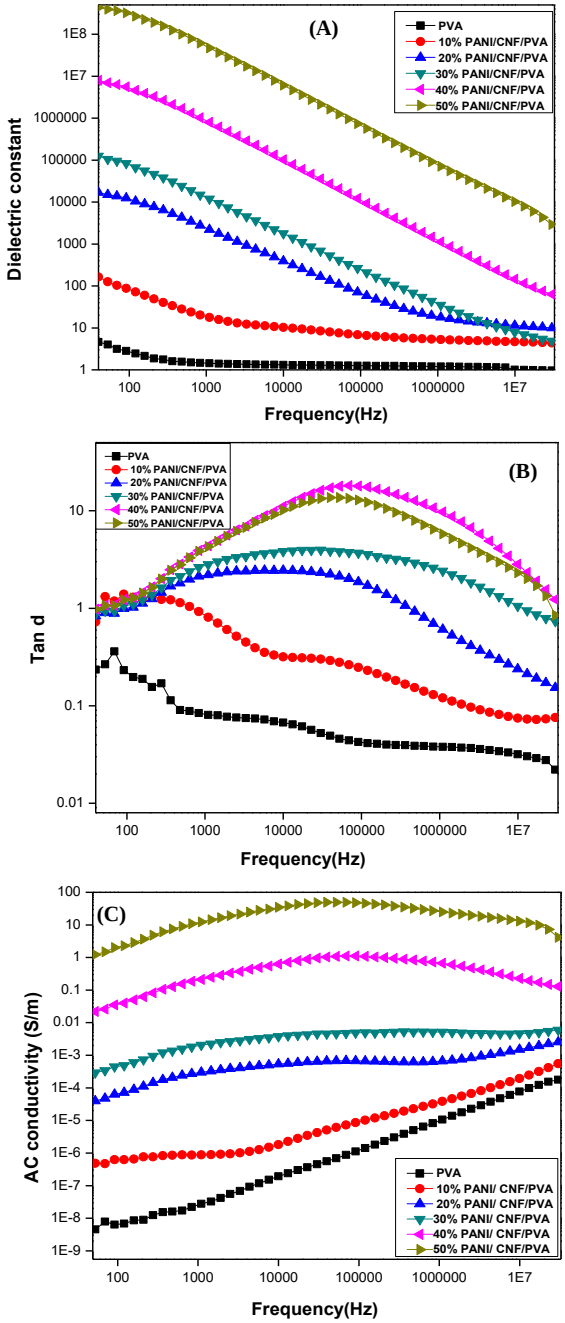

Figure 4.B.8: Dielectric properties of PANI/CNF/PVA composites A) variation of dielectric constant with frequency B) dielectric loss as a function of frequency and C) Variation of AC conductivity with frequency

4.B.3.2.2.2 Loss tangent

Variation of Tan d with frequency is plotted in the figure 4.B.8B. Except PVA all the composites exhibited peak at frequencies higher than 10^4 Hz. These are the relaxation peaks of the composites. Usually polymers possess three types of relaxations, such as α, β and γ. In the present study all the composites exhibit relaxation process called β relaxation. It is caused by the local movements of the side dipole groups of polyanilines. X-Ray diffractogram of the composites revealed the amorphous nature of the materials. In amorphous regions, the chains are irregular and entangled where as in crystalline regions the chains are regularly arranged. So, the movement of molecular chains is easy in the amorphous region than the crystalline region. Due to the well packing in the crystalline state, the density is high compared to the amorphous region. So, the side dipoles will orient themselves with certain frequency. Hence in the amorphous state these dipoles are freer to orient, thus it will contribute to absorption at wide frequency [32,33].

4.B.3.2.2.1 AC conductivity

AC conductivity of the composites was calculated from the permittivity and loss tangent values using the following equation

$$\sigma_{AC}=2\pi f\varepsilon\varepsilon^{*}\tan\delta \quad \text{.....4.B.1}$$

Where, ε is the permittivity of vacuum, f is the frequency of the applied frilled, ε* is permittivity of the material and tan δ is the loss tangent. The external electric field produces the induced charges on the surface of the material. Hence as the frequency increases the charge concentration also increases which will result in the enhanced AC conductivity at higher frequency ranges. The conductivity increase can be otherwise related to the

homogenous dispersion of the conductive filler in the matrix. Good dispersion produces uniformity of charges in the composites. Sudden increase of conductivity is observed or lower wt.% composites. At higher frequencies, all the composites attain almost constant conductivity. Hopping transition is the sudden increase followed by plateau region which occurs in AC conductivity curves, this kind of transition can be seen for pure PVA and lower wt.% composites. But for composites with higher fiber concentration does not lead to such a transition. The AC conductivity of the 50 % PANI/CNF/PVA composites reached a value of 29.59 S/m which is 10^8 times higher than that of pure PVA. Significant improvement in the dielectric properties of the composite is resulted by the incorporation of polyaniline coated carbon nanofibers in PVA matrix. The remarkable improvement is due to the better interaction between the fiber and the polymer matrix. Moreover, the high conductivity of PANI/CNF enhanced the dielectric properties than the corresponding cellulose composites.

4.B.3.2.3 Mechanical properties

4.B.3.2.3.1 Tensile strength

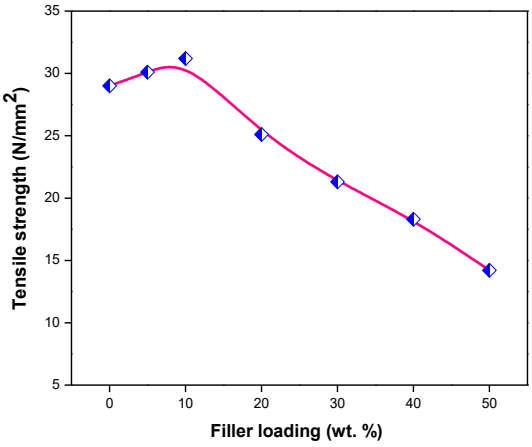

Figure 4.B.9: Variation of tensile strength with filler loading

Figure 4.B.9 shows the variation of tensile properties with PANI/CNF loading. Initially the tensile strength is increased owing to better interaction of polyaniline coated carbon nanofibers with the PVA matrix. The tensile strength of pure PVA is about 29 N/mm^2. The improvement of tensile strength can be explained by the formation of strong hydrogen bonding interaction between the fiber and the matrix. It results in the good dispersion of fibers in the matrix. Hence efficient load transfer occurs. As the concentration of the fiber increases above 10 wt.% reduction in the tensile strength is observed. Similar results are obtained for PANI/Cellulose/PVA composite also.

The FTIR spectra of the composite has established hydrogen bonding interaction between the polyaniline coated carbon nanofibers and PVA matrix. Various research groups have reported on the enhancement of the mechanical properties of the composite by the incorporation of carbonaceous materials [34-40]. Many reports have shown that high fiber loading might reduce the mechanical properties owing to the particle agglomeration [41]. At higher fiber loading due to the poor dispersion, agglomeration of PANI/CNF fibers occurs thereby causing weak filler matrix interface. Hence an efficient stress transfer is not occurring at higher concentration of the fiber. As a result, tensile strength decreases to about 14.2 N/mm^2 for 50 % PANI/CNF/PMMA composite.

4.B.3.2.3.2 Dynamic Mechanical Analysis

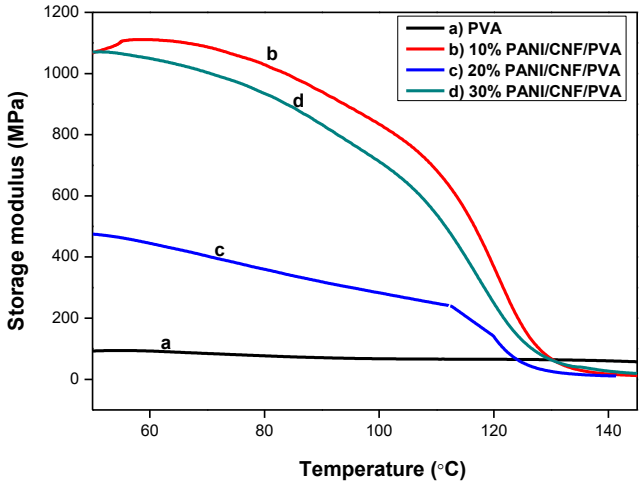

Figure 4.B.10: Storage modulus of PANI/CNF/PVA composites as a function of temperature

The dynamic storage modulus of PANI/CNF/PVA composite as a function of temperature at 1 Hz is represented in figure 4.B.10. The storage modulus of all the composite decreases with increase of temperature. Sudden decrease of storage modulus is observed for lower wt.% composites, while as the fiber content increases the storage modulus decreases gradually with temperature. Compared to cellulose based composites, incorporation of PANI/CNF in to PVA shows drastic increase of storage modulus. The storage modulus obtained for PVA is about 78 MPa, while it is increased to 1066 MPa for 10 % composite at 50 ºC. It indicates efficient stress transfer between PANI/CNF and PVA matrix. The storage modulus decreases after 10 wt.%, it may be due to the agglomeration of PANI coated CNF fibers. The improvement at low fiber content is because of the efficient reinforcing effect of the well dispersed polyaniline coated CNF fibers in PVA matrix. The hydrogen bonding interaction between polyaniline and PVA molecules

results in the uniform distribution of PANI/CNF fibers in PVA matrix. As a result, the PVA chains are immobilized and the storage modulus is increased. The effective immobilization of these chains is responsible for the drastic increase of storage modulus at lower fiber content. The improvement in the storage modulus of the composites depend on the aspect ratio of the dispersed fibers. Nanofiber being a rigid filler, possessing high aspect ratio the polymer interface adjacent to the fiber is highly restrained mechanically.

So it can be believed that the in-situ polymerization of aniline in presence of CNF is the successful way of incorporating CNF in the polymer matrix. Carbon nanofibers serve as nucleating agents for the polymerization of aniline. Hence it increases the dispersibility of CNF in the polymer matrix. The increased mechanical and electrical properties of the composite is due to the efficient distribution of conducting fibers in the PVA matrix. The agglomerating tendency of carbon nanofibers is reduced by the modification with polyaniline.

4.B.3.2.4 Thermogravimetric analysis

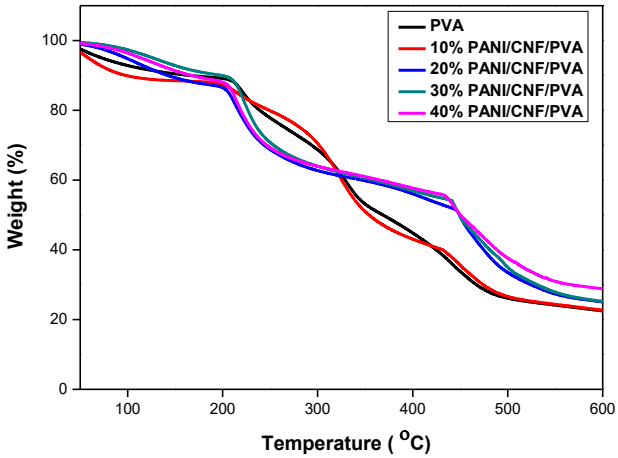

Figure 4.B.11: Thermogravimetric curves of PVA and PANI/CNF/PVA composites

To understand the effect of PANI coated CNF on the thermal properties of the PVA composite thermogravimetric analysis was carried out (Figure 4.B.11). There are two distinct steps in the TG curve of pure PVA, so it can be regarded as a two-step degradation process [42-44]. The first temperature loss corresponds to the breaking of hydroxyl groups of PVA chain. If PVA is heated above 120 °C water is eliminated to give conjugated double bonds, and it may result in the formation of ether cross-links. That means on heating PVA above the decomposition temperature, the polymer starts a rapid chain-stripping elimination of H_2O [45]. The elimination of water molecules from the PVA chain yields a polyene structure. The presence of hydroxyl groups of PVA is evident from the FTIR spectra of the composites. Tsuchiya and Sumi [46] reported the formation of conjugated polyene structures by the dehydration of PVA.

The second weight loss corresponds to degradation of whole polymer chain. It is the most important both in the rate of weight loss and in the total weight loss. The incorporation of PANI/CNF greatly improves the degradation temperature of PVA. The addition of polyaniline modified CNF makes the degradation of PVA more complex process. The degradation of PVA is shifted to higher temperatures. Moreover, the improved thermal stability of the composites can be understood from the weight of residue present for higher wt.% composites. As the content of PANI/CNF in PVA increases the residual mass of the char also increases.

For pure PVA the second weight loss appears at 325 ºC. The major degradation peak at 325 ºC can be an overlap of the continual eliminations

and chain scission reactions which require comparatively higher energy. The second weight loss of PVA is not much clear from the curves of higher wt.% composites. For polyaniline, the major weight loss occurring in a wide range of temperatures, between 350-500 ^{o}C is related to the oxidative decomposition.

4.B.3.2.5 Water absorption behaviour

The specimens for water absorption were immersed in water at room temperature. Initial weight of the sample was recorded and the amount of water absorption was analysed by weighing the sample at certain time intervals (30 min). The water absorbed at the surface was wiped out before weighing. The percentage of water absorption was calculated using the following equation

$$Mt\ (\%) = \frac{wt - wo}{wo} \times 100 \qquad \text{.....4.B.2}$$

Wt is the weight of the sample at time t, Wo is the initial weight of the sample.

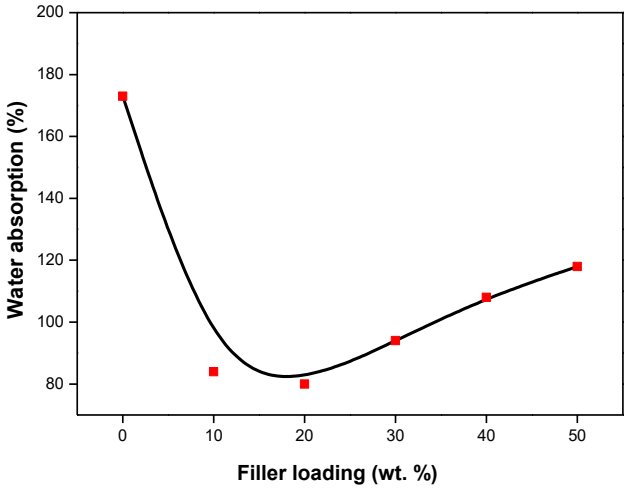

Figure 4.B.12: Water absorption behaviour of PANI/CNF/PVA composites

Figure 4.B.12 represents the percentage of water uptake as a function of filler concentration. The water absorption studies show that the addition of PANI/CNF in to PVA decreased the absorption of PVA. The water absorption increases with the content of PANI/CNF. Unlike PANI/Cellulose fibers, the PANI/CNF/PVA composites did not lead massive increase in the rate of water absorption. It is due to the hydrophobic nature of the CNF fibers incorporated in to the matrix. The rate of water diffusion through any solid material is determined by the diffusivity D, it is also known as flux. The rate of water absorption is more at the initial stages of exposure after that it is slowed down. This is in accordance with the Fickian diffusion process. The water absorption can take place in three different ways. Water can directly diffuse into the matrix, or it diffuses through the interfaces or it can be through the imperfections such as pores or cracks formed during the processing stages. Moreover, the transport of water through a material depends upon many factors like temperature, coating effects etc. [48].

At higher fiber concentrations the homogenous dispersion of fibers may not occur, hence it may result in the increased concentration of the agglomerates. Consequently, the effective interaction with the matrix reduces and more hydroxyl groups will be available for water absorption. In addition to that more cracks and pores will be formed in the composites with poor dispersion. So it enhances the transport of water through the cracks. The equilibrium is attained in 39 h of time which is less than that

of PANI/Cellulose/PVA composites where the composites reached the saturation stage only after 72 h.

4.B.4 Conclusion

Novel PANI/CNF/PVA composite were successfully prepared by solution cast method. The electrical, mechanical, thermal and dielectric characteristics were investigated. Compared to cellulose fiber composite, higher dielectric permittivity together with lower loss factor are achieved for CNF based nanocomposites in frequency range of 40 Hz to 30 MHz. PVA nanocomposite attained an AC conductivity of 29.9 S/m. The addition of PANI coated carbon nanofiber improved the tensile strength and storage modulus of the nanocomposites. But due to the poor compatibility at higher concentration the mechanical properties were decreased. TGA studies showed that the thermal stability of all the composites increased with the addition of fibers. The addition of PANI/CNF in to PVA reduced the percentage of water absorption. These novel nanocomposites with high dielectric performance can find applications in high-charge storage capacitors.

References

[1] H. L. Wang, Q. L. Hao, X. J. Yang, L. D. Lu, Wang, X. Nanoscale, 2010, 2, 2164

[2] J. Wang, Y. L. Xu, F. Yan, J. B. Zhu, J. P. Wang, J. Power Sources, 2011, 196, 2373

[3] W. K. Maser, A.M. Benito, M. A. Callejas, Mater. Sci. Eng., 2003, 23, 87

[4] S. Bhadra, D. Khastgir, N. K. Sinha, J. H. Lee Prog. Polym. Sci., 2009, 34, 783

[5] Q. Cheng, J. Tang, J. Ma, H. Zhang, N. Shinya, L. C. Qin, J. Phys. Chem. C, 2011, 115, 23584

[6] N. Roy, R. Sengupta, A. K. Bhowmick, Prog. Polym. Sci., 2012, 37, 781

[7] R. Sengupta, M. Bhattacharya, A. K. Bhowmick, Prog. Polym.Sci., 2011, 36, 638

[8] J. Jang, J. Bae, M. Choi, S. H. Yoon, Carbon, 2005, 43, 2730

[9] Y. K. Choi, K. Sugimoto, S. M. Song, Y. Ohkoshi, M. Endo, Carbon, 2005, 43, 2199

[10] Z. Wangxi, L. Jie, W. Gang, Carbon, 2003, 41, 2805

[11] J. L. Vilaplana, F. J. Baeza, O. Galao, E. Zornoza, P. Garcés, Materials, 2013, 6, 4776

[12] M. Endo, Y. A. Kim, T. Hayashi, K. Nishimura, T. Matusita, K. Miyashita, M. S. Dresselhaus, Carbon, 2001, 39, 1287

[13] F. Y. Wu, J. H. Du, C. G. Liu, L. X. Li, H. M. Cheng, New Carbon Mater., 2004, 19, 81

[14] J. H. Du, C. Sun, S. Bai, G. Su, Z. Ying, H. M. Cheng, J. Mater. Res., 2002, 17, 1232

[15] F. J. Baeza, O. Galao, E. Zornoza, P. Garcés, Materials, 2013, 6, 841

[16] M. L. Lake, J.-M. Ting, In: Carbon materials for advanced technologies, Burchell, T. D., Ed.; Pergamon: Netherlands, 1999

[17] R. J. Kuriger, M. K. Alam, D. P. Anderson, R. L. Jacobsen, Composites Part A, 2002, 33, 53

[18] E. Lonzo, V. Barrera, Journal of Applied Polymer Science, 2000, 79, 125

[19] R. D. Patton, C. U. Pittman Jr., L. Wang, J. R. Hill, Composites Part A, 1999, 30, 1081

[20] C. R. Martin, Handbook of Conducting Polymers. In: Skotheim TA, Elsenbaumer RL, Reynolds JR, editors. 2nd ed. New York: M Dekker, 1998, 409

[21] R. M. Karim, C. J. Lee, Y. T. Park, M. S. Lee, Synth Met., 2005, 151, 131

[22] Varesano, L. Dall'Acqua, C. Tonin, Polym. Degrad. Stab., 2005, 89, 125

[23] T. Badapanda, V. Senthil, S. Anwarb, L. S. Cavalcante, N. C. Batista, E. Longo, Current Applied Physics, 2013, 13, 1490

[24] J. A. Campbell, A. A. Goodwin, G. P. Simon, Polymer, 2001, 42, 4731

[25] C. Tsonos, L. Apekis, K. Viras, L. Stepanenko, L. Karabanova, L. Sergeeva, Solid State Ionics, 2001, 143, 229

[26] C. G. Koops. Phys Rev., 1951, 83, 121.

[27] L. Liu, S. Matitsine, Y. B. Gan, L. F. Chen, L. B. Kong, K. N. Rozanov, J. Appl. Phys., 2007, 101, 094106

[28] Z. -M. Dang, L. Wang, Y. Yin, Q. Zhang, Q. -Q. Lei, Adv. Mater., 2007, 19, 852

[29] J.-K. Yuan, W.-L. Li, S.-H. Yao, Y.-Q. Lin, A. Sylvestre, J. Bai, Appl. Phys. Lett., 2011, 98, 032901

[30] J. -K. Yuan, S. -H. Yao, Z.- M. Dang, A. Sylvestre, M. Genestoux, J. Bai, J. Phys. Chem. C, 2011, 115, 5515

[31] I. Tantis, G. C. Psarras, D.Tasis, eXPRESS Polym. Lett., 2012, 6, 283

[32] P. K. C. Pillai, P. Khurana, A. Tripattari, J. Mater. Sci. Lett., 1986, 5, 629

[33] R. C. Rastogi, K. L. Chopra, Thin Solid Films, 1975, 27, 311

[34] S. Roy, S. K. Srivastava, J. Pionteck, V. Mittal, Macromol. Mater. Eng., 2015, 300, 346.

[35] Z. Spitalsky, D. Tasis, K. Papagelis, C. Galiotis, Prog. Polym. Sci., 2010, 35, 357.

[36] S. Mallakpour, M. Madani, J. Appl. Polym. Sci., 2015, 132

[37] N. Domun, H. Hadavinia, T. Zhang, T. Sainsbury, G. H. Liaghat, S. Vahida, Nanoscale, 2015, 7, 10294.

[38] S. M. M. Dadfar, G. Kavoosi, Polym. Compos., 2015, 36,145.

[39] N. George, C. S. J. Chandra, A. Mathiazhagan, R. Joseph, Compos. Sci. Technol., 2015, 116, 33.

[40] M. Wegrzyn, O. Sahuquillo, A. Benedito, E. Gimenez, J. Appl. Polym. Sci., 2015, 132

[41] P. Alexy, D. Bakos, G. Crkonova, K. Kolomaznik, M. Krsiak, Macromolecular Symposia, 2001, 170, 41

[42] M. Wegrzyn, O. Sahuquillo, A. Benedito, E. Gimenez, J. Appl. Polym. Sci., 2015, 132

[43] J. W. Gilman, D. L. VanderHart, T. Kashiwagi, In: Nelson GL, editor. Fireand Polymers II: Materials and tests for hazard prevention. Washington, DC: American Chemical Society, 1994, 161

[44] W. W. Zhao, Y. Yamamoto, S. Tagawa. Journal of Polymer Science Part A Polymer Chemistry, 1998, 36, 3089

[45] C. F. Gullis, M. M. Hirshler, In the combustion of organic polymers. Claredon, Oxford, 1981

[46] Y. Tsuchiya, K. Sumi, Journal of Polymer Science Part A-1: Polymer Chemistry 1969, 7, 3151

[47] J. K. Kim, C. Hu, R. Woo, M. L. Sham, Compos. Sci. Technol., 2005, 65, 805

[48] A. Stamboulis, C. A. Baillie, S. K. Garkhail, H. G. H. Van Melick, T. Peijs, Applied Composite Materials, 2000, 7, 273

…..ൠ…..

Chapter 5

CONDUCTING POLYMER COMPOSITES BASED ON POLY(METHYL METHACRLATE)

Contents

Part A

Development of electrically conducting composites based on cellulose and poly(methyl methacrylate)

*High performance dielectric composites based on poly(methyl methacrylate) (PMMA), cellulose fibers and polyaniline were prepared. The electrical, dielectric, thermal and mechanical properties were studied as a function of fiber content, fiber dimensions and polyaniline content. The short cellulose fibers were size-reduced to micro and nano levels prior to coating with polyaniline. Fiber surface was coated with polyaniline by an in-situ polymerization technique in aqueous medium. The composites were prepared by solution casting method. An electrical conductivity of 0.0069 S/cm was achieved by 50 % PANI/Cellulose/PMMA composite. The composites showed a dielectric constant of 2.7 *10^4 at 40 Hz. For the micro- and nano-cellulose fiber composites the dielectric constant was increased to 2.5*10^5 and 1.3*10^8 respectively. The loss tangent of all the composites remained at less than 50. The PMMA nanocomposite attained an AC conductivity of 18.3 S/m. Minor improvement in the mechanical properties was achieved for 10 wt. % composites. Higher fiber loading resulted in the agglomeration and hence deteriorated the mechanical properties of the composite. The incorporation of PANI/Cellulose resulted significant improvement in the thermal stability of PMMA. Thus, it was confirmed that by controlling the size of the fiber used, it is possible to tune the properties to desired values over a wide range. These novel nanocomposites, combining high dielectric constant and low dielectric loss, can be effectively used in applications such as high-charge storage capacitors.*

5.A.1 Introduction

Poly(methyl methacrylate) (PMMA), having the IUPAC name of poly [1-(methoxy carbonyl)-methyl ethylene], is a transparent thermoplastic polymer widely used as the substitute for inorganic glass, because of its good impact strength, light weight and ease of processing. It is a promising material in optical, pneumatic actuation, sensing, analytical separation, and conductive devices [1-5]. It is a material of choice in biomedical applications such as drug delivery systems, polymer electrolytes, electro-osmotic flow etc. [6-10]. PMMA based bone cement has been found to be very efficient for the anchoring of artificial joints [11].

Most of the previous works on PMMA based composites used inorganic fillers for reinforcement [12,13]. Numerous inorganic fillers like talc, calcium carbonate, mica, fly ash etc. have been incorporated in recent years [14-22]. Extra effort has to be taken to use inorganic filler because of poor compatibility with PMMA matrix [23,24]. Attempts have also been made to combine biodegradable materials as fillers [25,26]. The composites based on cellulosic materials is an important area of current research. Cellulose fibers exhibit attractive properties like high specific strength, modulus and low density arising from the unique structural hierarchy derived from biological origin [27-29]. Hence cellulose is being widely used as reinforcing filler in polymer composites for various applications [30,31]. Cellulose–based conducting polymer composite is an attractive proposal. PMMA has been the subject of numerous composite studies focusing on the improvement of strength and durability [32-35]. PMMA nanocomposites have been prepared by the incorporation of

various nanofillers. Improvements in the mechanical properties, thermal stability and flame retardancy were obtained by the addition of nanoparticles [36-41]. The conductivity can be imparted to the cellulose fibers by the modification with suitable conducting polymers.

Contrast to bulk composites, nanocomposites possess several benefits like better biodegradability, good thermal resistance, flame retardancy, improvement in mechanical properties and they are more compatible [42-43]. Despite the good mechanical properties of PMMA, it shows rather low dielectric constant. The dielectric properties of the material can be improved by the incorporation of suitable conducting materials. The development of composite materials possessing high permittivity have become increasingly important for the capacitor applications [44]. Light weight, mechanical flexibility and low processing temperatures are the important characteristics of polymeric materials. Combining the advantages of polymers with those of high permittivity materials, polymer nanocomposites were made with low leakage current and high energy density for capacitor applications [45]. Earlier ceramic materials were employed for the development of high permittivity composites [46-48]. Ceramics were incorporated into the PMMA matrix to improve the overall permittivity of PMMA [49-52].

In this chapter, preparation and properties of cellulose fiber reinforced PMMA based composites are discussed. The dielectric and electrical properties of the composites are studied as a function of filler loading and filler size. The mechanical and thermal properties are also elaborated.

5.A.2 Experimental

5.A.2.1 Preparation of PANI/Cellulose/PMMA composites

The extraction of cellulose from coir fibers is described in chapter 4A. During the chemical treatments cementing materials like hemi-cellulose and lignin were removed. The cellulose fibers thus obtained were dispersed in 100 mL of 1 M hydrochloric acid by sonication for 1 h. Then 5 g of aniline was added and sonication was continued for another half an hour. 6.25 g of ammonium persulfate in 100 mL HCl was added to the reaction mixture from the burette. The polymerization reaction was continued for 24 h at 0-5 ^{o}C. The PANI-coated fibers were collected as solids on a filter, washed repeatedly with distilled water and acetone and dried at 80 ^{o}C for 24 h.

Conducting PANI/Cellulose filler was added to the solution of PMMA in dichloroethane. The composites were fabricated by the solution casting method and the loading of the filler was adjusted to get the 10, 20, 30, 40 and 50 wt.% compositions.

5.A.3 Results and discussion

5.A.3.1 Characterizations of the composite

5.A.3.1.1 Scanning Electron Microscopy

The untreated coir fiber has a diameter of 0.15 mm whereas the diameter of the treated fiber is 0.08 mm. After chemical treatments a decrease in diameter is observed. Polyaniline coating on the fiber surface can be confirmed from the increase in the diameter of the fiber. The

diameter increases from 0.08 mm to 0.13 mm. The formation of a network of PANI coated cellulose fiber in PMMA matrix is apparent from the SEM image (Figure 5.A.1). The network will help to improve the electrical conductivity of the composite. The diameter of fiber in PMMA matrix is found to be 0.12 mm. This shows that PANI is not easily delaminated when added to PMMA matrix.

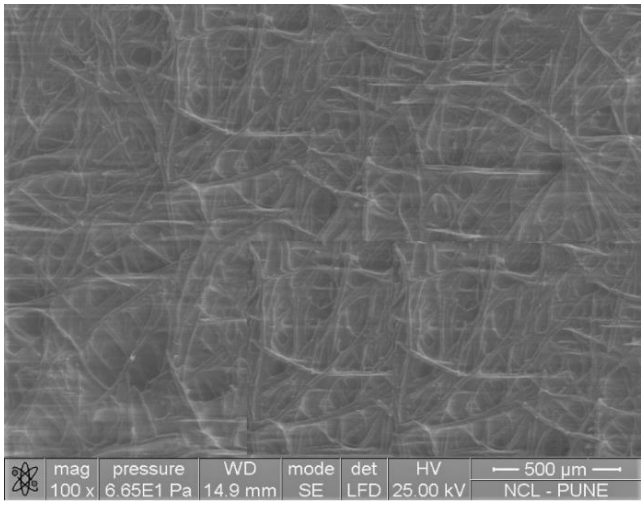

Figure 5.A.1: SEM image of PANI/Cellulose/PMMA composite

5.A.3.1.2 X-ray diffraction

Figure 5.A.2 illustrates the X-ray diffractograms of PMMA, PANI/Cellulose and PANI/Cellulose/PMMA composites in the 2θ range of 5-80 º. PMMA is an amorphous polymer. Absence of any sharp peak confirms its non-crystalline nature. Broad diffraction peaks are observed at 2θ values of 14.3 º and 30.3 º.

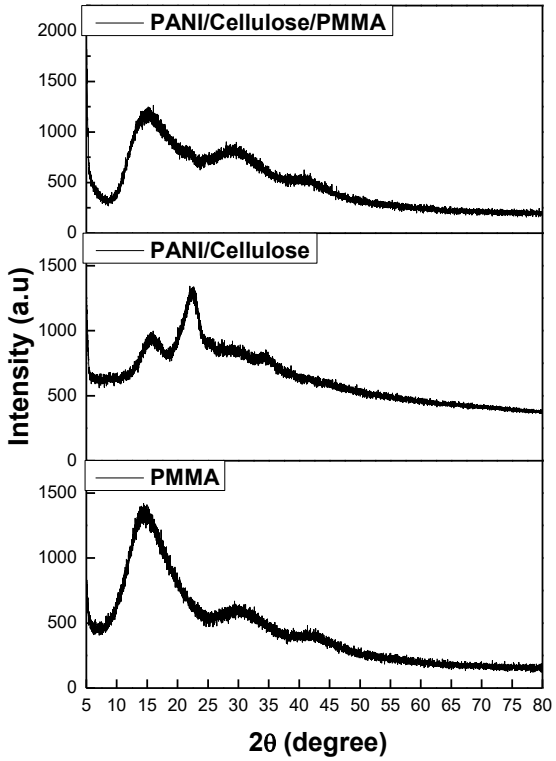

Figure 5.A.2: XRD pattern of PMMA, PANI/Cellulose and PANI/Cellulose/PMMA composite

Absence of sharp peaks at 6.7 º in the diffractogram of PANI/Cellulose indicates the amorphous nature of polyaniline. Conventional coating of polyaniline on cellulose surface results in the thick deposition on the surface. As the thickness increases the control over ordering of chains during polymerization is gradually lost. This results in the lower crystallinity of the composite. The X-ray diffractogram of PANI/Cellulose shows peaks around 2θ of 16 º, 22.5 º corresponding to the typical β-cellulose structure, for the crystallographic planes of (110) and (200) respectively.

5.A.3.2 Properties of the composite

5.A.3.2.1 DC conductivity

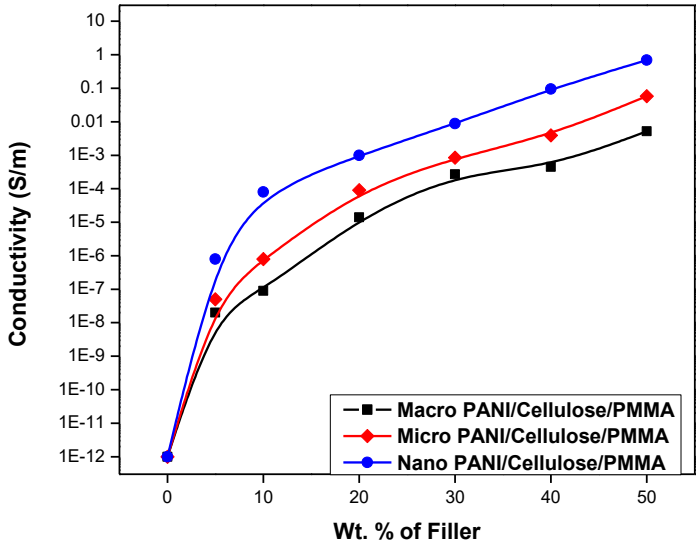

Figure 5.A.3: Variation of DC conductivity with concentration of PANI/Cellulose fiber

The room temperature conductivity of the PANI/Cellulose/PMMA composites against fiber concentration is shown in the figure 5.A.3. The incorporation of polyaniline-coated fibers results in the increase of conductivity. The conductivity of pure PMMA is about 10^{-12} S/m which is increased to about $6.9*10^{-1}$ S/m for 50 % nanocomposite. While such a tremendous increase is not observed for micro and macro composites. The highest conductivities of $5.2* 10^{-3}$ S/m and $5.8* 10^{-2}$ S/m are obtained for macro and micro composites respectively. For micro composite, the DC conductivity increases by 9 orders and for macro it is 8 orders in magnitude.

Inter-connected, conductive network is formed with increase of PANI/Cellulose reduces the conductive resistance at the interfaces. This result correlates directly with the morphological differences between the composites. The particle-particle contact becomes very efficient at low particle size. It is evident from the figure 5.A.3 that the percolation threshold for nano composites is much lower than the other two composites. So, with minimum PANI/Cellulose loading the composite exhibits maximum conductivity.

5.A.3.2.2 Dielectric properties

5.A.3.2.2.1 Dielectric permittivity

The change in the dielectric permittivity with the alteration of frequency is shown in the figure 5.A.5. For all sized composites, the dielectric constant decreases with applied frequency. The dielectric constant decrease is fast in the case of higher wt.% composites. That is the decrease is slow below the percolation threshold. It is clear from the images that a sudden increase of dielectric constant is observed after certain filler loading called percolation threshold. The permittivity at the vicinity of percolation threshold shows highest increase. That means beyond this point the filler particles are connected each other which will help to increase the dielectric value [53-55]. The increase in the permittivity near percolation threshold is more distinct at low frequency region. Frequency independent behaviour is observed for pristine PMMA. As the concentration of the conducting fiber increases the permittivity of the composites is more frequency dependent.

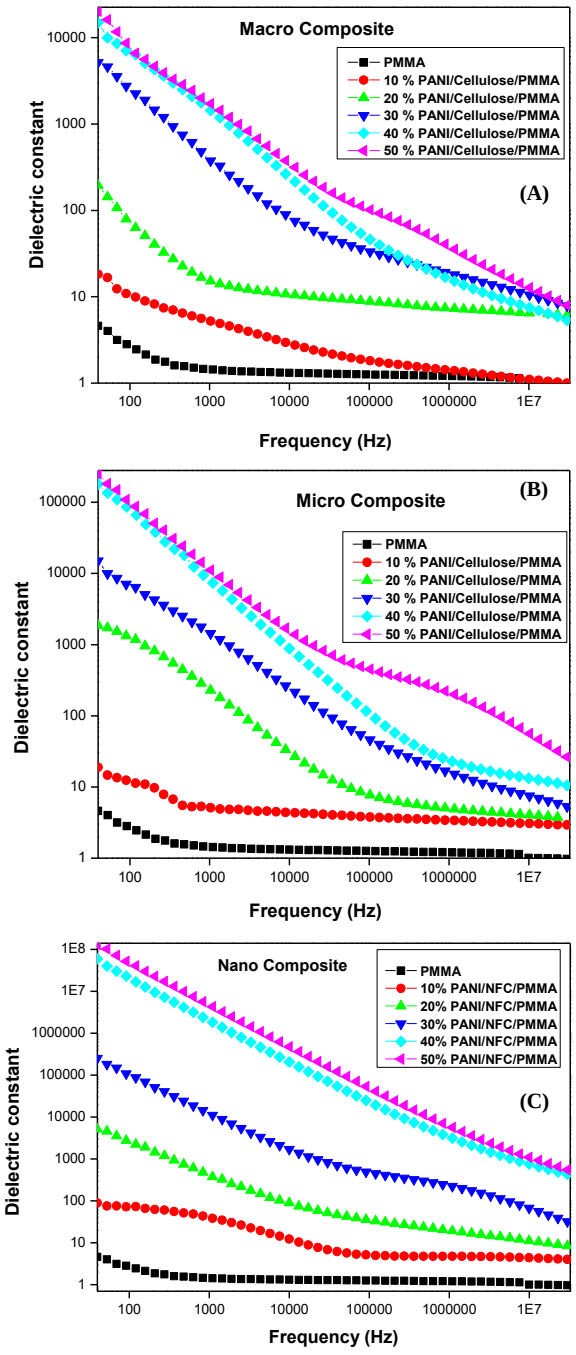

Figure 5.A.4: Dielectric constant as a function of frequency A) Macro composites B) Micro composites C) Nano composites

Compared to PMMA the dielectric constant of the composites is increased dramatically. The increase can be correlated to the interfacial polarization between the conducting PANI/Cellulose fibers and insulating PMMA matrix. The difference in the conductivity of the two causes the polarization at the interface.

The dielectric constant of about 2.7 $*10^4$ is obtained for 50 wt.% macro composites while the dielectric constant is comparatively more for micro composite ($2.5*10^5$). The nanocomposite exhibits very high permittivity of about $1.3*10^8$ for 50 wt.% composite. The size-dependent behaviour of dielectric properties can be easily understood from the permittivity values. The nanocomposite shows approximately 10^8 times higher permittivity. The abrupt increase of dielectric constant compared to pristine polymer is due to the formation of conductive paths in the nano cellulose composite. This significant improvement in nano composites can be related to the small size of the fibers. The nano size of the filler facilitates homogenous dispersion in the polymer matrix leading to the formation of more and more micro capacitor networks [56,57].

Table 5.A.1: Comparison of dielectric constants of three composites at different frequencies.

Frequency (Hz)	**Dielectric Constant**		
	Macro composite 50 %	**Micro composite 50 %**	**Nano composite 50 %**
40	$2.7*10^4$	$2.5*10^5$	$1.3*10^8$
1000	1719	11106	$4.8*10^6$
10000	315	1384	473750
30000000	7.9	26	550

A comparison of dielectric constants of three composites containing 50 wt. % filler at different frequencies is shown in Table 5.A.1. It is interesting to note that under the same filler loading the dielectric constant of nanocomposites is much higher than that of micro- and macro-composites. The nanocomposite shows a maximum of dielectric constant at very low frequency. For nanocomposite the highest dielectric constant is near $1.3*10^8$ and it is about $2.5*10^5$ for micro composite. As the size of the filler reduces the composite exhibits better properties. This dramatic increase in dielectric constant is possibly due to the formation of microcapacitor or nanocapacitor networks by neighbouring conducting polyaniline-cellulose fibers and the insulating PMMA in between. Up to the percolation threshold many conductive paths are formed by PANI coated cellulose fibers. Most of the conductive paths will be connected to each other and some will be isolated by the polymer matrix. But beyond the percolation threshold point high dielectric constant is obtained.

Moreover, Maxwell–Wagner–Sillars (MWS) polarization for heterogeneous systems, is well applicable to the current system [58]. According to MWS mechanism, at the insulator/conductor interface, the entrapment of free charges takes place. This effect is more pronounced at low frequency region where the dielectric constant is more dependent on frequency. The frequency-independent nature of lower wt.% composites below the percolation threshold can be related to the MWS effect. But just above the percolation threshold sudden increase of dielectric constant at low frequencies is observed. That means PANI/Cellulose particles are blocked by the PMMA layers and charges are accumulated at the interface causing interfacial polarization.

5.A.3.2.2.2 Loss tangent

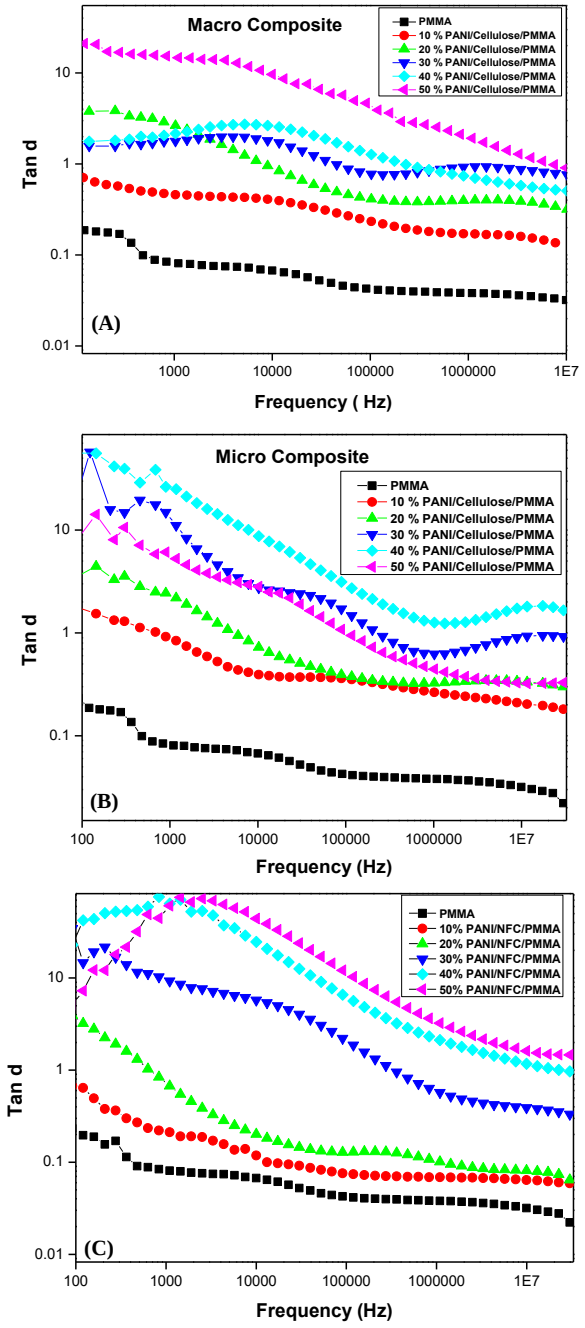

Figure 5.A.5: Dielectric loss as a function of frequency A) Macro composite; B) Micro composite; C) Nano composite

Frequency-dependence of loss tangent of macro, micro and nano composites are represented in the figure 5.A.5. Loss tangent values increase with the concentration of conductive particles. Heat dissipation increases with the energy storage capacity of the material. Hence high loss tangents are observed for high wt.% composites. The frequency-dependence of loss tangent also increases with filler loading. Small relaxation peaks are observed for the loss tangent curves. As represented in figure 5.A.6A, the tan δ values are found to decrease with increasing frequency which may be due to the fall in electrical conductivity of the composites. The increase in the dielectric properties with PANI/Cellulose content is related to the interfacial polarization present in heterogeneous systems [59,60]. Hydrochloric acid doped polyaniline contains electron withdrawing chlorine atoms. The presence of electron withdrawing groups will form strong interfaces with the polymer matrix. This in turn increases the dielectric properties of the composite.

5.A.3.2.2.3 AC conductivity

AC conductivity was calculated from the dielectric permittivity and dielectric loss by the equation

$$\sigma_{AC}=2\pi f\varepsilon\varepsilon^{*}\tan\delta \qquad \text{.....2.B.1}$$

Where, ε is the permittivity of vacuum, ε* is the permittivity of the material, f is the frequency and tan δ is the loss tangent of the material.

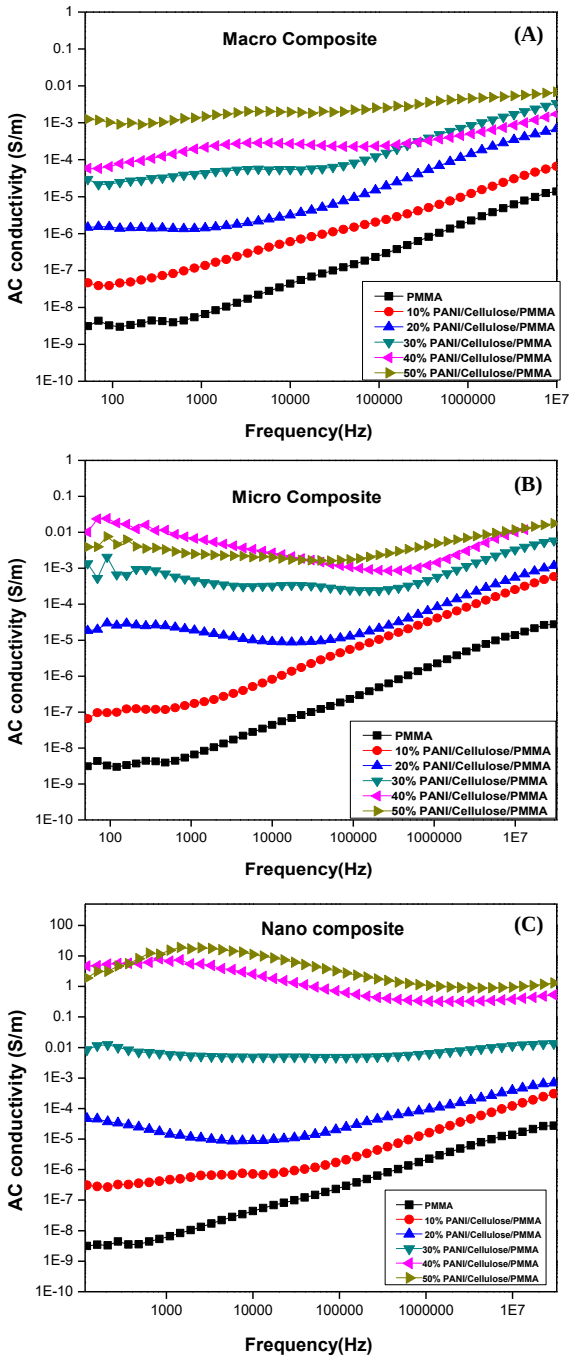

Figure 5.A.6: A) Plot of AC conductivity as a function of frequency for A) Macro composite, B) Micro composite and C) Nano composite

Conductivity of all the composites increase with increase of frequency. This can be attributed to the presence of induced surface currents created by the application of external electric filed. For nanofiber composite a linear increase of AC conductivity with frequency is observed at all fiber loadings. However, for micro and macro composites containing higher weight percentages of fiber a linear increase of AC conductivity is observed.

For composites containing higher fiber concentration a deviation from linear dependence is observed. The conductivity increases with the filler loading. This can be related to the good dispersion of conductive fillers in the matrix.

Usually the application of conductive nano particles to an insulating polymer matrix is supposed to induce an electrical conductivity when the volume fraction exceeds the percolation threshold. The percolation threshold is considered to be lesser for fiber-shaped fillers (high aspect ratio) than for spherical particles. The highest conductivity is achieved for 50 % nano PANI/Cellulose/PMMA composite. The obtained AC conductivity of the composites are 0.002 S/m, 0.014 S/m and 18.3 S/m respectively for macro, micro and nanocomposites.

5.A.3.2.3 Mechanical Properties

5.A.3.2.3.1 Tensile strength

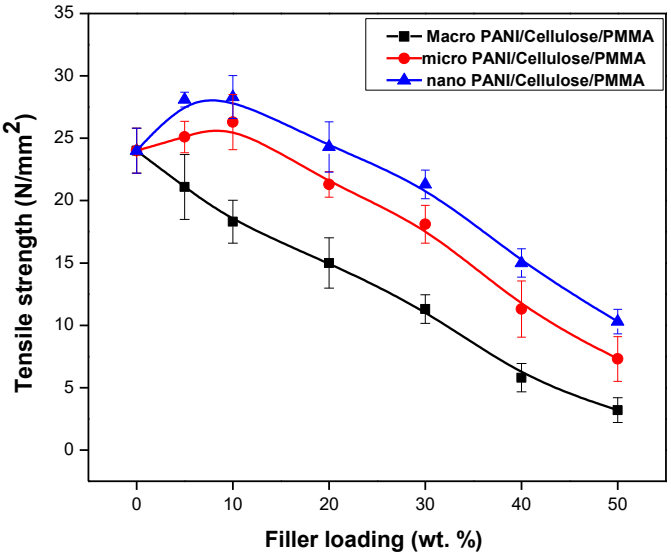

Figure 5.A.7: Variation of tensile strength with filler loading

Figure 5.A.7 shows the variation of tensile strength with PANI/Cellulose fiber at different loadings. The incorporation of polyaniline modified cellulose fibers leads to minor increase in the tensile strength. Up to 10 % fiber concentration the tensile strength increases and thereafter it decreases. It is due to the incompatibility of the fibers in the PMMA system. The composites become less compatible as the fiber content increases leading to lower tensile strength. Poor adhesion between matrix and fiber leads to voids at the fiber-matrix interface and the stress transfer to the fibers becomes inefficient [61]. For micro and nano composites the maximum tensile strength is achieved at 10 % filler concentration. The tensile strength of the nanocomposite increases by 17.9 %. But the increase is less pronounced for micro composite (9.5 %).

Unlike PVA based composites (Chapter 4A), there are no favourable interactions between the fibers and the matrix in case of PMMA composite. Good dispersion and effective interaction of fibers with the PVA matrix helps to increase the tensile strength.

5.A.3.2.3.2 Dynamic Mechanical Analysis

The reinforcing effect of polyaniline coated cellulose fibers in PMMA matrix was tested by dynamic mechanical analysis at a fixed frequency of 1 Hz at a temperature range of 40 to 150 ºC. The variation of storage modulus with temperature is shown in figure 5.A.8. The addition of macro PANI/Cellulose fibers in to PMMA matrix results in decrease of storage modulus. The storage modulus decreases from 1218 MPa to 495 MPa by the addition of 10 % macro PANI/Cellulose at 50 ºC. Unlike macro composite, sudden decrease of storage modulus is not observed for micro PANI/Cellulose/PMMA composite. 10 % micro composite possess similar storage modulus to that of pure PMMA. But further increase of fiber content decreases the storage modulus of the composites.

A higher storage modulus over a temperature range of 40-145 ºC is observed for the nanocomposites. Highest storage modulus is obtained for 10 % nanocomposite. The storage modulus is increased from 1218 MPa to 1558 MPa. The increase is due to the possibility of better interaction through higher surface area of the nano-sized fillers. But for 30 % nanocomposite slight reduction in storage modulus is observed. It can be ascribed to the agglomeration of the fibers.

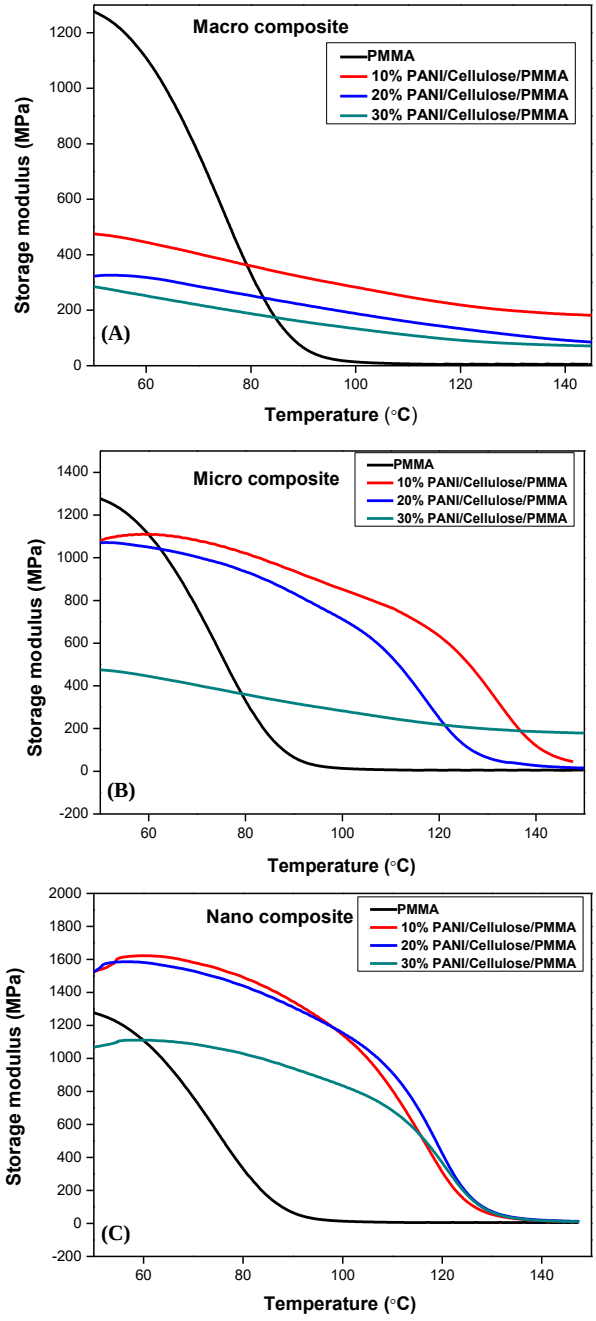

Figure 5.A.9: Storage modulus curves for A) Macro PANI/Cellulose/PMMA, B) Micro PANI/Cellulose/PMMA and C) Nano PANI/Cellulose/PMMA composites

The improvement in the storage modulus strongly depends on the aspect ratio of the dispersed fibers and their interaction with the polymer matrix [62-63]. The lower wt.% composites become stiff with nano PANI/Cellulose fibers. It suggests that better interfacial interaction is taking place with high aspect ratio fibers. The dispersion of the fibers is also found to improve with the size reduction. Pristine PMMA exhibits high storage modulus which decreases greatly with increase of temperature. Nanocomposites at all the wt.% show excellent storage modulus over a wide range of temperature.

5.A.3.2.4 Thermal properties of the composite

5.A.3.2.4.1 Thermogravimetric analysis

The thermal stability of pure PMMA depends on many factors like molecular weight, impurities present and the polymerization method [64-66]. Kashiwagi et al. [67] described the degradation in three different steps. The first step occurs below 200 ^{o}C due to the scissions of head to head linkages. The bond dissociation energy needed for the head to head linkages being less than the C-C back bond owing to large steric hindrance and inductive effect of vicinal ester groups. The second step is initiated by the scissions at unsaturated ends including the homolytic cleavage β to the vinyl group. The last step is the polymer chain degradation. It is caused by the random scissions. After the discovery of kashiwagi, Manring et al. [68] reported a thorough degradation mechanism of PMMA. According to him, the free radical involved in the reaction will be of small size and these free radicals are originating from the impurities present in the material.

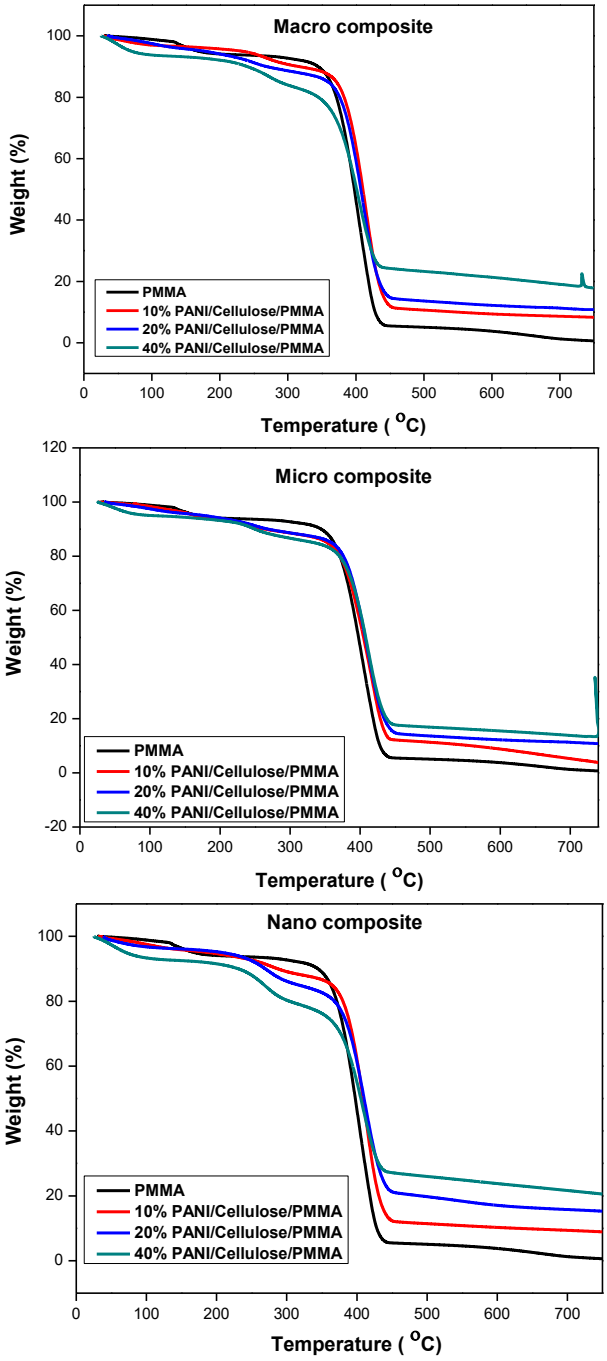

Figure 5.A.9: Thermogravimetric curves of macro composite, micro composite and nano composite

Moreover, he proposed that the main chain degradation is initiated by the homolytic scission of methoxy carbonyl side group. Recently a study of PMMA degradation performed by Holland and Hay [69] concluded that at low temperatures (340–360 ^{o}C) the degradation was initiated by a mixture of chain-end and random scission, followed by de-propagation and first-order termination. While at higher temperature (385–420 ^{o}C), initiation was a mixture of chain-end and chain scission processes followed by de-propagation to the end of the polymer chain.

Table 5.A.2: Thermal characteristics of the composites

Composite	**T onset (^{o}C)**	**T max (^{o}C)**	**Residue at 700 (%)**
PMMA	319.1	403.2	0.73
10% macro	322.3	414.3	8.06
20% macro	324.5	408.3	11.28
40% macro	331.1	409.3	14.40
10% micro	321.6	415.2	5.86
20% micro	327.5	411.9	11.35
40% micro	333.6	414.6	18.93
10% nano	325.6	416.9	10.72
20% nano	329.5	414.6	15.96
40% nano	336.1	413.3	21.55

The thermal stability of PMMA nanocomposite is improved by the addition of PANI/Cellulose fibers. The predominant improvement is observed in case of nano composites. The major degradation peak of PMMA is shifted to higher temperature by the addition of PANI/Cellulose fibers. In the case of nanocomposite, the decomposition peak is shitted to significantly higher temperature. The first stage of degradation of PMMA occurs at about 160 ^{o}C seen as a small peak in the figure 5.A.9. The other two degradations are not clear from the curves.

The degradation steps are not completely separated out. The weight loss of polyaniline occurs at 350-450 ^{o}C. However, the peaks due the polymer degradation and PANI weight loss are overlapped due to simultaneous decomposition of polyaniline and PMMA.

Table 5.A.2 gives the onset of degradation (Tonset), maximum degradation (Tmax) and residue (%). The percentage of char formation is increased in the presence of PANI/Cellulose. For PMMA 0.7 % char is produced which increases to about 14 % for macro composite, 18 % for micro composite and 21 % for nanocomposite. It shows that the composites are becoming thermally more resistant by the incorporation of polyaniline- coated cellulose fibers.

5.A.4 Conclusion

PANI/Cellulose/PMMA composite were successfully fabricated by solution cast method. The electrical, mechanical, thermal and dielectric characteristics were investigated. Three series of PANI/Cellulose/PMMA composites containing fibers in three size ranges i.e. macro, micro and nano were studied. Compared to macro and micro cellulose fiber composite, higher dielectric permittivity together with lower loss factor were achieved for nanocomposites in frequency range of 40 Hz to 30 MHz. Nanocomposite attained an AC conductivity of 18.3 S/m. The addition of PANI coated cellulose fiber improved the tensile strength and storage modulus for micro and nanocomposites. But due to the poor compatibility of macro fiber the mechanical properties were decreased. TGA studies showed that the thermal stability of all the composites increased with the addition of fibers. The result obtained here is an example of how nanoscopic changes in the structure of

conductive filler and the subsequent change in the interfacial polarization can affect the macroscopic properties of composites. These novel nanocomposites with high dielectric performance can find applications in high-charge storage capacitors.

References

[1] B. Adhikari, S. Majumdar, Progress in Polymer Science, 2004, 29, 699

[2] J. J. Shah, J. Geist, L. E. Locascio, M. Gaitan, M. V. Rao, W. N. Vreeland, Electrophoresis, 2006, 27, 3788

[3] L. H. Lee, W. C. Chen, Titania materials. Chem. Mater., 2001, 15, 1137

[4] A. C. Henry, T. J. Tutt, M. Galloway, Y. Y. Davidson, C. S. McWhorter, S. A. Soper, R. L. McCarley, Analytical Chemistry, 2000, 72, 5331

[5] H. Hashim, N. I. Adam, N. H. M. Zaki, Z. S. Mahmud, C. M. S. Said, M. Z. A. Yahya, A. M. M. Ali, Conference on Science and Social Research 2010 (CSSR 2010), Kuala Lumpur, Malaysia, 485

[6] S. Mishra, G. Sen, International Journal of Biological Macromolecules, 2011, 48, 688

[7] M. Shi, J. D. Kretlow, P. P. Spicer, Y. Tabata, N. Demian, M. E. Wong, F. K. Kasper, A. G. Mikos, Journal of Controlled Release, 2011, 152, 196

[8] D. T. Beruto, R. Botter, M. Fini, Biomaterials, 2002, 23, 2509

[9] J. Kost, R. Langer, Advanced Drug Delivery Reviews, 2012, 64, 327

[10] A. Isha, N. A. Yusof, M. Ahmad, D. Suhendra, W. M. Z. W. Yunus, Z. Zainal, Sensors and Actuators B: Chemical, 2006, 114, 344

[11] S. J. Breusch, P. R. Aldinger, M. Thomsen, V. Ewerbeck, k. M. Lukosche. Unfallchirurg, 2000,103, 918

[12] B. Kulyk, V. Kapustianyk, V. Tsybulskyy, O. Krupka, B. Sahraoui, J Alloys Compds., 2010, 502, 24

[13] S. Kim, C. A. Wilkie, Polym. Adv Technol., 2008, 19, 496

[14] S. Bose, P. A. Mahanwar, Journal of Minerals & Materials Characterization & Engineering, 2004, 3, 65

[15] D. C. Deb Nath, S. Bandyopadhyay, A. Yu, D. Blackburn, C. White, J. Mater Sci., 2010, 45, 1354

[16] K. Kishore, S. M. Kulkarni, D. Sunil, S. Sharathchandra, Polymer International, 2002, 51, 1378

[17] N. Chand, S. R. Vashishtha, Bull. Mater. Sci., 2000, 23, 103

[18] S. Bose, P. A. Mahanwar, Journal of Minerals & Materials Characterization & Engineering, 2004, 3, 23

[19] S. Bose, R. Pandey, M. B. Kulkarni, P. A. Mahanwar, Journal of Thermoplastic Composite Materials, 2005, 18, 393

[20] C. Y. Tang, L. C. Chang, J. Z. Liang, K. W. E. Cheng, T. L. Wong, Journal of Reinforced plastics and Composites, 2002, 21, 1337

[21] J. Z. Liang, Journal of Thermoplastic Composite Materials, 2005, 18, 407

[22] A. K. Sharma, P. A. Mahanwar, Int J. PlastTechnol., 2010, 14, 53

[23] H. Lin, D. E. Day, J. O. Stoffer, Polymer Engineering & Science, 1992, 32, 344

[24] K. H. Rao, K. S. E. Forssberg, W. Forsling, Colloids and Surface A: Physicochemical and Engineering Aspects, 1998, 133, 107

[25] A. C. Albertson, O. Ljungquist, Acta Polym., 1998, 39, 95.

[26] N. Tudorachi, C. N. Cascaval, M. Rusu, J Polym.Eng., 2000, 20, 287

[27] V. Favier, G. R. Canova, J. Y. Cavaille, H. Chanzy, A. Dufresne, C. Gauthier, Polym. Adv. Technol., 1995, 6, 351

[28] W. J. Orts, J. Shey, S. H. Imam, G. M. Glenn, M. E. Guttman, J. F. Revol, J. Polym. Environ., 2005, 13, 301

[29] M. Samir, F. Alloin, A. Dufresne, Biomacromolecules, 2005, 6, 612

[30] S. Vitta, V. Thiruvengadam, Current Science, 2012, 102, 1398

[31] S. Tanpichai, F. Quero, M. Nogi, H. Yano, R. J. Young, T. Lindstrom, Biomacromolecules, 2012, 13, 1340

[32] Z. M. Dang, J. K. Yuan, J. W. Zha, T. Zhou, S. T. Li, G. H. Hu, Prog. Mater. Sci., 2012, 57, 660

[33] B. Marrs, J. Biomed. Mater. Res., 2006, 77, 269

[34] Z. M. Li, Carbon, 2005, 43, 2397

[35] J. N. Coleman, U. Khan, Y. K. Gun'ko, Adv. Mater., 2006, 18, 689

[36] V. Skakalova, U. Dettlaff-Weglikowska, S. Roth, Synth. Met., 2005, 152, 349

[37] J. Dai, Q. Wang, W. Li, Z. Wei, G. Xu, Mater. Lett., 2007, 61, 27

[38] M. Marinovic´-Cincovic´, M. C. Popovic´, M. M. Novakovic´, J. M. Nedeljkovic´, Polym. Degrad. Stab., 2007, 92, 70

[39] K. Daimatsu, H. Sugimoto, Y. Kato, E. Nakanishi, K. Inomata, Y. Amekawa, K. Takemura, Polym. Degrad. Stab., 2007, 92, 1433

[40] M. C. Costache, D. Wang, M. J. Heidecker, E. Manis, C. A. Wilkie, Polym. Adv. Technol., 2006, 17, 272

[41] W. J. Lee, S. E. Lee, C. G. Kim, Compos. Struct., 2006, 76, 406

[42] S. S. Ray, M. Bousmina, A. Maazouz, Polym. Eng. Sci., 2006, 46, 1121

[43] S. S. Ray, M. Okamoto, Prog. Polym. Sci., 2003, 28, 1539

[44] Z. Jin, Chem. Phys. Lett., 2001, 43, 337

[45] M. Dang, J. K. Yuan, S. H. Yao, R. J. Liao, Adv. Mater., 2013, 25, 6334

[46] C. J. Dias, D. K. Das Gupta, IEEE Trans., Dielectr. Electr. Insul., 1996, 35, 706

[47] D. K. Das Gupta, Trans Tech., Aedermannsdorf, Switzerland, 1994

[48] R. E. Newnham, Annu. Rev. Mater. Sci., 1986, 16, 47

[49] E. A. Stefanescu, X. Tan, Z. Lin, N. Bowler, M. R. Kessler, Polymer, 2010, 51, 5823

[50] Y. Kobayashi, A. Kurosawa, D. Nagao, M. Konno, Polym. Eng. Sci., 2009,.49, 1069

[51] B. Hussien, Eur. J. Sci. Res., 2011, 52, 236

[52] P. Thomas, R. S. Ernest Ravindran, K. B. R. Varma, J. Poly. Engg. Sci., 2014, 54, 551

[53] L. Liu, S. Matitsine, Y. B. Gan, L. F. Chen, L. B. Kong, K. N. Rozanov, J. Appl. Phys., 2007, 101, 094106

[54] Z. M. Dang, L. Wang, Y. Yin; Q. Zhang, Q. Q. Lei, Adv. Mater., 2007, 19, 852

[55] J. K. Yuan, W. L. Li, S. H. Yao, Y. Q. Lin, A. Sylvestre, J. Bai, Appl. Phys. Lett., 2011, 98, 032901

[56] Z. M. Dang, L. Wang, Y. Yin, Q. Zhang, Q. Q. Lei, Adv. Mater., 2007, 19, 852

[57] Z. M. Dang, J. P. Wu, H. P. Xu, S. H. Yao, M. J. Jiang, J. B. Bai, Appl. Phys. Lett., 2007, 91, 072912

[58] Z. M. Dang, L.Wang, Y. Yin, Q. Zhang, Q. Q. Lei, Adv. Mater., 2007, 19, 852.

[59] H. T. Vo, F. G. Shi, J. Microelectron., 2002, 33, 409

[60] G. C. Psarras, E. Manolakaki, G. M. Tsangaris, Compos. Part A, 2002, 33, 375

[61] S. Dmitri, T. Elvira, K. Andres, M. Pille, Materials Science, 2011, 17, 1392

[62] Y. Dong, D. Bhattacharyya, J. P. Hunter, Composites Science and Technology, 2008, 68, 2864.

[63] A. Maryam, S. Moradian, Polymer plastics technology & Engineering, 2011, 50, 732

[64] J. D. Peterson, S. Vyazovkin, C. A. Wight, Macromol. Rapid Commun., 1999, 20, 480

[65] T. Hirata, T. Kashiwagi, J. E. Brown, Macromolecules, 1986, 19, 2160

[66] T. Kashiwagi, A. Inaba, J. E. Brown, K. Hatada, T. Kitayama, E. Masuda, Macromolecules, 1985, 18, 1410

[67] T. Kashiwagi, A. Inaba, J. E. Brown, K. Hatada, T. Kitayama, E. Masuda, Macromolecules, 1986, 19, 2160

[68] L. E. Manring, D. Y. Sogah, G. M. Cohen, Macromolecules, 1989, 22, 4652

[69] B. J. Holland, J. N. Hay, Polymer, 2001, 42, 4825

Part B

Development of electrically conducting composites based on carbon nanofiber and poly(methyl methacrylate)

Polymer composite based on polyaniline/carbon nanofiber and poly(methyl methacrylate) was prepared by the solution casting method. The prepared thin films were characterized by FTIR, XRD and SEM analysis. The electrical, dielectric, thermal and mechanical properties of the composite were studied as function of fiber concentration. Mechanical properties of the composite were enhanced by the incorporation of polyaniline modified carbon nanofibers. Compared to pure PMMA 10.64 % improvement in tensile strength was observed for 10 wt.% PANI/CNF composites. TGA studies showed that the thermal stability of all the composites increased with the addition of fibers. The 50 % PANI/CNF/PMMA composite exhibited a dielectric constant of $1.4*10^8$ at 40 Hz. This novel nanocomposite combining good electrical, thermal and mechanical properties can be effectively used as charge storage batteries and electromagnetic wave absorbers.

5.B.1 Introduction

In this chapter preparation and characterization of PMMA based composites containing carbon nanofiber as modifying filler is discussed. The electrical and dielectric properties are studied in detail. Research on the development of high performance composites with excellent conductivity and dielectric properties is gaining momentum in nanoscience [1-5]. The synergistic combination of high conductivity of carbon based materials and excellent capacitance of conducting polymers is found to potential breakthrough for the development of efficient composite materials [6-8]. Among the conducting polymer composites, PANI has

frequently been used in the preparation of composites with carbonaceous materials [9,10]. It improves the conductivity of the polyaniline and reduces the agglomeration of the carbonaceous materials [11,12]. Among carbon based materials carbon nanofiber is selected as promising carbon nano morphology. Since it is cheaper than carbon nanotubes and possessing promising properties like high aspect ratio, unique structure resulting from the stacking of individual graphene layers. It is reported that nitrogen containing polymers are used as binder and membrane material which enhances the dispersion of carbonaceous materials [13,14]. The strong π-π interaction between the carbonaceous materials and polymer modulates the electronic properties of the individual components.

In this chapter the preparation of novel nanocomposite system consisting of poly(methyl methacrylate) and polyaniline-coated carbon nanofibres (CNF) is presented. The composites were characterized by various methods. The mechanical, thermal, dielectric and electric properties of the composite were studied as a function of filler loading.

5.B.2 Experimental

5.B.2.1 Preparation of the composites

3 g of CNF was dispersed in 100 mL of 1 M hydrochloric acid solution by ultrasonication for 1 h. Then the dispersion was kept at 0-4 ^{o}C temperature followed by addition of 10 g of aniline. 12.50 g of ammonium persulfate was dissolved in 100 mL 1 M HCl solution and was taken in a burette. The APS/HCl was added drop-wise into the aniline-fiber solution to initiate polymerization reaction. The polyaniline-coated

fibers (PANI/CNF) were then isolated. Different weight percentages of modified fibers were then mixed with poly(methyl methacrylate) solution in dichloroethane at 50 ^{o}C followed by ultrasonication for 2 h. Films were prepared by casting and dried slowly at room temperature for 24 h.

5.B.3 Results and discussion

5.B.3.1 Characterizations of PANI/CNF/PMMA composites

5.B.3.1.1 Scanning Electron Microscopy

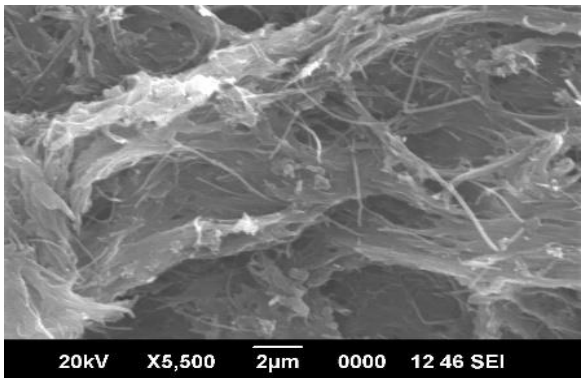

Figure 5.B.1: SEM micrograph of the PANI/CNF/PMMA composite

To provide the insight in to the structural formation and the formation of conductive networks, the composites were characterized by SEM. Well defined conductive paths were formed in the case of PVA-based composites (Chapter 4B). It could be ascribed to the formation of extensive hydrogen bonding between the matrix and filler particles. Whereas such an evenness cannot be observed in PMMA composites. Well dispersion of nanofiber in the polymer matrix is crucial to electrical, dielectric, thermal and mechanical properties of the composite. The formation of conductive network depends on concentration, dispersion

and orientation of conductive fillers [15-17]. It greatly enhances the conductivity of the composites. Sufficient filler concentration is one of the criteria for high contact conductance.

During the polymerization of aniline, aniline oligomers get absorbed on the carbon nanofiber surface. As a result, the diameter of CNF increases from 90 nm to about 400 nm. Figure 5.B.1 represents the surface morphology of PANI/CNF/PMMA composite. The average diameter of PANI coated carbon nanofibers is approximately 400 nm. Hence it demonstrates the deposition of polyaniline on the surface of CNF. The SEM micrograph of the composite suggests low DC conductivity than the PVA analogue.

5.B.3.1.2 FTIR Spectroscopy

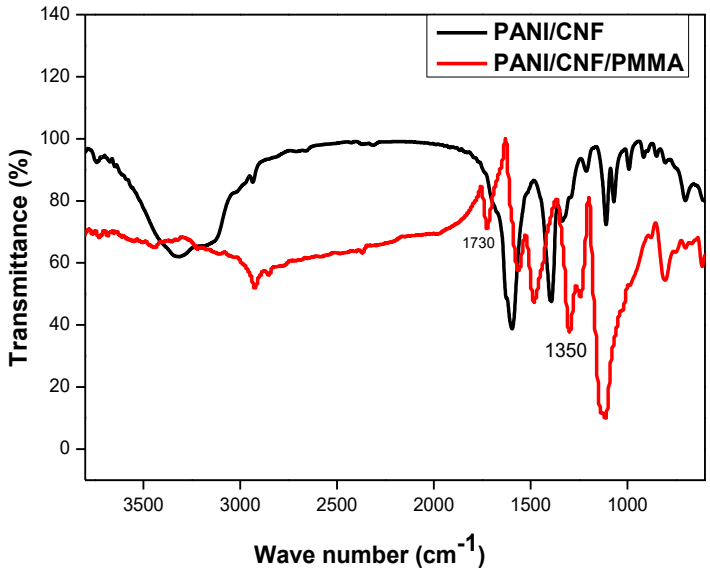

Figure 5.B.2: FTIR spectra of PANI/CNF and PANI/CNF/PMMA composites

Figure 5.B.2 depicts the FTIR spectra of PANI/CNF fibers and PANI/CNF/PMMA composite. All the characteristic peaks of PANI are seen in the spectrum of PANI/CNF. The peak at 1339 cm^{-1} is due to the strong aromatic C-N stretching vibrations present in polyaniline. The peaks around 1550-1600 cm^{-1} and 1390 cm^{-1} correspond to the signatures of PANI backbone stretching vibrations of quinoid and benzenoid rings. The peak around 3200 cm^{-1} is attributed to the N-H stretching vibration of polyaniline [18]. The characteristic vibration bands of PMMA appear at 1730 cm^{-1} (C=O stretching mode). The small peak at 2800 cm^{-1} correspond to the methylene C-H stretching of PMMA while the bands at 1350 $cm^{-1}$and 1450 cm^{-1} are associated with C-H symmetric and asymmetric stretching modes of the same group, respectively. The characteristic vibration peaks of polyaniline indicate that the PANI/CNF is well preserved during the preparation of the composite. FTIR spectra reveal that there is no change in the characteristic peaks. The chances for intermolecular interactions such as hydrogen bonding, dipolar interactions can be neglected. Favorable nanofiller polymer interactions will increase better dispersion of nanofibers in the matrix which in turn enhances the properties of the composite. So, in PANI/CNF/PMMA composite no favorable interactions are taking place between polyaniline-coated carbon nanofibers and PMMA matrix. It may lead to deterioration of the properties of the composite.

5.B.3.1.3 X-ray Diffraction

Comparison of X-ray diffractograms of PMMA, PANI/CNF and PANI/CNF/PMMA composite are shown in the figure 5.B.3. The

diffractogram of PMMA shows one major maximum at 2θ of 14.3 ° and a small peak at 30.3 °.

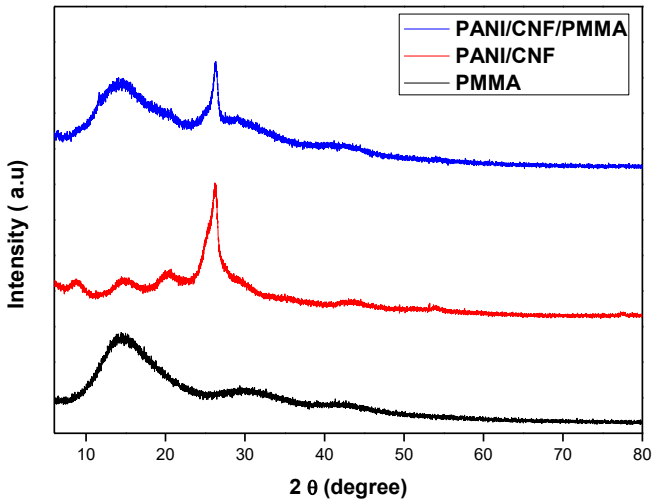

Figure 5.B.3: X-Ray Diffractogram for PMMA, PANI/CNF and PANI/CNF/PMMA composite

The broad peak indicates the ordered packing of polymer chains whereas the small peak gives the effect of ordering inside the main chains. Sharp crystalline peaks are absent in PMMA diffractogram which suggests amorphous nature of PMMA film. Pure CNF exhibits a sharp peak at 2θ of 26.4 °. It can be ascribed to the (002) plane diffractions from the graphitic carbon of CNF. Less intense peaks can also be seen at higher 2θ values correspond to the (100), (101) and (004) planes of the CNF. It shows that carbon nanofibers are well preserved in the composite. The amorphous peak of polyaniline appears at lower 2θ values.

5.B.3.2 Properties of the composites

5.B.3.2.1 Electrical conductivity

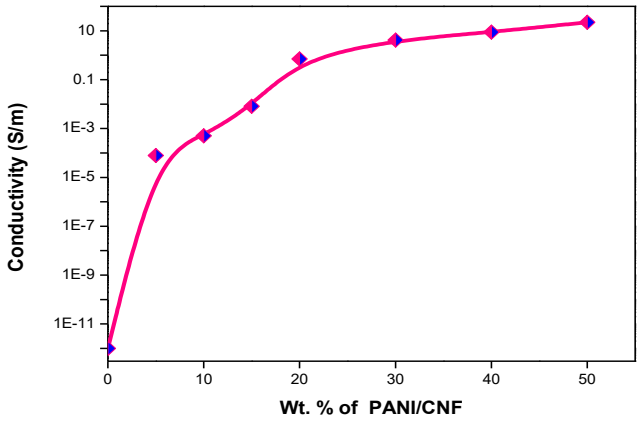

Figure 5.B.4: Change of DC conductivity with PANI/CNF concentration

Figure 5.B.4 shows the bulk electrical conductivity of the PANI/CNF/PMMA composites as a function of PANI/CNF loading. The electrical conductivity of the composite is dependent on the filler volume fraction. The conductivity of pure PMMA is about 10^{-12} S/m. The addition of 5 % PANI/CNF increases the conductivity to 10^{-4} S/m. Tremendous increase of conductivity is observed for even 5 % composite. Conductivity continuously increases with the further addition of conductive filler. The conductivity is increased 10^{13} times at 50 % addition. As the concentration of PANI/CNF in PMMA increases it leads to the formation of conductive network which will produce good interconnectivity between conducting fibers. This in turn reduces the conductive resistance formed by the band gap at the interfaces. The network formation at higher filler concentration is responsible for the sharp increase of conductivity.

The critical loading at which sudden increase of conductivity is called as percolation threshold. It is evident from the figure 5.B.4 that the percolation threshold for PANI/CNF/PMMA composite is below 5 % concentration. After the percolation threshold, the rate of increase of conductivity is not much sharp as before. Connected components are absent below the percolation threshold; above that point, connectivity is established.

Low percolation threshold compared to cellulose-based composites can be attributed to the large aspect ratio of CNF. Once CNF concentration exceeds the percolation threshold, the DC conductivity of the composite increases gradually and attains a stable value. It is interesting to note that the composite with 5 wt.% achieves satisfied electrical conductivity of about $5.0*10^{-4}$ S/m. Further increase of concentration results in an excellent electrical conductivity of about 12 S/m.

5.B.3.2.2 Dielectric properties

5.B.3.2.2.1 Dielectric permittivity

Figure 5.B.5A represents the dielectric constant of PANI/CNF/PMMA composites as function of frequency. Large enhancement is observed for the dielectric permittivity by the addition of PANI/CNF in to PMMA. The dielectric constant of pure PMMA is about 4.9 and it increases to 33450 by the incorporation of 10 % PANI/CNF. As the content of PANI/CNF fibers increases the dielectric permittivity of the composite attains very high values. The dielectric constant for 50 % PANI/CNF/PMMA composite is about $1.4*10^{8}$. This value is higher than the corresponding

cellulose composite. The higher permittivity of CNF based composite can be attributed to the high conductivity of the carbon nanofiber compared to the cellulose nanofiber. The dielectric constant for 50 % PANI/CNF/PMMA is 10^8 times higher than that of pure PMMA. The increase in the dielectric permittivity can be ascribed to the formation of micro capacitor networks in PMMA with the increase of PANI/CNF content in the matrix, as explained in chapter 5A. Polyaniline- coated carbon nanofiber introduces the polar groups in the matrix which will lead to increase the dielectric constant. Polyaniline is a good dielectric material. The observed polarization of a dielectric material has contribution from electronic, ionic and orientational polarizations. Electronic polarization occurs during very short interval of time (10^{-15} s); ionic polarization occurs in the range of (10^{-13}-10^{-12} s) whereas the orientational polarization requires comparatively longer time. Polyaniline noticeably enhances the electrical conductivity as well as the polarizability of the composite. Hydrochloric acid doped polyaniline contains chlorine atoms. Presence of these groups in the composites will increase interfacial polarization. The higher the possibility of polarization the larger will be its dielectric constant.

The dielectric constant of the PANI/CNF/PMMA composites decreases linearly with frequency. However, at higher frequencies the dielectric constant tends to be independent of frequency. High dielectric permittivity is observed at low frequency region which is the signature for all carbon-based materials [19-21]. The frequency-dependent behaviour of the composites at low frequency region can be attributed to the Maxwell- Wagner- Sillar polarization [22,23].

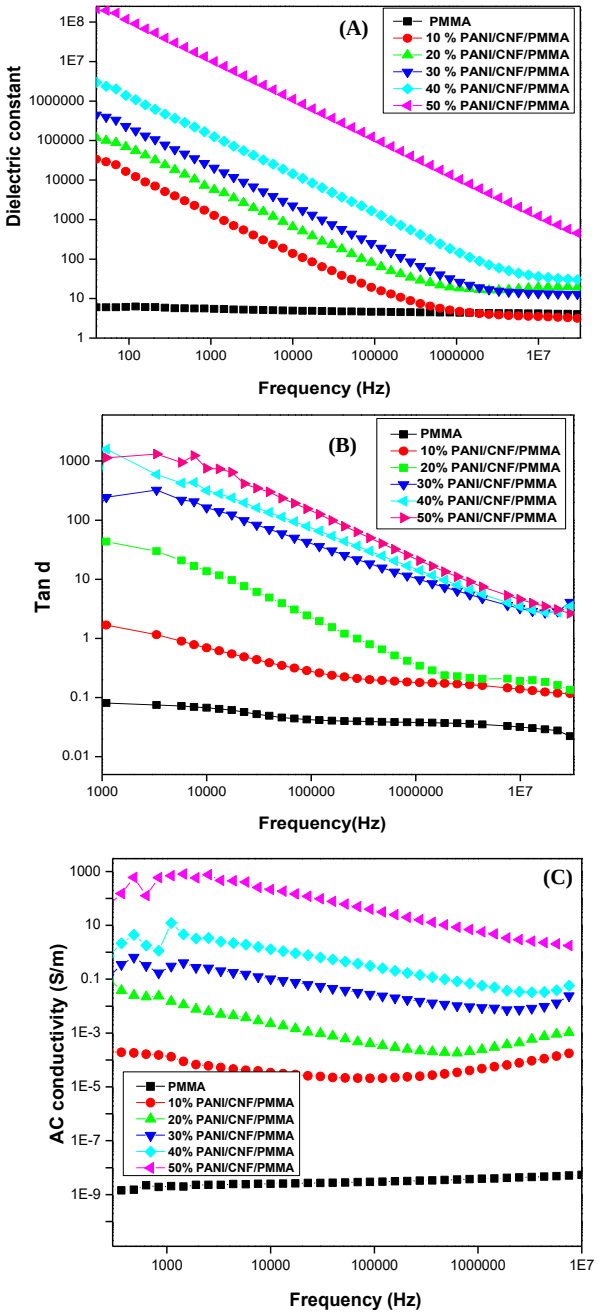

Figure 5.B.5: Dielectric properties of PANI/CNF/PMMA composites A) variation of dielectric constant with frequency B) dielectric loss as a function of frequency and C) Variation of AC conductivity with frequency

The initial frequency-dependent region inflection point shifts to higher frequencies with fiber content. The inflection point for 40 % composite is close to 1MHz, and for 50 % composite it is more than 30 MHz. It may be recalled that in the case of PANI/CNF/PVA composites the inflection points for 40 % and 50 % composites are beyond 30 MHz frequency region. The change in the behaviour of inflection points can be related to the evenness of the conducting fiber dispersed in the polymer matrix. Compared to PANI/CNF/PVA composite lower dielectric constant is obtained for PANI/CNF/PMMA composite. It is mainly due to the poor dispersion of conducting fibers in the PMMA matrix. Hydrogen bonding interaction between PANI/CNF and PVA helps to get a well dispersed structure. But absence of such kind of interaction in PANI/CNF/PMMA composite results in comparatively low dielectric constant.

The percolation threshold of material is dependent on the homogenous dispersion of the filler in the matrix. Near the percolation threshold, the electrical conductivity and dielectric permittivity of the composites increase by several orders of magnitude. When the frequency is greater than $1*10^{-6}$ Hz, the dielectric permittivity of all the composites attains a stable value. Due to the conductivity difference between PANI/CNF fibers and PMMA matrix, accumulation of charges at the interface occurs. As a result, interfacial polarization occurs. At low frequencies the dipoles have the tendency to orient with the applied field. However, at high frequencies dipoles will not get time to orient with the applied field. Hence the dielectric constant decreases at high frequency. The increase of dielectric constant is due to the formation of microcapacitor structures, which is explained in chapter 5A.

5.B.3.2.2.2 Loss tangent

Figure 5.B.5B represents the dissipation factor of the composite as a function of fiber loading and frequency. The dissipation factor of the composite increases with the concentration of PANI/CNF in the composite. At high frequencies, the loss tangent is found to be low as the orientation polarization due to chain motion of polymer becomes out of phase with the rapidly oscillating electric field. Composites which exhibit large dielectric constant also show high loss tangent which can be related to the leakage current. Leakage current will be more pronounced near the percolation threshold when there is direct contact between conductive fillers. Leakage current can be minimized by preventing the contact between conductive fillers.

AC conductivity of the composites was calculated using the equation

$$\sigma_{AC}=2\pi f\varepsilon\varepsilon^{*}\tan\delta \quad \text{.....5.B.1}$$

Where, ε is the permittivity of vacuum, ε* is the permittivity of the material, f is the frequency and tanδ is the loss tangent of the material.

Variation of AC conductivity with frequency is given in the figure 5.B.5C. AC conductivity curves show frequency-independent behaviour. The external electric field produces the induced charges on the surface of the material. Hence as the frequency increases the charge concentration also increases which will result in the enhanced AC conductivity at higher frequency ranges. The highest conductivity is achieved for 50 % PANI/CNF/PMMA composite which is about 672 S/m.

5.B.3.2.3 Mechanical properties

5.B.3.2.3.1 Tensile properties

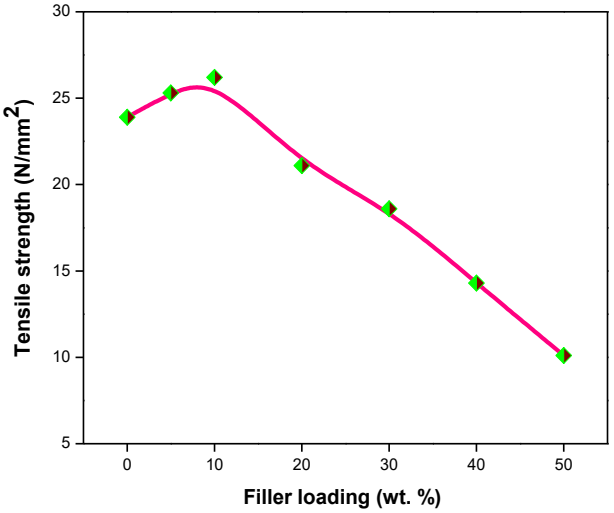

Figure 5.B.6: Tensile strength Vs % of filler loading for PANI/CNF/PMMA composite

The mechanical properties of PANI/CNF/PMMA composites are studied by tensile and dynamic mechanical analysis. Considerable improvement is not observed in the mechanical properties for PANI/CNF/PMMA composite.

The effect of PANI/CNF concentration on the tensile strength of the composite is shown in the figure 5.B.6. At lower filler loading slight increase of tensile strength is observed. The tensile strength of pure PMMA is about 23.9 N/mm^2, by the addition of 10 wt.% PANI/CNF the tensile strength is increased to 26.4 N/mm^2. But after 10 wt.%, the filler particles tend to agglomerate resulting in the reduction in the tensile strength. As a result, the filler particles cannot carry the load applied to

the system. Agglomeration of filler particles at the interface produces stress concentration points. The agglomeration, mostly occurs above 10 wt.% loading. Hence the reduction in the tensile strength is observed. The 10.46 % improvement in the tensile strength can be attributed to the large surface area of the PANI/CNF fibers which facilitates better interaction between the fibers and the polymer. By the improved interaction between filler and matrix, the chain mobility of the polymer will get reduced which in turn increases the tensile strength. A sudden decrease in the tensile strength can be observed beyond 10 wt. % composites. At higher loading, the compatibility reduces, leading to the inefficient stress transfer and thereby reduces the tensile properties [24,25].

5.B.3.2.3.2 Dynamic mechanical analysis

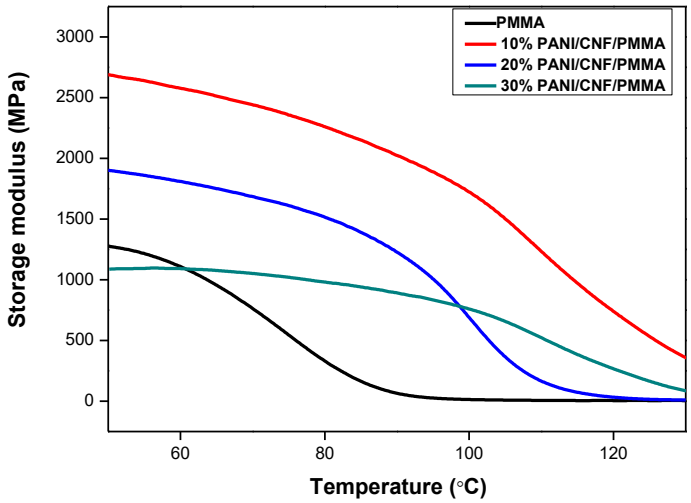

Figure 5.B.7: Variation of storage modulus with temperature

The effect of PANI coated CNF on the viscoelastic properties of PMMA was analysed by dynamic mechanical analysis. The storage modulus of the composites as a function of temperature is shown in the

figure 5.B.7. Significant increase of storage modulus is observed by the addition of PANI/CNF in to PMMA matrix. The effect of fiber is pronounced at lower temperature region. At higher temperatures all the composites acquire almost similar storage modulus values. It can be related to the increased segmental mobility of the polymer chain. At lower temperature the highest storage modulus is obtained for 10 % PANI/CNF/PMMA composite. Compared to PMMA 104 % improvement is obtained. This behaviour is due to the reinforcing effect imparted by polyaniline coated carbon nanofibers. Hence it allows efficient stress transfer at the interface. However, the restraining effect of fibers is significantly operative at the lower temperature region. From the FTIR spectra of the composite, it is evident that there are no favourable specific interactions between PMMA and PANI/CNF. Nevertheless, upon increasing the concentration of PANI/CNF, the mechanical properties decrease.

5.B.3.2.4 Thermal properties

5.B.3.2.4.1 Thermogravimetric analysis

Many reports are available on the thermal degradation of PMMA [26-28], which is described in chapter 5A. The first stage of degradation occurs at about 160 ºC which is seen as a small peak in the figure 5.B.8. The other two degradations are not clear from the curves. The stages are not completely separated out.

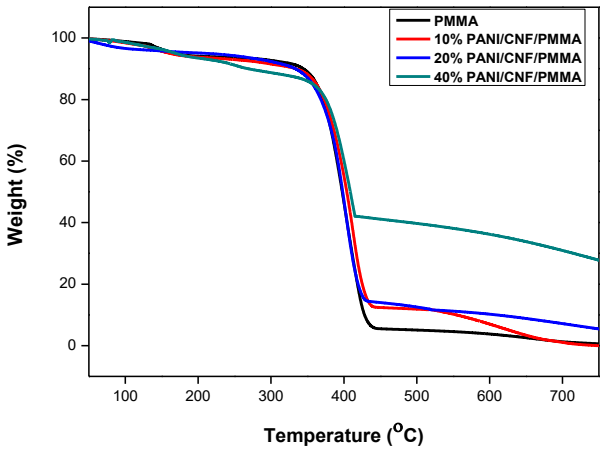

Figure 5.B.8: Thermogravimetric curves of PANI/CNF/PMMA composites

Table 5.B.1: Thermal characteristics of the composite

Composite	T onset (°C)	T max (°C)	Residue at 700 °C (%)
PMMA	319.1	403.2	0.73
10% PANI/CNF/PMMA	321.2	405.3	1.9
20% PANI/CNF/PMMA	323.8	407.6	7.4
40% PANI/CNF/PMMA	325.6	413.2	29.5

The weight loss of polyaniline occurs at 350-450 °C. However, here the peaks due the polymer degradation and PANI weight loss are overlaid resulting in overlapping decomposition of polyaniline and PMMA. Pure PMMA produces char after the elimination of methoxy carbonyl side groups resulting in an unsaturated conjugated system [29]. Whereas the percentage of char formation is increased by the addition of PANI/CNF in to the composite. For pure PMMA, 0.7 % char is produced, which increases to about 30 % by the incorporation of 40 % PANI/CNF in to the

system. It shows that the composites are becoming thermally stable by the incorporation of polyaniline coated carbon nanofibers.

5.B.4 Conclusion

In situ polymerisation of aniline in presence of carbon nanofibers resulted in the uniform coating of polyaniline on CNF surface. Ultra-sonication assisted dispersion reduced the agglomeration of PANI/CNF in PMMA matrix. Unlike PANI/CNF/PVA composites hydrogen bonding interactions are absent in these composites. Hence the property improvement is not as good as in PVA composites. The composite exhibited a dielectric constant of $1.4*10^8$ at 40 Hz. In contrast to PANI/Cellulose/PMMA composites, higher dielectric permittivity together with lower loss factor are achieved for CNF based nanocomposites in frequency range of 40 Hz to 30 MHz. Mechanical properties of the composite were enhanced by the incorporation of polyaniline modified carbon nanofibers. Compared to pure PMMA 10.64 % improvement was observed in the tensile strength of 10 wt.% PANI/CNF. The storage modulus of the composite increases indicating better dispersion of the PANI/CNF in the matrix. TGA studies showed that the thermal stability of all the composites increased with the addition of fibers.

References

[1] Y. Yan, Q. Cheng, G. Wang, C. Li, J. Power Sources, 2011, 196,7835

[2] X. Yan, J. Chen, J. Yang, Q. Xue, P. Miele, Appl. Mater. Interfaces, 2010, 2, 2521

[3] E. Frackowiak, V. Khomenko, K. Jurewicz, K. Lota, F. Beguin, J. Power Sources, 2006, 153, 413

[4] M. Ertas, R. M. Walczak, R. K. Das, A. G. Rinzler, J. R. Reynolds, Chem. Mater., 2012, 24, 433

[5] D. W. Wang, F. Li, J. P. Zhao, W. C. Ren, Z. G. Chen, J. Tan, Z. S. Wu, I. Gentle, G. Q. Lu, H. M. Cheng, ACS Nano, 2009, 3,1745

[6] W. Fan, C. Zhang, W. W. Tjiu, K. P. Pramoda, C. He, T. Liu, ACS Appl. Mater. Interfaces, 2013, 5, 3382

[7] G. A. Snook, P. Kao, A. S. Best, J. Power Sources, 2011, 196, 1

[8] K. Zhang, L. L. Zhang, X. S. Zhao, J. Wu, Chem. Mater., 2010, 22, 1392

[9] N. A. Kumar, H. J. Choi, Y. R. Shin, D. W. Chang, L. Dai, J. B. Baek, ACS Nano, 2012, 6, 1715

[10] Y. Liu, R. Deng, Z. Wang, H. J. Liu, Mater. Chem., 2012, 22,13619.

[11] L. Li, Z. Y. Qin, X. Liang, Q. Q. Fan, Y. Q. Lu, W. H. Wu, M. F. Zhu, J. Phys. Chem. C, 2009, 113, 5502

[12] H. Wang, Q. Hao, X. Yang, L. Lu, X. Wang, Nanoscale, 2010, 2, 2164

[13] G. G. Tibbetts, G. L. Doll, D. W. Gorkiewicz, J. J. Moleski, T. A. Perry, C. J. Dasch, M. J. Balogh, Carbon, 1993, 31, 1039

[14] M. Okamoto, T. Fujigaya, N. Nakashima, Adv. Funct. Mater., 2008, 18, 1776

[15] S. I. White, B. A. DiDonna, M. Mu, T. C. Lubensky, K. I. Winey, Phys. Rev. B, 2009, 79, 024301

[16] S. Nam, H. W. Cho, S. Lim, D. Kim, H. Kim, B. J. Sung, ACS Nano, 2013, 7, 851

[17] H. W. Cho, S. Nam, S. Lim, D. Kim, H. Kim, B. J. Sung, J. Appl. Phys., 2014, 115, 154307

[18] M. Amrithesh, S. Aravind, S. Jayalekshmi, R. S. Jayasree, J. Alloys Compd., 2008, 449, 176

[19] A. Higginbotham, J. Stephenson, R. Smith, D. Killips, L. C. Kempel, J. M. Tour, J. Phys. Chem. C, 2007, 111, 17751

[20] C. Xiang, Y. Pan, X. Liu, X. Sun, X. Shi, J. Guo, Appl. Phys. Lett., 2005, 87, 1231031

[21] C. A. Grimes, E. C. Dickey, C. Mungle, K. G. Ong, D. Qian, J. Appl. Phys., 2001, 90, 4134

[22] F. He, S. Lau, H. L. Chan, J. T. Fan, Adv. Mater., 2009, 21, 710

[23] Z. M. Dang, L. Wang, Y. Yin, Q. Zhang, Q. Q. Lei, Adv. Mater., 2007, 19, 852

[24] S. Dmitri, T. Elvira, K. Andres, M. Pille, ISSN 1392–1320 Material science, 2011, 17, 1

[25] B. Elif, U. Nuray, O. Aysen, W. Youjiang, O. Mustafa, A. Onur, U. Mehmet, D. Ali, J. Appl. Polymer Sci., 2012, 125, 2882

[26] L. E. Manring, Macromolecules, 1989, 22, 2673

[27] L. E. Manring, Macromolecules, 1991, 24, 3304

[28] L. E. Manring, Macromolecules, 1988, 21, 528

[29] H. Nobuyuki, S. Hideki, N. Masazo, Macromolecules, 1989, 22, 4652

Part C

Impact of bis –(3-triethoxysilylpropyl)tetrasulphide on the properties of PMMA/Cellulose composite

Poly(methyl methacrylate) (PMMA)-microcrystalline cellulose composites with improved interfacial interaction were prepared by solution casting method using Bis-(3-triethoxysilylpropyl) tetrasulphide (Si69) as coupling agent. The incorporation of microcrystalline cellulose into PMMA enhanced the mechanical as well as thermal properties over that of base polymer but not remarkably. So in the current study Bis-(3-triethoxysilylpropyl) tetrasulphide (Si69) is used as a coupling agent to improve PMMA-Cellulose adhesion. The composites were characterized using FTIR, ^{13}C NMR, UV-Vis, ^{29}Si NMR, XRD and SEM analysis. The results indicated that Si69 formed chemical bonds with both PMMA and cellulose. The effect of Si69 on the physical and mechanical properties of PMMA/Cellulose composite was investigated. Thermogravimetric analysis and differential scanning calorimetry studies showed that the degradation temperature and glass transition temperature of PMMA shifted to higher temperature. The addition of silane coupling agent in to the PMMA/Cellulose improved the mechanical properties. The impact strength increased up to 72 %, flexural strength by 37 %. The composite exhibited 49 % higher tensile strength and 50 % storage modulus than pristine PMMA. The addition of cellulose to PMMA increased the dielectric constant and attained an AC conductivity of $1.4*10^{-4}$ S/m. The result proved that Si69 is compactable to both PMMA and cellulose and can be used as an effective coupling agent for PMMA/Cellulose system.

5.C.1 Introduction

Recent surge in the ecological awareness and efforts to protect environment have led to the manufacture of low cost biodegradable materials with enhanced properties. Cellulose and its derivatives being abundant, renewable and eco-friendly gained great attention, as

reinforcing filler in polymer composite [1-8]. These include composites based on thermoplastic and rubbers [9-11]. Because of the flexibility during the processing and high stiffness and cheap rate of plastic lead to the drastic use as a matrix for fibers. Natural fiber reinforced composite with excellent tensile properties has achieved for the fiber/thermoset resin composites [12].

PMMA is a versatile synthetic polymer with many desirable properties and industrial as well as pharmaceutical applications. High strength, excellent optical clarity and dimensional stability are some of the special features of PMMA.

Use of organic cellulose fibers as filler in the PMMA matrix is expected to make it stronger and more environmental friendly. This area is not much explored as others. Liu et al. [26] prepared PMMA-cellulose composites by solvent casting method. Dong et al. [27] extracted nanocrystal cellulose from wood systems and used to reinforce PMMA fibers. The enhancement in the properties of PMMA by the incorporation of cellulose nanoparticles was studied by Sain et al. [28]. Fahma et al. observed the improvement in the mechanical and thermal properties of PMMA system by the incorporation of nanocellulose [29].

The mechanical properties of the composite strongly dependent on the linkage between the filler and matrix. The nature of interaction between the hydrophilic cellulose and the hydrophobic PMMA is critical in the development of strong composites. Coupling agents are the chemical substances that can create a chemical bridge at the interface between the matrix and filler to improve the strength in such composites. Silanes are

efficient coupling agents extensively used in composites. Large variety of silane coupling agents are available in the market, among them I have chosen Bis –(3-triethoxysilylpropyl)tetrasulphide (Si69) for this study in order to get better the compatibility and dispersion of cellulose fiber in PMMA matrix.

This work is designed to develop PMMA/Cellulose micro composites and to study the effect of the coupling agent, Si69, on the dynamic mechanical, dielectric and thermal properties. The characterization of the composite has been done using FTIR, UV-Vis ,^{13}C NMR, ^{29}Si NMR, XRD and SEM analysis.

5.C.2 Experimental

5.C.2.1 Preparation of composites

The composites were fabricated by the solution casting method. PMMA was dissolved in 1,2-dichloroethane at 80 ^{o}C. Micro crystalline cellulose and Si69 (10 wt. % of the filler) were added to the solution of PMMA. Then the reaction mixture was stirred using mechanical stirrer for two hours. After that it was solvent casted at 60 °C. The thickness of casted films was about 2 mm. After that the films were crushed mechanically. The resulting blends were injection molded in DSM Explore, micro 12 cc injection molding machine at 190 °C for 8 minutes, to prepare test samples for impact, tensile, and flexural testing according to the relevant ASTM standards. The samples for XRD were prepared by cracking injection molded specimens with sharp tools.

5.C.3 Results and discussion

5.C.3.1 Characterization of cellulose

5.C.3.1.1 Scanning Electron Microscopy

The morphology of microcrystalline cellulose was explored using Scanning Electron Microscopy. Image depicts fiber like morphology with an average diameter of 20 μm.

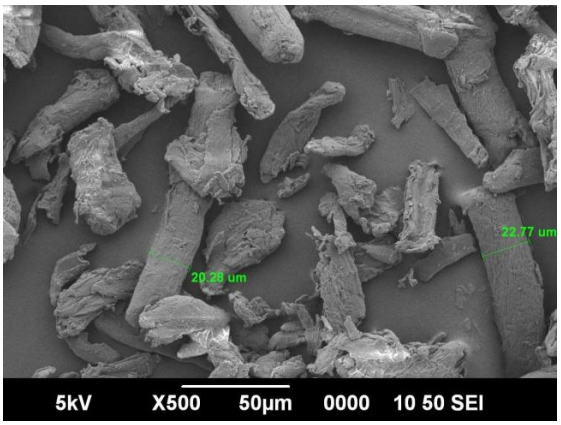

Figure 5.C.1: SEM image of microcrystalline cellulose

5.C.3.1.2 BET surface area analysis

The surface area and porosity of the cellulose were measured by nitrogen adsorption-desorption experiments at 77.3 K (Figure 5.C.2). Following the general classification of adsorption isotherms, the shape obtained is of type IV isotherm. BET surface area is found to be 0.9198 m^2/g. The average pore diameter obtained for cellulose is about 19.3 nm, indicating a mesoporous nature of the fibers.

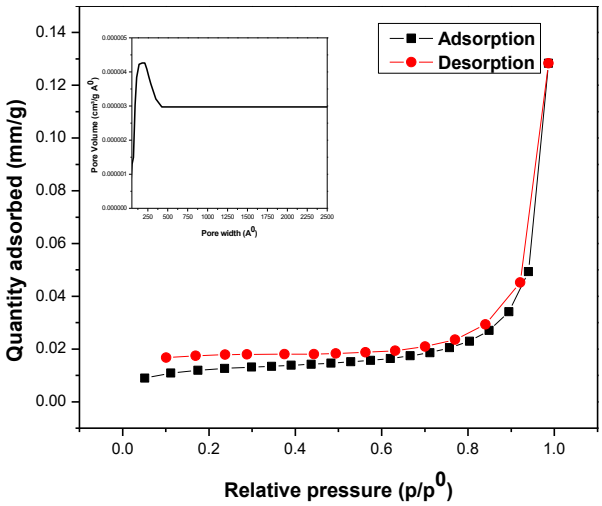

Figure 5.C.2: Adoption-desorption isotherm and pore size distribution of cellulose

5.C.3.1.3 Particle size analysis

Dynamic light scattering method was adopted to find out the size of cellulose used for composite preparation. Particle size was determined by measuring the random changes in the intensity of light scattered from the water suspension of cellulose. The size distribution of cellulose is given in figure 5.C.3A.

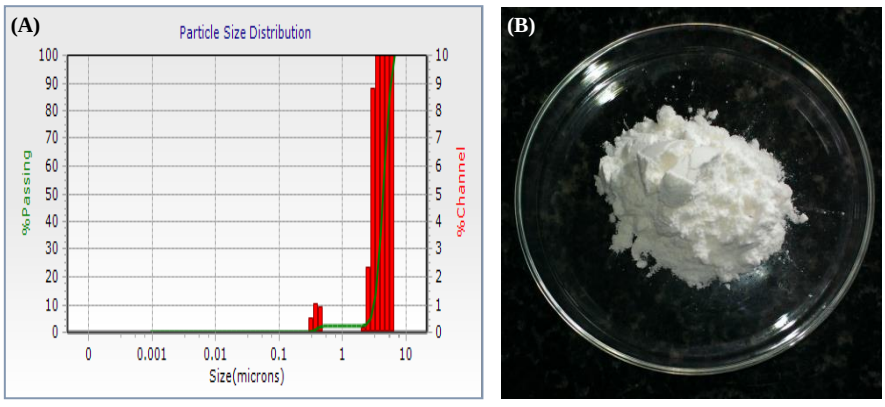

Figure 5.C.3: A) Particle size distribution from DLS spectrum and B) optical photograph of microcrystalline cellulose powder

The spectrum reveals that the size of most of the particles falls on the micrometer range i.e. about 10 μm. The optical photograph of microcrystalline cellulose powder is shown in the figure 5.C.3B.

5.C.3.2. Mechanical properties of the composites

5.C.3.2.1 Tensile properties

The tensile strength as well as elongation at break as a function of increasing cellulose loading is shown in Figure 5.C.4. The tensile strength of the composites increases with the incorporation of cellulose whereas the elongation at break decreases with filler loading. The tensile strength increases linearly with cellulose content up to 10 wt.% and then drops with further cellulose loading. The composite shows 40 % improvement in tensile strength at optimum fiber loading. For the composite containing the coupling agent, the corresponding increase is 49 %. The increase in tensile properties can be related to the high surface area of cellulose so that it interacts with PMMA thereby reduces the chain mobility hence increasing the tensile properties.

The addition of cellulose increased the strength and stiffness as well as considerable improvement in toughness. At higher cellulose loading the tensile properties get decreased due to the inadequate wetting of the filler with the matrix. The poor adhesion between PMMA and cellulose leads to voids at the fiber matrix interface so that it will not direct an efficient stress transfer between PMMA and cellulose; hence it lowers the tensile properties. The decrease at higher cellulose loading is less for silane added composite, i.e. from 67 N/mm^2 to 64 N/mm^2 whereas for PMMA/Cellulose composite tensile strength decreases from 63 N/mm^2 to

58 N/mm^2. It confirms that the cellulose fibers are well wetted in the matrix in presence of Si69, and at higher loading also efficient stress transfer taking place. Unlike PMMA/Cellulose composite a decrease of tensile strength for PMMA/Flyash composite has been reported by Mahanwar et al. [30], the tensile strength was reduced from 68 MPa to 57 MPa.

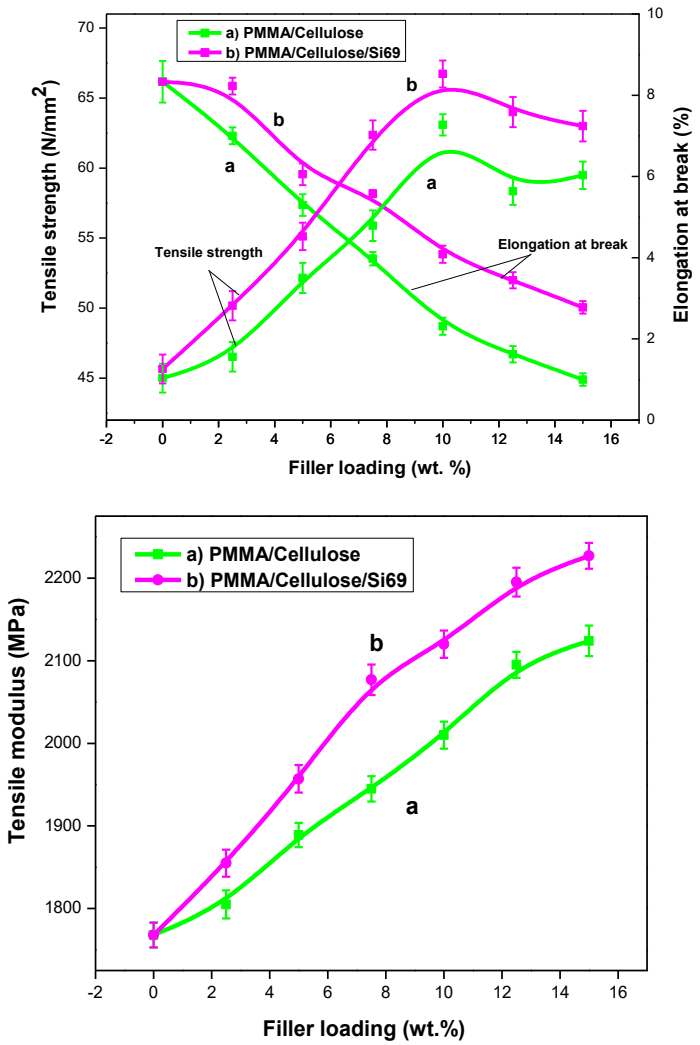

Figure 5.C.4: Tensile strength and Elongation at break Vs wt.% of filler loading for PMMA/Cellulose and PMMA/Cellulose /Si69 composites.

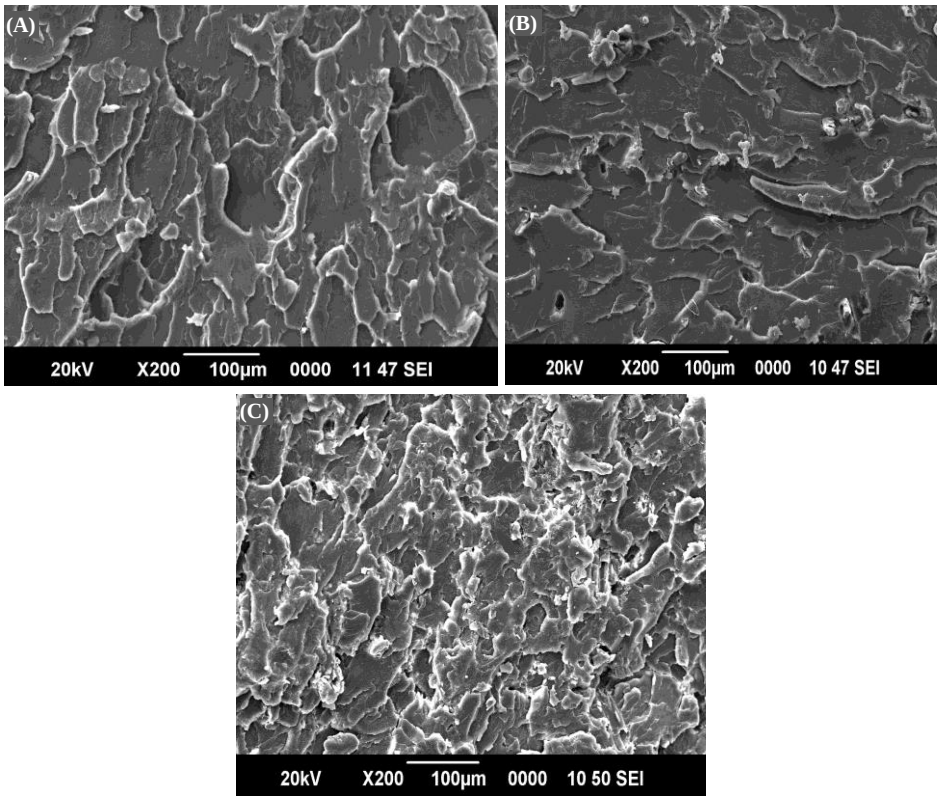

Figure 5.C.5: SEM micrographs of tensile fractured surfaces of A) PMMA, B) PMMA/Cellulose and C) PMMA/Cellulose/Si69 composites

The figure 5.C.5 shows tensile fractured surfaces of PMMA, PMMA/Cellulose and PMMA/Cellulose/Si69 composites. In PMMA and PMMA/Cellulose the cracks possess sharp tips. The sharp edges of particles and holes on the fractured surface indicate poor interfacial adhesion between the particles [31], whereas in PMMA/Cellulose/Si69 the cracks are with blunt tips. Cracks with sharp tips propagate easily compared to cracks with blunt tips. This indicates the ductile fracture of PMMA/Cellulose/Si69composite. In ductile materials the plastic deformation at a crack tip blunts the crack.

5.C.3.2.2 Impact properties

The crack initiation energy is directly related to the nature of matrix, filler morphology and the adhesion between the filler and matrix. The figure 5.C.6 shows the comparison of impact strength of PMMA/Cellulose and PMMA/Cellulose/Si69 composite. For both composites the impact strength increases with the incorporation of cellulose but the increase is prominent in the presence of silane coupling agent.

It is well understood from the figure that Si69 coupled composites need more energy to break by impact. The energy increases with cellulose loading this agrees the enhanced ability of the composites to resist the fracture under stress. After reaching maximum energy it began to reduce for higher weight percentage composites. Cellulose can inhibit the propagation of cracks and it can act as load transfer medium in PMMA matrix. The major factors which play role in the properties of the composite are particle–particle interaction and particle–matrix interactions. The particle-particle interaction deteriorates the performance of the sample where as filler-matrix interaction improves the properties of the composites. For higher weight percentage composites, it achieves minimum strength. This can be ascribed to the agglomeration of cellulose particles which lead to adverse impact on particle-particle interaction. Hence the performances of the composite deteriorate.

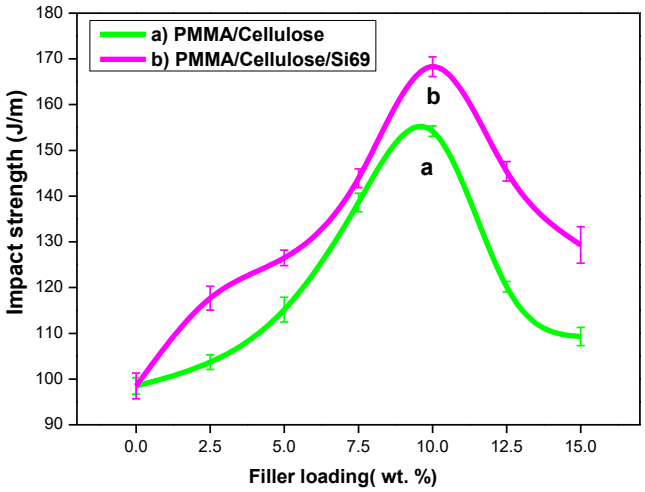

Figure 5.C.6: Variation of impact strength of the PMMA/Cellulose composite- Effect of Si69.

Maximum impact strength is observed for 10 wt.% combination for both PMMA/Cellulose and PMMA/Cellulose/Si69 composites. Sharp increase from 98 to 155 J/m is observed for PMMA/Cellulose composite, and then it decreases to 109 J/m for 15 % composite. Whereas for silane added composite the increase is more prominent it increases up to 169 J/m for 10 % composites then reduces to 129 for 15% PMMA/Cellulose/Si69 composites. Excess energy is needed to break the bond formed between Si69 with PMMA matrix and cellulose. The impact test clearly shows some sort of extra energy is utilized to break silane coupled composites. The mechanical properties of PMMA/Flyash composites were studied by Mahanwar et al. For PMMA/Flyash composite [30] the addition of flyash into PMMA leads to decrease the strength from 42 to 35 J/m for 10wt% composite. But in case of PMMA grafted talc on PVC reported by Aznizam Abu Bakar et al. resulted an increase of impact strength [32].

Figure 5.C.7 shows the surface morphology of the fractured cross sections of impact samples of the pure PMMA and composites.

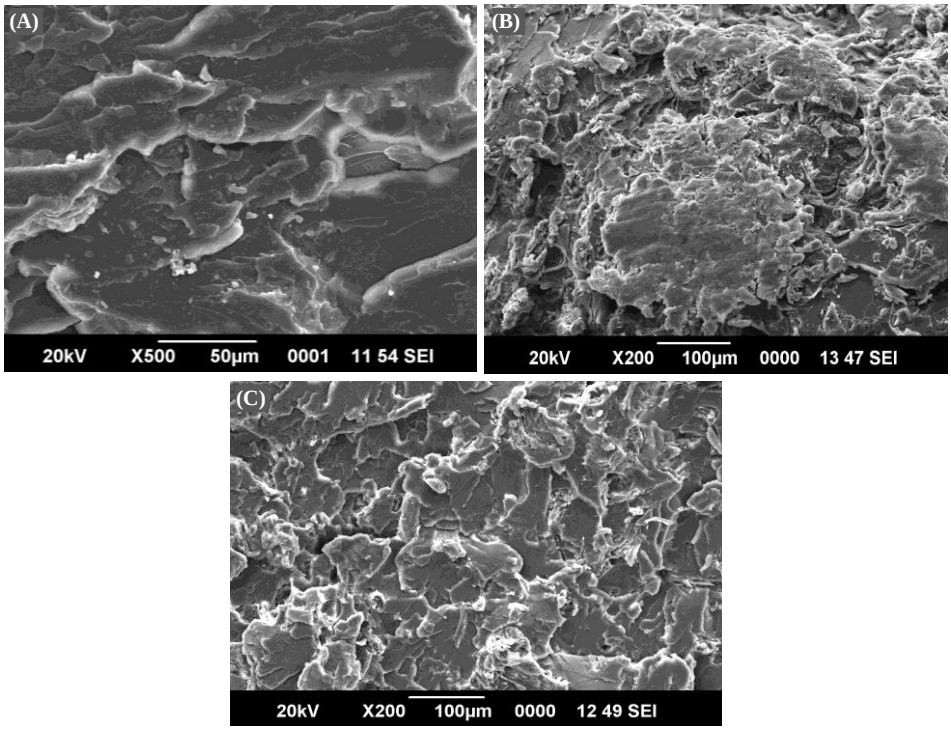

Figure 5.C.7: SEM micrographs of impact fractured surfaces of A) PMMA, B) PMMA/Cellulose and C) PMMA/Cellulose/Si69 composites

Since the mechanical properties of the composites are influenced by the morphology as well as interfacial interaction between components, so the consideration of morphologies will be very valuable. Pure PMMA exhibit a flat and featureless morphology. For PMMA/Cellulose composite shows a weak interface between the dispersed phase (cellulose) and the continuous phase (PMMA). It results in reduction of properties due to the agglomeration. Agglomeration may be due to the incompatibility between the hydrophilic cellulose surface and hydrophobic PMMA [33,34]. Contrast to PMMA and

PMMA/Cellulose composites PMMA/Cellulose/Si69 exhibit stable cracks. This indicates extensive plastic deformation ahead of crack, which reveals better stress transfer between the components.

5.C.3.2.3 Flexural properties

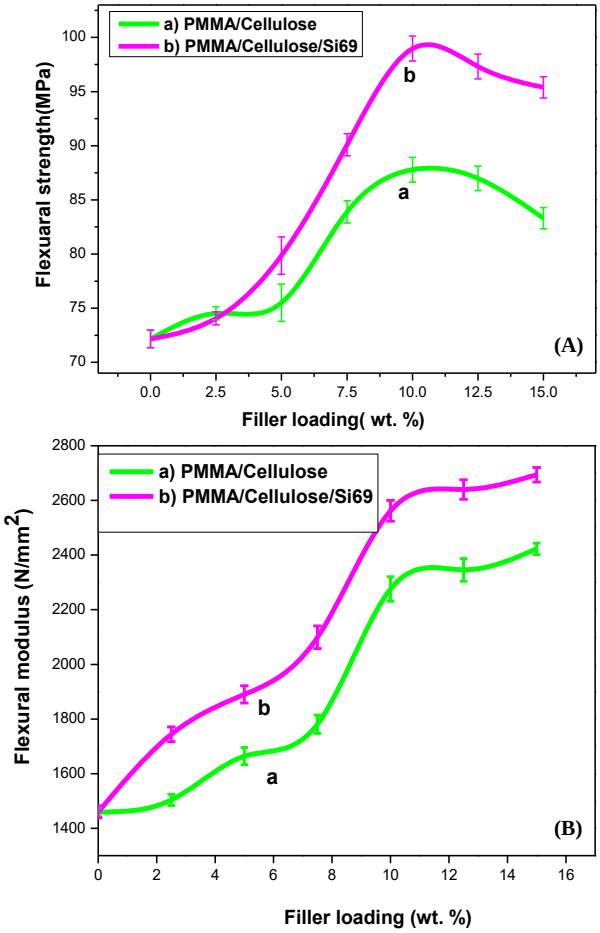

Figure 5.C.8: Effect of the addition of Si69 on the A) flexural strength and B) flexural modulus of the PMMA/Cellulose composite

Flexural properties show a trend similar to tensile strength with varying fiber content. Flexural strength of the composites is shown in the

figure 5.C.8A. The addition of cellulose fiber increases the flexural strength, achieves maximum strength and then decreases. The predominant increase is observed by the coupling of silane with cellulose and PMMA. The increase in flexural strength is due to the increased compatibility and interfacial adhesion between the cellulose and PMMA polymer in presence of Si69. The interaction between Si69 and PMMA/Cellulose lead to form a strong interface which can sustain stress at fracture. The highest flexural modulus 99 MPa is obtained for 10 % PMMA/Cellulose/Si69 composite, and then it reduces to 94 MPa for 15 % composite. But without silane the highest value obtained is 87 MPa. For PMMA/Hydroxyapetite composites reported by Naderi et al. [33] the flexural strength and flexural modulus increases up to 2.5 wt.% composites then it decreases. But for PMMA/Flyash [30] composites the increase of flexural strength is more predominant than hydroxyapetite it increases from 115 to 129 MPa for 10 wt.% composite. The increase of flexural strength indicates that the PMMA/Cellulose/Si69 composite became more rigid and less flexible.

5.C.3.3 Characterization of the composites

5.C.3.3.1 X-ray diffraction

Comparison of X-Ray diffractogram of PMMA/Cellulose and PMMA/Cellulose/Si69 is shown in the figure 5.C.9. The spectrum obtained for cellulose is similar to the cellulose-I structure with peaks at 2θ of 16 ° and 22.5 °. The intensity of the crystalline peak at 22.5 ° increases with cellulose content in the composite. The crystallite size was calculated by using the Scherrer equation, $L_{h,k,l} = K\lambda / b\cos\theta$,

where, K = 0.94.

The diffractogram of PMMA show one major maximum at 2θ of 14.3 ° and a small peak at 30.3 °. The broad peak indicates the ordered packing of polymer chains whereas the small peak gives the effect of ordering inside the main chains. [34] Sharp crystalline peaks are absent in PMMA diffractogram which suggests amorphous nature of PMMA film. As the filler concentration increases the intensity of the crystalline peak of cellulose at 22.5° increases.

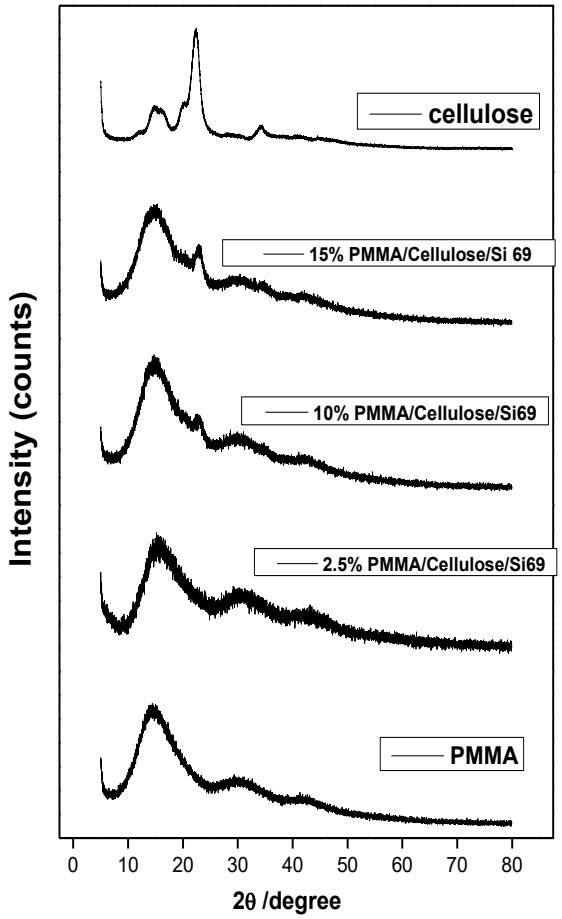

Figure 5.C.9: X-Ray Diffractogram for different compositions of PMMA/Cellulose and PMMA/Cellulose/Si69

5.C.3.3.2 FTIR spectroscopy

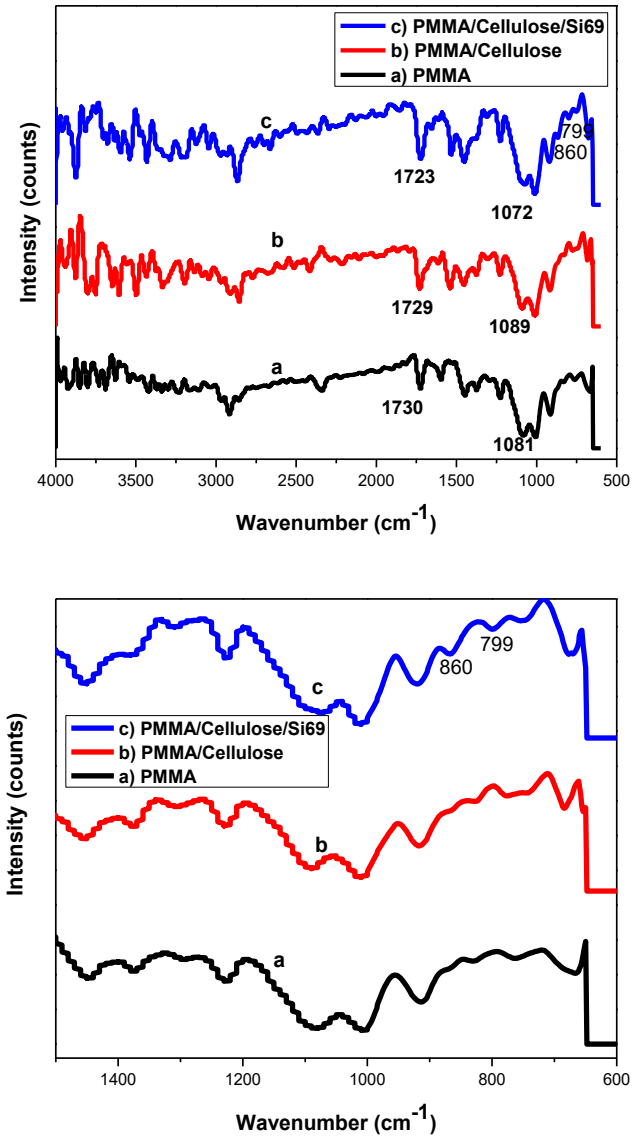

Figure 5.C.10: FTIR spectra of PMMA, PMMA/Cellulose and PMMA/Cellulose/Si69 composites and expanded region from 500-1500 cm^{-1}

Figure 5.C.10 depicts the FTIR spectra of neat PMMA, PMMA/Cellulose and PMMA/Cellulose/Si69 composites. It is evident that all the three spectra look more or less similar except for some changes in the spectra of the silane added composite. But no major differences are observed between the FTIR spectra of pure PMMA and PMMA/Cellulose composites. The characteristic vibration bands of PMMA appear at 1730 cm^{-1} (C=O stretching mode). The small peak at 2800 cm^{-1} correspond to the methylene C-H stretching of PMMA while the bands at 1350 $cm^{-1}$and 1450 $cm^{-1}$are associated with C-H symmetric and asymmetric stretching modes of the same group, respectively. Absence of any additional bands by the addition of cellulose indicates no chemical bond is formed between PMMA and cellulose in PMMA/Cellulose composite [34,35].

A minor change in the C=O stretching frequency is observed for the PMMA/Cellulose/Si69 composite. For pure PMMA the peak obtained is at 1730 cm^{-1} while that for the composite it is about 1723 cm^{-1}. Compared to PMMA a lower C=O stretching frequency is observed for PMMA/Cellulose/Si69 composite. This can be related to the interaction of carbonyl group of PMMA with Si69, thereby making carbonyl bond less stiff. New peak appeared at 860 cm^{-1} in the spectrum of PMMA/cellulose/Si69 composite is probably due to the S-S stretching of Si69. This suggests that S-S bond is not breaking in the formation of the composite.

5.C.3.3.3 ^{29} Si NMR spectroscopy

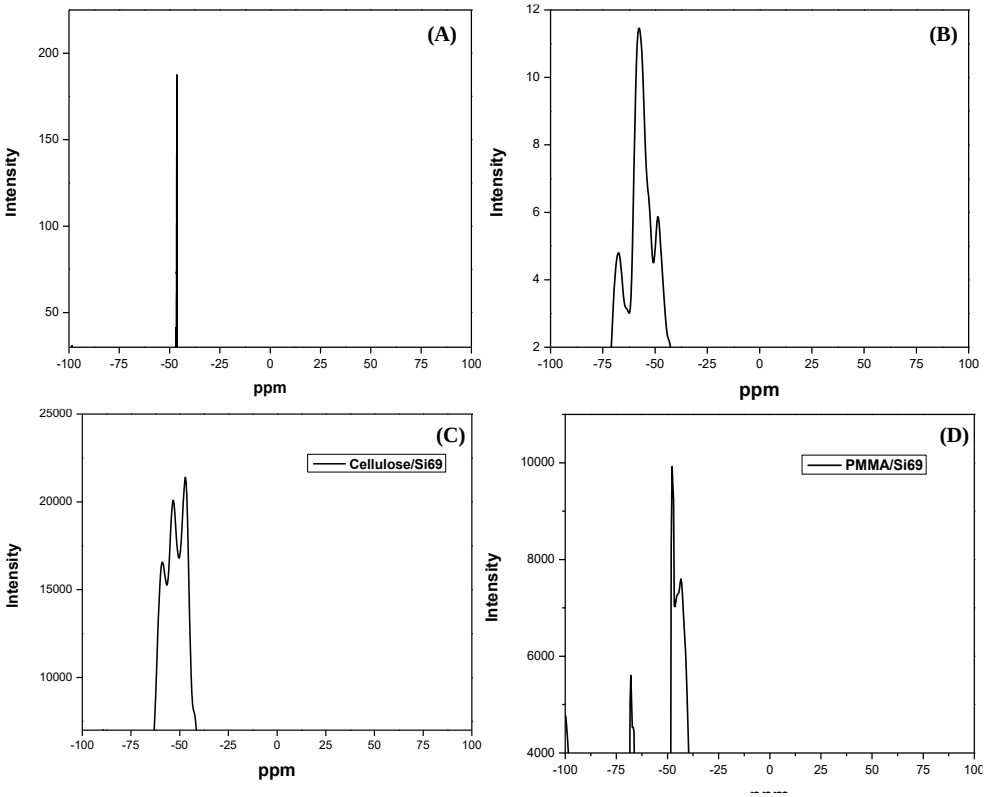

Figure 5.C.11: ^{29}Si CP/MAS spectra of (A) Si69 and (B) PMMA/Cellulose/Si69 composite(C) Cellulose/Si69 (D) PMMA/Si69

The interaction of silane coupling agent with cellulose and PMMA can easily be understood from the ^{29}Si CP/MAS spectra of pure Si69 (figure 5.C.11A) and the composite (figure 5.C.11B). For silane coupling agent a single peak is obtained at -47 ppm. Whereas for the composite three peaks were obtained at -47.5, -57 and -67 ppm. The peak at -47.5 ppm is due to the unreacted silane present in the composite. The two ethoxy (OEt) groups of silane can react with hydroxyl group of cellulose as well as the carbonyl carbon of PMMA.

Then two different silicon atoms will be formed in the composite which can give two different peaks. The change in the absorption maxima is due to the different chemical environment. When the ethoxy group reacts with the carbonyl carbon of PMMA, the carbon from PMMA is connected to two oxygen atoms. This will lead more down field shift compared to the reaction of silane with cellulose. The peak at -57 ppm is more intense than the one at -67 ppm. It can be attributed to the difference in degree of reaction of silane with cellulose and PMMA. The silane is more prone to react with hydroxyl group of cellulose than the carbonyl group of PMMA. So the ^{29}Si spectra evidently show that, the two Si atoms of the coupling agent is connected to two different atoms, i.e. it can bond to cellulose as well as PMMA. For better understanding I have performed ^{29}Si NMR separately for cellulose and coupling agent as well as for PMMA and coupling agent. The peaks obtained for cellulose (figure 5.C.11C) and PMMA (figure 5.C.11D) are at -56 ppm and -65 ppm respectively, which is similar to the peaks obtain for the composite (figure 5.C.11B).

5.C.3.3.4 ^{13}C NMR spectroscopy

Figure 5.C.12 shows the ^{13}C NMR spectra obtained for PMMA/ Cellulose and for PMMA/Cellulose/Si69 composites. Though all the peaks are present after the addition of Si69, the main difference appears to be in the intensity. The intense peak at 52 ppm corresponds to the methoxy group of PMMA. Methyl and methelene carbon peaks of PMMA can be seen at 17 ppm and 58 ppm respectively.

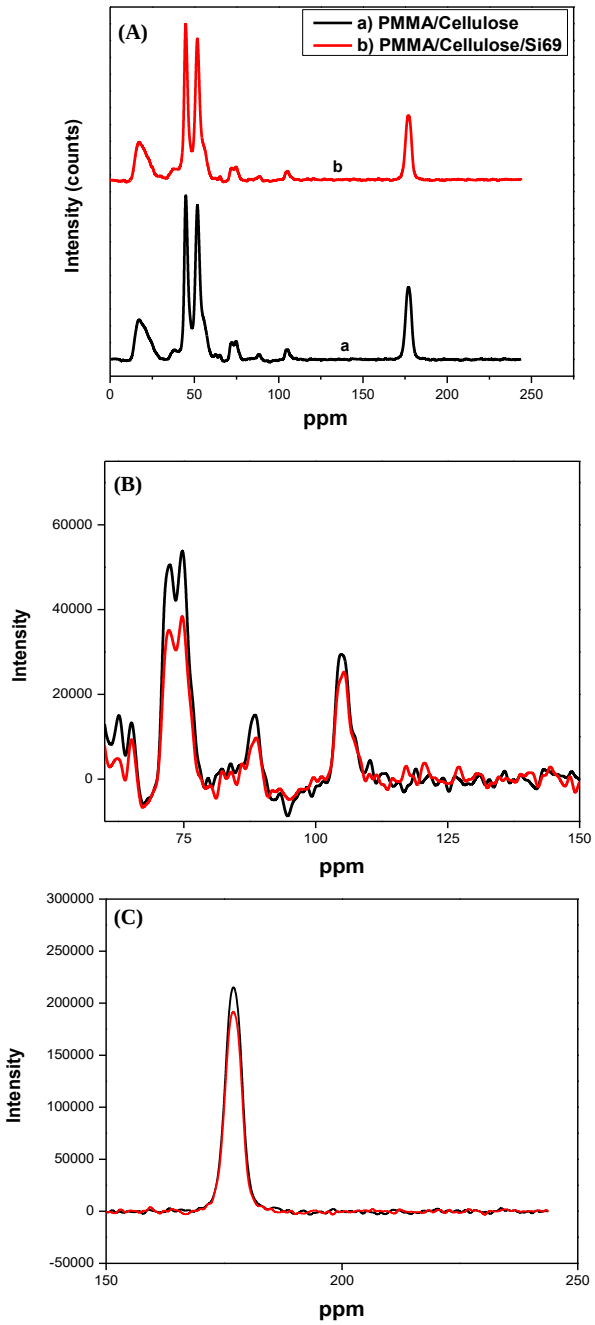

Figure 5.C.12: A) ^{13}C spectra of PMMA/Cellulose and PMMA/Cellulose/Si69 composites, B) expanded region of hydroxyl peak of cellulose, C) expanded region of carbonyl peak of PMMA

The chemical shifts of PMMA/Cellulose/Si69 are virtually identical to those obtained for PMMA/Cellulose composites. However, the intensity of the signals changes after the addition of Si69. This could be due to the reaction of Si69 with cellulose and PMMA. Carbonyl group of PMMA has a peak at 170 ppm, the intensity of the peak is reduced after the incorporation of Si69 in to the composite which can be attributed to the reaction of carbonyl carbon of PMMA with silane coupling agent. A significant reduction in the C-OH peak intensity can be seen in the spectrum at 74 ppm (figure 5.C.12B). This also agrees with the result obtained from the ^{29}Si NMR. In every case the observed reduction in intensity is only marginal as the total amount of Si 69 added is very small (10 wt.% on cellulose content).

5.C.3.3.5 UV-Vis spectroscopy

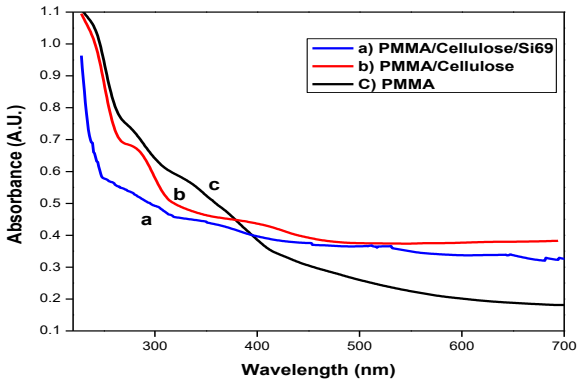

Figure 5.C.13: UV-Vis spectra of PMMA, PMMA/Cellulose and PMMA/Cellulose/Si69 composites

UV analysis of PMMA, PMMA/Cellulose and PMMA/Cellulose/Si69 is represented in the figure 5.C.13. The spectrum of PMMA indicates an

absorption band of high intensity around 230 nm and a low intense band at 280 nm. The intense peak around 230 nm represents the π-π^* transition. It is the characteristic peak of PMMA carbonyl group acting as the chromophor. In symmetry terms the most typical transition of carbonyl compounds (n-π^*) is forbidden. Hence the corresponding peak will be of low intensity. The peak obtained for PMMA at 280 nm will be corresponding to the n-σ^* transition. A slight change in the peak intensity of PMMA is observed for the PMMA/Cellulose composite. But there is significant reduction in the intensity of the carbonyl peaks for PMMA/Cellulose/Si69 composite indicating the interaction of carbonyl group of PMMA. The spectrum reveals that no absorption peak is seen at longer wavelength >285 nm. The absorbance of PMMA reduces abruptly after 325 nm. In the visible region it shows very low absorbance confirming to its high optical transparency. However, for the composites containing cellulose fibers, the transparency is marginally reduced, as indicated by the relatively higher absorption in the visible region.

The possible interface between cellulose and PMMA in presence of Si69 is shown in the figure 5.C.14. The mechanism is supported by the FTIR, UV-Vis, ^{29}Si and ^{13}C NMR spectroscopy etc. All the spectroscopic results suggest that silane coupling agent reacts differently with PMMA and cellulose. One end of silane reacts with hydroxyl group of cellulose eliminating a molecule of ethanol. Without breaking of S-S linkage of silane the other end reacts with PMMA. The existence of S-S bond in the composite is evident from the FTIR spectra. Presence of two different Si atoms in the composite gives different absorption peaks in the ^{29}Si spectra

of PMMA/Cellulose/Si69 composite. This illustrates the S-S bond in Si69 is not breaking in the composite, which supports the proposed reaction mechanism.

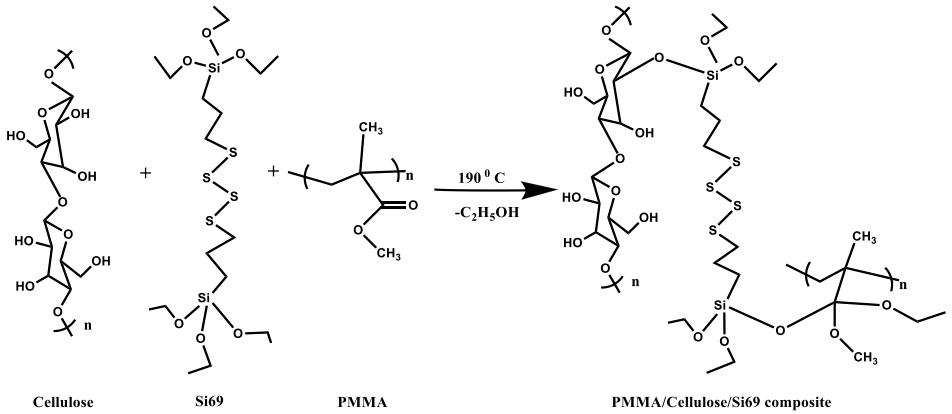

Figure 5.C.14: Schematic diagram of the possible interface between the cellulose, Si69 and PMMA

5.C.3.3.6 Dynamic Mechanical Analysis

The dynamic storage modulus of PMMA/Cellulose and PMMA/ Cellulose/Si69 composites as a function of temperature is shown in the figure 5.C.15. For all the composites the storage modulus decreases with temperature. This can be related to the increased segmental mobility of the polymer chains. All composites possess higher storage modulus than the pure PMMA at all the temperature range. But at lower temperature the highest storage modulus is observed for 10 % PMMA/Cellulose composite whereas at higher temperature ranges 15 % PMMA/Cellulose composite exhibits maximum storage modulus. Compared to pure PMMA, 24 % increase in storage modulus can be observed for PMMA/Cellulose composites.

A sharp increase of storage modulus can be seen in silane coupled composites, which indicate efficient stress transfer between the matrix and filler in presence of Si69. The results are consistent with other mechanical properties obtained for the composite. Comparison of storage modulus at 40 °C for PMMA/Cellulose and PMMA/Cellulose/Si69 composites is shown in the figure 5.C.16.

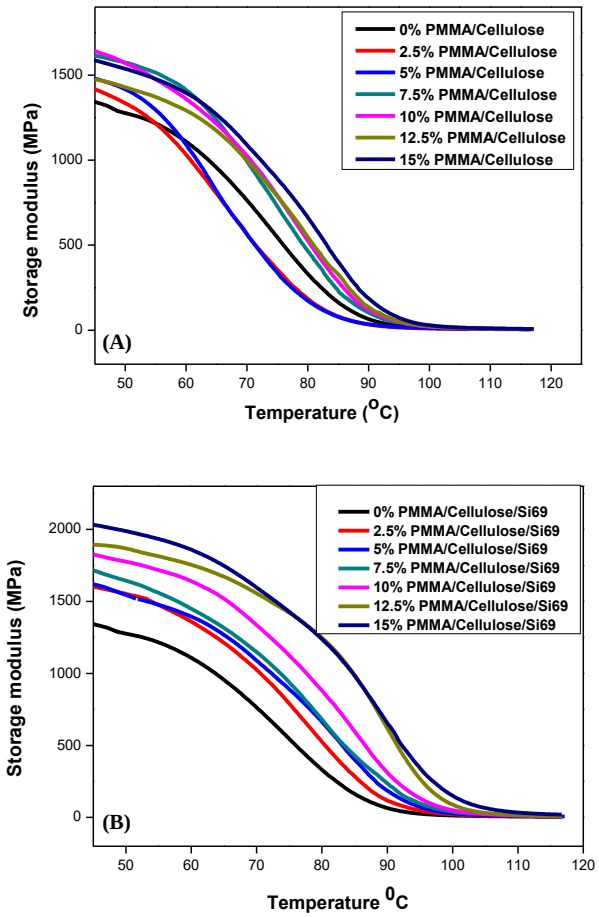

Figure 5.C.15: Storage modulus curves A) PMMA/Cellulose and B) PMMA/Cellulose /Si69composites

It is evident from the figure 5.C.16 that the storage modulus for PMMA/Cellulose decreases at higher weight percentage composites. Whereas in silane coupled composites storage modulus increases continuously with cellulose content. That means by the formation of chemical bond between silane to PMMA and cellulose efficient stress transfer occurs. Absence of chemical interaction in PMMA/Cellulose composite results in agglomeration in the case of higher weight percentage composites resulting in lower storage modulus.

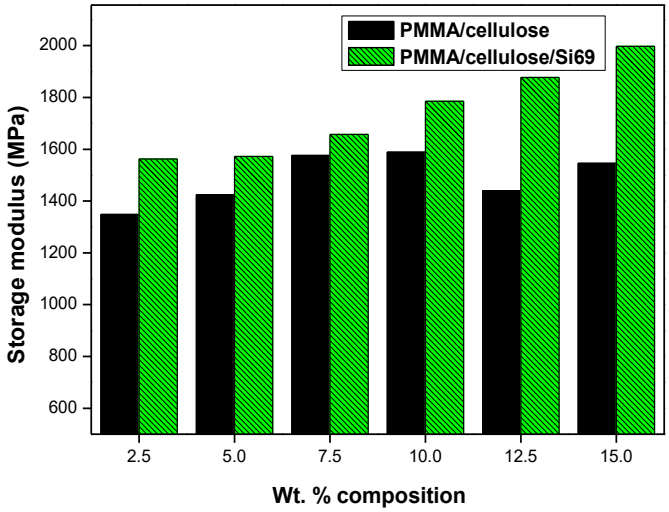

Figure 5.C.16: Comparison of storage modulus of PMMA/Cellulose and PMMA/Cellulose /Si69.

Tan δ in dynamic mechanical analysis represents the damping in the material and it is related to the macroscopic physical transitions. In both composites (PMMA/Cellulose & PMMA/Cellulose/Si69) the glass transition temperature (Tg) values increase with cellulose content (figure 5.C.17). For pure PMMA, the glass transition temperature obtained is about 91 °C. But it increased up to 99 °C for 15 % PMMA/Cellulose

composite. This increase in Tg is due to immobilization of polymer molecules resulting from the good dispersion of cellulose in PMMA matrix. Further increase is found in PMMA/Cellulose/Si69 composite. In this case maximum glass transition temperature achieved is 105 °C, indicating better dispersion in the matrix. As the dispersion increases the mobility of the macromolecular chain gets reduced and results in high value of Tg.

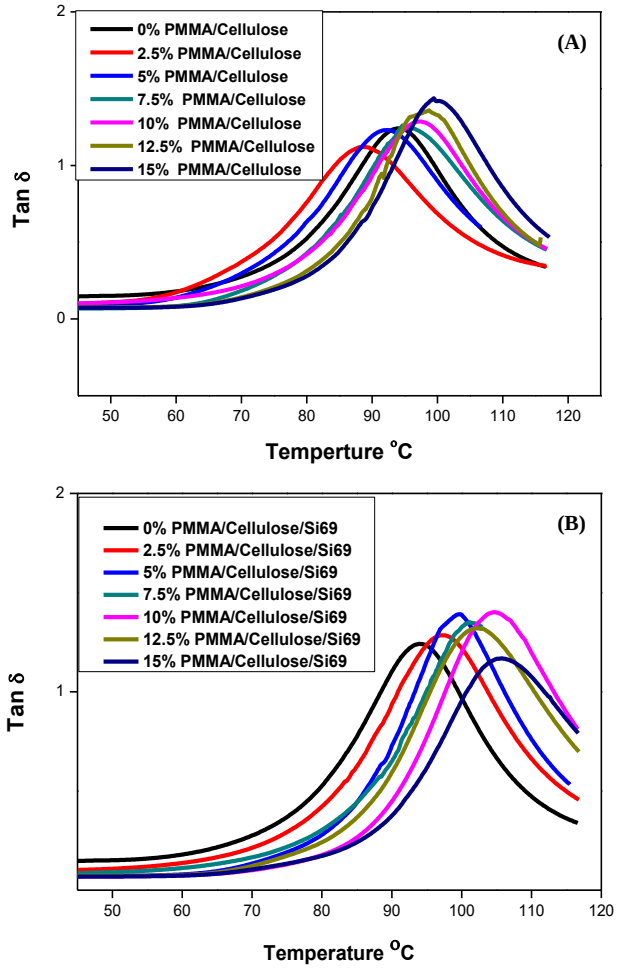

Figure 5.C.17: Tan δ curves of A) PMMA/Cellulose and B) PMMA/Cellulose/Si69 composites

The shift of the tan δ peak towards the high temperature side indicates the restricted mobility of PMMA chains by the interaction with silane molecule. Figure 5.C.18 shows the comparison of tan δ values obtained for PMMA/Cellulose and PMMA/Cellulose/Si69 composites. All the silane-coupled composites show higher Tg value than the PMMA/Cellulose composite. This implies the importance of chemical bond formed between the coupling agent with PMMA and cellulose. The mobility of PMMA chains is significantly reduced after the bond formation thereby increasing the tan δ value.

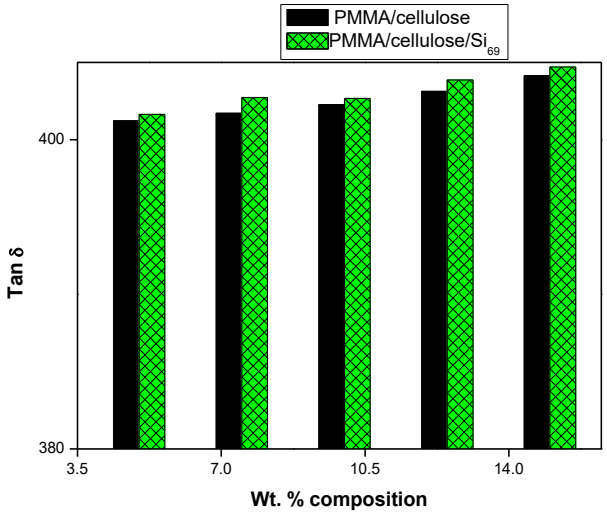

Figure 5.C.18: Comparison of tan δ value of PMMA/Cellulose and PMMA/Cellulose /Si69

5.C.3.4 Thermal properties

5.C.3.4.1 Thermogravimetric analysis

To understand the effect of Si69 on the thermal properties of the composite thermogravimetric analysis was carried out (Figure 5.C.19). The degradation temperature of pure PMMA is 398 °C, it increases with

the addition of cellulose and Si69. The temperature increases up to 406 °C for PMMA/Cellulose/Si69 and 404 °C for PMMA/Cellulose composite. It shows that the thermal stability of the composite is enhanced upon the addition of cellulose. There is a slight increase in the case of silane coupled composite compared to PMMA/Cellulose composite. Enhancement of the thermal stability of the composites can be attributed to better filler-matrix interaction where the restrained matrix delays the volatilization of the products generated at the time of thermolysis of the PMMA.

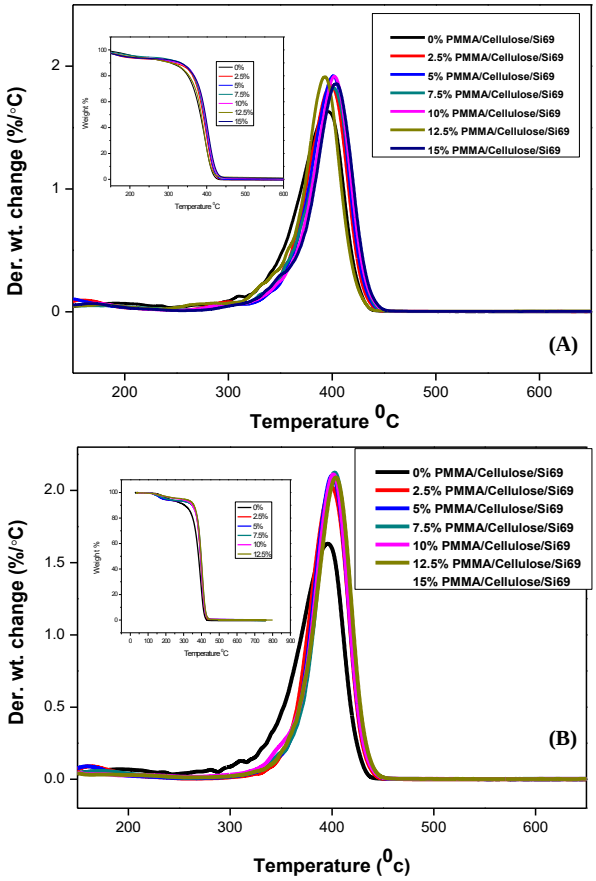

Figure 5.C.19: Thermogravimetric curves of A) PMMA/Cellulose and B) PMMA/Cellulose/Si69 composites

PMMA/Cellulose/Si69 composites show superior thermal stability than PMMA/Cellulose composites. In PMMA/Cellulose composites cellulose is not chemically bonded to PMMA. But in PMMA/Cellulose/ Si69 composites Si69 is covalently bonds to PMMA and immobilization of PMMA chains takes place at higher temperature. Hence the PMMA/ Cellulose/Si69 composite is thermally more stable than PMMA/Cellulose composite.

5.C.3.4.2 Differential Scanning Calorimetry

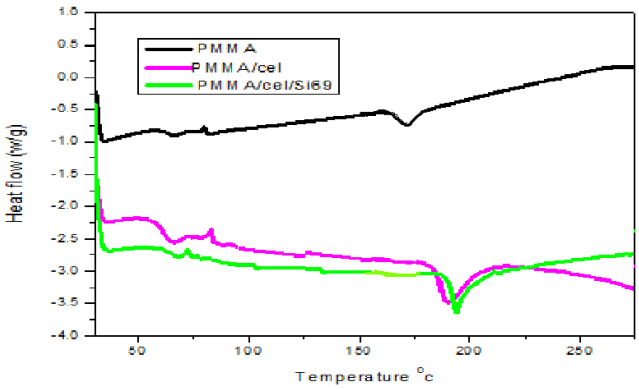

Figure 5.C.20: DSC heating curves of PMMA, PMMA/Cellulose and PMMA/Cellulose/Si69 composites

Figure 5.C.20 shows the DSC curves of pure PMMA, PMMA/ Cellulose, and PMMA/Cellulose/Si69 composites. The glass transition temperature (Tg) of pure PMMA is 64 °C whereas the Tg for PMMA/Cellulose and PMMA/Cellulose/Si69 is shifted to 67 °C and 69 °C, respectively. The melting point obtained for pure PMMA is about 173 °C. The addition of cellulose to PMMA increased the melting point to 188 °C for PMMA/Cellulose composite. The presence of Si69 takes it further to 196 °C. The shift of melting temperature (Tm) to a higher temperature

indicates constrained mobility of the PMMA molecules in the composites. The presence of Si69 can induce a restricted mobility of polymer chains by forming covalent bonds. In PMMA/Cellulose composite hydrogen bonding between cellulose and PMMA results an increase of melting temperature, whereas prominent increase for PMMA/Cellulose/Si69 is due to the covalent bonding between the silane coupling agent with PMMA and cellulose.

5.C.3.5 Dielectric Properties

5.C.3.5.1 Dielectric permittivity

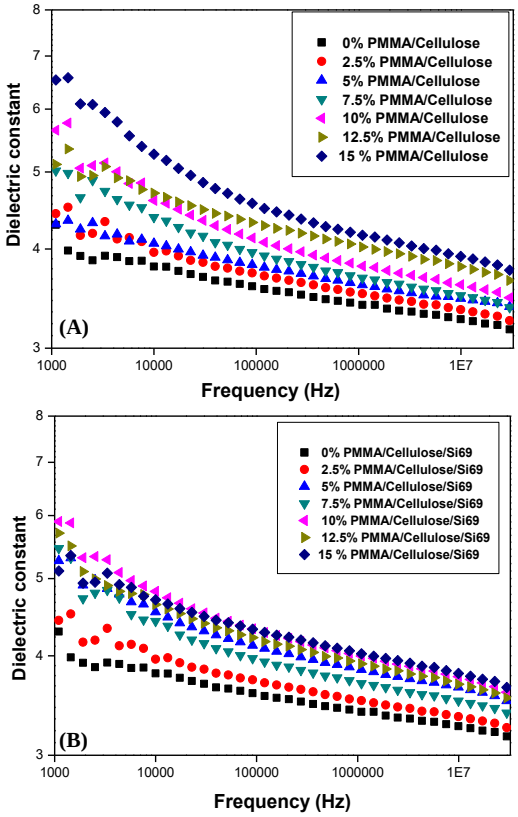

Figure 5.C.21: Dielectric constant as a function of frequency for A) PMMA/Cellulose and B) PMMA/Cellulose /Si69 composites.

The variation of dielectric permittivity with applied frequency is shown in the figure 5.C.21. For all the composites, dielectric permittivity decreases with increase of frequency. The decrease is more predominant at low frequency regions, as the frequency increases all the composites acquire more or less similar dielectric constant.

From the above figure, it is apparent that the dielectric constant obtained is more for PMMA/Cellulose composite compared to PMMA/Cellulose/Si69. It indicates that by the addition of Si69 to the PMMA/Cellulose composite reduces the number of polar groups in the molecule. It means that Si69 couples with both cellulose and PMMA. The dielectric property of polymer depends on the charge distribution and statistical thermal motion of the polar groups. This also clearly shows that the coupling agent reacts with cellulose and the polymer matrix resulting in reduction of polar groups. Compared to PMMA/Cellulose, silane coupled composite shows a slow decrease of dielectric constant with frequency. Since the orientation polarization due to the ionic groups of PMMA/Cellulose composites reduces quickly with the alternation of electric filed. This reduction is deliberate in case of PMMA/Cellulose/Si69 composite. Decrease of dielectric constant with frequency is due to dielectric dispersion as a result of the lag of the molecules in the alternating electric field.

5.C.3.5.2 Loss Tangent

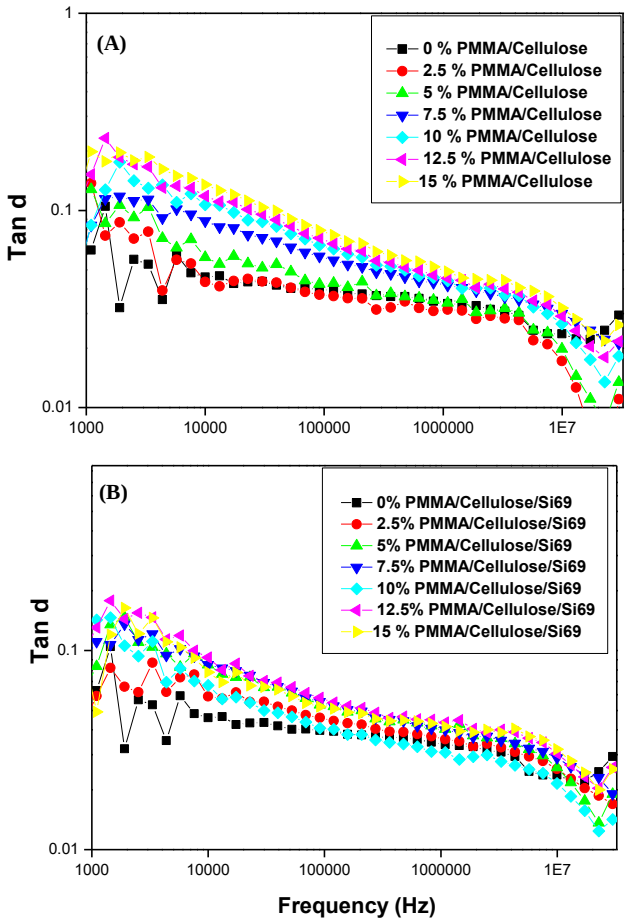

Figure 5.C.22: Dielectric loss as a function of frequency for A) PMMA/Cellulose and B) PMMA/Cellulose/Si69 composites

Loss tangent for all the composite decreases with increase of frequency. At higher frequencies all the composites acquire more or less similar value. At very high frequencies, the loss tangent is found to be marginally lower as the chain motion of polymer becomes out of phase with the rapidly oscillating electric field.

5.C.3.5.3 AC Conductivity

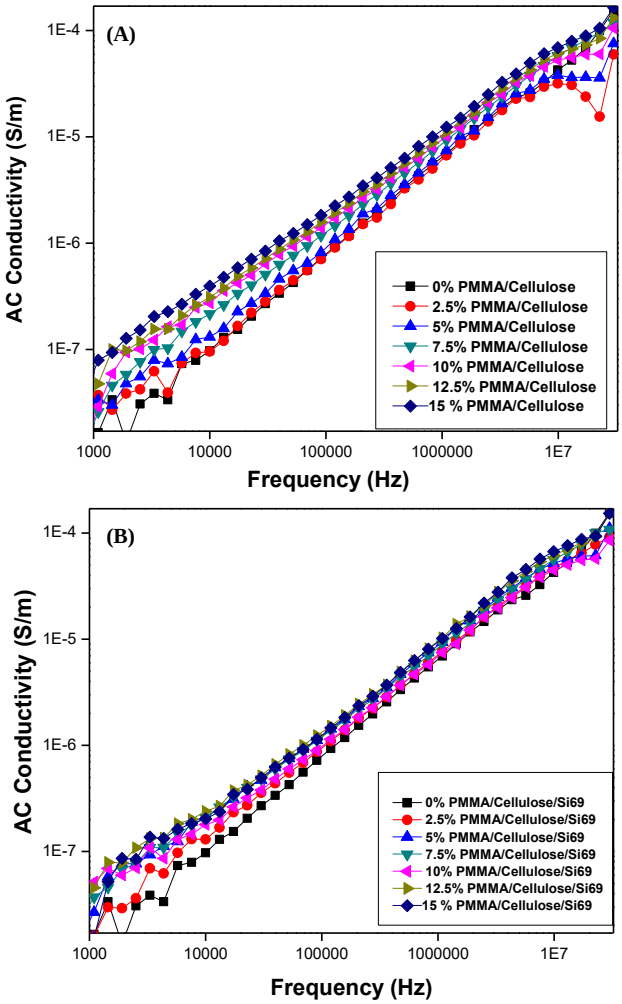

Figure 5.C.23: AC Conductivity as a function of frequency for A) PMMA/Cellulose and B) PMMA/Cellulose/Si69 composites

AC conductivity for all the composites were calculated from the dielectric permittivity and loss tangent using the equation $\sigma_{AC}=2\pi f\varepsilon\varepsilon^{*}\tan\delta$, ε is the permittivity of vacuum. Figure 5.C.23 shows the variation of AC

conductivity with frequency as a function of cellulose loading. At lower frequencies jump of AC conductivity is observed and it attains almost constant value at higher frequency. This type of transition is called hopping transition. AC conductivity increases at lower frequencies which are due to the induced surface currents by the external electromagnetic field. At lower frequencies the conduction will be due to the displacement currents created by the dipoles, but at higher frequencies these dipoles cannot get oriented with alternation of electric field. Hence the displacement current will be diminished. For PMMA/Cellulose composite AC conductivity reaches value of $4.1*10^{-4}$ S/m which is higher than that of PMMA/Cellulose/Si69 composite ($1.4*10^{-4}$ S/m).

5.C.4 Conclusion

The PMMA/Cellulose and PMMA/Cellulose/Si69 composites were fabricated by solution cast method. FTIR, UV-Vis, ^{13}C NMR, ^{29} Si CP/MAS and XRD techniques showed the presence of covalent bond formed between silane coupling agent to PMMA and cellulose. The presence of Si69 in the composite marginally increases the Tg of PMMA. The results proved that Si69 can be used for reinforcing PMMA/cellulose system very effectively. The Si69 remarkably improves the tensile strength, impact strength and flexural strength. The storage modulus of silane-coupled composites is much greater than that of pure PMMA. SEM images revealed well dispersion of cellulose in PMMA matrix in presence of Si69. This is in good agreement with the improved strength of the composite. But for higher filler weight percentage composites the properties are decreased due to the agglomeration of microcrystalline

cellulose. The incorporation of cellulose into PMMA matrix increased the dielectric properties and AC conductivity reached a value of $1.4*10^{-4}$ S/m. In short, PMMA/Cellulose/Si69 composite can be used as high strength material with improved thermal properties, tensile strength, high impact energy and high storage modulus.

References

[1] G. Ahlblad, A. Kron, B. Stenberg, polymer Int. 33 (1994) 103-109

[2] S. Varghese, B. Kuriakose, S. J Appl Polym Sci. 53 (1994) 1051-1060

[3] S. Jain, R. Kumar, U.C. Jindal, 27 (1992) 4598-4604

[4] A.K. Bledzki, J. Gassan, Prog. Polym. Sci. 24 (1999) 221–274

[5] M. Jawaid, H.P.S. Abdul Khalil, Carbohydrate Polymers 86 (2011) 1– 18.

[6] O. Faruk, A.K. Bledzki, H.P. Fink, M. Sain, 2000–2010, Prog. Polym. Sci. 37 (2012) 1552– 1596

[7] V.P. Anju, S.K. Narayanankutty, AIP Advances 6 (2016) 015109 -015113

[8] K.Y. Lee, Y. Aitomäki, L. A. Berglund, K. Oksman, A. Bismarck, 105(2014)15-27.

[9] G.C. Escamilla, J.R. Laviada, J.I. Cauich-Cupul, E. Mendizabal, J.E. Puig, P.J. Composites: Part A: Applied Science and Manufacturing 33 (2002) 539-549.

[10] A.K. Bledzki, J. Gassan, Angew Makromol Chem. 236 (1996) 129-138

[11] V.G. Geethamma, R Joseph, S. Thomas, J Appl Polym Sci. 55 (1995) 583-594.

[12] K. Oksman, J Reinf Plast Compos 20 (2001) 621–627.

[13] H. Liu, D. Liu, F. Yao, Q. Wu, Bioresour. Technol. 101 (2010) 5685-5692.

[14] H. Dong, K.E. Strawhecker, J.F. Snyder, J.A. Orlicki, R.S. Reiner, A.W. Rudie, Carbohydr. Polym. 87 (2012) 2488-2495.

[15] S. Sain, D. Ray, A. Mukhopadhyay, Polymer Composites 36 (2015) 1748-1758.

[16] F. Fahma, N. Hori, T. Iwata, A. Takemura, J Appl Polym Sci. 128 (2013) 1563–1568.

[17] M.B. Kulkarni, P.A. Mahanwar, Journal of Minerals & Materials Characterization & Engineering 11 (2012) 365-383.

[18] K. Pravin, K. Rajendra, H. Sangeetha, B. Neelima, J. P. Jog, Journal of Applied Polymer Science 81 (2001**)** 1786-1792

[19] A. Hassan, Noor Izyan Syazana Mohd Yusoff , A. Abu Bakar, J Polym Eng. 32 (2012) 275–282.

[20] S.M. Zebarjad, S.A. Sajjadi, T.E. Sdrabadi, A. Yaghmaei, B. Naderi, Nanocomposite Engineering 3 (2011) 795-801.

[21] S. Ahmad, S. Ahmad, S.A. Agnihotry, Bull Mater Sci. 30 (2007) 31-35.

[22] S. Sain, D. Ray, A. Mukhopadhyay, S. Sengupta, T. Kar, C.J. Ennis, P.K.S.M. Rahman, J Appl Polym Sci. 126 (2012) 127–134.

…..ꕥ…..

Chapter 6

APPLICATION STUDIES OF THE COMPOSITES

Contents

Part A

Development of flexible carbon nanofiber and nanofibrillated cellulose based composite sheet as excellent electromagnetic shielding material

This chapter describes the microwave characterization and EMI shielding property of poly(vinyl alcohol) based thin and flexible composite films containing carbon nanofibers (CNF) and nanofibrillated cellulose (NFC). Microwave properties of the composites were studied in terms of permittivity, loss tangent, skin depth and absorption coefficient. High permittivity, absorption coefficient and low skin depth were obtained for carbon nanofiber based composites owing to its good electrical conductivity. The shielding effectiveness (SE) of two composites was measured in the 2-4 GHz (S-band) and 8-12 GHz (X-band) frequency range. Abrupt increase of SE with increasing fiber concentration was observed for CNF based composite. An electromagnetic shielding effectiveness of about -31.5 dB in the S-band and of -32.2 dB in the X band was achieved at 0.12 mm thickness. The SE due to absorption (SE_A) and reflection (SE_R) were increased with increase of PANI/CNF content. Additionally, CNF based composite film had a very low density of 0.21 g/cm^3. Compared to metals and other carbonaceous materials, this composite film exhibited a high specific EMI shielding efficiency of -153.3 dB cm^3/g.

6.A.1 Introduction

The advancement in communication technology has its share of undesirable effect on the environment in the form of electromagnetic radiation pollution. There is a pressing need now to protect the environment as well as the sensitive circuits from such radiations. The research in the field of electromagnetic interference shielding, microwave absorption and the evaluation of dielectric properties are drawing great attention [1-7]. Over the last few decades metal based shielding material have emerged as a viable option up owing to their good conductivity, high dielectric constant and small skin depth [8-10]. Nevertheless, low proccessability, heavy weight and poor flexibility restrict its wide acceptability. Polymer composites with high permittivity and electrical conductivity are emerging as alternate option. Nanomaterial embedded composites have been found to exhibit broader bandwidth, good compatibility and exceptional EMI shielding properties [11-13]. Among the different EMI shielding materials conducting polymers have profound advantage due to tunable conductivity, corrosion resistance, lower density, cost effectiveness and availability of good processing techniques. Doped polyaniline, polypyrrole and poly(3,4-ethylenedioxythiphene) have emerged as promising alternatives for metal-based EMI shielding devices [14-16]. Conducting polymer/metal composites, multilayer sheets etc. [17] have also been used for EMI shielding applications. Poly(vinyl alcohol) with hydroxy functional group attached to backbone has good film forming property and is highly flexible. When properly adjusted, it can be used as a good host matrix for preparing excellent EMI shielding composites.

EMI shielding effectiveness of a composite depends on factors like the conductivity of filler and aspect ratio. Recently carbon-based materials such as carbon nanotubes, graphite flakes, carbon nanofibers and carbon black have been used in the preparation of EMI shielding materials [18-21]. Among the carbon-based materials, carbon nanofiber has been widely explored owing to its large aspect ratio, comparatively low cost, exceptional electrical and mechanical properties [22-24]. Another major advantage of CNF based composites is their ability to form thin film with excellent EMI shielding efficiency. Insulating fibers can also be used for EMI shielding applications by providing them with a thin coating of a conducting polymer such as polyaniline on the surface.

In this study I report, the microwave dielectric properties, EMI shielding efficiency of two light weight and flexible composites based on carbon nanofiber and cellulose fiber. PVA was used as the matrix. Microwave characteristics and EMI shielding efficiency were studied over a wide frequency range. Electromagnetic interference shielding of a material can be represented as the sum of the contribution from electromagnetic parameters i.e. its complex permittivity and permeability. In case of non-magnetic materials, the contribution from complex permeability can be neglected and it solely depends on the permittivity. Hence the measurement of the microwave dielectric properties leads to the direct calculation of EMI shielding. I have adopted cavity perturbation technique using vector network analyzer, simple and non-destructive technique for the evaluation of permittivity.

6.A.2 Experimental

Modification of nano-fibrillated cellulose (NFC) and carbon nanofiber (CNF) using aniline

3 g of NFC or CNF was dispersed in 100 mL of 1 M hydrochloric acid solution by ultrasonication for 1 h. Then the dispersion was kept at 0-4 ^{o}C temperature followed by addition of 10 g of aniline. 12.50 g of ammonium persulfate was dissolved in 100 mL 1M HCl solution and was taken in a burette. The APS/HCl was added drop-wise into the aniline-fiber solution to initiate polymerization reaction. The polyaniline-coated fibers (PANI/CNF or PANI/NFC) were then isolated. Different weight percentages of modified fibers were then mixed with poly(vinyl alcohol) solution in water at 90 ^{o}C followed by ultrasonication for 2 h. Films were prepared by casting and dried slowly at 70 ^{o}C for 24 h. Thus, the casted composite films were thin and easily foldable. The folding nature of the film is illustrated in the figure 6.A.2.

6.A.3 Results and discussion

6.A.3.1 Scanning Electron Microscopy

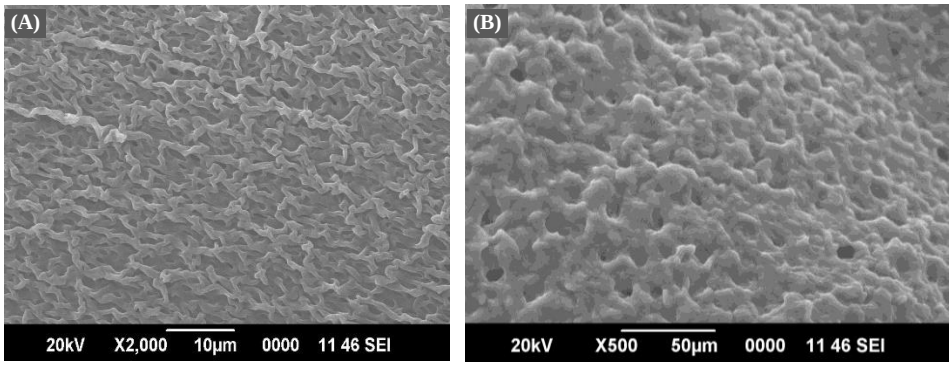

Figure 6.A.1: SEM images of A) PANI/CNF/PVA and B) PANI/NFC/PVA composites

SEM micrographs of the composites are given in figure 6.A.1. It shows a uniform distribution of fibers in the polymer matrix. Shielding efficiency of the composite is directly related to the conductivity of the fibrous fillers. On the other hand, the conductivity is dependent on the even distribution of the conducing fibers in the matrix. High conductivity will contribute to the SE of the composite. Continuous network of CNF/NFC suggests high conductivity and shielding efficiency for the composites.

6.A.3.2 Physical properties of the composite film

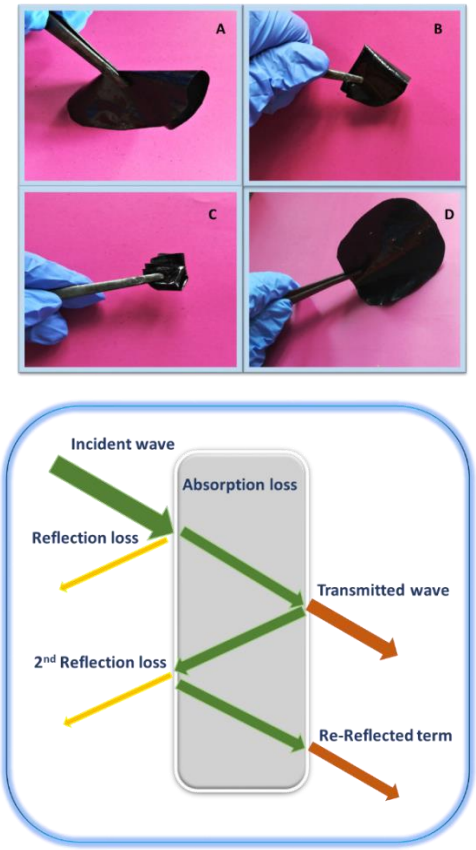

Figure 6.A.2: Illustrates the folding nature of the film.

The density of PANI/CNF/PVA and PANI/NFC/PVA films is about 0.23 g/cm^3 and 0.25 g/cm^3 respectively. The flexibility of the film is clear from the figure 6.A.2. It illustrates multiple folds and the unfolded form of PANI/CNF/PVA composite. Thus, the composites films prepared using CNF is of light weight and easily foldable.

6.A.3.3 Microwave dielectric properties

6.A.3.3.1 Dielectric permittivity

The real and imaginary permittivity of both CNF and NFC based composites in 8-12 GHz frequency range are shown in the figure 6.A.3. Four different concentrations were analyzed for each composite i.e. 10, 20, 30 and 40 wt.% in X-band at four different frequencies. It can be noticed that the permittivity value is increased substantially by the addition of PANI/CNF and PANI/NFC fibers into PVA matrix. It is due to the conductive nature of fibers incorporated in the matrix.

For all the composites, significant improvement in the permittivity is observed with increase of fiber loading. Better increase is observed for PANI/CNF/PVA composite. Koops et al. described the dielectric permittivity as the inverse of the square root of resistivity [25]. The CNF based composites show higher permittivity than NFC composites owing to the conductivity difference of the fibers. For PANI/CNF/PVA composites a dielectric permittivity of 62 is obtained at 8.55 GHz frequency. While for PANI/NFC/PVA composite, the value is much lower, it is only about 38 at the same frequency range. This is evidently related to the conductivity of the particles in the matrix. Well defined conductive network is formed at the higher wt.% of the fiber. But these fibers are widely dispersed in the insulating PVA matrix. Greater the

polarizability of the material greater will be the permittivity. Figure 6.A.4 is the cross plot of real permittivity with fiber loading at four different frequencies. It shows an abrupt increase of permittivity with fiber loading and slight reduction with increase of frequency.

The variation of imaginary permittivity with fiber content and the frequency is shown in the figure 6.A.5. The ε'' increases with fiber content as the conductivity is improved in the presence of PANI-coated fibers. Slight reduction in the permittivity values can be observed with increase of frequency (figure 6.A.4). As the applied frequency increases the dipoles will not get enough time to orient with the frequency and consequently the permittivity reduces.

The prepared composites are heterogenous mixtures of conducting fibers and insulating poly(vinyl alcohol). The permittivity of such composites is achieved by the interfacial polarization as well as the intrinsic electric dipole polarizations. Due to the high conductivity difference between polyaniline coated nanofibers and insulating PVA molecules, charge accumulation taking place at the interface of the two. It is known as Maxwell-Wagner-Sillars (MWS) effect [26-28]. Insitu polymerization of aniline was carried out in presence of hydrochloric acid dopant molecules. The doped polyaniline molecules possess positively charged nitrogen atoms surrounded by chloride ions. Hence dipolar polarization is also contributing to the total permittivity of the composites but not to a good extend. Since the contribution from dipolar and space charge polarization to the total permittivity decreases at microwave frequencies. At this frequency, the major contribution is by the electronic

and ionic polarizations. The reduction in the permittivity values can be attributed to the reduction in the space charge polarization with frequency. Compared to the lower wt.% composites more reduction in the permittivity values is observed for higher wt.% composites. It indicates that the prominent contribution of space charge polarization at higher fiber loading. As the concentration of PANI coated fibers in the PVA matrix increases, more conducting regions are formed in the composite. Consequently, there will be more interfacial polarization.

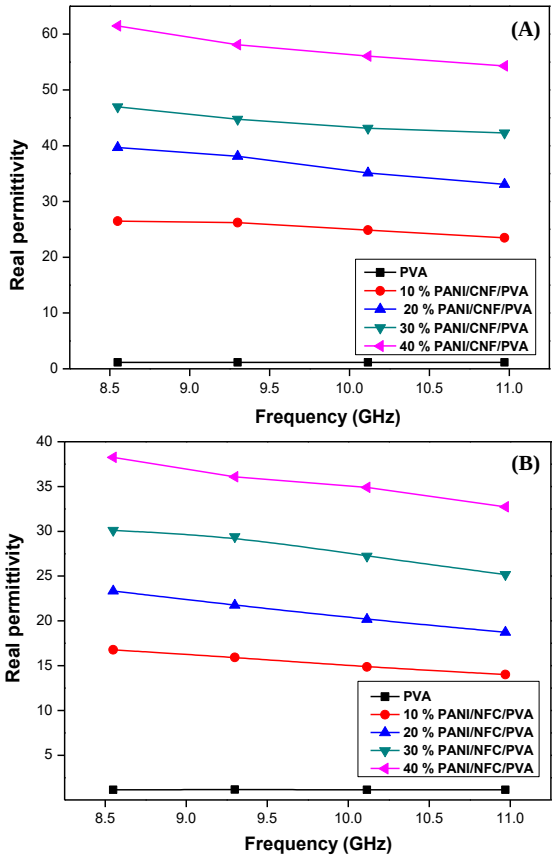

Figure 6.A.3: Variation of real permittivity with frequency for A) PANI/CNF/PVA and B) PANI/NFC/PVA composites

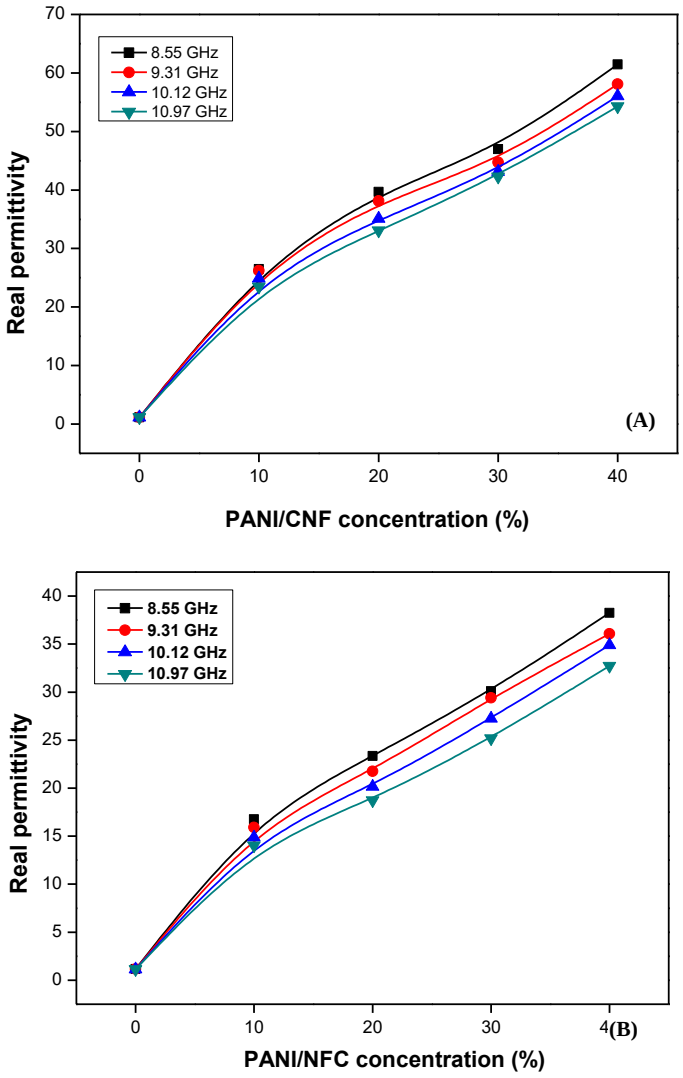

Figure 6.A.4: Variation of real permittivity with A) PANI/CNF concentration and B) PANI/NFC concentration

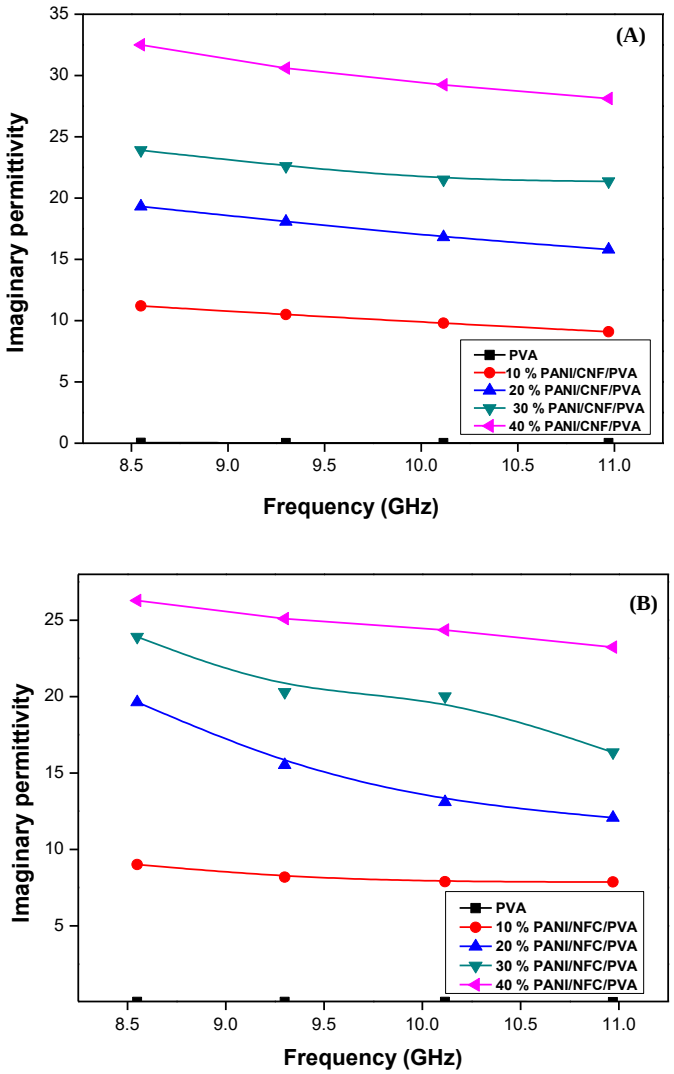

Figure 6.A.5: Variation of imaginary permittivity with frequency for A) PANI/CNF/PVA and B) PANI/NFC/PVA composites

6.A.3.3.2 Loss tangent

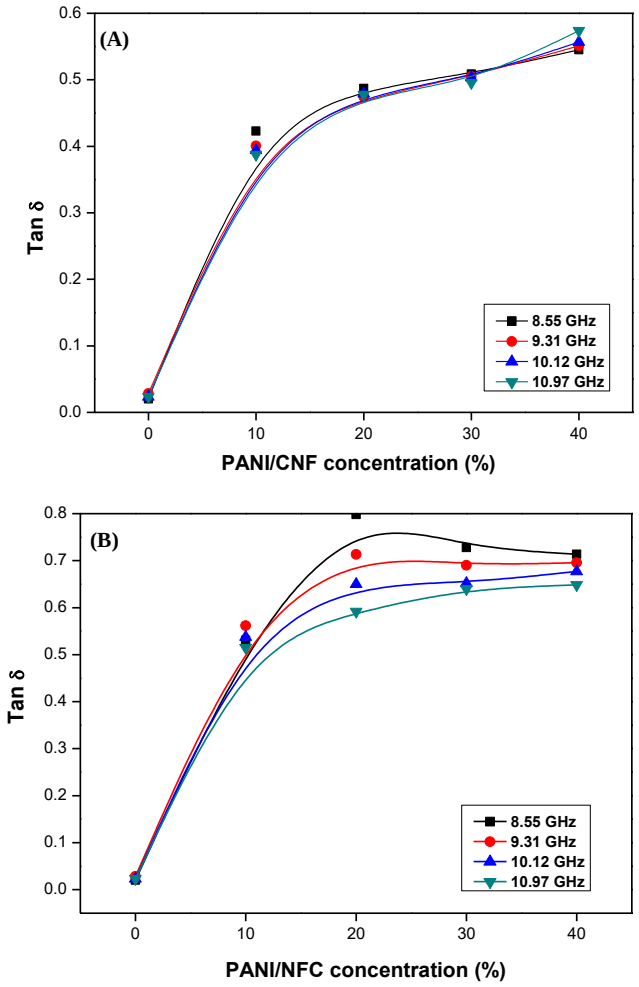

Figure 6.A.6: Variation of tan δ with A) PANI/CNF concentration and B) PANI/NFC concentration

Real and imaginary permittivities are related to each other by the dissipation factor tan δ. Loss tangent is the tangent of the angle δ between the vector for the amplitude of the total current and the amplitude of the charging current [29]. Figure 6.A.6 represents the frequency dependence

of loss tangent in the X-band region. Loss tangent of all the composite reduces with the applied frequency. Because of the leakage current, the composites with higher permittivity also show higher loss tangent. At the percolation threshold, the leakage current is more distinct because of the direct contact between the conducting fibers. Owing to the difference in the conductivity and permittivity of the particles, charge builds up occurs at the macroscopic interface. This kind of charge accumulation at the heterogenous interface causes field distortions and dielectric loss to the materials. The involvement of ionic conduction in the total loss becomes outstanding with decrease in frequency of applied field. When the frequency is increased the interfacial polarization, decreases resulting a reduction in the polarizability and loss factor. The higher the dielectric constant of the material greater will be its dielectric loss. Hence it absorbs more microwaves and becomes more opaque to electromagnetic radiation as the concentration of the conducting fibers increases.

6.A.3.3.3 AC Conductivity

Microwave conductivity is derived directly from the dielectric loss of the material. Hence the plots are much similar to that of the imaginary part of permittivity.

$$\varepsilon'' = \frac{\sigma}{2\pi f \varepsilon_0} \quad \text{.....6.A.1}$$

$$\sigma = 2\,\pi\, f\, \varepsilon_0\, \varepsilon'' \quad \text{.....6.A.2}$$

where, ε'' is the imaginary part of permittivity, σ is the electrical conductivity, ε_0 is the permittivity of vacuum, and f is the applied frequency. AC conductivity of all the wt.% composites increases with the

addition of polyaniline coated fibers. This can also be related to the improvement of the dielectric loss of the composites. Conductivity of a composite material mainly depends on the shape and the intrinsic conductivity of the filler and also the surface tension between filler and matrix.

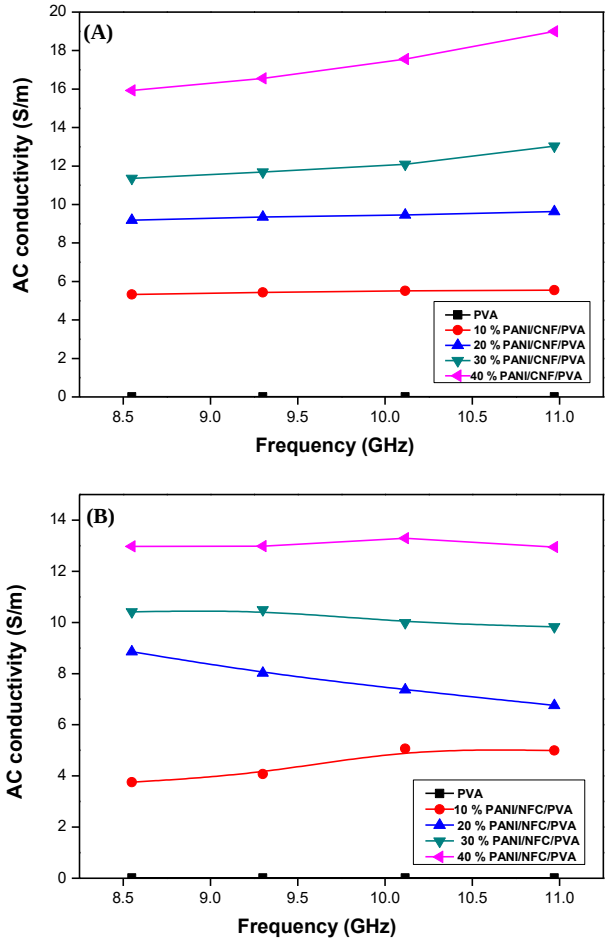

Figure 6.A.7: Variation of AC conductivity with frequency
A) PANI/CNF/PVA, B) PANI/NFC/PVA composites

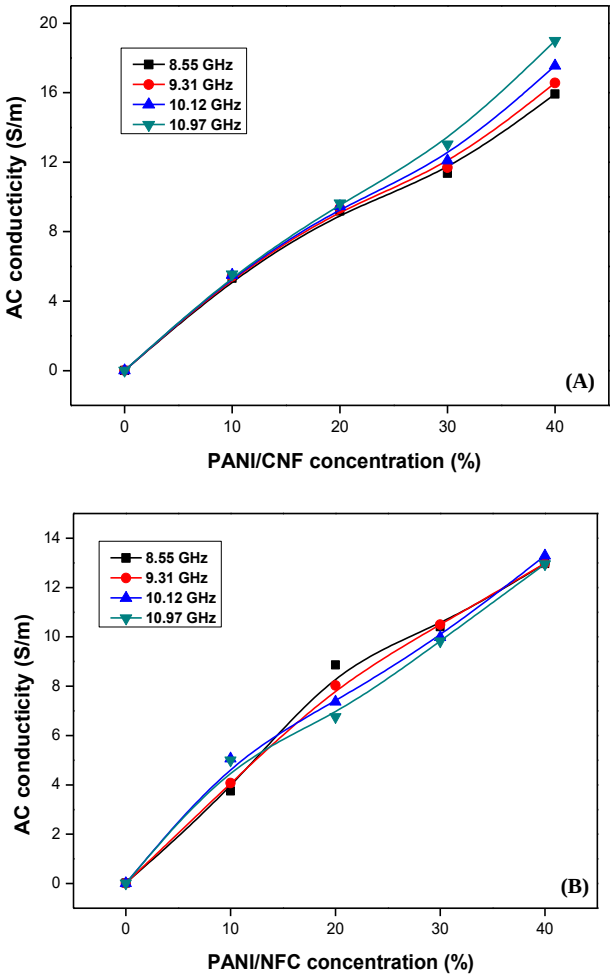

Figure 6.A.8: Variation of AC conductivity with A) PANI/CNF concentration and B) PANI/NFC concentration

Fibrous particles are expected to have more inter particle contact. This results in low percolation threshold. Sharp increase of conductivity is observed for PANI/CNF/PVA composites when compared to PANI/NFC/PVA. It is evident from the figure 6.A.8 that the percolation threshold is much lesser for CNF composites. Even with 10 wt.% of the filler the composite shows very sharp increase of conductivity. The

conductivity is increased from 0.014 S/m (PVA) to 6.1 S/m for 10 wt.% PANI/CNF/PVA composites. At the same fiber content, the NFC composite shows a conductivity of 3.2 S/m. Maximum conductivity of 19.1 S/m is obtained for PANI/CNF/PVA composite at 10.97 GHz.

6.A.3.2.4 Absorption coefficient, Skin depth and Heating coefficient

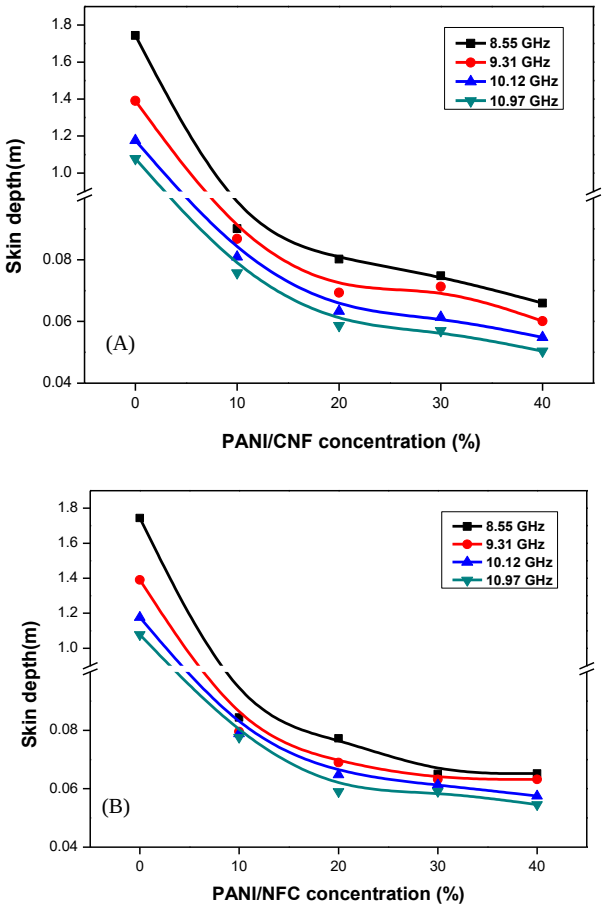

Figure 6.A.9: Skin depth variation with A) PANI/CNF B) PANI/NFC concentration

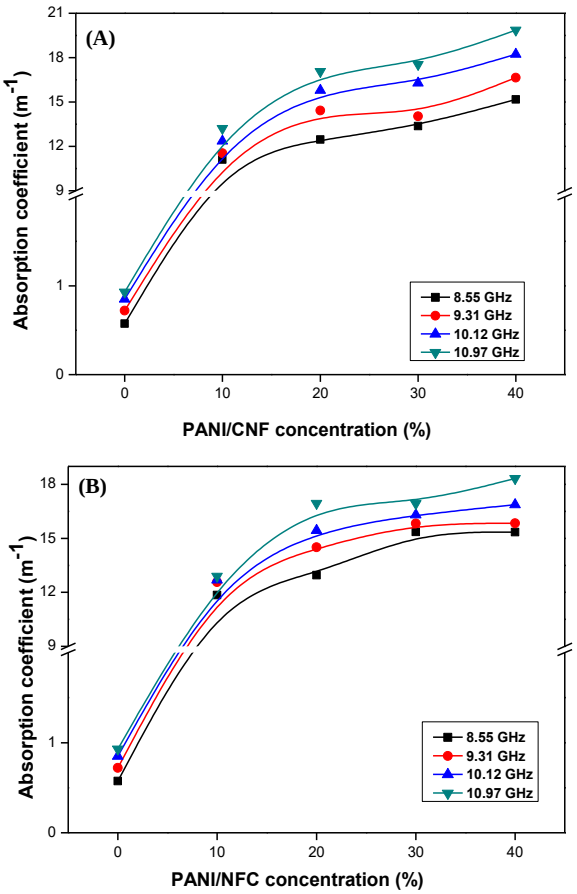

Figure 6.A.10: Variation of absorption coefficient with A) PANI/CNF B) PANI/NFC concentration

The electromagnetic radiation at high frequencies cannot penetrate deep in to the material. It penetrates only in to the near surface of the material. It is called the penetration depth or skin depth. The skin depth is usually defined as the depth in to a material where the microwave power is dropped in to 36.8 % of its initial value. The penetration depth of composites can be calculated from other dielectric parameters. At fixed dielectric properties, the penetration depth of material is inversely

proportional to the applied frequency. So as the frequency increases the skin depth decreases and hence deeper penetration can be expected at the lower frequency range. More surface heating is observed at higher frequency values. The skin depth is reduced from 1.744 to 0.055 and 0.050 for PANI/NFC/PVA and PANI/CNF/PVA composites, respectively. Absorption coefficient is a direct function of complex permittivity. It describes the propagation and absorption of electromagnetic waves during the passage within the material. It is the measure of transparency of the medium. Since the absorption coefficient derived from the dielectric loss, the curves are similar to the tan δ curves. The absorption coefficient exhibits sharp increase with PANI coated fiber concentration in the composite. Better increase is observed for PANI/CNF/PVA composite due to the high conductivity and good dispersion of the polyaniline modified CNF fibers. For pure PVA the absorption coefficient is about 0.5732 m^{-1}. It increases to 19.85 m^{-1} for CNF based composite and to 18.32 m^{-1} for PANI/NFC/PVA composite. The skin depth is inversely proportional to the absorption loss of the material. The contribution of absorption to the total shielding effectiveness increases for the CNF composites. Hence the composites exhibit lower skin depth. The higher aspect ratio and excellent conductivity of CNF results in better EMI shielding and strong skin effect. Variation of heating coefficient with concentration of PANI/CNF and PANI/NFC is given in the figure 6.A.11. Heating coefficient of both composites decreases with frequency and fiber loading.

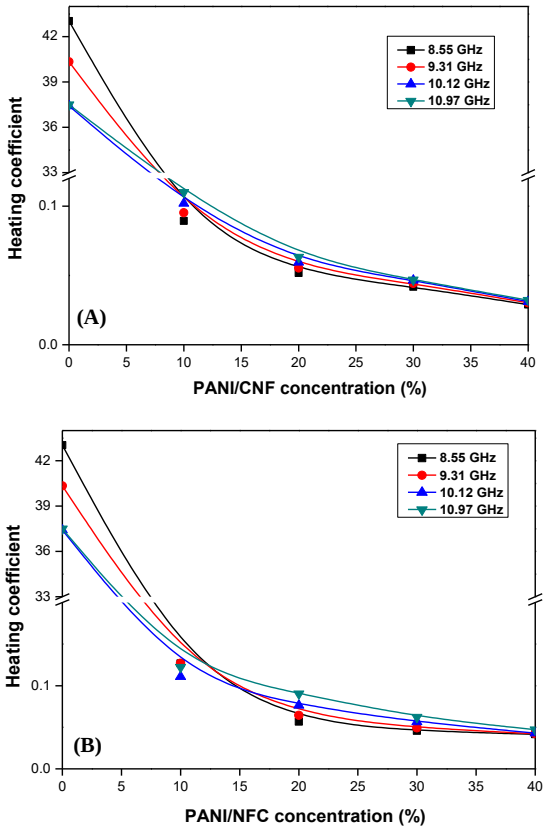

Figure 6.A.11: Heating coefficient Vs fiber concentration
A) PANI/CNF/PVA and B) PANI/NFC/PVA

6.A.3.3 EMI shielding effectiveness

We have measured the EMI shielding efficiency of the composite films at 10, 20,30, 40 wt.% fiber concentrations. EMI shielding efficiency of a material can be defined as the ratio between the incident power and the transmitted power of an electromagnetic wave. SE is expressed in decibels (dB)

$$SE = 10\log\left(\frac{PI}{PT}\right) = 20\log\left(\frac{EI}{ET}\right) \quad \text{.....6.A.3}$$

Here, PI is the power of incident wave and PT is the power on transmitted wave. The shielding effectiveness of PANI/CNF/PVA and PANI/NFC/PVA composites containing different weight percentages of conducting filler were studied for S-band and X-band frequency range. When an electromagnetic radiation is incident on shielding material mainly three different processes are taking place: reflection, absorption and internal multiple reflections [30]. So, the total EMI SE can be described as the sum of the contribution from reflection, absorption and multiple reflections.

$$SE_T = SE_R + SE_A + SE_M \quad \text{6.A.4}$$

According to Schelkunoff' s theory for single layered materials with SE> 10dB the contribution from the multiple reflections can be neglected [31].

$$SE_T = SE_R + SE_A \quad \text{6.A.5}$$

SE increases with the addition of PANI/NFC and PANI/CNF into the polymer matrices. Initially both PANI/CNF/PVA and PANI/NFC/PVA composite have lower SE values. With increasing PANI/NFC and PANI/CNF content, SE is improved significantly. It is interesting to note that under the same fiber concentration the shielding efficiency of PANI/CNF/PVA composite is much higher than PANI/NFC/PVA composite. PANI/CNF/PVA nanocomposites containing 10 wt.% PANI/CNF produces SE of approximately -9 dB while it rises to -31 dB upon the addition of 40 % PANI/CNF. For NFC based composite the highest SE is about -5.1 dB at S band frequency range. Figure 6.A.12

gives the total SE of the PANI/CNF/PVA and PANI/NFC/PVA composites at 2-4 GHz. It can be seen that the SE of the PANI/CNF/PVA composite is significantly higher than that of PANI/NFC/PVA composites at all frequencies.

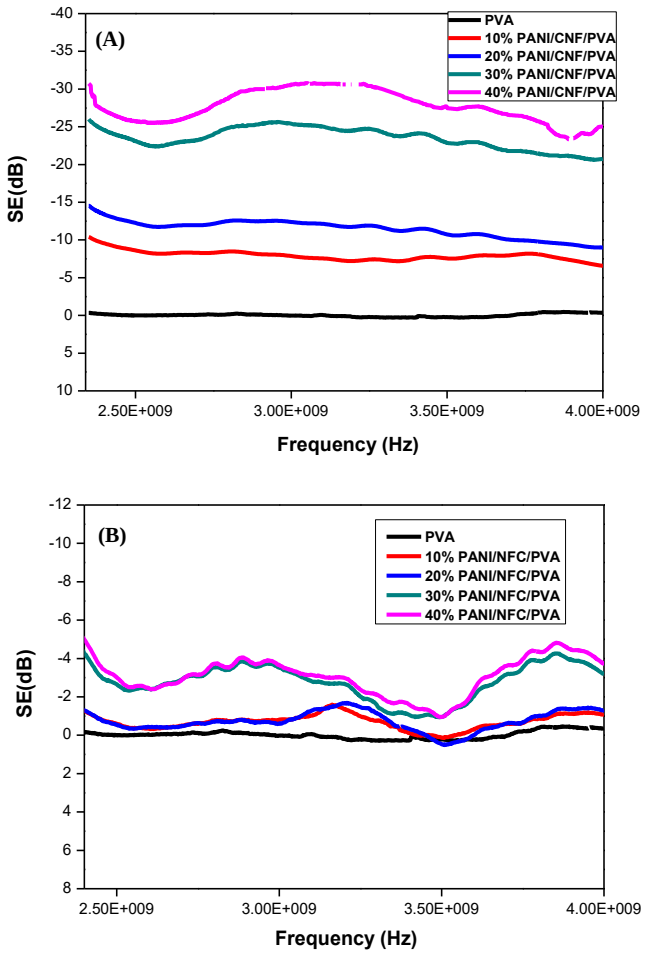

Figure 6.A.12: Total SE as a function of frequency range of 2-4 GHz for A) PANI/CNF/PVA B) PANI/NFC/PVA composites

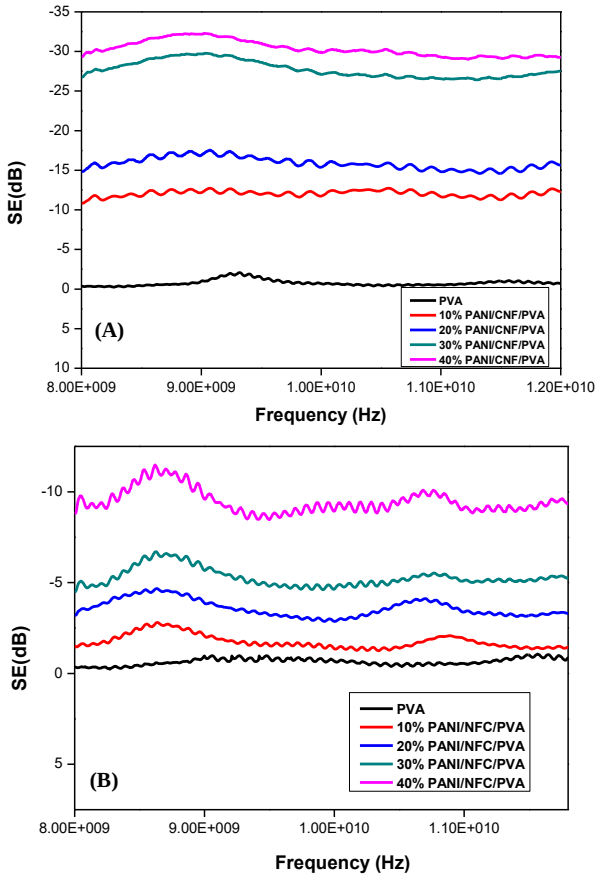

Figure 6.A.13: Total SE as a function of frequency range of 8-12 GHz for A) PANI/CNF/PVA B) PANI/NFC/PVA composites

The shielding efficiency of PVA composites containing different concentrations of PANI/CNF and PANI/NFC in the X-band frequency range is represented in the figure 6.A.13. It shows a trend similar in the S band. The SE of both composites increases with the fiber content. The figures indicate that sudden increase of SE is obtained in case of CNF composites, whereas the SE gradually increases with PANI/NFC concentration. The SE increases from -0.35 dB to -32.2 dB by the addition of 40 % PANI/CNF.

Conductivity of the nanoparticle plays an important role in determining the shielding effectiveness of the composite. When the shielding material is conducting, the electrical and varying magnetic fields of electromagnetic radiation induce currents in the material. In turn, the current generates the counteracting fields. So, the shielding material can reduce the effect of EM field. Studies have revealed that for efficient shielding, the filler in the polymer matrix should possess satisfactory conductivity and dielectric constant [32,33]. As the conductive filler concentration in the matrix increases the incoming radiation interacts more with the particles and improves the shielding effectively. But unlike DC conductivity EMI SE does not require conducting network formation unless it interacts with the conductive particles and impede the radiation [34]. CNF being a good conducting material, the shielding efficiency of PANI/CNF/PVA composite results from the synergistic effect of CNF and PANI. The shielding observed for PANI/NFC composites is due to the presence of polyaniline on cellulose fibers.

Polymer composites containing conductive fillers are good shielding materials. Owing to the skin effect of the shielding material, the material should have small unit size and high conductivity. So, while considering the two different fillers such as NFC and CNF, CNF is of smaller in size and it has higher conductivity. High aspect ratio of the fiber particles helps in achieving good connectivity. Contrast to NFC, CNF achieved high aspect ratio which will result connectivity of the conducting fillers thereby increasing the conductivity of the composite.

According to percolation theory, for a material with high aspect ratio the formation of conductive network results at lower wt.%. The EMI shielding efficiency of the material increases rapidly in the vicinity of percolation threshold. All the properties favor the use of CNF as fillers in the matrix. The effect of percolation is more evident from the SE curves in the X-band region. Significant improvement in SE is observed for PANI/CNF/PVA composite at lower filler concentration itself. At 10 wt.% of PANI/CNF a SE of -10 dB is achieved. Further increase of fiber concentration in PVA matrix yields a continuous increase of shielding effectiveness. It shows that the percolation threshold for CNF based composite lies below 10 %. But such a tremendous increase at lower wt.% concentration is not observed for PANI/NFC/PVA composite.

The high shielding efficiency of metals is due to the reflection of radiation from the surface owing to the excellent conductivity. The shielding effectiveness of the conducting polymers can be attributed to both reflection and absorption. The most important mechanism of EMI shielding is the reflection which takes place when electromagnetic radiation is incident on the field. It occurs by the interaction of the electromagnetic radiation with the free electrons present on the surface of the shielding material. In order to have the free electrons on the surface the material should be electrically conducting.

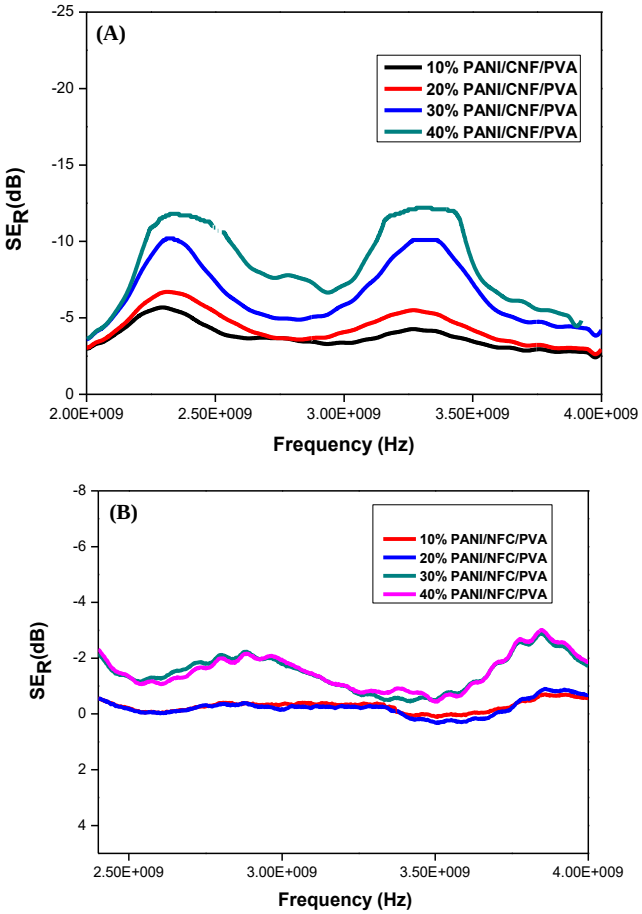

Figure 6.A.14: Reflection component as a function of frequency range of 2-4 GHz for A) PANI/CNF/PVA B) PANI/NFC/PVA composites

Absorption is secondary process of EMI shielding mechanism where the electric dipoles present in the shield interacts with radiation. If the material is more prone to polarization it can have more absorption value than the reflection component. There are mostly three types of polarization mechanisms occur in dielectric material such as electronic polarization, ionic polarization and orientation polarization. Electronic

polarization is present in all types of materials, whereas ionic polarization and orientation polarizations occur when ions and permanent dipoles are present in the molecule. Another involvement to polarization is the space charge or it can be the accumulation of mobile charges at the interfaces. So, in the present case mostly interfacial polarization is contributing to the SE_A. Hydrochloric acid was used for the doping of polyaniline, therefore the presence of electron withdrawing groups on the surface of polyaniline will enhance the interfacial polarization [35,36]. Absorption loss is a function of $\sigma^*\mu$, here, σ is the electrical conductivity and μ is the magnetic permeability. Hence absorption loss increases with the conductivity of the material.

The calculated absorption and reflection components are plotted against frequency (Figure 6.A.14,15,16,17). It is observed that with the addition of conducting fillers both reflection and absorption increases. The absorption process is found to be dominant in all the composites. The SE_R increases with the incorporation of PANI/CNF and PANI/NFC. Better increase in SE_R is observed for PANI/CNF/PVA composites. The number of free electrons on the surface of PANI/NFC/PVA composite are not enough to interact with the incoming radiation, yielding low SE_R. From the results it is found that shielding efficiency due to absorption varies from -7.43 to -24.1 dB in the S-band and from -6.41 to -22.6 dB in the X-band frequency region for PANI/CNF/PVA composite. As a corresponding increase is not observed in SE_R, it can be deduced that the contribution of reflection to SE is relatively small.

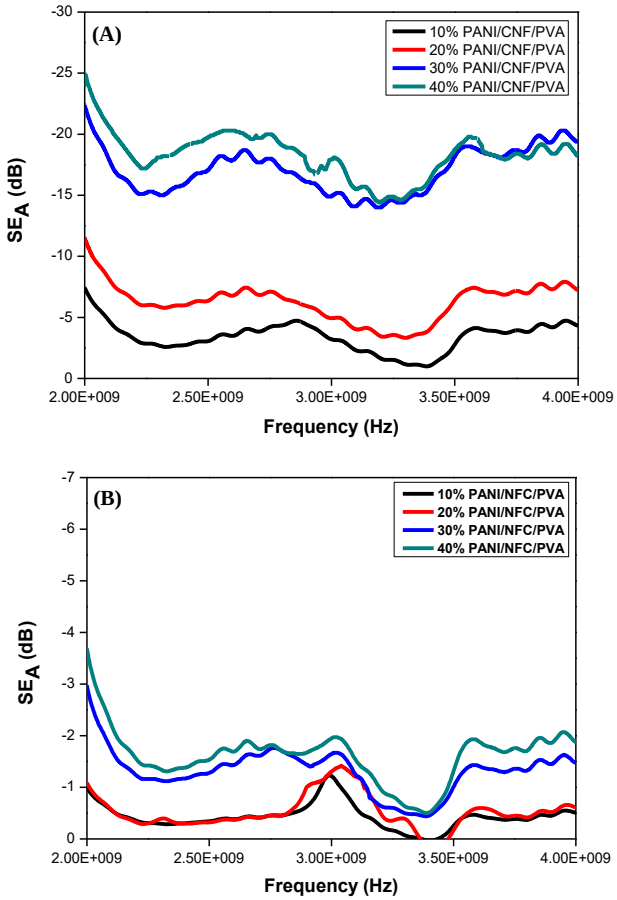

Figure 6.A.15: Absorption component as a function of frequency range of 2-4 GHz for A) PANI/CNF/PVA B) PANI/NFC/PVA composites

For PANI/CNF/PVA composite the percentage of absorption increases from 59 to 78 %. It is evident from the table 6.A.1 that the total shielding efficiency is dominated by absorption rather than reflection. The contribution by the absorption increases with the increase of polyaniline coated fiber content, it can be related to the improvement in the electrical conductivity and surface area of the composite film.

Table 6.A.1: Calculated SE_R and SE_A values of the composites in the 2-4 GHz frequency range

Composite	10 %				20%				30%				40%			
	SE_R	SE_A	SE_T	% of absorption	SE_R	SE_A	SE_T	% of absorption	SE_R	SE_A	SE_T	% of absorption	SE_R	SE_A	SE_T	% of absorption
PANI/CNF/ PVA	3.21	4.65	7.86	59	4.07	8.3	12.37	67	5.8	19.5	25.3	77	6.9	23.7	30.6	78
PANI/NFC/ PVA	0.68	0.9	1.58	56	0.76	1.16	1.92	60	1.5	1.84	3.34	55	1.58	2.15	3.73	57

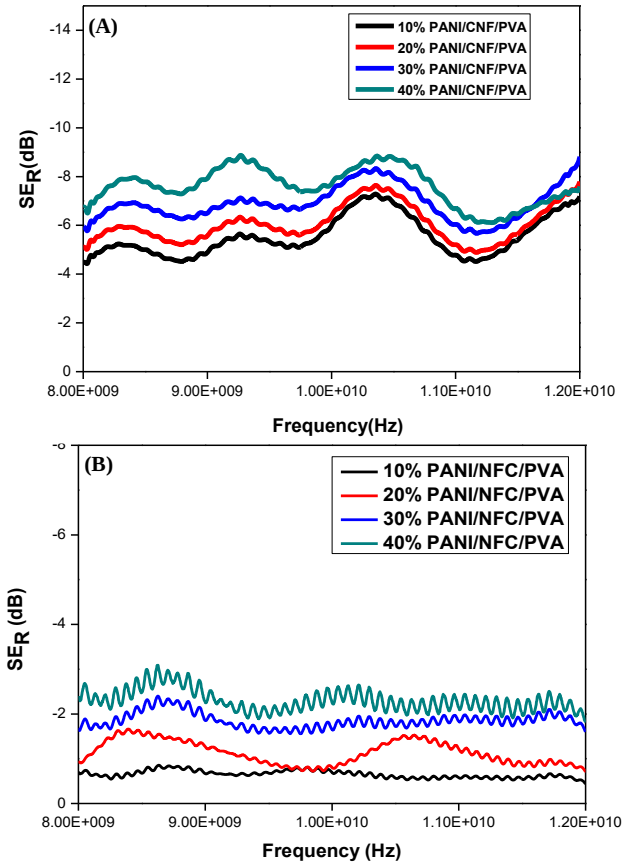

Figure 6.A.16: Reflection component as a function of frequency range of 8-12 GHz for A) PANI/CNF/PVA A) PANI/NFC/PVA composites

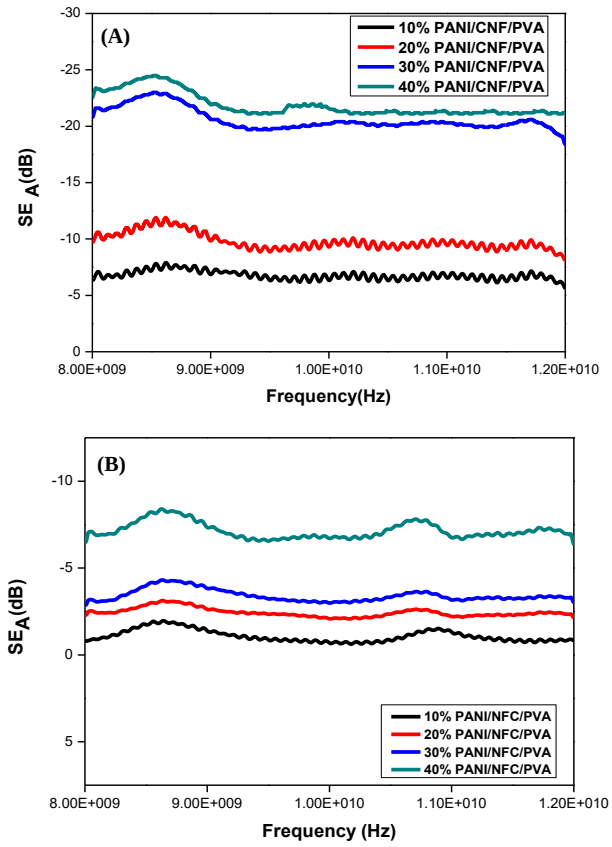

Figure 6.A.17: Absorption component as a function of frequency range of 8-12 GHz for A) PANI/CNF/PVA B) PANI/NFC/PVA composites

Table 6.A 2: Calculated SE_R and SE_A values of the composites in the 8-12 GHz frequency range

Composite	10 %				20%				30%				40%			
	SE_R	SE_A	SE_T	% of absorption	SE_R	SE_A	SE_T	% of absorption	SE_R	SE_A	SE_T	% of absorption	SE_R	SE_A	SE_T	% of absorption
PANI/CNF /PVA	4.47	6.41	10.88	59	5.11	9.76	14.87	65	5.94	20.8	26.74	77	6.23	22.1	28.33	78
PANI/NFC /PVA	0.715	0.838	1.452	55	0.947	2.0	3.241	61	1.68	2.9	4.58	63	2.4	6.51	9.23	70

As the shielding efficiency is related to the thickness of the material, the challenge is to develop the material with lowest thickness possessing higher SE. Comparison of shielding efficiency of various composites are given in the table 6.A.3. It important to indicate the density of the composite film is much less compared to the literature reports. The density of 40 % PANI/CNF/PVA composite film is about 0.21 g/cm^3. The composite exhibited maximum total shielding effectiveness of -32.2 dB at a thickness of 0.12 mm. Therefore, the material meets the requirements for commercial EMI shielding applications. The efficiency increases with the thickness of the sample. Moreover, the EMI shielding efficiency can be further improved by increasing thickness or filler loading. The significance of EMI shielding efficiency can be effectively described in terms of specific EMI SE. Compared to other carbonaceous materials PANI/CNF/PVA composite exhibits very high specific EMI SE.

Table 6.A.3: Comparison of specific EMI SE of with different carbon-based composites reported in the literature

Composites	**Density (g/cm-3)**	**thickness (mm)**	**EMI SE (dB)**	**specific EMI SE (dB cm^3/g)**
graphene/PMMA	.79	2.4	13-19 [37]	17-25
MnO_2 /Graphene		3	57 [38]	
Fe3O4/MWCNT/Wax		3	75 [39]	
PS/Graphene	0.45	2.5	29 [40]	64.4
MCMB/MWCNT	0.26	0.6	31-56 [41]	119-215
MWCNT/epoxy		0.35	19 [42]	
MWCNT/resin	0.51	0.14	32.4 [43]	63.5
polyimide/graphene	0.28	.8	17-21 [44]	60-75
CNT/PS	0.56		19 [45]	33.1
graphene/PEVA		0.36	23-27 [46]	
Fe_3O_4/RGO/PANI		2.5	26 [47]	
carbon foam/MWCNT	0.54	2.75	85 [48]	163
PMMA/CNT		.57	29 [49]	
Fe_3O_4/RGO PEI	0.40	2.5	14.3-18.2 [50]	35-45
Fe_3O_4/Graphene	0.78	.03	21-24 [51]	26-31
PANI/CNF/PVA	**0.21**	**0.12**	**32.2**	**153.3**

6.A.3.4 Dependence of shielding efficiency on conductivity

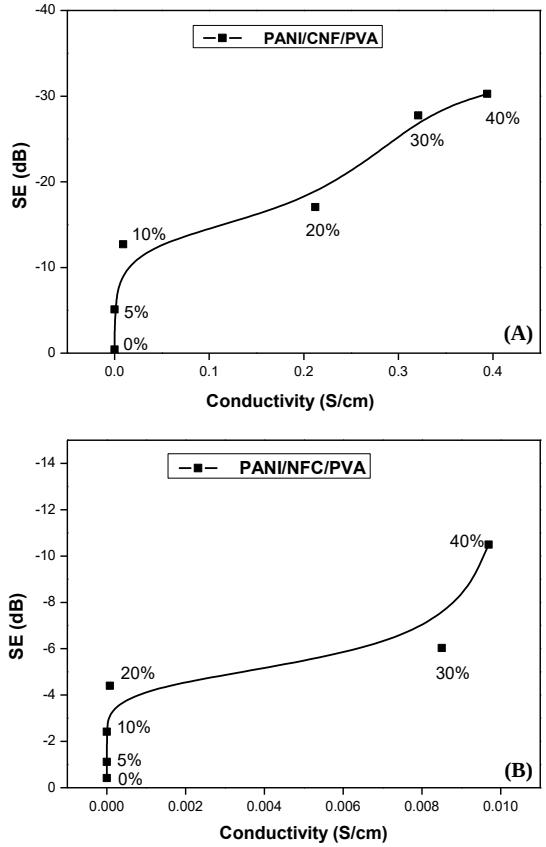

Figure 6.A.18: Shielding efficiency as a function of DC conductivity at 9 Hz for A) PANI/CNF/PVA, B) PANI/NFC/PVA composites

The dependence of shielding effectiveness on the conductivity of the composite can be understood from the figure 6.A.18. It is clear from the figure that for PANI/CNF/PVA composite the rapid increase of SE starts at lower wt.%. But gradual increase is observed for NFC composite. The change in the shielding efficiency at lower concentration of PANI/NFC is low. On inclusion of 10 wt.% PANI/NFC, DC conductivity increases five orders from 10^{-11} to 10^{-6}. But at that concentration the SE rises faintly

from -0.41 to -1.1dB. That means small change in the PANI/NFC concentration makes abrupt changes in the DC conductivity while the influence on the shielding efficiency is low (the variation is not much clear from the figure). Similar behavior is observed for PANI/CNF/PVA composite also. For 5 wt.% composite the DC conductivity increases from 10^{-11} to $5* 10^{-8}$ S/cm and SE increase -0.41 to -5.2 dB. After the percolation threshold, the composites exhibit the reverse trend. The variation of DC conductivity becomes low and the change of SE becomes quite significant. Similar variation of SE has been reported in the literature [52,53]. It shows that the conductivity is originated from the network of conductive fillers while the SE requires only conductive particles to interact and impede the electromagnetic radiation. It can be evidenced from the figure that the conductivity is not the only aspect for controlling the SE of the material. In addition to that the size of the filler also plays significant role. The high aspect ratio of the material helps to achieve low percolation threshold for the composites. The BET analysis of PANI/CNF and PANI/NFC fibers (chapter 5A) shows the high surface area for PANI/CNF fibers. The interaction of electromagnetic waves with the material increases with the surface area. Thus, the increased shielding efficiency of PANI/CNF/PVA composite is due the combination of conductivity and high surface area of the fibers.

6.A.4 Conclusion

PANI/CNF/PVA and PANI/NFC/PVA composites were prepared by ultrasonication-assisted mixing of PANI coated CNF/NFC fibers with poly(vinyl alcohol) solution. The composite films are of light weight, flexible and easily foldable which exhibits high permittivity and excellent

EMI shielding properties in both S and X-band frequencies. The composites were characterized in terms of permittivity, loss tangent, skin depth and heat generated during microwave irradiation. The effect of conductivity of the two nanofibers on the microwave properties of the composites were studied. The results obtained here have outlined how the conductivity variation effecting the microwave properties. High permittivity with good EMI shielding efficiency was obtained for CNF compared to NFC based composites. It is due to the high conductivity of carbon nanofibers. Beside good electrical conductivity, high surface area of carbon nanofiber makes PANI/CNF/PVA composite efficient for EMI shielding. The results clearly indicate how the conductivity of the filler is able to significantly affect the electromagnetic properties at the microwave frequencies. Maximum shielding effectiveness of -32.2 dB was achieved for PANI/CNF/PVA composite at 0.12 mm thickness. High specific EMI SE of 153.3 dB cm^3/g was obtained for PANI/CNF/PVA composite which is more than the values reported for carbon-based composites. Easily foldable polymer composite film with excellent absorption dominated electromagnetic interference shielding can be an excellent EMI shielding material.

References

[1] R. C. Che, L. M. Peng, X. F. Duan, Q. Chen, X. L. Liang, Adv Mater, 2004, 16, 401

[2] Y. L. Yang, M. C. Gupta, K. L. Dudley, R. W. Lawrence, Nano Lett., 2005, 5, 2131

[3] M. S. Cao, X. L. Shi, X. Y. Fang, H. B. Jin, Z. L. Hou, W. Zhou, Appl Phys Lett., 2007, 91, 2031101

[4] W. L. Song, M. S. Cao, Z. L. Hou, X. Y. Fang, X. L. Shi, J. Yuan, Appl Phys Lett., 2009, 94, 2331101

[5] N. Li, Y. Huang, F. Du, X. B. He, X. Lin, H. J. Gao, Nano Lett., 2006, 6, 1141

[6] Y. Huang, N. Li, Y. F. Ma, D. Feng, F. F. Li, X. B. He, Carbon, 2007, 45, 1614

[7] X. L. Shi, M. S. Cao, J. Yuan, Q. L. Zhao, Y. Q. Kang, X. Y. Fang, Appl Phys Lett, 2008, 93, 1831181

[8] R. Panigrahi, S. K. Srivastava, Sci. Rep., 2015, 5, 7638.

[9] R. Che, L. M. Peng, X. F. Duan, Q. Chen, Adv. Mater., 2004, 16, 401

[10] H. S. Cho, S. S. Kim, IEEE Trans. Magn., 1999, 35, 3151

[11] D. Micheli, C. Apollo, Compos Sci Technol., 2010, 70, 400

[12] K. Y. Park, J. H. Han, Compos. Sci. Technol., 2009, 69, 1271

[13] J. Cao, F. Wuyou, Mater Sci Eng B, 2010, 175, 56

[14] N. F. Colaneri, L. W. Shacklette, IEEE Trans. Instrum. Meas., 1992, 41, 291

[15] J. Joo, A. J. Epstein, Appl. Phys. Lett., 1994, 65, 2278

[16] T. Makela, S. Pienimaa, T. Taka, S. Jussila, H. Isotalo, Synth. Met., 1997, 85, 1335

[17] J. Joo, C. Y. Lee, H. G. Song, J.-W. Kim, K. S. Jang, E. J. Oh, A. J. Epstein, Mol. Cryst. Liq. Cryst., 1998, 316, 367

[18] X. Luo, D. D. L. Chung, Carbon, 1996, 34, 1293

[19] W. L. Song, M. S. Cao, Z. L. Hou, J. Yuan, X. Y. Scr, Mater., 2009, 61, 201

[20] D. D. L. Chung, Carbon, 2001, 39, 279

[21] Z. F. Liu, G. Bai, Y. Huang, Y. F. Ma, F. Du, F. F. Li, Carbon, 2007, 45, 821

[22] M. A. Montes-Moran, F. W. J. Van Hattum, J. P. Nunes, A. Martinez-Alonso, J. M. D. Tascon, C. A. Bernardo, Carbon, 2005, 45, 1795

[23] M. A. Montes-Moran, R. J. Young, Carbon, 2002, 40, 857

[24] M. S. Cao, W. L. Song, Z. L. Hou, B. Wen, J. Yuan, Carbon, 2010, 48, 788

[25] C. G. Koops, Phys Rev., 1951, 83, 121

[26] R. Tamura, E. Lim, T. Manaka, M. Iwamotoa, J. Appl. Phys., 2006, 100, 114515

[27] Z. M. Dang, L. Wang, Y. Yin, Q. Zhang, Q. Q.Lei, Adv. Mater., 2007, 19, 852

[28] F. He, S. Lau, H. L. Chan, J. T. Fan, Adv. Mater., 2009, 21,710

[29] T. A. Ezquerra, F. Kremmer, Wegner, Progress in electromagnetic research. Vol 6, Elsevier, New York,1992.

[30] Y. Yang, M. C. Gupta, K. L. Dudley, R. W. Lawrence, Nano Lett., 2005, 5, 2131

[31] P. Saini, V. Choudhary, B. P. Singh, R. B. Mathur, S. K. Dhawan, Mater. Chem. Phys., 2008

[32] D. D. L. Chung. Carbon, 2001, 39, 279

[33] S. Y. Yang, K. Lozano, A. lomeli, H. D. Foltz, R. Jones, Compos Part A, 2005, 36, 691. 5

[34] D. D. L. Chung, Carbon, 2001, 39, 279–285

[35] Q. Li, Q. Z. Xue, X. L. Gao, and Q. B. Zheng, Polymer Letters, 2009, 3, 769

[36] V. P. Anju, Sunil K. Narayanankutty, AIP Advances, 2016, 6, 015109

[37] H. B. Zhang, Q. Yan, W. G. Zheng, Z. He, Z. Z. Yu, ACS Appl. Mater. Interfaces, 2011, 3, 918

[38] T. K. Gupta, B. P. Singh, V. N. Singh, S. Teotia, A. P. Singh, I. Elizabeth, S. R. Dhakate, S. Dhawan, R. Mathur, J. Mater. Chem. A, 2014, 2, 4256

[39] M. S. Cao, J. Yang, W. L. Song, D. Q. Zhang, B. Wen, H. B. Jin, Z. L. Hou, J. Yuan, ACS Appl. Mater. Interfaces, 2012, 4, 6949

[40] D. X. Yan, P. G. Ren, H. Pang, Q. Fu, M. B. Yang, Z. M. Li, J. Mater. Chem., 2012, 22, 18772

[41] A. Chaudhary, S. Kumari, R. Kumar, S. Teotia, B. P. Singh, A. P. Singh, S. K. Dhawan, S. R. Dhakate, ACS Appl. Mater. Interfaces, 2016, 8, 10600

[42] B. Singh, V. Choudhary, P. Saini, S. Pande, V. Singh, R. Mathur, J. Nanopart. Res., 2013, 15, 12

[43] S. Teotia, B. P. Singh, I. Elizabeth, V. N. Singh, R. Ravikumar, A. P. Singh, S. Gopukumar, S. Dhawan, A. Srivastava, R. Mathur, RSC Adv., 2014, 63, 33168

[44] Y. Li, X. Pei, B. Shen, W. Zhai, L. Zhang, W. Zheng, RSC Adv., 2015, 5, 24342

[45] Y. Yang, M. C. Gupta, K. L. Dudley, R. W. Lawrence, Nano Lett., 2005, 5, 2131

[46] W. L. Song, M. S. Cao, M. M. Lu, S. Bi, C. Y. Wang, J. Liu, J. Yuan, L. Z. Fan, Carbon, 2014, 66, 67

[47] K. Singh, A. Ohlan, V. H. Pham, R. Balasubramaniyan, S. Varshney, J. Jang, S. H. Hur, W. M. Choi, M. Kumar, S. Dhawan, B.-Y. Kong, J. S. Chung, Nanoscale, 2013, 5, 2411

[48] R. Kumar, S. R. Dhakate, T. Gupta, P. Saini, B. P. Singh, J. Mater. Chem. A, 2013, 18, 5727.

[49] K. Hayashida, Y. Matsuoka, Carbon, 2015, 85, 363

[50] B. Shen, W. Zhai, M. Tao, J. Ling, W. Zheng, ACS Appl. Mater. Interfaces, 2013, 5, 11383

[51] W. L. Song, X. T. Guan, L. Z. Fan, W. Q. Cao, C. Y. Wang, Q. L. Zhao, M. S. Cao, J. Mater. Chem. A, 2015, 3, 2097

[52] V. K. Sachdev, S. Bhattacharya, K. Patel, S. K. Sharma, N. C. Mehra, R. P. Tandon, J. appl. Polym. Sci., 2014, 131, 40201

[53] [53] V. K. Sachdev, S. K. Sharma, M. Tomar, V. Gupta, R. P. Tandon, RSC Adv., 2016, 6, 45049

Part B

Effect of dopants on the antimicrobial activity of PANI/CNF/PMMA composites

Polymeric composites based on poly(methyl methacrylate), carbon nanofiber and polyaniline were prepared and the effect of various dopants on the morphology and antibacterial property was evaluated. CNF was given a coating of PANI by in situ polymerization method and was used to prepare the composite by solution casting method. The activity of the composites against Escherichia coli, Klebsiella pneumoniae and Bacillus subtilis bacteria was evaluated by agar well diffusion method. The antibacterial activity was assessed by measuring the inhibition zone diameter and minimum inhibitory concentration. The composites showed variable toxicity indicating a dependence on the type of doping agent used. A zeta potential value of +39.60 mV was obtained for phosphoric acid doped PANI/CNF composites, indicating its antibacterial property. The results showed that the antibacterial activity of this composites is tunable.

6.B.1 Introduction

The antibacterial properties of polymers have been recognized in the past decades [1]. Among the several polymer types, conducting polymer received much attention because of good cellular response [2,3]. The redox properties of polyaniline have opened up new opportunities such as immobilization platform for tissue growth, biosensors, controlled drug delivery systems and neural probes etc. [4-9]. The antibacterial activity of polyaniline is greatly influenced by its hydrophilicity, molecular weight and the electrostatic attraction between PANI and bacteria. The electrical conductivity of polyaniline can be controlled by dopant ions [10-12] and the addition of inorganic ions [13]. The dopant molecule is one of the key factors that controls the properties of PANI.

Polymeric nanocomposite has gained special attention over the last decades because of the increased surface area to volume ratio, interesting possibilities for their structural modification, prominent activity compared to its micro and macro counter parts etc. [14,15]. A combination of polymeric nanocomposite and microbiology can prime the development of novel antibacterial agents. Carbon based nanomaterials have evolved as novel antimicrobial agents [16-19]. It has been reported that carbon based nanomaterials can damage the bacterial membranes owing to the oxidative stress [20-23]. The size and surface area of particles play significant role in their antibacterial activity [24]. In the nanometer scale the surface area will be more and consequently there will be more chance for interaction with the bacterial cells. On the basis of this carbon nanomaterial is used in PMMA/PANI to develop antibacterial polymer composites. Several studies have shown that carbon based nanoparticles such as single walled nanotubes and graphene oxide exhibited significant cytotoxicity to animal cells. The present study explores the antibacterial activity of PANI/CNF/PMMA composite with emphasis on the role of dopants.

Poly(methyl methacrylate) is used as the matrix since it is biocompatible and it can act as host matrix for material embedding. PMMA based bone cement has been found to be very efficient for the anchoring of artificial joints [25]. During the implantation, it is at high risk of infection. Pioneering work of Buchholz and Engelbrech has cemented the way to reduce the infection rate [26]. Successively the contribution of Thierse [27] Wannske and Tscherne [28] proved that

significant reduction in the infection rate could be achieved after the addition of antibacterial agents in to PMMA molecules [29].

In view of growing importance of antibacterial drugs, I report the preparation of PANI/CNF/PMMA nanocomposite by insitu polymerization of aniline using various doping agents. Even though the antibacterial activity of polyaniline has been extensively reported, the effect of dopants has not been studied systematically. This work aims to design and develop antibacterial composite by tuning the properties of PANI through proper selection of dopants.

6.B.2 Experimental

6.B.2.1 Method of Preparation

0.3 g of CNF was dispersed in 1.25 M acid dopant solution by sonication for 1 h. To the well dispersed solution of CNF, 5 g of aniline was added and ultrasonication was continued for another half an hour. The reaction mixture was kept at 0-4 °C under constant magnetic stirring and ammonium persulfate (7.5 g in 50 mL 1M HCl) solution was added from the burette. The polymerization of aniline was continued for 24 h at low temperature. Then the green colored polyaniline coated CNF was filtered washed recurrently with distilled water, finally it was washed with acetone and dried at 75 °C for 24 h. The same procedure was followed for all the acid dopants.

Poly(methyl methacrylate) was dissolved in DMSO at 70 °C. The synthesized PANI/CNF was added to the PMMA solution. The filler loading was adjusted to get 10, 20, 40, 50, 60, 70, and 80 wt. %.

6.B.2.2 Antibacterial activity study

The antibacterial activity of the PANI/CNF/PMMA nanocomposites was tested against *Escherichia coli, Klebsiella pneumoniae and Bacillus subtilis* microorganisms. The bacterial test was performed by agar well diffusion method. All the test bacteria were grown in nutrient agar medium and it was incubated at 37 °C for 24 h. The nutrient agar medium was prepared by using peptone (5 g), NaCl (5 g), yeast extract (2 g), agar (20 g) in 1000 mL distilled water. The agar medium was sterilized in autoclave. Then a sterile cotton swab was dipped either in gram-positive or gram-negative culture. The excess inoculum present was eliminated by pressing the saturated swab against the internal wall of culture tube. The entire agar surface was spread over the plate to ensure the substantial growth over the whole surface. The plates were dried for 5 minutes. Wells on the agar plates were created (6 mm) by employing the gel puncture. One drop of various concentrations of PANI/CNF/PMMA composite was added to each well using sterile micropipette and it was incubated for 24 h at 37 °C. The diameters of inhibition zone formed around each well were determined in millimeter. The experiments were repeated under the same conditions and the average diameter was considered. Pure DMSO was used as negative control.

6.B.2.3 Minimum inhibitory concentration (MIC) analysis

MIC of H_3PO_4 doped PANI/CNF/PMMA composite was determined by agar well diffusion method. Different concentrations of the composites (10 %, 20 %, 30 %, 40 %, 50 %, 60 %) were prepared. All the concentration of PANI/CNF in PMMA matrix was tested against *Escherichia coli,*

Klebsiella pneumoniae and Bacillus subtilis microorganisms. All MIC values reported here is based on three experimental repeats revealing the reproducibility of the obtained results.

6.B.3 Results and discussion

6.B.3.1 Characterizations of the composites

The size of the particle is an important factor in determining the antibacterial activity. The SEM images of the polyaniline coated CNF fibers are given in chapter 3. SEM images of PANI/CNF show an average diameter of CNF fiber after PANI coating with various dopants is about 340 nm. i.e. the fiber diameter is increased from 90 nm to 340 nm. Phosphoric acid doped PANI/CNF composite exhibit much lower diameter, approximately 152 nm, i.e. half of the diameter of other PANI/CNF composites. Recent reports have indicated that the size of the particles plays a significant role in the inactivation of microorganisms [32].

In order to obtain additional evidence for the size variation PANI coated CNF fibers the surface area and porosity of all five different PANI/CNF composites were measured by nitrogen sorption experiments at 77.3 K. The nitrogen adsorption/desorption isotherms are given in chapter 3. The surface area obtained for the CNF is about 45 m^2/g while it is reduced to 33-14 m^2/g range for PANI/CNF composites. The surface area is found to vary with different doping agents. In a comparison of the BET surface area of the composites, it is obvious that the highest surface area is obtained for H_3PO_4 doped PANI/CNF composites. Apart from this, H_3PO_4 composite exhibited lowest pore diameter, it is about 15.25 nm.

The pore diameter of the PANI/CNF fibres is distributed in the mesoporous region, i.e. 10-35 nm. H_3PO_4-PANI composite shows highest N_2 absorption at $P/P_0=1$.

6.B.3.1.1 Zeta potential analysis

Zeta potential measurement was carried out to comprehend the stability of nanoparticles in the solution and to examine the effect of PANI/CNF particles on the membrane surface potential. The zeta potential analysis (figure 6.B.1) confirmed a positive surface charge of + 39.60 mV for the PANI/CNF nanoparticles. As a result, the nanoparticles will absorb on to the negative bacteria cell wall, destabilizing the microbial cell wall. Ahn et al. [39] have reported that the use of cationic aluminium ions affected the surface negativity of the root cell membranes, resulting the destabilization of the membranes. Harkes et al. [40] witnessed the absence of growth of microorganisms (*E. coli*) on the positively charged poly(methyl methacrylate) films. So, in the process of cation induced activity, there is significant impact on the measurement of zeta potential. The cations present in the composite interfere with the membrane bound ATPs, effecting the membrane potential. APTase are responsible for regulating the membrane potential by the movement of hydrogen ions. So, the zeta potential analysis of the current study reveals the potential application of PMMA composite as an antibacterial agent.

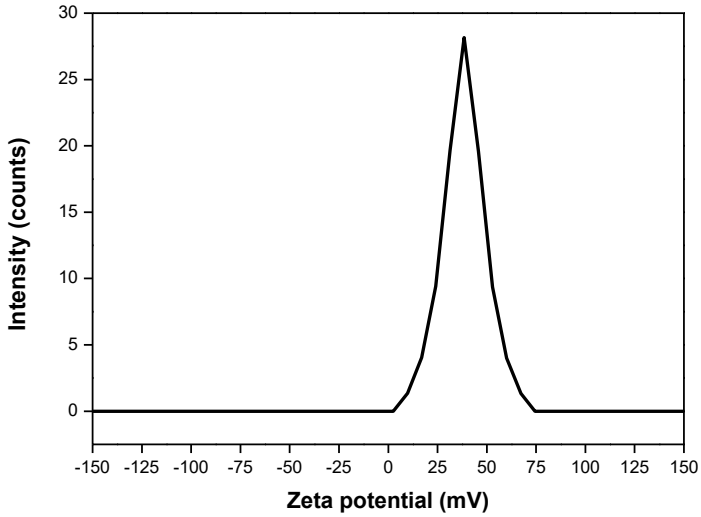

Figure 6.B.1: Plot of zeta potential Vs intensity for PANI/CNF/PMMA composite

6.B.3.2 Anti-bacterial properties

The agar well diffusion method was adopted to explore the antibacterial activity of PANI/CNF/PMMA composites. The test was carried out for three bacterial strains viz. *Escherichia coli, Klebsiella pneumoniae* and *Bacillus subtilis.* The zones of inhibition obtained for PANI/CNF/PMMA composites containing various dopants are shown in the figure 6.B.2. All the composites exhibit good resistance against the *E. coli. E. coli* was inhibited strongly by H_3PO_4-PANI/CNF/PMMA composite.

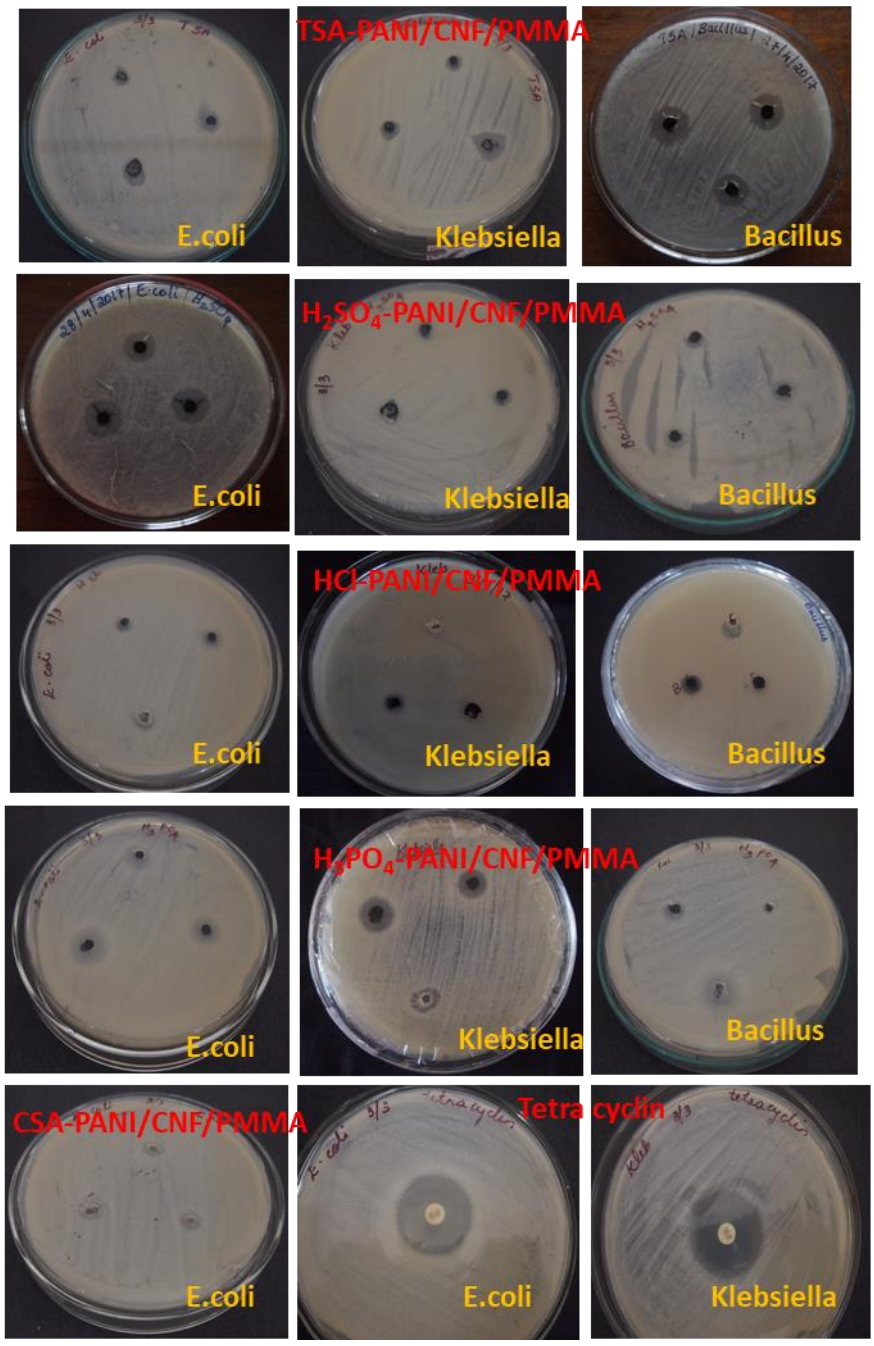

Figure 6.B.2: Average zones of inhibition obtained for different nanocomposites against *Escherichia coli*, *Klebsiella pneumoniae* and *Bacillus subtilis*.

The antibacterial activity of the compounds can be classified as the strong, moderate and low depending on the zone of inhibition diameter. When the zone of inhibition is greater than 16 mm it is strong activity. For moderate antibacterial activity, the zone of inhibition lies in the range of 10-16 mm and low activity is reported when the diameter is less than 10 mm. Strong antibacterial activity is observed for the PANI/CNF/PMMA composite when the PANI/CNF concentration is greater than 50 wt.%.

Polyaniline exhibits strong antimicrobial activity due to electrostatic attraction between polyaniline and the organisms, hydrophilic nature of PANI, the possibility of direct contact between the polyaniline molecules and bacterial cell wall and the high molecular weight of the polymer [41-44]. After doping, the polyaniline chain will be positively charged and the dopant anions will be present around the positively charged nitrogen atom. By the electrostatic interaction between the positive charge on the polyaniline surface and the negative bacterial cell wall, PANI chains will get anchored to the cell wall at several positions on the membrane. Ion channels present on the cell membrane are responsible for the passive transport of positively and negatively charged ions across the biological membranes. When PANI is anchored to the cell wall the ion channel experiences, changes in the potential gradient which will cause to destroy the normal influx-efflux of electrolyte [45]. When polyaniline is anchored on to the cell wall, PANI releases the dopant ions attached to it resulting a change in the potential of hydrogen. In turn, it affects the permeability of the bacterial cell. The PANI molecules attached to the cell wall breaks inside the cell and damages the cells through the interaction with DNA and protein present. It may also alter the cell composition and leads to cell lysis.

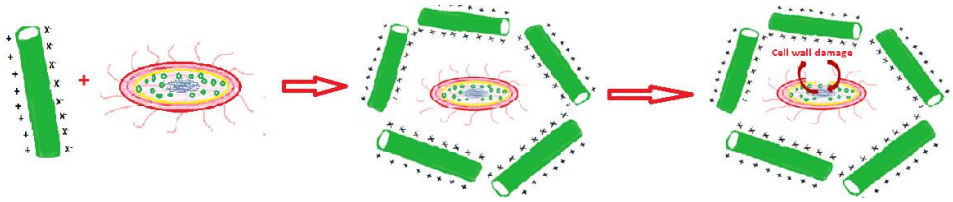

Figure 6.B.3: Mechanism of action of PANI/CNF/PMMA composite against microorganisms.

The activity of the different acid doped samples depends on the nature of the dopant used. The activity increases with the acid strength. It is well explained in the literature that polyaniline is highly electroactive at low pH values [46]. But exceptionally high activity is obtained for phosphoric acid doped PANI composite. It can be related to the smaller size of the particles. Several reports are available in the literature on the antibacterial activity of nanoparticle and composite because of the high surface area and the size [47-49]. From the SEM micrographs of PANI/CNF composites it is evident that phosphoric acid doped PANI has the smallest size. Surface area and size of particles also play a major role in determining the toxicity against microorganisms. As the size reduces particles are capable of reacting more with outer membrane of the cells. All the five different PANI/CNF composites have same length, but the difference is in the thickness of coating. So, the aspect ratio will be very high for phosphoric acid doped PANI/CNF composite. The high aspect ratio of the composites increases the opportunity of the composites to react with microorganisms.

SEM micrographs and DLS measurement revealed particle size of about 100 nm diameter for H_3PO_4 doped composite. BET surface area measurement indicated very high surface area of the phosphoric acid doped PANI/CNF particles in comparison to other PANI/CNF

composites. The smallest particles present in the composite can penetrate into the cell wall, and it will interfere with the metabolic pathways such as ATP synthesis and DNA replication [50]. The particles can reach the nuclear content of the bacteria much easily for H_3PO_4 doped composite when compared to other composite particles. The larger particles present interact with the bacterial cell membranes, which in turn disturbs in-cell transport or respiratory functions of the bacteria [51]. Due to the high surface area of H_3PO_4 doped PANI/CNF particles stronger bactericidal interaction is possible [52,53]. Furthermore, the electrostatic interaction between positively charged particles and negatively charged bacterial cell wall is another significant aspect for the antimicrobial activity. The zeta potential analysis of the particles revealed positive surface charge of +39.60 mV indicating the effectiveness of these material as a cell toxin. As most of the bacteria carries a net negative charge, so the positive charged materials can adhere in to the bacterial cell wall. Therefore, the cationic surfaces are suggested as efficient antibacterial coatings so that these materials can bind to the microorganisms by strong multivalent electrostatic attraction, thus effecting the bacterial viability.

Table 6.B.1: Average of inhibition zones formed for various composites (40 wt.%) against three bacterial strains.

Sl. No.	Sample	E. coli (Gram negative) Zone of Inhibition in mm	Klebsiella (Gram negative) Zone of Inhibition in mm	Bacillus (Gram positive) Zone of Inhibition in mm
1	PANI-TSA/CNF/PMMA	10	11	13
2	PANI-H_2SO_4/CNF/PMMA	13	7	8
3	PANI-HCl/CNF/PMMA	9	12	10
4	PANI-H_3PO_4/CNF/PMMA	14	10	13
5	PANI- CSA/CNF/PMMA	8	NIL	NIL
	Tetra cyclin	24	27	--

It is surprising to note that the highest toxicity against K. pneumoniae, a cause for many respiratory infections, is observed for HCl-PANI/CNF/PMMA composite. But the size of HCl-PANI/CNF composite is approximately 524 nm. In this case size cannot play a key role; instead the pKa value of the acid dopant has significant effect on the activity of the composite. Since hydrochloric acid is being strong, the chloride counter ion presents in the polyaniline molecule creates comparatively low pH. As a consequence, PANI/CNF/PMMA composite also exhibit more antibacterial activity. The average diameter of the inhibition formed for various composites against three bacterial stains are given in the table 6.B.1.

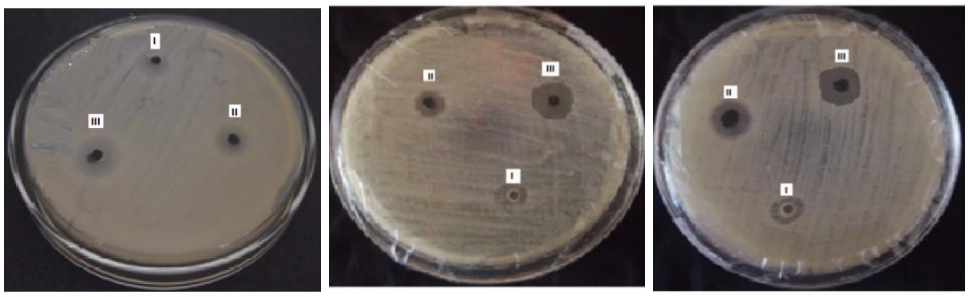

Figure 6.B.4: Antibacterial activity against *Klebsiella* sp., *E. coli* and *Bacillus Sp.* [(I) 40 %,(II) 50 %, (III) 60 % of H_3PO_4-PANI/CNF/PMMA]

On comparing the activities of these composites, a higher zone of inhibition is observed for H_3PO_4-PANI/CNF/PMMA composite. Hence this composite was further studied for MIC. The average size of inhibition zones against concentration of H_3PO_4-PANI/CNF in PMMA matrix is shown in the figure 6.B.4 and 6.B.5. No or weak antibacterial activity is observed up to 20 wt.% PANI/CNF concentrations. After that the activity

increases sharply as the concentration of PANI/CNF increases. The inhibition zones increase from 8 to 16 mm for *Bacillus sp.*,10 to 17 mm for *E. Coli* and 6 to 12 mm for *Klebsiella sp*. This result reveals that the PANI coated carbon nanofibers are the chief biocide in nanocomposite systems.

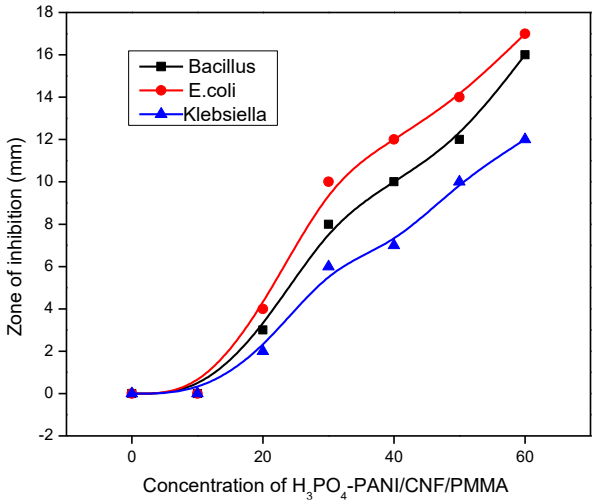

Figure 6.B.5: Plot of zone of inhibition against the concentration of H_3PO_4-PANI/CNF/PMMA composite

The results reveal that the antimicrobial activity of polyaniline based composites can be tuned by proper doping. The antimicrobial activity can be increased by the unique redox properties of polyaniline which will enhance the controlled ion transport through the membrane. So, I believe that these novel PMMA based composite can be a good alternative choice for the bone cement with low infection rate.

6.B.4 Conclusion

Novel PANI/CNF/PMMA composites were prepared by solution casting method. Polyaniline was coated over the carbon nanofiber surface by chemical oxidative polymerization of aniline using five different dopants. Several spectral characterization techniques were used to comprehend the effect of dopant on the properties of PANI in the composite. The antibacterial activity of various acid doped PANI/CNF/PMMA composite was studied against *Escherichia coli*, *Klebsiella pneumoniae* and *Bacillus subtilis* employing agar well diffusion method. The composite showed variable toxicity with different doping agents. The highest antibacterial activity was observed for phosphoric acid doped PANI/CNF/PMMA composite owing to its smallest size, highest surface area and the greatest surface charge compared to other composites. This novel nanocomposite has high potential in biomedical applications such as PMMA based bone cement.

References

[1] M. R. Gizdavic-Nikolaidis, A.J. Easteal, S. Stepanovic, Bioactive aniline copolymers, US patent (2010) 20100196306A1.

[2] R. Balint, N. J. Cassidy, S. H. Cartmell, Acta Biomater, 2014, 10, 2341

[3] H. Nam, T. An, G. Lim, Nanoscale Res. Lett., 2014, 9, 566

[4] Banerjee, J. P. Saikia, A. Kumar, B. K. Konwar, 2010, 21, 045101

[5] M. R. Gizdavic-Nikolaidis, J. Travas-Sejdic, G. A. Bowmaker, R. P. Cooney, P. A. Kilmartin, Synth. Met. 2004, 140, 225

[6] M. Li, Y. Guo, Y. Wei, A. G. MacDiarmid, P. I. Lelkes, Biomaterials, 2006, 27, 2705

[7] D. Wei, A. Ivaska, Chem. Anal., 2006, 51, 839

[8] H. Peng, L. Zhang, C. Soeller, J. Travas-Sejdic, Biomaterials, 2009, 30, 2132

[9] M. Gizdavic-Nikolaidis, J. Travas-Sejdic, G. A. Bowmaker, R. P. Cooney, C. Thompson, P.A. Kilmartin, CurrAppl Phys, 2004, 4, 347

[10] M. M. Ayad, E. A. Zaki, European Polymer Journal, 2008, 44, 3741

[11] S. F. Chung, T. C. Wen, A. Gopalan, Materials Science and Engineering B, 2005, 116, 125

[12] Y. Long, Z. Chen, N. Wang, J. Li, M. Wan, Physica B: Condensed Matter, 2004, 344, 82

[13] L. Li, J. Jiang, F. Xu, Materials Letters, 2007, 61,1091

[14] G. R. Bardajee, Z. Hooshyar, H. Rezanezhad, J. Inorg. Biochem., 2012, 117, 367

[15] V. P. Anju, S. K. Narayanankutty, AIP Advances, 2016, 6, 015109

[16] S. Liu, L. Wei, L. Hao, N. Fang, M. W. Chang, R. Xu, Y. Yang, Y. Chen, ACS Nano, 2009, 3, 3891

[17] G. Jia, H. Wang, L. Yan, X. Wang, R. Pie, T. Yan, Y. Zhao, X. Guo, Environmental Science and Technology, 2005, 39, 1378

[18] L. Dong, A. Henderson, C. Field, Journal of Nanotechnology, 2012, 2012, 1

[19] C. Yang, J. Mamouni, Y. Tang, L. Yang, Langmuir, 2010, 36, 16013

[20] S. Gurunathan, J. W. Han, A. A. Dayem, V. Eppakayala, J. H. Kim, Int. J. Nanomedicine, 2012, 7, 5901

[21] A. A. Shvedova, A. Pietroiusti, B. Fadeel, V. E. Kagan, Toxicol Appl Pharmacol, 2012, 261,121

[22] C. D. Vecitis, K. R. Zodrow, S. Kang, M. Elimelech, ACS nano, 2010, 4, 5471

[23] M. Pacurar, Y. Qian, W. Fu, D. Schwegler-Berry, M. Ding, V. Castranova, N. L. Guo, J Toxicol Environ Health A, 2012, 75, 129

[24] C. Buzea, Ii. Pacheco, K. Robbie, Biointerphases, 2007, 2, 17

[25] S. J. Breusch, P. R. Aldinger, M. Thomsen, V. Ewerbeck, k. M. Lukosche, Unfallchirurg, 2000, 103, 918

[26] H. W. Buchholz, H. Engelbrecht, Chirurg, 1970, 11, 511

[27] L. Thierse, M. Erfahrungen, Z Orthop, 1978, 116, 847

[28] M. Wannske, H. Tscherne, Ortho, Bern: Hans Huber, 1979, 12, 201

[29] G. Josefsson, G. Gudmundsson, L. Kolmert, S. Wijkstrom, ClinOrthop, 1990, 253, 173

[30] M. Paligova,´ J. Vil_ca´kova,´ P. Sa´ha, V. Kr˘esa´lek, J. Stejskal, O. Quadrat, Physica A, 2004, 335, 421

[31] H. Dong, S. Prasad, V. Nayme, Jr. E. J. Wayne, Chem. Mater, 2004, 16, 371

[32] S. Kang, M. Herzberg, D. F. Rodrigues, M. Elimelech, Langmuir, 2008, 24, 6409

[33] H. S. O. Chan, S. C. Ng, W. S. Sim, S. H. Seow, K. L. Tan, B. T. G. Tan, Macromolecules, 1993, 26, 144

[34] Y. Guo, Y. Zhou, Eur. Poly. J., 2007, 43, 2292

[35] I. Sedenkove, M. Trchova, N. V. Blinova, J. Stejskal, Thin Solid Films, 2006, 515, 1640

[36] N. Kuramoto, E. M. Genies, Synth. Met., 1995, 68, 191

[37] L. Zhang, Electrochim. Acta, 2007, 52, 6969

[38] K. S. W. Sing, PureAppl.Chem., 1985, 57, 603

[39] S. J. Ahn, M. Sivaguru, H. Osawa, C. Chung, H. Matsumoto, Plant Physiol, 2001, 126, 1381

[40] G. Harkes, J. Dankert, J. Feijen, Journal of Biomaterials Science Polymer Edition, 1992, 3, 403

[41] P. K. Prabhakar, S. Raj, P. R. Anuradha, S. N. Sawant, M. Doble, Colloids Surf., B. Biointerfaces, 2011, 86, 146

[42] X. Liang, M. Sun, L. Li, R. Qiao, K. Chen, Q. Xiao, F. Xu, Dalton Trans., 2012, 41, 2804

[43] N. P. S. Chauhan, R. Ameta, R. Ameta, S. C. Ameta, J. Indian Counc. Chem., 2010, 27, 128

[44] H. Zuo, D. Wu, R. Fu, J. Appl. Polym. Sci., 2012, 125, 3537

[45] N. Shi, X. Guo, H. Jing, J. Gong, C. Sun, K. Yang, J. Mater. Sci. Technol., 2006, 22, 289

[46] A. A. Syed, M. K. Dinesan, Talanta, 1991, 38, 815

[47] A. Panacek, L. Kvitek, R. Prucek, M. Kolar, R. Vecerova, N. Pizurova, V. K. Sharma, T. Nevecna, R. Zboril, J. Phys. Chem. B, 2006, 110, 16248

[48] S. Vijay Kumar, N. M. Huang, H. N. Lim, A. R. Marlinda, I. Harrison, C. H. Chia, Chem. Eng. J., 2013, 219, 217

[49] K. Amarnath, J. Kumar, T. Reddy, V. Mahesh, S. R. Ayyappan, J. Nellore, Colloids Surf., B Biointerfaces, 2012, 92, 254

[50] P. Dallas, V. K. Sharma, R. Zboril, Adv. Colloid Interface Sci., 2011, 166, 119

[51] G. A. Sotiriou, S. E. Pratsinis, Curr. Opin. Chem.Eng., 2011, 1, 3

[52] G. A. Martinez-Castanon, N. Ni˜no-Mart´ınez, F. Mart´ınez- Gutierrez, J. R. Mart´ınez-Mendoza, F. Ruiz, Journal of Nanoparticle Research, 2008, 10, 1343

[53] S. Pal, Y. K. Tak, J. M. Song, Applied and Environmental Microbiology, 2007, 73, 1712

Part C

Highly flame-resistant composites based on nanofibers/polyaniline/poly(vinyl alcohol) composite

The flammability and the thermal stability of the polyaniline/carbon nanofiber/poly(vinyl alcohol) and polyaniline/carbon nanofiber/poly(methyl methacrylate) composites were studied using vertical burning test and thermogravimetric analysis. High Limiting Oxygen Index (LOI) value of 42 was obtained for 50 % PANI/CNF/PVA composite. The drastic increase of LOI value suggest the possibility of structural changes and chemical reactions in composites during heat treatment. The thermogravimetric analysis of the composite showed that the degradation temperature of PVA shifted from 381 ^{o}C to 588 ^{o}C. The evolved gas analysis and the elemental analysis suggested that the nitrogen atoms were retained even after the high temperature treatment. The formation of graphene like structures during heating was confirmed by the XRD analysis of the char residues. Detailed X-ray photoelectron spectroscopy analysis of the samples showed that pyridinic type nitrogen as the major component at higher temperatures. Hence the high thermal stability of the PVA composite could be attributed to the formation of polyconjuagted ladder structures through dehydrogenation and cyclization reactions.

6.C.1 Introduction

Though polymer nanocomposites with excellent electromagnetic interference shielding properties have found a wide range of applications [1-5], one of the disadvantages of these composites are the high flammability. Various additives such as halogenated materials [6], metal hydroxides [7], nanoclay [8], and graphene [9] has been tried as flame retardants. Though halogenated additives impart good flame retardancy [10,11], they emit

toxic gases during burning [12-15]. Halogen-free flame retardant is one of challenging effort of the chemists [16,17]. Carbon nanofibers is a non-halogen filler that can improve flame-resistance apart from improving EMI shielding efficiency and mechanical properties of the composite.

The hydroxyl groups available in PVA matrix can exhibit latent charring property. The charring can be improved by the addition of various flame retardants. Chen et al. [7] reported the self-synthesized bis neopentyl glycol dithio pyrophosphate with melamine formaldehyde (MF) in PVA solution to produce flame retardant polymer. They have achieved a flame retardancy of 31.8. A number of studies have been carried out to improve the flame retardant properties of PVA. The flame retardant system could accelerate the dehydration and char formation of PVA [18-22]. Still, the high LOI values these polymers are not commercially successful as the added flame retardants greatly reduce the properties of the composite [23-25].

Poor compatibility between the flame retardants and polymer always results in the migration of retardant particles to the surface [26-29]. Polyaniline containing alternating amine and imine groups, is one of the important conjugated polymer in this context. Gu et al. reported that polyaniline functioned as a coupling agent to improve the dispersion of nanoparticles in epoxy matrix [30,31]. So, it is expected that combination of CNF and PANI can impart excellent flame retardancy to PMMA and PVA apart from improving mechanical, electrical and dielectric properties.

6.C.2 Experimental

A detailed description of the methods employed for the preparation PANI/CNF/PVA and PANI/CNF/PMMA composites is given in chapter 4B and 5B.

Polyaniline was prepared by the chemical oxidative polymerization. 5 g of aniline monomer was dispersed in 200 mL distilled water for 1 h. The solution was pre-cooled to 0-4 ^{o}C in an ice bath. 6.25 g of ammonium persulfate (APS) was dissolved in 100 mL 1M HCl solution and was taken in a burette. The APS/HCl was added drop-wise into the aniline solution to initiate polymerization reaction. PANI/PVA composites were prepared by mixing different wt.% of polyaniline with poly(vinyl alcohol) solution in water at 90 ^{o}C followed by ultrasonication for 2 h. Films were prepared by casting and dried slowly at 70 ^{o}C for 24 h.

6.C.3 Results and discussion

6.C.3.1 Flammability of PMMA and PVA composites

Limiting Oxygen Index (LOI) of the composites was determined by the vertical burning test. LOI measures the relative permeability of polymers by burning the material in a controlled atmosphere of nitrogen and oxygen. It is based on the ranking of polymers on their combustibility. The index is measured by increasing the concentration of oxygen and reducing the concentration of nitrogen. The increase in the oxygen level will support the combustion of the samples. The sample is placed vertically and it is ignited with flame. It burns downward in to the material.

The limiting oxygen index is the lowest percentage of oxygen which is used to support flame combustion. Since the normal oxygen level in air is about 21 %, so in order to have good fire resistance the material should possesses limiting oxygen index greater than 21. The materials with index below 21 will burn easily under normal conditions. The values of PMMA and PVA composites are listed in the table 6.C.1.

Pure PMMA is flammable, as indicated by the low LOI value of 18. It shows serious dripping behaviour. LOI value of the composite increases with PANI/CNF content. It increases to about 24 for 50 % PANI/CNF/PMMA composite.

Table 6.C.1: Limiting Oxygen Index values of the PANI/CNF/PMMA composites

PANI/CNF/PMMA Composites*	LOI	PANI/CNF/PVA composite**	LOI
PM0	18	PV0	20
PM10	19	PV10	24
PM20	20	PV20	30
PM30	21	PV30	34
PM40	23	PV40	39
PM50	24	PV50	42

* PM0 to PM50 stand for PMMA composites with 0 to 50 wt.% PANI/CNF.
** PV0 to PV50 stand for PVA composites with 0 to 50 wt.% PANI/CNF.

In contrast to PMMA, PVA is marginally more fire resistant with an LOI value of 20. It is due to the presence of hydroxyl groups in PVA chain. After ignition for few seconds, PVA film is burned rapidly with formation of fine ash. The incorporation of 50 wt.% polyaniline-modified carbon nanofiber increases the LOI value up to 42. The flame spread is also reduced considerably in the case of the PVA composites. The char formation is increased noticeably for PVA composites.

Compared to the PMMA based composites significant improvement in LOI is observed for PVA composites. In PVA composite, PANI/CNF fibers are strongly interacting with matrix. Hence the motion of the polymer chains is limited, as explained in the chapter 4A. This result in additional stabilization in case of PVA composites. The charring quality of the composite is related to the even distribution of the flame retardants in the polymer matrix. Poor dispersion of the PANI/CNF fibers in PMMA matrix results in low LOI value. Nanoparticles are found to interact with the polymer chains in a way that forces the arrangement of macro molecular chains and restricts the thermal motions of polymer domains [32,33]. The thermal stability of polymer composites depends on the wt.% and the dispersion of the nanoparticles. The good compatibility of PANI/CNF fibers and PVA matrix helps to increase the LOI value better than in PMMA composites.

It is usually well accepted that the high fire resistance in nanocomposites is mainly due to the char formation which hinders the out diffusion of decomposition products. Despite this the exact degradation mechanism of PVA composites is not clear. Such a behavior is probably associated with the structural changes in the PVA molecular chain in the composites.

The significance of polyaniline on the thermal stability of PVA system is studied in detail. Different wt.% of PANI/PVA composites were prepared and the fire resistance was measured. The LOI values of the PANI/PVA composite indicates efficient fire resistance of the material even in the absence of carbon nanofibers. Like PANI/CNF/PVA composite,

significant increase in the LOI value of the composite is observed for PANI/PVA composite. It increases from about 20 to 38 (table 6.C.2).

Table 6.C.2: Limiting Oxygen Index values of the PANI/PVA composites

Sample	LOI
PVA	20
PANI/ PVA 20	27
PANI/PVA 50	38

The photographs of the PANI/CNF/PVA composites after LOI test are presented in the figure 6.C.1. Pure PVA and lower wt.% composites show serious dripping in the burning test. When 20 % PANI/CNF is added the dripping is partly reduced. The higher wt.% composites results in the formation of intumescent char layer on the surface. It could effectively hinder the mass and heat flow and thus improves the flame resistance of the composite [34].

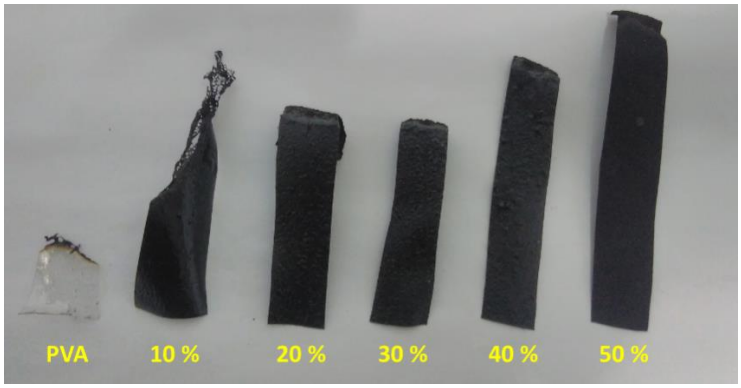

Figure 6.C.1: Micrographs of the sample residues during the burning test

A protective char layer on the surface of the composite reduces the flammability of the material. It reduces the transfer of heat, supply of oxygen and other flammable gas molecules through the material. As a result, more amount of oxygen is needed to make the material flammable. The efficient char formation will prevent the heat and mass transfer between the flame zone and the burning material. Thus, it protects the remaining substrate from further burning (figure 6.C.2).

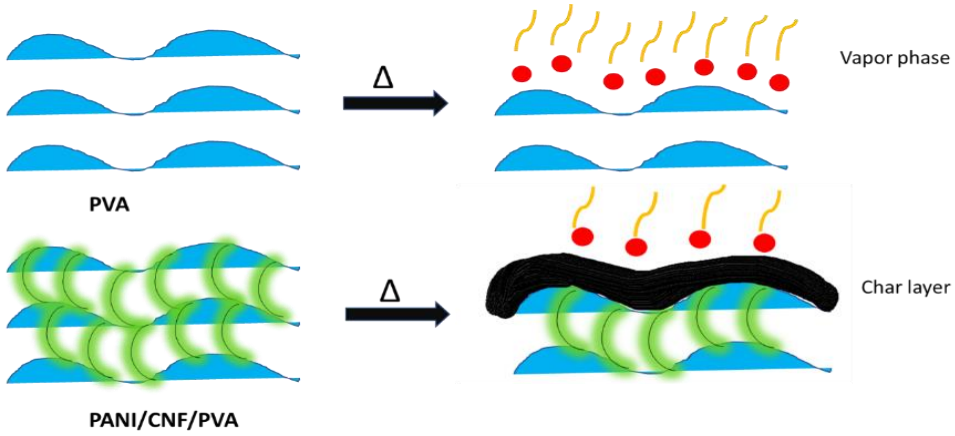

Figure 6.C.2: Formation of protective char layer on the surface of PANI/CNF/PVA film.

The mechanism of flame retardancy can be of three types, physical, chemical or combination of the two. It can function in the condensed phase or in the vapor phase.

In the condensed phase, char formation has significant effect in improving the flame retardancy of the polymer composite. Thin wall products have much dependence on the surface properties than the thick wall products. Hence, the surface char formation produces high impact on the properties of thin films. During burning both PMMA and PVA based

composites lead to the formation of char on the surface. As the concentration of flame retardant PANI/CNF in the polymer matrix increases, the composite produces char more quickly than the lower wt. % composites. Therefore higher wt. % composites are exhibiting higher efficiency.

6.C.3.2 Thermogravimetric analysis

To better understand the thermal stability of PVA composites thermogravimetric analysis was performed. Thermal stability was determined by heating the samples up to 700 ºC under nitrogen, air and oxygen atmospheres at a heating rate of 10 ºC/min using thermogravimetric analyzer coupled with differential scanning calorimeter and mass spectrometry. The effect of PANI/CNF on the degradation temperature of PVA is determined. Under nitrogen atmosphere the major degradation of pure PVA takes place at 381 ºC and two small peaks are observed at 444 ºC and 480 ºC (Figure 6.C.4A). While in presence of air, the degradation shifts to comparatively lower temperature of 328 ºC (Figure 6.C.4B).

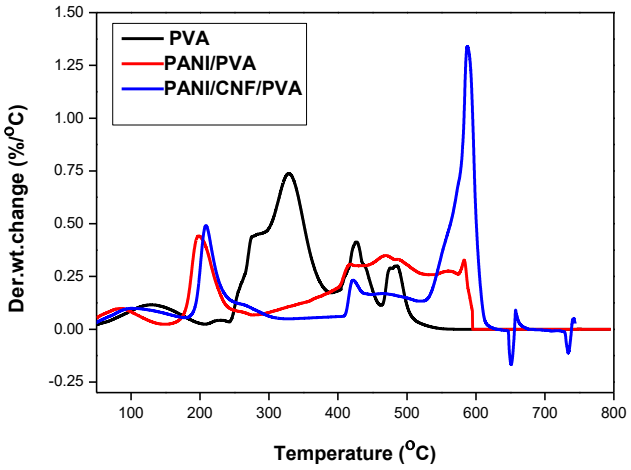

Figure 6.C.3: Thermogravimetric curves of PVA, PANI/PVA and PANI/CNF/PVA in air

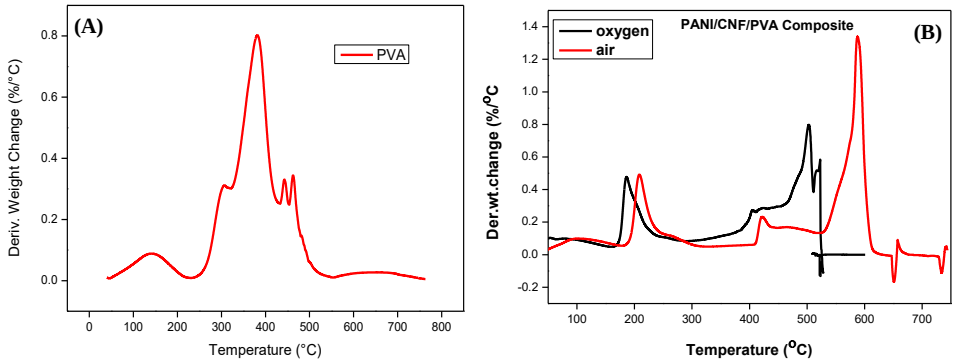

Figure 6.C.4: Thermogravimetric curves of A) PVA in nitrogen atmosphere, B) PANI/CNF/PVA composite in air and oxygen atmospheres

While the thermal degradation of PVA composite is sufficiently dominant compared to pure PVA. With the addition of PANI/CNF, the thermal degradation mechanism tends to be more complex. Due to the retardant effect of PANI/CNF it is more difficult to be degraded. Hence it requires more reaction activation energy during the process. In air, the major degradation of PANI/CNF/PVA composite takes place around 588 ^{o}C. The shift in the degradation peak towards higher temperature indicates the changes in the molecular structure of the PVA chain. The difference in the degradation pattern of the curves implies that the degradation mechanism of the nanocomposite differs from that of pure PVA.

The effect of polyaniline on the thermal stability of PVA was studied. The thermal behaviour of 50 % PANI/PVA composite was studied by thermogravimetric analysis and the degradation curves are plotted in the figure 6.C.3. The degradation patterns of the two composites (PANI/CNF/PVA and PANI/PVA) are almost similar. Both composites exhibit enhanced thermal stability to pure PVA. Both composites firstly degrade and release the dopants from the polyaniline at

a temperature around 200 ^{o}C. Hence it indicates that, polyaniline plays a key role in reducing the flammability and enhancing the thermal stability of the composite.

The presence of carbon nanofibers in PANI/CNF/PVA makes the composite more stable than PANI/PVA composite. From the DTG curves of the two composites, it is clear that the PANI/CNF/PVA composite shows wider degradation peak than the PANI/PVA composite. Due to the improvement in thermal resistance of PANI/CNF/PVA composite, the whole degradation process of the nanocomposite is protracted.

Thermogravimetric analysis provides quantitative information on the mass change of the sample. The combination of thermogravimetric analyser with DSC and mass spectrometer allows the nature of gaseous reaction products formed. Several gases are evolved during heating, MS spectra characterizes specific gases eliminated.

6.C.3.3 Mass spectroscopy

The mass spectra of the evolved gases during heat treatment for PVA and composites is shown in the figure 6.C.5. The mass spectra indicate the evolution of high amount of carbon monoxide, showing the high intense peak at molecular weight 28. At the degradation temperature of pure PVA and the composites, CO_2 elimination is high. The peaks at the molecular mass of 30, 44 and 62 is corresponding to the evolution of nitrogen oxides. But the intensity of these bands is very less. It implies that the nitrogen atoms of the composite are not eliminating in the form of oxides from the composite.

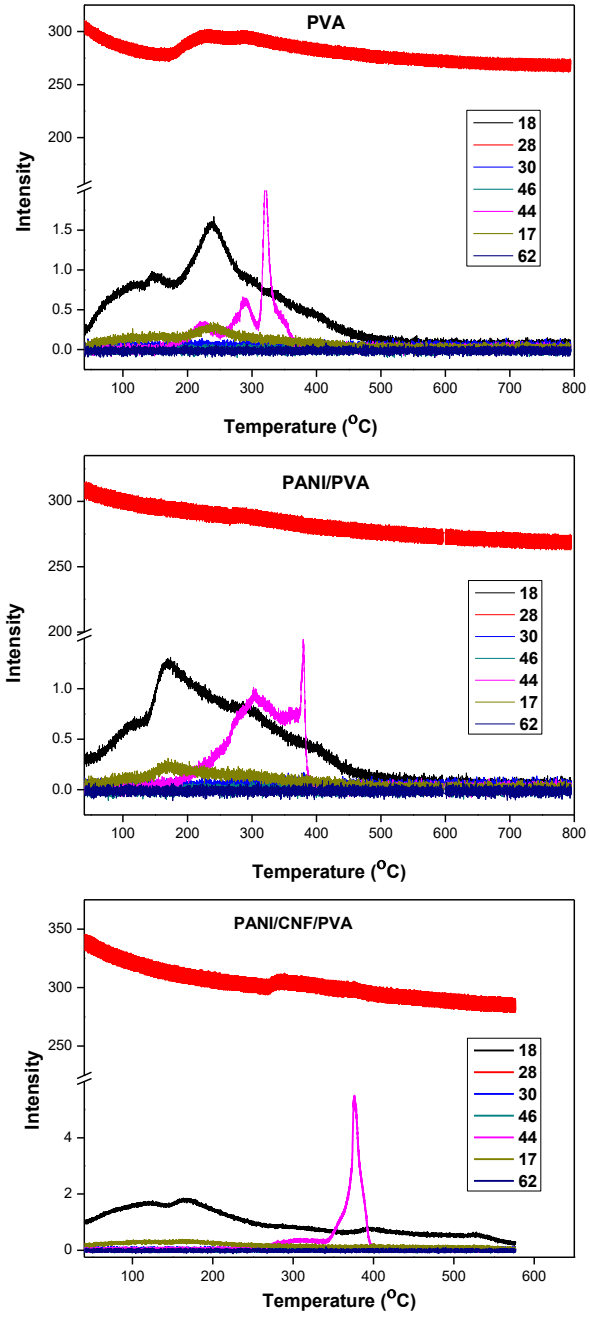

Figure 6.C.5: Mass spectra of the evolved gases during heat treatment

6.B.3.4 Differential Scanning Calorimetry

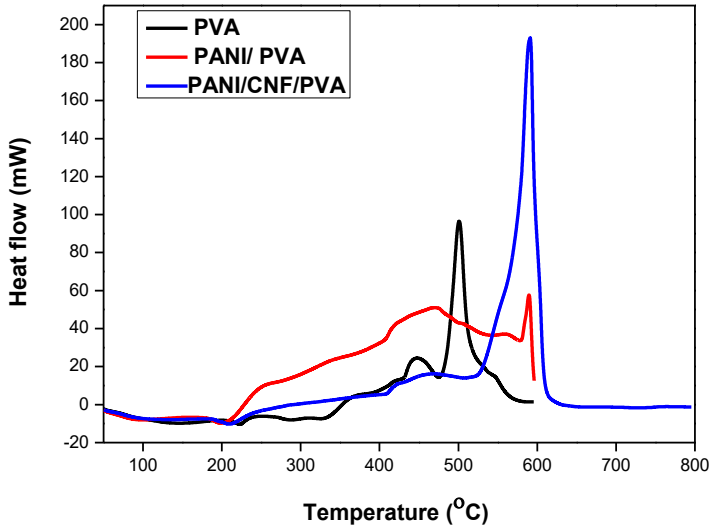

Figure 6.C.6: DSC heating curves of PVA, PANI/PVA and PANI/CNF/PVA composites

Differential scanning calorimetry displays the temperature at which the composite decomposes. The decomposition peak is obtained from the temperature at which the maximum reaction rate occurs. Figure 6.C.6 shows the DSC thermograms during the heating process. A small endothermic peak around 220 ºC indicates the glass transition temperature of pure PVA and the composites. With increase of temperature, the exothermic nature increases and it results in an intense exothermic peak at the degradation temperature. A high intense peak is observed for PANI/CNF/PVA composite. The exothermic nature of the composite during degradation is evident from the DSC heating curves.

6.C.4 Residue analysis

To investigate the form of components and the reaction mechanism in the heated system the char residues were analysed by different techniques. For this char residues were collected under similar conditions at 400 ºC, 500 ºC and 600 ºC temperatures.

6.C.4.1 Scanning Electron Microscopy

The microstructure of the char residue formed after burning was investigated by scanning electron microscopy. The figure 6.C.7 shows the SEM images of char from pure PVA, PANI/CNF/PVA and PANI/CNF/PMMA composites. No residue is left after the ignition of pure PMMA, so the SEM image is not included here.

PVA exhibits smooth and continuous char layer indicating the rapid volatilization at the surface of the material. While the surface of the PVA composite is not much smooth as that of pure polymer, many char fragments are observed for the composite. The presence of holes in the char of PVA composite indicates the possibility of the evolution of gases during heating. But the nature of PMMA composite is different (figure 6.C.7C). It indicates that the gases are trapped in between the layers and have more chances to undergo secondary reactions. Hence the degradation pathways could be promoted in case of PMMA composites resulting in low LOI values. Due to the char formation at the surface of PVA composites, the surface becomes impermeable to gases. Hence it limits the oxygen diffusion inside the nanocomposites during thermal degradation. So, at higher temperature, the surface restrains the diffusion of gases evolved during degradation.

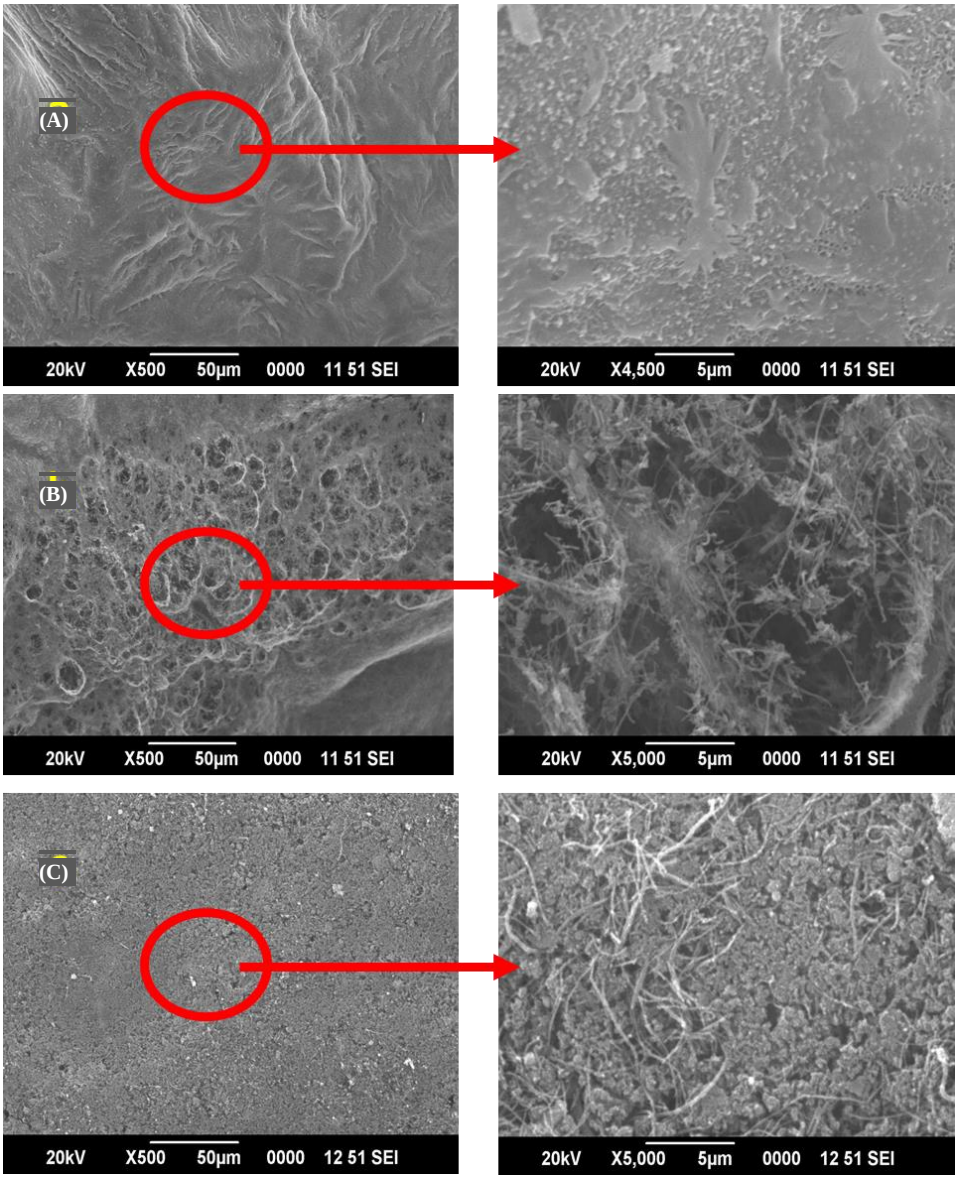

Figure 6.C.7: SEM images of char residues A) PVA, B) PANI/CNF/PVA composite and C) PANI/CNF/PMMA composite

6.C.4.2 Elemental analysis

Char residue was further investigated by elemental analysis. It provides the wt.% of carbon, nitrogen and hydrogen present in the sample. Little difference is noted in the elemental profiles of the char residues at three different temperatures.

Table 6.C.3: The elemental analysis of the char residues at different temperatures

Sample	N wt.%	C wt.%	H wt.%
Residue at 400 °C	7.39	74.55	3.34
Residue at 500 °C	7.11	79.86	1.68
Residue at 600 °C	6.87	80.24	0.94

The presence of nitrogen atoms in the structure is evident from the elemental analysis. The percentage of nitrogen atoms in the composite remain more or less unaltered even at higher temperatures. The result is consistent with the evolved gas analysis. The wt.% of carbon in the composite increases with the increase of temperature. Whereas the wt.% of hydrogen in the composite is reducing. It reduces from 3.34 wt.% to 0.94 wt.%. The increase of carbon wt.% and decrease of hydrogen wt.% may be due to the elimination of hydrogen from the system. Hence the aliphatic structures are converting to more stable aromatic forms. The elemental analysis indicates that the high thermal stability of the composite is due to the formation of more stable aromatic structures with retention of nitrogen atoms. At higher temperature polyconjugated structures are formed with the dehydrogenation and cyclization reactions. Hence these graphitic structures are thermally stable and withstands up to higher temperatures. The reduction in the wt.% of hydrogen without reducing the wt.% carbon indicates the possibility of dehydrogenation reactions.

6.C.4.3 X-ray Diffraction

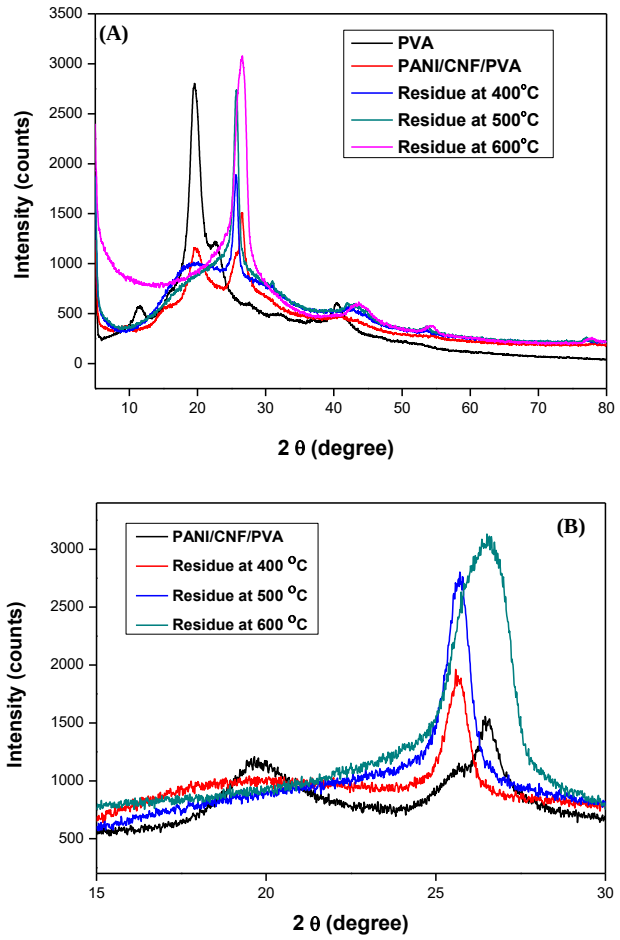

Figure 6.C.8: X-ray diffractogram of A) PVA, PANI/CNF/PVA and its char residues at different temperatures B) zoomed version of the peak

X-ray diffraction pattern of PVA, PANI/CNF/PVA and the char residues of PANI/CNF/PVA at different temperatures are shown in the figure 6.C.8. XRD pattern of pure PVA indicates a sharp peak at 19.6 °, typical of crystalline PVA. High degree of crystallinity of PVA can be attributed to the regularity in the molecular structure. In the case of

nanocomposites, the intensity of crystalline peak of PVA is reduced and is broader. This may be due to a different thermal history of the composites and the presence of filler that interacts with the matrix chains. Similar amorphous peak has been reported in the case of hot pressed PVA molecules [35].

Pure CNF exhibits a sharp peak at 2θ of 26.4 º. It can be ascribed to the (002) plane diffractions from the graphitic carbon of CNF. Less intense peaks can also be seen at higher 2θ values correspond to the (100), (101) and (004) planes of the CNF. When the composite is heated to higher temperatures the peak at 26.4 º becomes broader.

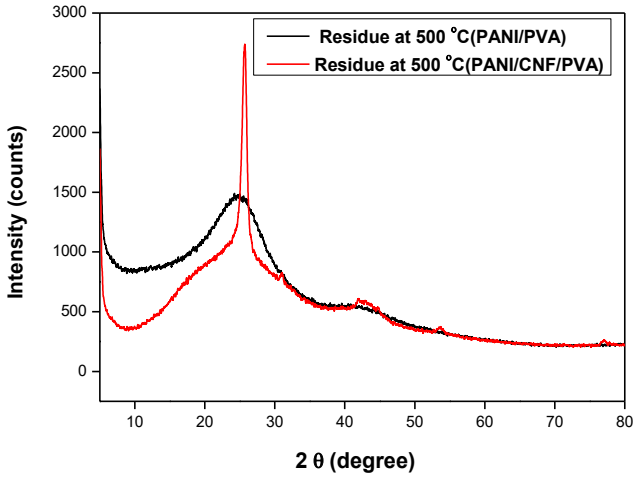

Figure 6.C.9: X-ray diffractogram of char residues of PANI/PVA and PANI/CNF/PVA composites at 500 ºC

The heating of PANI/PVA composite resulted in a wide peak around 25º. It indicates the presence of graphite like crystallites in presence of polyaniline and poly(vinyl alcohol). So it can be confirmed that the graphene like structures are formed in even in absence of carbon nanofiber. It is evident from the figure 6.C.9.

6.C.4.4 ^{13}C NMR analysis

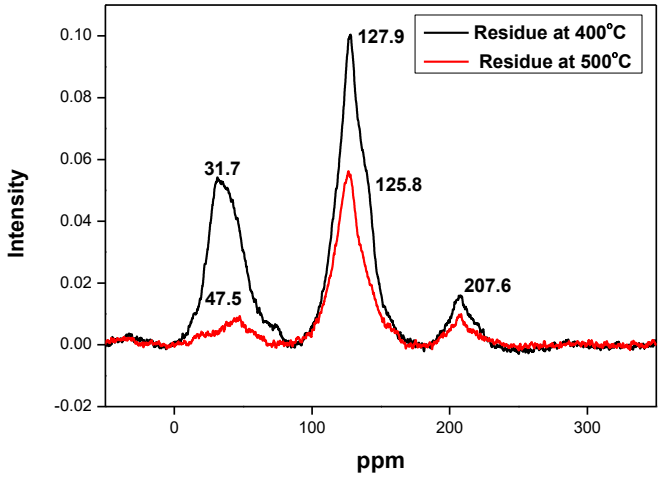

Figure 6.C.10 : ^{13}C NMR spectra of char residues of PANI/CNF/PVA composite at different temperatures

Figure 6.C.10 shows the ^{13}C NMR spectra of char residues at different temperatures. Though all the peaks are present after the high temperature treatment, the major difference appears to be in the intensity. The appearance of peaks at low ppm (30-40) corresponds to the aliphatic carbons. It can be seen that at 500 ºC, significant reduction occurs in the intensity of the peak. The aromatic carbons possess peaks around 127 ppm. High temperature treatment does not alter the intensity of the peak at 127 ppm. That means the peak intensity of aromatic carbons is not decreased as aliphatic carbons. It could be due to the presence of more number of aromatic rings at higher temperatures indicating more stability to the composite.

6.C.4.5 FTIR spectroscopy

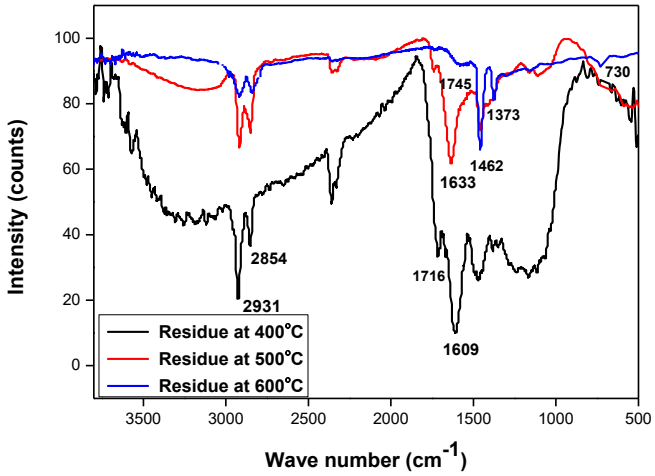

Figure 6.C.11: FTIR spectra of char residues of PANI/CNF/PVA composite at different temperatures

FTIR spectra of PANI/CNF/PVA composite char residues at different temperatures is shown in the figure 6.C.11. The indication of the chemical reaction in the composite during heat treatment is apparent from the FTIR spectra. The absorption bands at 2931 cm^{-1} and 2854 cm^{-1} is due to the alkyl C-H vibrations. But as the heating temperature increases the intensity of the peak reduces. It may be due to the conversion of aliphatic groups to more stable aromatic rings. The characteristic peaks of carbonyl absorption are present for the char residues at 400 ºC and 500 ºC. After the high temperature treatments at 500 ºC, the absorption bands at 1745 cm^{-1}, 1633 cm^{-1} disappeared and new absorption bands at 1462 cm^{-1}, 1373cm^{-1} and 730 cm^{-1} are appeared. The peaks at 1462 cm^{-1},1373 cm^{-1} and 730 cm^{-1} can be attributed to C-H, C-N stretching vibrations and C-H stretching in aromatic structures respectively. So, the FTIR spectroscopy specifies the formation of aromatic structures with the inclusion of nitrogen atoms.

6.C.4.6 Raman Spectroscopy

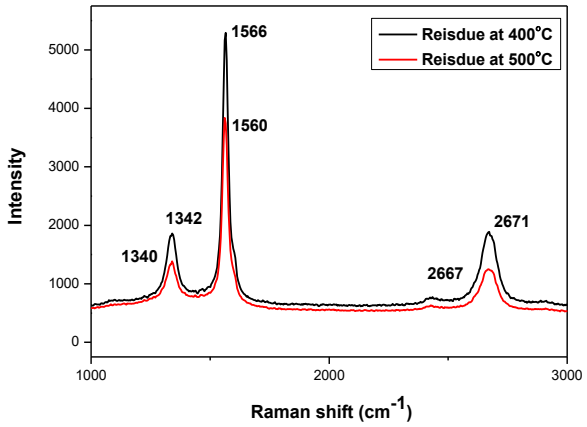

Figure 6.C.12: Raman spectra of PANI/CNF/PVA composite at 400 ºC and 500 ºC

Carbonaceous materials typically show two characteristics bands in the Raman spectrum. The bands present around 1340 cm^{-1} and 1560 cm^{-1} are assigned to the disordered turbostratic structures and ordered graphitic structures. The intensity ratio of the D and G bands (I_D/I_G) can be used to estimate the extent of disorder within the samples. Raman spectroscopy provides excellent information about the defects in the graphitic structure [36]. Hence Raman spectroscopy was employed to study the chemical changes after the heat treatments. Figure 6.C.12 shows the Raman spectra of the composite residue at different temperatures. Both samples exhibit similar pattern, but differ in the intensity of the peak and position. The D, G and 2D bands respectively occurred at 1342 cm^{-1}, 1566 cm^{-1} and 2671 cm^{-1}. Slight change in the peak is observed for the composites after 500 ºC heating. The bands are shifted to 1340 cm^{-1}, 1560 cm^{-1} and 2667 cm^{-1}respectively. The appearance of D, G and 2D band with more intensity indicates the presence of ladder polyconjugated structures at higher temperatures. Hence this results the higher thermal stability to the

composites. The I_D/I_G ratio is calculated for the composite residue at 400 ^oC is about 0.5 and it is increased to 0.64 for the residue at 500 ^oC. The higher I_D/I_G ratio indicates more defects in the composite [37], suggesting the formation of less ordered graphitic structure. The ratio of D band and G band intensities increases with the pyrolysis temperature.

6.C.4.7 X-ray Photoelectron spectroscopy

X-ray photoelectron spectroscopy provides useful information about the elemental composition and the nitrogen content. Furthermore, it helps to identity the nitrogen present in the samples based on the bonding interactions. In the full survey of XPS spectra, three major peaks are obtained corresponding to C 1s, O 1s, N 1s. The intense peak at 284.45 eV is due to the C 1s sp^2 carbon. The nitrogen and oxygen peaks are observed respectively at 400 eV and 530 eV. The atomic percentages of elements in two samples were measured. High nitrogen content is obtained in the char residue at higher temperature of 500 ^oC.

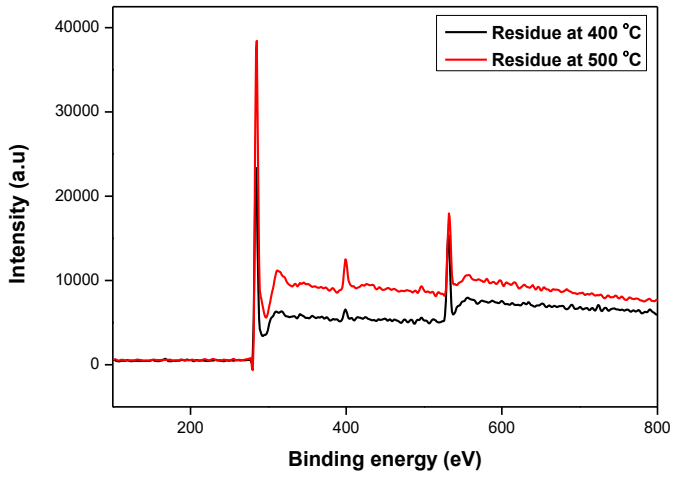

Figure 6.C.13: Full survey of XPS spectra of the PANI/CNF/PVA composite char residues at different temperatures

Table 6.C.4: Atomic percentages from the area of XPS peaks

	Residue at 400 ºC (at. %)	**Residue at 500 ºC (at. %)**
Carbon	84.93	86.45
Nitrogen	2.66	5.87
Oxygen	12.42	7.68

The carbon/oxygen ratio of the composite at 400 ºC is 6.83. After high temperature treatment this is increased to 11.25, signifying the removal of oxygen moieties from the composite. The carbon/nitrogen ratio is decreased from 31.92 to 14.72. So it indicates that after high temperature treatment the oxygen containing groups are removed from the composite and nitrogen groups are retained.

The characteristic C1s, N1s and O1 s peaks were subjected to further scrutiny in order to ascertain the nature groups in each sample. The figures (6.C.14, 6.C.15, 6.C.16) represent the deconvoluted C 1s, N 1s and O 1s peaks for the two samples.

In the deconvoluted peak of C 1s, the intense peak at 284.45 eV is due to the presence of sp^2 carbons [38-41]. After high temperature treatment, the peak corresponding to the carbon in sp^3 configuration at 285.25 eV is significantly increased. This indicates the partial conversion of sp^2 carbons to sp^3 configurations.

The peaks corresponding to the oxygen functional groups are reduced significantly after high temperature treatment. Hydroxyl groups result in a peak around 286.59 eV and carbonyl groups at 288.33 eV [42-44]. These two peaks are visible in the C 1s deconvoluted spectrum of the char

residue at 400 °C. While after high temperature treatment the two new peaks are formed corresponding to the nitrogen functional groups in sp^2 (286.05 eV) and sp^3 (286.76 eV) configurations [45].

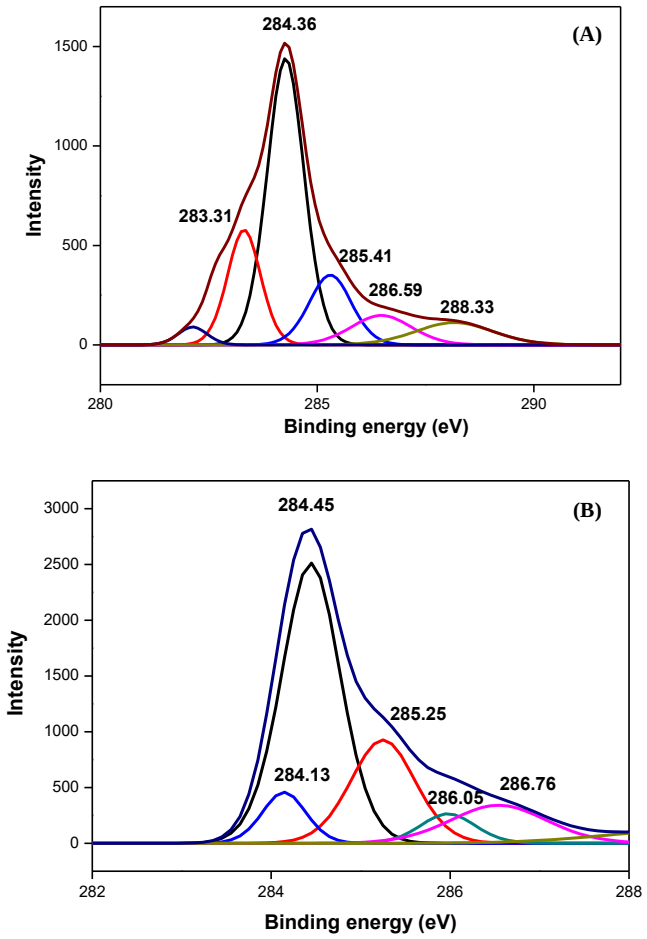

Figure 6.C.14: The deconvoluted C 1s spectra of the PANI/CNF/PVA composite at A) 400 °C and B)500 °C

The nitrogen deconvoluted spectra of the composite char residues are shown in the figure 6.C.15. In the composite at 400 ^{o}C, the major peak is located at 399.12 eV. It may be corresponding to the pyrrolic nitrogen atom in the structure. In the residue at 500 ^{o}C, the N 1s peak is deconvoluted into four major peaks corresponding to the binding energies of 398.74, 399.57, 400.45, 401.11 eV, which can be assigned to pyridinic, pyrrolic, graphitic and oxidized nitrogen respectively. It is evident from the figure 6.C.15, that at 400 ^{o}C, the pyrrolic nitrogen is the major component. With increase of temperatures, the intensity of peak at 399.57 eV increased, indicating the increased contribution of pyridinic nitrogen atoms. It suggests the formation more stable aromatic structures. Moreover, the intensity of the graphitic nitrogen at 400.45 eV is increased at higher temperature. This is also consistent with the other characterization techniques. Among the various types of nitrogens, both pyridinic and pyrrolic nitrogens contribute to the conjugated π-system in the graphene layers. The relative intensity of oxidic type (at 401.11 eV) and pyrrolic nitrogen decreases with increase of reaction temperature. It suggests that the highly stable structures are formed at temperature between 400 ^{o}C and 500 ^{o}C. Hence it results thermal stability to the composite. A portion of nitrogen is also found to present as amine functional groups which is manifested as a peak at 397.02 eV [46,47]. The intensity of this peak is more at low temperature. It is significantly reduced after high temperature treatment.

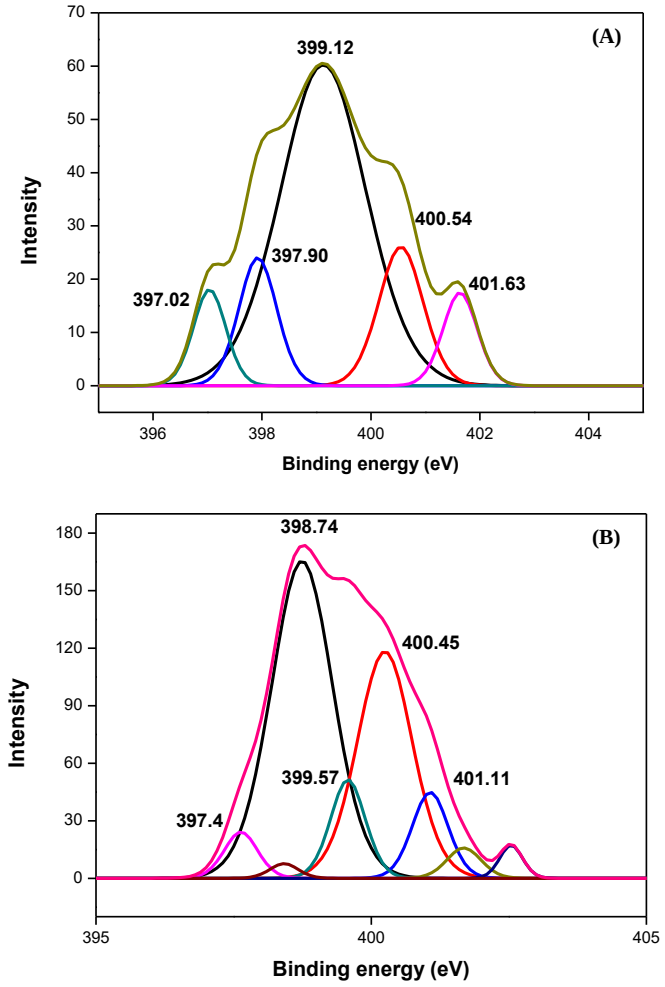

Figure 6.C.15: Deconvoluted N 1s spectra of PANI/CNF/PVA composite at A) 400 ºC and B)500 ºC

A comparison of deconvoluted O 1s part is given in the figure 6.C.16. The figure reveals that both the samples have almost similar pattern. The peak at 531.37 eV can be assigned to the organic C-O groups. While a new peak located at 532.47 with high intensity arises after the high temperature treatment. It corresponds to the C=O group functionalization [48,49]. The existence of C=O groups is mainly due to

the ketones and quines located at the edges of graphene like structures. It can also be found at the basal plane as the carbonyl groups [50,51]. The presence of carbonyl groups is also manifested from the FTIR spectra of the char residues.

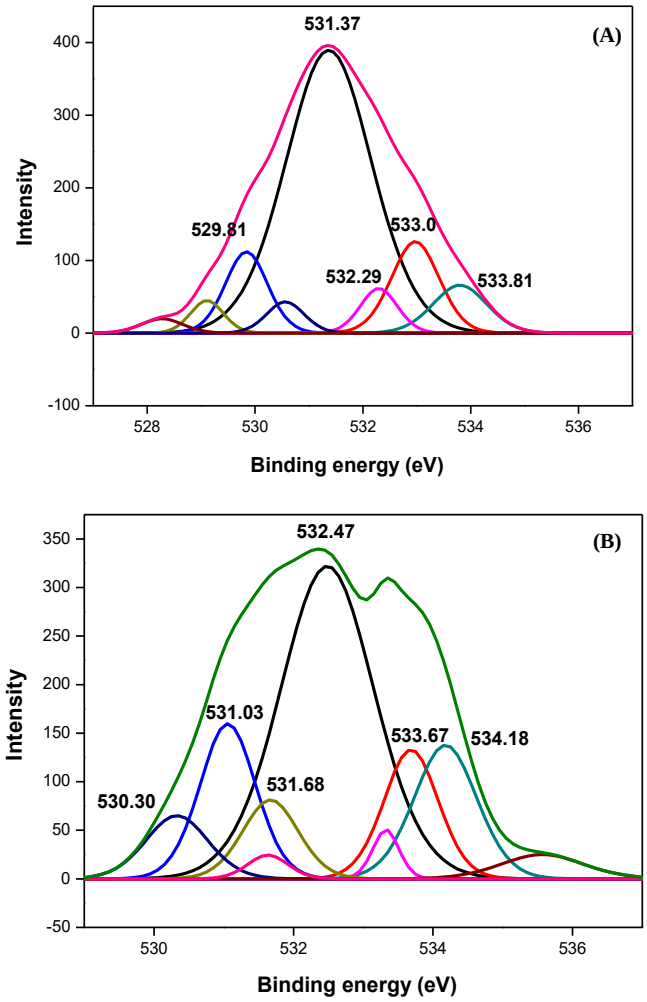

Figure 6.C.16: Deconvoluted O 1s spectra of PANI/CNF/PVA composite at A) 400°C and B) 500 °C

X-ray photoelectron spectroscopy demonstrated the formation of graphene like polyconjugated structures. The results showed that the polyconjugated structures are not formed below 400 ºC. It is formed in the temperature range of 400-500 ºC. The changes in the molecular structure of PVA and hence the formation of graphene like structures makes the PANI/CNF/PVA composites fire resistant.

6.C.5 Conclusion

The flame retardancy of PANI/CNF/PVA and PANI/CNF/PMMA were analysed by the vertical burning test. Compared to PANI/CNF/PMMA composite, PANI/CNF/PVA exhibited high limiting oxygen index. The LOI value of pure PVA was about 20, it increased to 42 for 50 % PANI/CNF/PVA composite. The drastic increase of LOI value suggest the possibility of structural changes and chemical reactions involved during heat treatment. The thermal stability of the composite increased from 381 ºC to 588 ºC. The presence of nitrogen in the char is confirmed by the elemental analysis. In addition to that the evolved gas analysis showed no or less nitrogen oxides eliminating from the composite. X-ray diffractogram exhibited a peak at 25 º indicating the formation of graphene like structure. X-ray photoelectron spectroscopy analysis indicate that it not the nitrogen content but nitrogen bonding configuration especially pyridinic and graphitic types play major role in the enhanced thermal stability. Hence the high thermal stability of the PANI/CNF/PVA composite can be attributed to the formation of polyconjuagted ladder structures by the dehydrogenation and cyclization reactions.

References

[1] P. Barber, S. Balasubramanian, Y. Anguchamy, S. Gong, A. Wibowo, H. Gao, H. Ploehn, H. Loye, Materials, 2009, 2, 1697

[2] R. Panigrahi, S. K. Srivastava, Sci. Rep., 2015, 5, 7638.

[3] P. Brochu, Q. Pei, Macromol. Rapid Commun., 2010, 31, 10

T. Mirfakhrai, J. D. W. Madden, R. H. Baughman, Mater Today, 2007, 10, 30

[4] X. L. Shi, M. S. Cao, J. Yuan, Q. L. Zhao, Y. Q. Kang, X. Y. Fang, Appl Phys Lett., 2008, 93, 1831181

[5] J. S. Lin, L. Chen, Y. Liu. J Appl Polym Sci., 2012,125,3517

[6] D. L. Wang, Y. Liu, D. Y. Wang. Polym Degrad Stab., 2007, 92, 1555

[7] G. B. Huang, H. D. Liang, Y. Wang. Mater Chem Phys., 2012, 132, 520

[8] G. B. Huang, J. R. Gao, X. Wang, Mater Lett., 2012, 66, 187

[9] D. Hong, J. H. Chen, Polymer, 1998, 39, 711.

[10] S. M. Sayed, H. M. Hamid, R. M. Radwan, Radiat Phys Chem., 2004, 69, 339

[11] G. A. Wang, C. C. Wang, C. Y. Chen, Polym. Degrad. Stab., 2006, 91, 2683.

[12] H. Vahabi, L. Ferry, C. Longuet, B. Otazaghine, C. Negrell-Guirao, G. David, J. M. Lopez-Cuesta, Mater. Chem. Phys., 2012, 136, 762.

[13] C. L. Chiang, S. L. Chiu, J. Polym. Res., 2009, 16, 637.

[14] A. Laachachi, M. Cochez, E. Leroy, M. Ferriol, J. M. Lopez-Cuesta, Polym. Degrad. Stab., 2007, 92, 61.

[15] I. Watanabe, S. Sakai, Environ Int., 2003, 29, 665.

[16] Z. Cui, B. J. Qu, Chin J Polym Sci., 2010, 28, 563

[17] C. X. Zhao, Y. Liu, D. Y. Wang, D. L. Wang, Y. Z. Wang, Polym. Degrad. Stab., 2008, 93, 323

[18] K. Wu, L. Song, Z. Wang, Y. Hu, Polym. Adv. Technol., 2008, 19, 1914

[19] H. Lu, C. A. Wilkie, M. Ding, L. Song, Polym. Degrad. Stab., 2011, 96, 1219

[20] J. Zuo, Y. Su, S. Liu, Q. Sheng, J. Polym. Res., 2011, 18, 1125

[21] B. J. Holland, J. N. Hay, Polymer, 2001, 2, 6775

[22] S. Pourjafar, A. Rahimpour, M. J. Jahanshahi.IndEngChem. Res., 2012, 18, 1398

[23] S. Mallakpour, M.Madani, Prog Org Coat., 2012, 74, 520

[24] D. Banerjee, A. Jha, K. K. Chattopadhyay, Macromol Res., 2012, 20, 1021

[25] P. Jash, C. A. Wilkie, Polym. Degrad. Stab., 2005, 88, 401

[26] P. Alexy, D. Bakos, G. Crkonova, Z. Kramarova, J. Hoffmann, M. Julinova, Polym. Test., 2003, 22, 811

[27] D. Y. Wang, Y. Z. Wang, J. S. Wang, D. Q. Chen, Q. Zhou, B. Yang, Polym. Degrad. Stab., 2005,87, 171

[28] D. L. Wang, Y. Liu, D. Y. Wang, C. X. Zhao, Y. R. Mou, Y. Z. Wang, Polym. Degrad. Stab., 2007, 92, 1555

[29] H. Gu, S. Tadakamalla, X. Zhang, Y.-D. Huang, Y. Jiang, H. A. Colorado, Z. Luo, S. Wei, Z. Guo, J. Mater. Chem. C, 2012, 1, 729

[30] H. Gu, S. Tadakamalla, Y. Huang, H. A. Colorado, Z. Luo, N. Haldolaarachchige, D. P.Young, S. Wei, Z. Guo, ACS Appl. Mater. Interfaces, 2012, 4, 5613

[31] A. Leszczy´nska, J. Njuguna, K. Pielichowski, J. R. Banerjee, Thermochim. Acta, 2007, 454, 1

[32] J. Ge, H. Hou, Q. Li, J. Graham Matthew, A. Greiner, H. Reneker Darrell, W. Harris Frank, Z. Cheng, J. Am.Chem. Soc., 2004, 126, 15754

[33] S. Bourbigot, M. Le Bras, S. Duquesne, M. Rochery, Macromol. Mater. Eng., 2004, 289, 499.

[34] Z. M. Dang, L. Wang, Y. Yin, Q. Zhang, Q. Q.Lei, Adv. Mater., 2007, 19, 852

[35] A. Das, S. Pisana, B. Chakraborty, S. Piscanec, S. K. Saha, U. V. Waghmare, K. S. Novoselov, H. R. Krishnamurthy, A. K. Geim, A. C. Ferrari, A. K. Sood, Nat. Nanotechnol., 2008, 3, 210

[36] J. Dong, X. Qu, L. Wang, C. Zhao, Xu, J. Electroanal. Chem., 2008, 20, 1981

[37] H. Ago, T. Kugler, F. Cacialli, W. R. Salaneck, M. S. P. Shaffer, A. H. Windle, R. H. Friend, J. Phys. Chem. B, 1999, 103, 8116

[38] S. Kundu, Y. Wang, W. Xia, M. Muhler, J. Phys. Chem. C, 2008, 112, 16869

[39] X. Mei, J. Ouyang, Carbon, 2011,49, 5389–5397

[40] H. L. Poh, F. Šaněk, A. Ambrosi, G. Zhao, Z. Sofer, M. Pumera, Nanoscale, 2012, 4, 3515

[41] H. Wang, T. Maiyalagan, and X. Wang, ACS Catal., 2012, 2, 81

[42] O. C. Compton, D. A. Dikin, K. W. Putz, L. C. Brinson, S. T. Nguyen, Adv. Mater., 2010, 22, 892

[43] D. Sun, X. Yan, J. Lang, and Q. Xue, J. Power Sources, 2013, 222, 52

[44] Z. H. Sheng, L. Shao, J. J. Chen, W. J. Bao, F. B. Wang, X. H. Xia, ACS Nano, 2011, 5, 4350.

[45] J. Kim, D. Jung, Y. Park, Y. Kim, D. W. Moon, and T. G. Lee, Appl. Surf. Sci., 2007, 253, 4112

[46] B. Ruelle, S. Peeterbroeck, R. Gouttebaron, T. Godfroid, F. Monteverde, J.-P. Dauchot, M. Alexandre, M. Hecq, P. Dubois, J. Mater. Chem., 2006, 17, 157

[47] S. Kundu, Y. Wang, W. Xia, M. Muhler, J. Phys. Chem. C, 2008, 112, 16869.

[48] K. V. Voitko, R. L. D. Whitby, V. M. Gun'ko, O. M. Bakalinska, M. T. Kartel, K. Laszlo, A. B. Cundy, S. V. Mikhalovsky, J. Colloid Interface Sci., 2011, 361, 129.

[49] W. W. Cai, R. D. Piner, F. J. Stadermann, S. Park, M. A. Shaibat, Y. Ishii, D. X. Yang, A. Velamakanni, S. J. An, M. Stoller, J. H. An, D. M. Chen, R. S. Ruoff, Science, 2008, 321, 1815

[50] T. Szabo, O. Berkesi, P. Forgo, K. Jose povits, Y. Sanakis, D. Petridis and I. Dekany, chemistry of materials, 2006, 18, 2740.

…..ꕥ…..

Chapter 7

THE DEVELOPMENT OF DEVICES

Contents

Part A

Novel humidity sensor based on nanofibers/polyaniline/poly(vinyl alcohol) composite

An efficient sensor for monitoring humidity was fabricated using nanofibers, polyaniline and poly(vinyl alcohol). The sensor was fabricated using two nanofibers, i.e. carbon nanofiber (CNF) and nano-fibrillated cellulose (NFC). The sensor film was prepared by casting of the hot aqueous PVA solution containing the nanofibers modified with polyaniline. The composites (PANI/CNF/PVA and PANI/NFC/PVA) were studied using TEM, SEM, and FTIR spectroscopy. The response of the sensor was evaluated from the change in capacitance with varying humidity levels. The analysis revealed that the sensors had a short response time (41 s) and good shelf life. The AC capacitance of the sensor film was measured over a relative humidity (RH) range of 30 % to 100 %. Compared to PANI/NFC/PVA composite, PANI/CNF/PVA composite exhibited higher sensitivity, shorter response time (41 s) and better recovery (46 s). The change of sensitivity for CNF based composite was from 290 % to 6570 % at 100 Hz frequency.

7.A.1 Introduction

Polymer based sensing material gained much attention in the development of electronic systems owing to their low cost, easy preparation, relatively simple modulation of properties by functionalization [1,2]. Among various of chemical and biological sensors known humidity sensing materials are widely used for the measurement of relative humidity. Humidity sensing has become essential for weather prediction, historic preservation, environmental studies and mobile electronics etc. [2-4]. Diverse materials like organic polymers, inorganic composite materials and ceramics have been used for the sensing applications [5-9]. Polymer based humidity sensors are classified into resistive or capacitive type sensors. In distinction to resistive type sensors, capacitive sensors feature ease of fabrication, less power requirement and possess much better linearity. The capacitive type sensors make use of the variation of capacitance of the hygroscopic dielectric layer [10] with relative humidity. Presently electric hygrometers are preferred to the traditional hair hygrometers owing to high precision and compact size [11-12].

The most challenging part is to find out suitable materials for the purpose. Conducting polymer based sensors possess some advantages like short response and recovery times. Among the conducting polymers, polyaniline has extensively been investigated as sensing polymer due to its conducting property and chemical stability [13-15]. PANI can be synthesized by a fast and facile in-situ polymerization technique. Moreover, the size and morphology of the PANI particles can be controlled during the synthesis. It also opens up a way to industrial processing. The cost of sensor fabrication and maintenance are thus likely

to be low. In the pioneering work of Chani et al. [16], the polyaniline sensors in the form of pellets responded towards humidity, but the response time was approximately 3-4 minutes. So, the development of novel and high-performance humidity and gas sensor with good sensitivity, stability and response remains a challenge.

In recent decades, a number of studies have indicated that poly(vinyl alcohol) responds well to humidity owing to the large number of hydroxyl groups present that can interact through hydrogen bonds [17-20]. By absorbing water molecules, PVA swells indicating altering of chain conformation. Ogura et al. [21] and Ming-Zhi Yang et al. [22] deployed a combination of PANI-PVA for the fabrication of extremely sensitive and linear resistive humidity sensor. But the sensitivity of as-prepared sensor was very low.

The low sensing response of polyaniline lowered the pace of development of PANI based sensors. To boost the properties of PANI and PVA I have used carbon nanofiber (CNF) and nano-fibrillated cellulose (NFC) separately. The effect of nanofibers on the sensing properties was studied in terms of change in capacitance and recovery times. The synergetic effect of the fibers along with PANI and PVA has not been studied. Hence efforts are aimed at developing nanocomposite humidity sensor with high selectivity, sensitivity and stability. In this I describe the cost-effective development of polyaniline/poly(vinyl alcohol)/carbon nanofiber based humidity sensor. A comparison humidity sensing property of PANI/CNF/PVA and PANI/NFC/PVA composites was carried out. The moisture sensitivity, hysteresis, repeatability and response time were evaluated at room temperature.

7.A.2 Experimental

7.A.2.1 Modification of nano-fibrillated cellulose (NFC) and carbon nanofiber (CNF) using aniline

3 g of NFC or CNF was dispersed in 100 mL of 1 M hydrochloric acid solution by ultrasonication for 1 h. Then the dispersion was kept at 0-4 ^{o}C temperature followed by addition of 10 g of aniline. 12.50 g of ammonium persulfate was dissolved in 100 mL 1M HCl solution and was taken in a burette. The APS/HCl was added drop-wise into the aniline-fiber solution to initiate polymerization reaction. The polyaniline-coated fibers (PANI/CNF or PANI/NFC) were then isolated. Different weight percentages of modified fibers were then mixed with poly(vinyl alcohol) solution in water at 90 ^{o}C followed by ultrasonication for 2 h. The wt.% of the fiber was adjusted to make 10, 20, 30 and 40 % compositions. Films were prepared by casting and dried slowly at 70 ^{o}C for 24 h. Circle shaped samples of diameter 20 mm and thickness of 0.2-0.5 mm was used for humidity sensing applications.

7.A.2.2 Humidity response measurement

The response of sensors towards the changing humidity was measured by customized humidity chamber. The humidity inside the chamber was controlled by placing fused calcium chloride. The reference sensor used was HTC-2 Digital Thermo-Hygrometer with a resolution of 0.1/0.2 and an accuracy of ±3 %RH. The variation of capacitance with humidity for a frequency range of 40 Hz to 30 MHz was measured by using Agilent 4294A impedance analyser. The impedance analyser was connected to a computer and the changes were monitored. The humidity inside the chamber was

maintained constant by adding adequate quantity of calcium chloride and the sensor response was measured until the capacitance registered constant value. All the measurements were carried out at a constant temperature of 30 ºC.

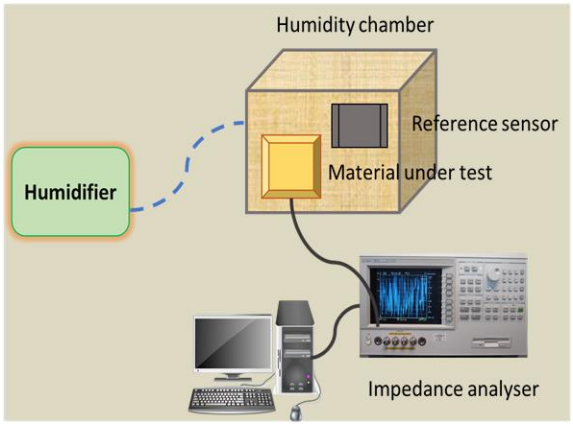

Figure 7.A.1: Schematic diagram of the humidity sensor showing humidifier, humidity chamber and measurement setup.

7.A.3 Results and discussion

7.A.3.1 Characterizations

7.A.3.1.1 Transmission Electron Microscopy

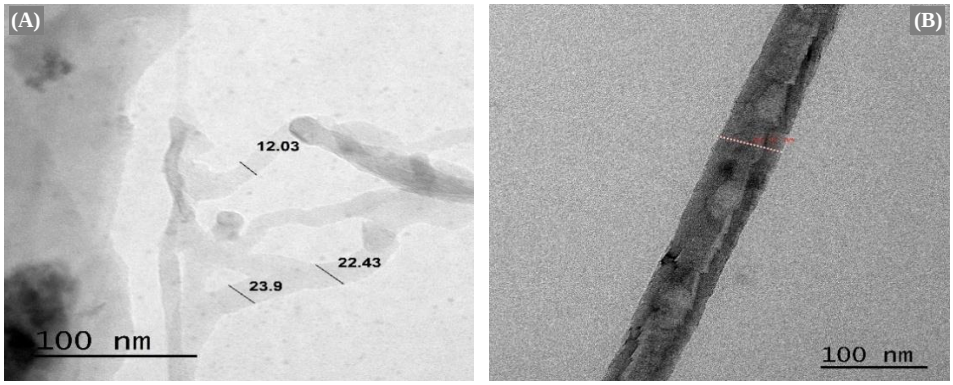

Figure 7.A.2: TEM micrographs of nano-fibrillated cellulose (A) and carbon nanofiber (B)

The morphological structures and average diameter of NFC and CNF are shown in the figure 7.A.2. The length of both fibers falls in micrometer range and the diameter of NFC is much smaller than that of CNF. The length of carbon nanofiber is about 2.3 μm while that of cellulose nanofiber is approximately 1 μm. The diameter of the NFC comes around 23 nm whereas the diameter of CNF is approximately 60 nm. Consequently, the aspect ratios of both the fibers are similar. Larger the surface to volume ratio the larger will be the response towards humidity. Shirale et al. [23] observed higher sensitivity with increasing aspect ratio in the case of single polypyrrole nanowire. So, in terms of aspect ratio both fibers are expected to show comparable sensitivity. As the diameter of the nanofiber decreases the number of surface charges increases. Hence it will reduce the interrupted conduction resulting an increased conductivity. Elfström et al. [24] proved that the sensitivity is a function of sensor surface area. TEM analysis suggests that both the composites will exhibit similar sensing properties.

7.A.3.1.2 Scanning Electron Microscopy

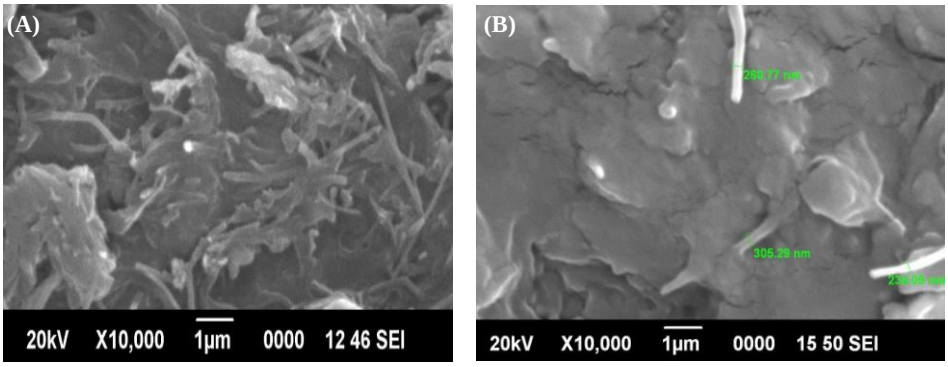

Figure 7.A.3: SEM images of PANI/CNF/PVA composites A) before water absorption, B) after water absorption

Figure 7.A.3 shows the SEM images of the composites. A network of PANI coated NFC fibers is seen in the figure 7.A.3A. After water absorption PVA swells. As a result, the fibers get separated out as seen in figure 7.A.3B. The water absorbing capacity of the composite can be well understood from the SEM images of the composites. The water molecules are a kind of polar molecules having long relaxation time. The water molecules are bonded to PVA molecules by hydrogen bonding. Water molecules being polar are easily polarized resulting in significant increase in the capacitance.

7.A.3.1.3 FTIR spectroscopy

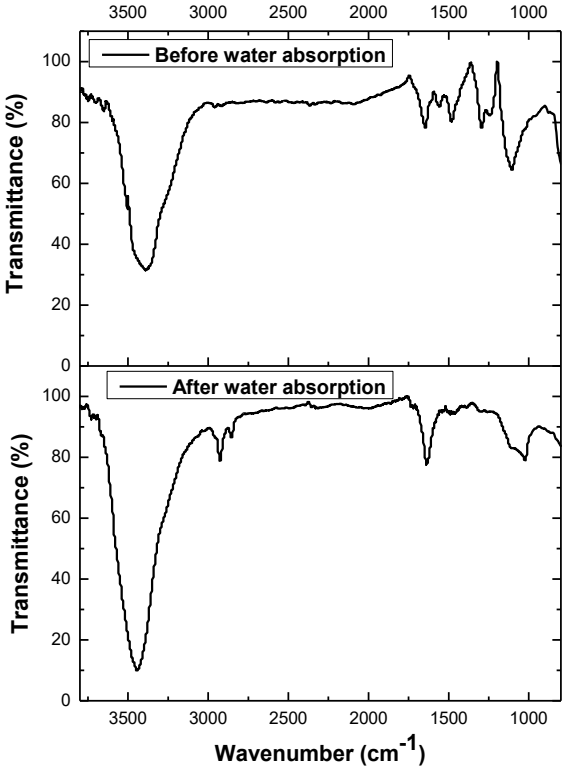

Figure 7.A.4: FTIR spectra of the PANI/CNF/PVA composites before and after water absorption

Figure 7.A.4 depicts the FTIR spectra of the PANI/CNF/PVA composite before and after water absorption. The peaks at 1550-1600 cm^{-1} correspond to the stretching vibrations of quinoid and benzenoid rings of polyaniline. For the water swollen composite the peak at 1598 cm^{-1} is merged and appears at 1648 cm^{-1}. The bending vibration of water molecules appears as absorption at 1643 cm^{-1}. The lower frequency vibrations of the water molecules are attributed to the stronger hydrogen bonds whereas the higher frequency vibrations are due to the weaker hydrogen bonds [25]. The O-H stretching band at around 3231 cm^{-1} shows strong evidence for the absorption of water molecules and the shift to lower frequency indicates the intermolecular hydrogen bonding. The peak at 2328 cm^{-1} corresponds to the C-H stretching vibration. FTIR spectra show that the composite absorbs good amount of water and results in hydrogen bonding interaction.

7.A.3.2 Humidity Sensing

The effect of humidity was explored by measuring the variation of capacitance with frequency under a wide range of humidity levels. Poly(vinyl alcohol) based composites were found to be very effective humidity sensor owing to its water absorbing and desorbing property. Figure 7.A.5 A-I represent variation of capacitance with frequency over a range of 100-30 % RH. For both PANI/NFC/PVA and PANI/CNF/PVA composites the capacitance decreases with decrease of humidity. It is evident from the figure 7.A.5 that all composites exhibit higher sensitivity than that of pure PVA. The variation of capacitance with humidity is more apparent at lower frequencies, while at higher

relative humidity levels all composites exhibit more or less similar capacitance. The variation is not as much clear as at low frequency. This can be attributed to the fact that the absorbed water molecules introduce leak conduction [26].

The equation for capacitance with leak current can be expressed as [27]

$$C=\varepsilon^*C_0=(\varepsilon_r - i\frac{\gamma}{\omega\varepsilon 0})C_0 \quad \text{.....7.A.1}$$

where ε^*, ε_r, C_0, represent the complex dielectric constant, relative dielectric constant and capacitance of ideal capacitor, respectively. ω is the angular frequency, ε_0 gives the permittivity of the free space and γ is the conductance. From this relationship, it is evident that capacitance of a material is inversely proportional to the frequency of the applied field and is directly related to the conductance of the medium. So, for all the composites the capacitance decreases with the frequency. The conductance of the composites increases with the number of absorbed water molecules. As the humidity increases the absorbed water also increases. Consequently, more will be its conductance. As a result, the composites exhibit higher capacitance value at higher humidity.

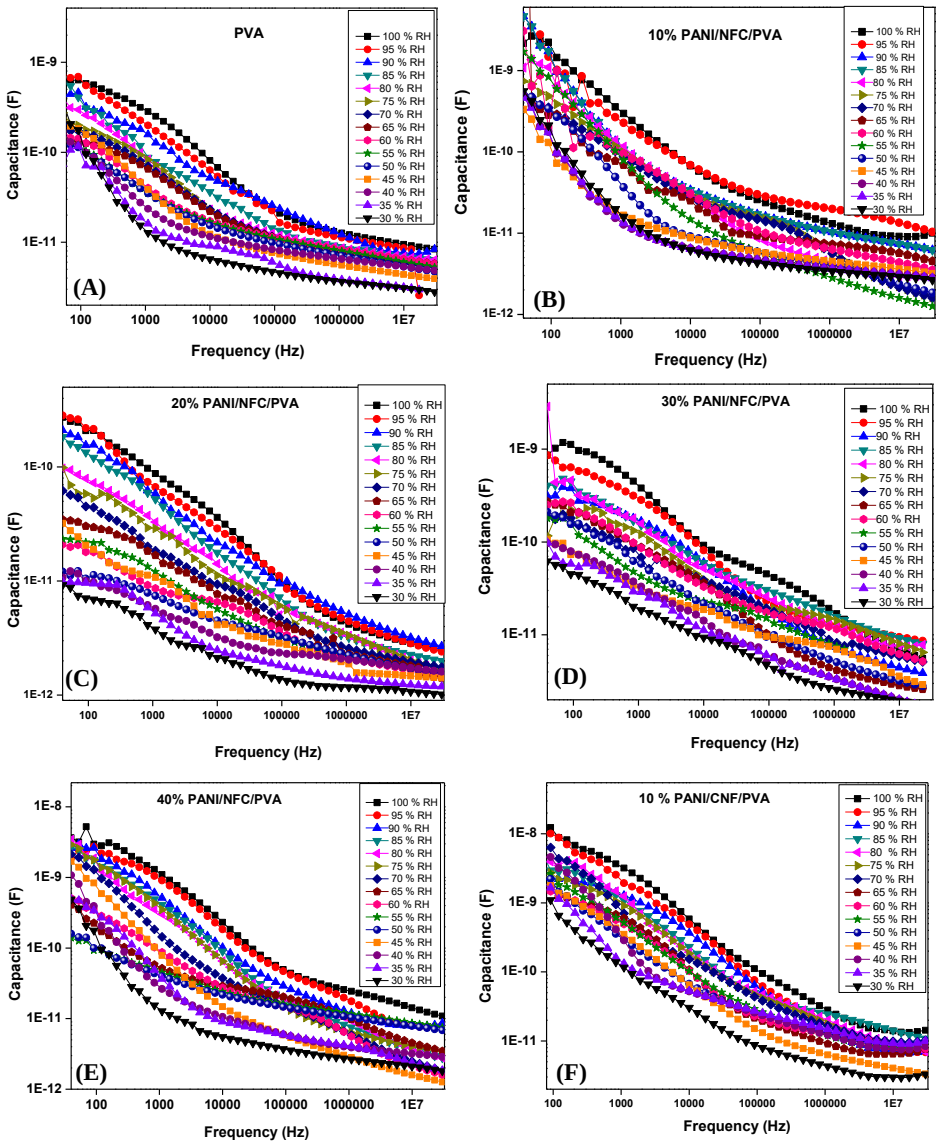

Figure 7.A.5: Capacitance variation as a function of frequency
A) PVA, B) 10 % PANI/NFC/PVA, C) 20 % PANI/NFC/PVA,
D) 30 % PANI/NFC/PVA, E) 40 % PANI/NFC/PVA,
F) 10 % PANI/CNF/PVA,

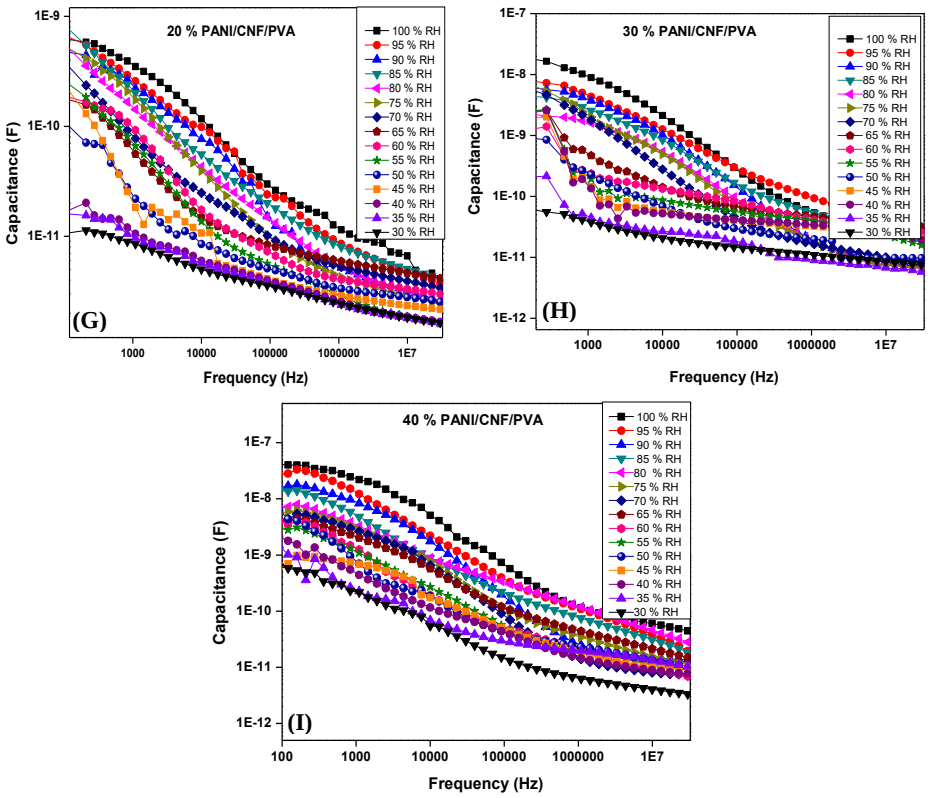

Figure 7.A.5: Capacitance variation as a function of frequency
G) 20 % PANI/CNF/PVA, H) 30 % PANI/CNF/PVA,
I) 40 % PANI/CNF/PVA

A cross plot of capacitance against relative humidity is given in figure 7.A.6. It shows that the composites have better sensitivity to relative humidity compared to PVA. For PVA the variation of capacitance is very limited. This is improved in the case of the composites. As the PANI-modified fiber concentration in the matrix increases the sensitivity increases. For composites with higher fiber content, the change in capacitance is relatively rapid. At lower humidity levels, a gradual increase of capacitance is observed. In contrast to PVA, all the composites exhibit good capacitance response for the range of humidity

studied. Significant improvement is observed for PANI/CNF/PVA composites in all the humidity levels in the frequency range 40 Hz-30 MHz. The best response of the capacitance is observed for 40 wt.% composite. For 40 % PANI/CNF/PVA composite the capacitance at 30 RH % is about 70 pF which increases to 3400 pF at 100 RH %.

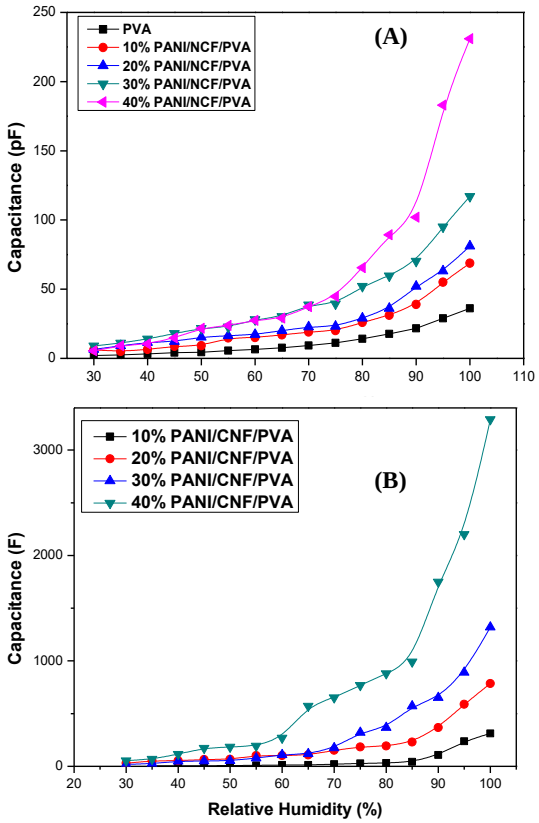

Figure 7.A.6: Capacitive response with relative humidity for different concentrations of PANI/NFC/PVA composite (A) and PANI/CNF/PVA composite (B) at 10 KHz

Hydrochloric acid doped polyaniline contains positively charged nitrogen atoms surrounded by negative chlorine atoms. After the modification of cellulose by polyaniline, the chlorine atoms of PANI will be

hydrogen bonded to the hydroxyl groups of cellulose whereas only Van der Waals interaction exists between carbon nanofiber and PANI. The mechanism of water absorption can be explained on the basis of proton transport and polarization of OH groups. Under low humidity levels the water molecules will be hydrogen bonded to the hydroxyl groups of PVA and chlorine atoms of PANI. More chlorine atoms will be available in case of PANI/CNF/PVA composites than that of PANI/NFC/PVA composites. Since in PANI/NFC/PVA composite, the polyaniline modification of cellulose results in the hydrogen bonding interaction between chlorine atoms of PANI and hydroxyl groups of cellulose. Whereas only Vander walls interaction is taking place between CNF and polyaniline. So, the chlorine atoms of polyaniline are more available for the hydrogen bonding interaction with the incoming water molecules. So, in PANI/CNF/PVA composites more active sites are available for hydrogen bonding interaction for the water molecules. Hydrogen bonding interaction plays significant role on the humidity sensing mechanism, since the water molecules can get transferred through the bonds [29]. Hence stronger water absorption can be observed in CNF based composite. It results in the formation of continuous water layer on the surface of the composite. With increase of humidity, the sites for hydrogen bonding will get saturated. The further increase of humidity, the excess water molecules will get attached to the water molecules which are in direct contact with the PVA molecules. At the first layer, the water molecules are highly bonded to the hydroxyl groups on the surface. Hence these water molecules cannot move freely. Whereas the water molecules in the other layers, are bonded by weak hydrogen bonds and they are easy to get polarized. At higher humidity values, weakly bonded water molecules will

get ionized producing huge number of hydronium ions. In contrast to PANI/NFC/PVA composites PANI/CNF/PVA composites exhibit high sensitivity towards the variation of humidity (figure 7.A.7). This is attributed to the more number of hydronium ions and chloride ions released during the absorption of water molecules which will act as charge carriers by the application of external electrical field. Consequently, it will enhance the capacitance.

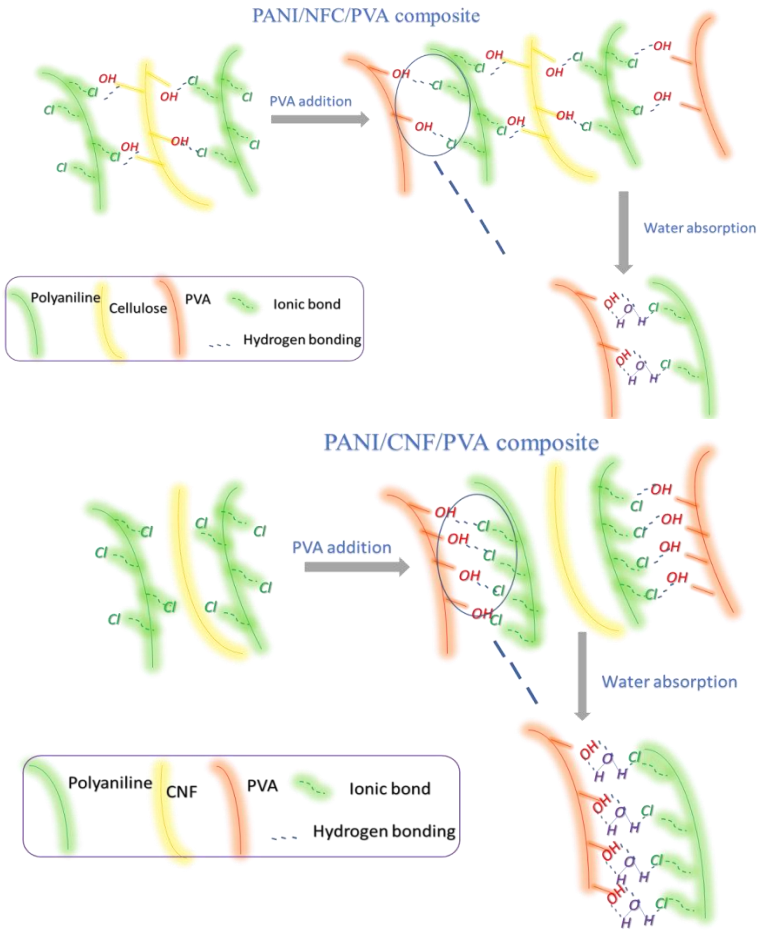

Figure 7.A.7: The mechanism for the improved humidity sensitivity of PANI/NFC/PVA and PANI/CNF/PVA composites

The capacitance of PANI/CNF/PVA composite is more due to the increased number of absorbed water molecules in the system. For instance, the capacitance value for 40 % PANI/CNF/PVA is 3290 pF at 100 % RH whereas it is only 231 pF for 40 %PANI/NFC/PVA composite at the same humidity. This increase is due to the conductive nature of CNF compared to cellulose and the increased water absorption.

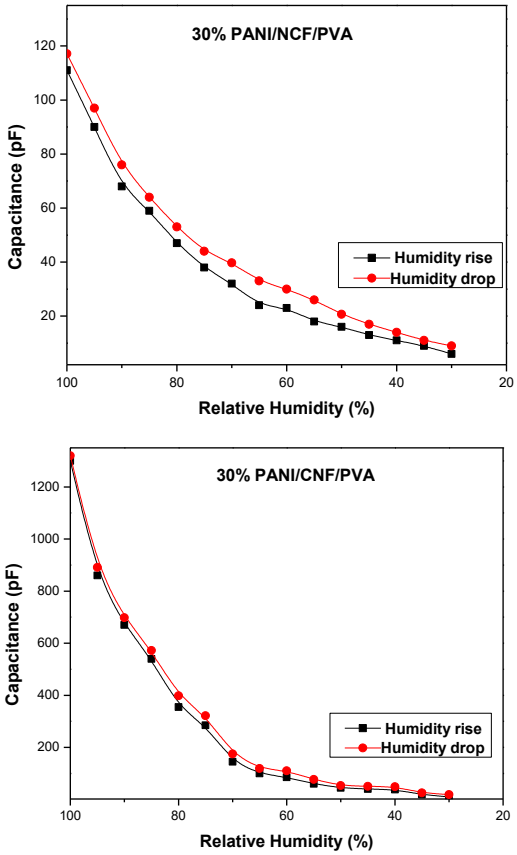

Figure 7.A.8: Hysteresis – relative humidity relationship for 30 % PANI/NFC/PVA and PANI/CNF/PVA composites

The relationship between capacitance and relative humidity during absorption-desorption processes is important for any sensor applications

of the composite. In order to evaluate the repeatability of the sensor the capacitance was measured at 30 % RH to 100 % RH in 50 minutes time to ensure absorption saturation. Then the chamber humidity was reduced to 30 % RH at the same rate as earlier. The figure 7.A.8 represents the change of capacitance with the variation of humidity in the case of humidity increase and dehumidification processes. The increase of capacitance during the water absorption is faster than the decrease during the water desorption process. Steady increase of water absorption is observed up to 75 % RH. Beyond that the capacitance increases rapidly. The field produced by the dipoles of water molecules will be enough to saturate the polarization of hydroxyl groups of poly(vinyl alcohol) at 75 % RH or lower relative humidity ranges. So up to 75 % RH the water molecules will be hydrogen bonded into the matrix and after that the excess water molecules will be physisorbed on to the composite leading to the sharp increase of capacitance. During the water desorption process the weakly bonded water molecules are removed first, followed by the removal of chemisorbed water molecules. But the rate of removal is comparatively slow. The higher capacitance values during desorption process indicate incomplete removal of water molecules because of the positive energy necessity for the desorption process. Therefore, the water molecules will contribute more to the effective capacitance, consequently yielding high capacitance value. As a result of this rate difference, hysteresis is observed at higher humidity levels. The hysteresis in not seen at lower by humidity ranges.

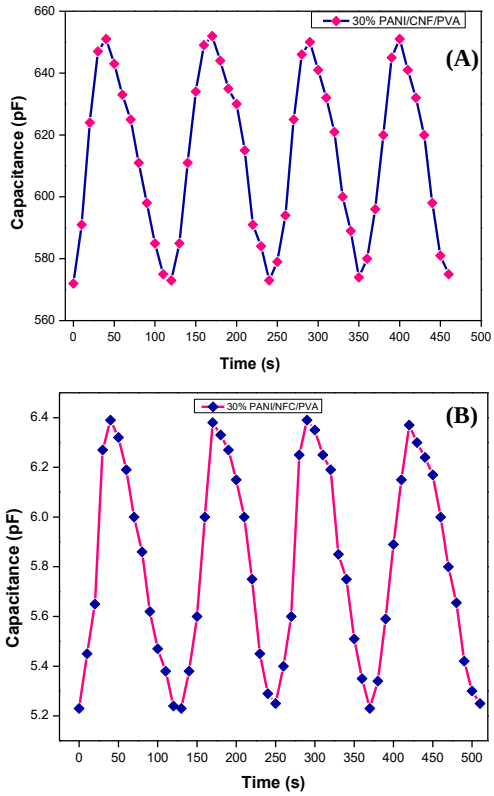

Figure 7.A.9: Response time curves for A) 30 % PANI/CNF/PVA and B)30 % PANI/NFC/PVA composites

For the evaluation of a sensor performance the important characteristics are recovery and response times. The time taken by the sensor to attain 90 % of the total capacitance change is the response time or the recovery time during the adsorption or desorption process of water molecules. The figure 7.A.9 A & B represent the change in capacitance with time in seconds for PANI/CNF/PVA and PANI/NFC/PVA composites, respectively. From the figure, it is seen that for NFC based composites the response time is of about 47 s when the humidity level is increased from 30 % to 100 % and the recovery time is 58 s when it is dehumidified from 100 % to 30 %. But PANI/CNF/PVA composite respond more quickly

than NFC composite. The response time for CNF composite is about 41 s and takes 50 s to come back to the original state. CNF based composites exhibit higher sensitivity, better response and recovery times.

Wen Chuang et al. defined an equation correlating capacitance variation and relative humidity [30].

$$S\ (\%)=\frac{C_{RH}-C_{30}}{C_{30}} * 100 \quad \text{.....7.A.2}$$

Here C_{RH} represents the capacitance measured at a particular RH value and C_{30} represents the capacitance at RH 30 %. The effect of frequency on the sensing parameters are examined by monitoring the capacitance response with relative humidity under 5 different frequencies and the variation of capacitance at different humidity values is plotted. As evident from the figure 7.A.10 that the sensitivity variation is higher at lower frequencies. As the frequency increases the capacitance variation and sensitivity are lowered. At 100 Hz, the sensitivity increases from 290 % to 6570 % whereas at 1000 Hz variation is from 200 % to 3500 %.

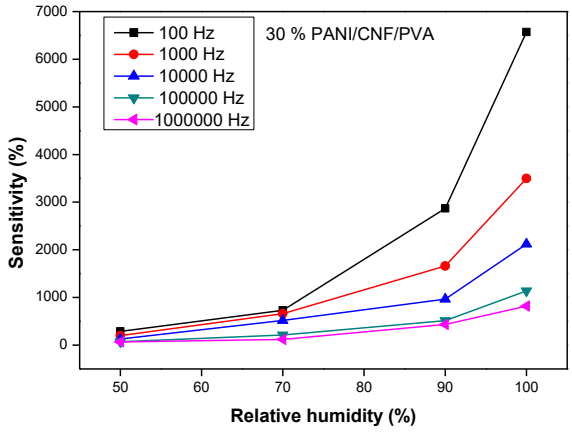

Figure 7.A.10: Sensitivity response with relative humidity for 30 % PANI/CNF/PVA composite

The sensor reported here represents small but acceptable degree of hysteresis. All the above results show that PVA composite based on polyaniline-modified fibers can be used as humidity sensor with good sensitivity and stability.

7.A.4 Conclusion

PANI/CNF/PVA and PANI/NFC/PVA composites were prepared by ultrasonication-assisted mixing of PANI coated CNF/NFC fibers with poly(vinyl alcohol) solution. The composites performance as humidity sensor was investigated at room temperature. The results revealed that the synergic effect of PANI/CNF and PVA led to high selectivity and fast response towards humidity. PVA is a water absorbing material. The absorbing capacity was improved by the presence of PANI/CNF or PANI/NFC which in turn altered the capacitance of the matrix. The influence of nanofibers on the sensing property was investigated. The response and recovery times, sensitivity and the stability of the sensing films were evaluated for both composites. Compared to PANI/NFC/PVA composite PANI/CNF/PVA composite exhibited higher sensitivity, faster response and recovery times and better stability towards humidity sensing. Thus, the prepared PANI/CNF/PVA composite offers great practical application as excellent humidity sensor.

References

[1] B. Adhikari, S. Majumdar, Prog. Polym. Sci., 2004, 29, 699

[2] Z. Chen, C. Lu, Sensor Lett., 2005, 3, 274

[3] W. Xuan, X. He, J. Chen, W. Wang, X. Wang, Y. Xu, Z. Xu, Y.Q. Fu, J. K. Luo, Nanoscale, 2015, 7, 7430

[4] Y. Sakai, Y. Sadaoka, M. Matsuguchi, Sens. Actuators B, 1996, 35, 85

[5] Y. Sakai, Y. Sadaoka, M. Matsuguchi, Y. Kanakura, M. J. Tamura, Electrochem. Soc.,1991, 138, 2474

[6] J. Wang, B. K. Xu, G. F. Liu, J. C. Zhan, T. Zhang, Sens. Actuators B, 2000, 66, 159

[7] Q. Qi, T. Zhang, Q. J. Yu, R. Wang, Y. Zeng, L. Liu, H. B. Yang, Sens. Actuators B, 2008, 133, 638

[8] Q. Qi, T. Zhang, L. J. Wang, Appl. Phys. Lett., 2008, 93, 023105

[9] J. Wang, F.-Q. Wu, K.-H. Shi, X.-H. Wang, P.-P. Sun, Sens. Actuators B, 2004, 99, 586

[10] P. G. Su, Y. L. Sun, C. C. Lin, Sens. Actuators B, 2006, 113, 883

[11] T. J. Harpster, B. Stark, K. Najafi, Sensors and Actuators A: Physical, 2002, 95, 100

[12] L. Gu, Q. A. Huang, M. Qin, Sensors and Actuators B, 2004, 99, 491

[13] A. Oprea, N. Barsan, U. Weimar, M. L. Bauersfeld, D. Ebling, J. Wöllenstein, Sensors and Actuators B, 2008, 132, 404

[14] H. J. Sharma, D. V. Jamkar, S. B. Kondawar, Proc. Mater. Sci., 2015, 10, 186

[15] C. Steffens, M. L. Corazza, E. Franceschi, F. Castilhos, P. S. Herrmann, J. V. Oliveira, Sensors and Actuators B, Chemical, 2012, 171, 627

[16] H. Xu, D. Ju, W. Li, H. Gong, J. Zhang, J. Wang, B. Cao, Sens. Actuators B, 2016, 224, 654

[17] M. T. S. Chani, K. S. Karimov, F. A. Khalid, S. A. Moiz, Solid State Sci., 2013, 18, 78

[18] T. Fei, K. Jiang, F. Jiang, R. Mu, T. Zhang, J. Appl. Polym. Sci., 2014, 131, 397261

[19] M. V. Fuke, P. V. Adhyapak, U. P. Mulik, D. P. Amalnerkar, R. C. Aiyer, Talanta, 2009, 78, 590

[20] Y. Li, B. Ying, L. Hong, M. Yang, Synth. Met., 2010, 160, 455

[21] S.-H. Hwang, D. Kang, R. S. Ruoff, H. S. Shin, Y.-B. Park, ACS Nano, 2014, 8, 6739

[22] M.-Z. Yang, C.-L. Dai, W.-Y. Lin, Sensors, 2011, 11, 8143

[23] N. Elfström, R. Juhasz, I. Sychugov, T. Engfeldt, A. E. Karlström, J. Linnros, Nano Lett., 2007, 7, 2608

[24] D. J. Shirale, M. A. Bangar, W. Chen, N. V. Myung, A. Mulchandani, J. Phys. Chem. C, 2010, 114,13375

[25] N. Kitadai, T. Sawai, R. Tonoue, S. Nakashima, M. Katsura, K. Fukushi, J. Solution Chem., 2014, 43, 1055

[26] C. McDonagh, P. Bowe, K. Mongey, B. D. MacCraith, Journal of Non-Crystalline Solids, 2002, 306, 138

[27] J. Wang, X.-H. Wang, X.-D. Wang, Sens. Actuators B Chem., 2005, 108, 445

[28] W. C. Wang, Y. T. Tian, K. Li, E. Y. Lu, D. S. Gong, X. J. Li, Appl. Surface Sci., 2013, 273, 372

Part B

Novel ammonia sensor based on nanofibers/polyaniline/poly(vinyl alcohol) composite

A sensor for ammonia gas monitoring was fabricated using nanofibers, polyaniline and poly(vinyl alcohol). The sensor film was prepared by casting of the hot aqueous PVA solution containing the nanofibers modified with polyaniline (PANI). The response of the films to ammonia was investigated over a range of 0-100 ppm at room temperature. The observed sensitivity of the film was varied from 10 to 84. PANI/CNF/PVA composite was found to have much better response time (46 s) and sensitivity for ammonia sensing. This improvement in the sensing performance of CNF composite was attributed to the higher pores size.

7.B.1 Introduction

Recently, gas sensors have been developed very fast all over the world due to their wide application in various fields such as environmental monitoring, modern industry and agriculture, military affairs, national defence and even disease diagnosis [1-10]. Polymer based sensing material gained much attention in the development of electronic systems owing to their low cost, easy preparation, relatively simple modulation of properties by functionalization [11,12]. In view of environmental pollutions, it is crucial to detect and measure the accurate amount of the toxic pollutant gases. Anhydrous NH_3 is such a toxic gas which causes irritation to eyes, skin and respiratory organs. At present metal oxide semiconductors are being used for monitoring toxic gases. Usually these sensors entail high working temperature, moderate selectivity and are expensive. So, our interest lies in the room temperature-sensing of ammonia gas. The most challenging part is to find out suitable materials for the purpose. It is understood that conducting polymers can play a key role in ammonia sensing. Conducting polymer

based sensors possess some advantages like short response and recovery times. Among the conducting polymers, polyaniline has extensively been investigated as gas sensing polymer due to its conducting property and chemical stability [13-16]. PANI can be synthesized by a fast and facile in-situ polymerization technique. Moreover, the size and morphology of the PANI particles can be controlled during the synthesis. It also opens up a way to industrial processing. The cost of sensor fabrication and maintenance are thus likely to be low.

The sensing property of PANI and PVA was compared by the incorporation of two nanofibers; carbon nanofiber (CNF) and nano-fibrillated cellulose (NFC) separately. The effect of nanofibers on the sensing properties was studied in terms of change in resistance and recovery times. The synergetic effect of the fibers along with PANI and PVA has not been studied. Hence efforts are aimed at developing nanocomposite ammonia sensors with high selectivity, sensitivity and stability.

Here, I report the cost-effective development of polyaniline/ poly(vinyl alcohol)/carbon nanofiber based ammonia sensors. A comparison of ammonia sensing properties of PANI/CNF/PVA and PANI/NFC/PVA composites was carried out. From the obtained results it could be concluded that this material had the potential to sense ammonia gas.

7.B.2 Experimental

7.B.2.1 Modification of nano-fibrillated cellulose (NFC) and carbon nanofiber (CNF) using aniline

3 g of NFC or CNF was dispersed in 100 mL of 1 M hydrochloric acid solution by ultrasonication for 1 h. Then the dispersion was kept at 0-

4 °C temperature followed by addition of 10 g of aniline. 12.50 g of ammonium persulfate was dissolved in 100 mL 1M HCl solution and was taken in a burette. The APS/HCl was added drop-wise into the aniline-fiber solution to initiate polymerization reaction. The polyaniline -coated fibers (PANI/CNF or PANI/NFC) were then isolated. Different weight percentages of modified fibers were then mixed with poly(vinyl alcohol) solution in water at 90 °C followed by ultrasonication for 2 h. The wt.% of the fiber was adjusted to make 10, 20, 30 and 40 % compositions. Films were prepared by casting and dried slowly at 70 °C for 24 h. Circle shaped samples of diameter 20 mm and thickness of 0.2-0.5 mm was used for humidity sensing applications.

7.B.2.2 Ammonia gas sensing

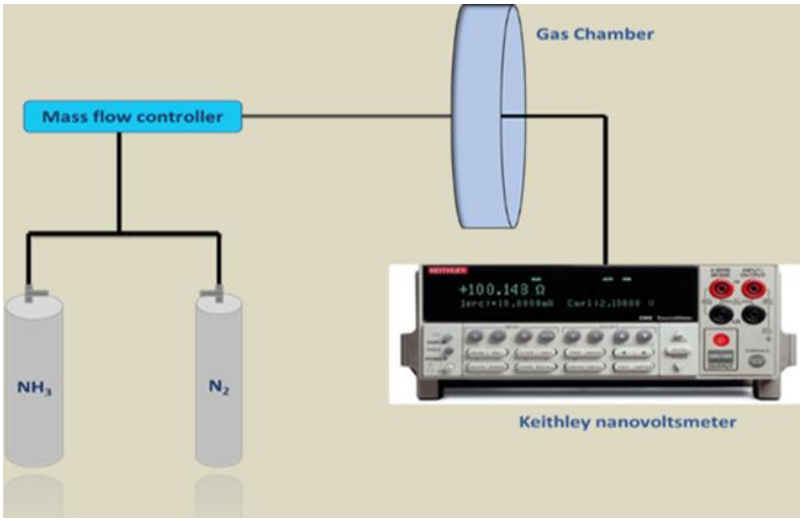

Figure 7.B.1: Schematic diagram of the ammonia sensor showing gas containers, mass flow controller, gas chamber and measurement setup.

Figure 7.B.1 shows the schematic representation of the gas sensor device. The sample was placed in the gas chamber and the desired NH_3

concentrations was achieved by diluting the concentrated NH_3 gas (1%) with nitrogen. The sensitivity measurements are carried out at room temperature. The resistance variation with NH_3 was measured using Keithley two-probe Nanovoltmeter.

7.B.3 Results and discussion

7.B.3.1 Characterization of the fiber

7.B.3.1.1 BET surface area analysis

The surface area and pore size distribution of the sensing material play a key role in the overall performance of the sensors. I have measured the surface area and porosity of PANI/CNF and PANI/NFC composites by nitrogen sorption experiments at 77.3 K. According to the usual classification of adsorption isotherms, shape of the isotherm is of type IV. The surface area and porosity of PANI/CNF is higher than PANI/NFC composites. The BET surface area for PANI/CNF composites is 34 m^2/g and the average pore diameter is 21.2 nm. Whereas, the surface area is 17 m^2/g and the pore diameter is 17.1 nm for PANI/NFC composite. If the solubility of ammonia gas is similar in both PANI/CNF and PANI/NFC composites the gas diffusion is directly related to the pore size of the material [17]. The surface area and pore size distribution analysis suggest that PANI/CNF/PVA composite might show superior gas sensitivity.

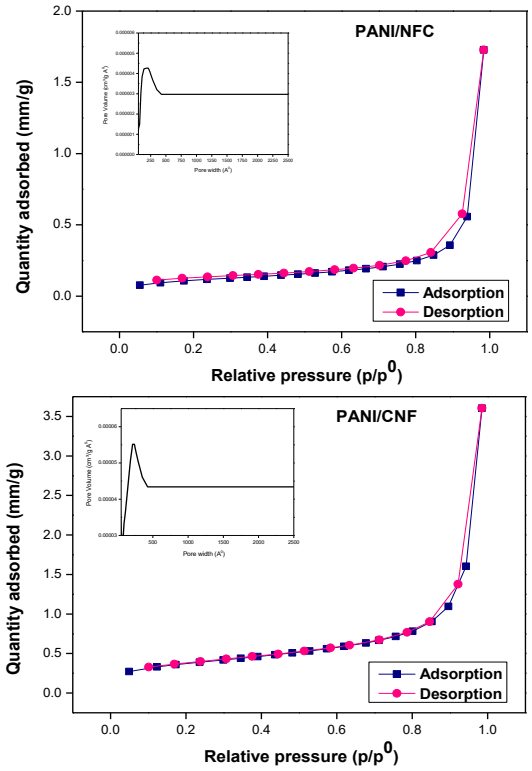

Figure 7.B.2: Adsorption-desorption isotherm and pore size distribution of PANI/NFC and PANI/CNF composites

7.B.3.2 Ammonia Sensing

To investigate the ammonia gas sensing properties of the composite a device was fabricated (Figure 7.B.3) and the responses of the PANI/CNF/PVA and PANI/NFC/PVA under different ammonia gas concentrations at room temperature were studied. The sensitivity to various gas concentrations under effective response time can be defined as

$$S=\frac{R-R_0}{R_0}=\frac{\Delta R}{R_0} \quad \text{.....7.B.1}$$

where R is the steady state resistance of the material when exposed to NH_3 gas at a particular concentration, R_0 is the initial resistance in pure

N_2. Figure 7.B.3 gives the change in sensitivity of the two composites with varying ammonia gas concentration.

The response of CNF based composites is much linear than the NFC composites. At 20 ppm of NH_3, 30 % PANI/CNF/PVA composite exhibits a sensitivity of 10 where as it is only 4.4 for 30 % PANI/NFC/PVA composite. While at higher concentration of about 100 ppm NH_3 the sensitivity is increased to 83 and 34 for CNF and NFC composites respectively. Very high response at high NH_3 concentration indicate that the availability of maximum number of active sites on the sensing material. As the concentration of PANI in the composites increases the number of reactive sites for NH_3 molecules also increases [18]. Moreover, for high wt.% composites the CNF concentration is also high and this will increase the pore sites for the absorption of ammonia molecules, thereby increasing the sensitivity of the composites.

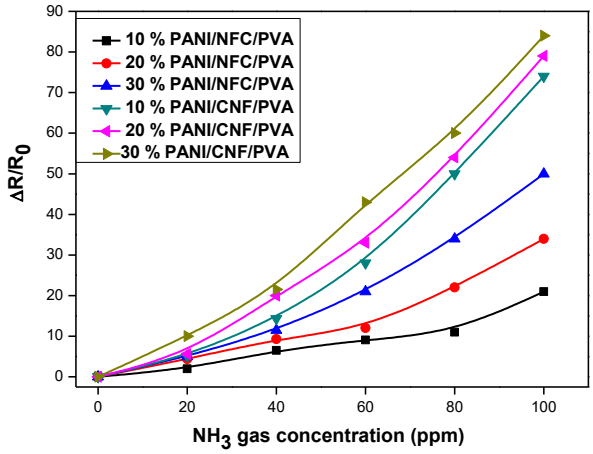

Figure 7.B.3: Variation of sensitivity of the composites with 0-100 ppm NH_3 gas concentration

It shows that PANI/CNF/PVA composites exhibits higher sensitivity to ammonia. This may be due to the fact that the hydrogen ion availability around nitrogen atom is more in PANI/CNF/PVA composites. Polyaniline bonds with nano-fibrillated cellulose is stronger than with CNF. In PANI/NFC/PVA composites the surface hydroxyl groups of cellulose provide more binding sites for polyaniline and a conduction path is formed. Consequently, it results in less number of hydrogen atoms available for interacting with NH_3 molecules. As a result, resistance of the material changes only marginally. Whereas in PANI/CNF/PVA composites, NH_3 molecules react with hydrogen ions of polyaniline to form NH_4^+ ions.

The doping of polyaniline results in the formation positively charged localized centers around the nitrogen atoms. The doping and the number of sites can be controlled by the doping agents. When polyaniline is exposed to the ammonia gas, the NH_3 molecules takes up the protons of NH groups of polyanilines, there by forming neutral polyaniline and NH_4^+ ions. Polyaniline in its base form is non-conducting, so when polyaniline is exposed to NH_3 the resistance of the composite increases. When NH_3 atmosphere is removed the NH_4^+ ion decomposes giving NH_3 molecule and hydrogen. The protonation-deprotonation reaction of polyaniline is reversible (figure 7.B.4).

The sensing properties of a material is highly dependent on the porosity of the material. In contrast to NFC, CNF possesses a porous structure. As a result, it is easy for gas molecules to diffuse from all the directions. This has significant influence on the sensing properties of the

composites. PANI/CNF/PVA composites exhibit high sensitivity than PANI/NFC/PVA composites. The sensitivities of the tested devices are 84 and 50 for PANI/CNF/PVA and PANI/NFC/PVA composites respectively.

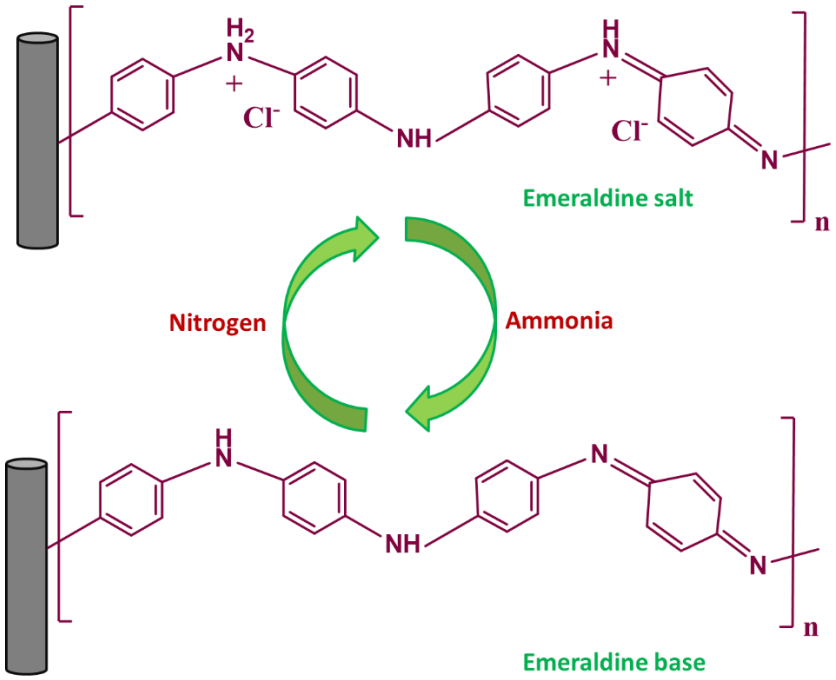

Figure 7.B.4: NH_3 gas detection mechanism of PANI/CNF composites

The reproducibility study of the sensor reveals that the composite maintained the initial resistance value with short response as well as recovery times. The figure 7.B.5 represents the response of the composites as the sensors are alternatively exposed to NH_3 and N_2 gases at 60 ppm. Both sensors recovered their initial resistance after the removal of NH_3 atmosphere, with only very minimal baseline shift. It suggests that both composites exhibit almost complete desorption of NH_3 molecules from the composites.

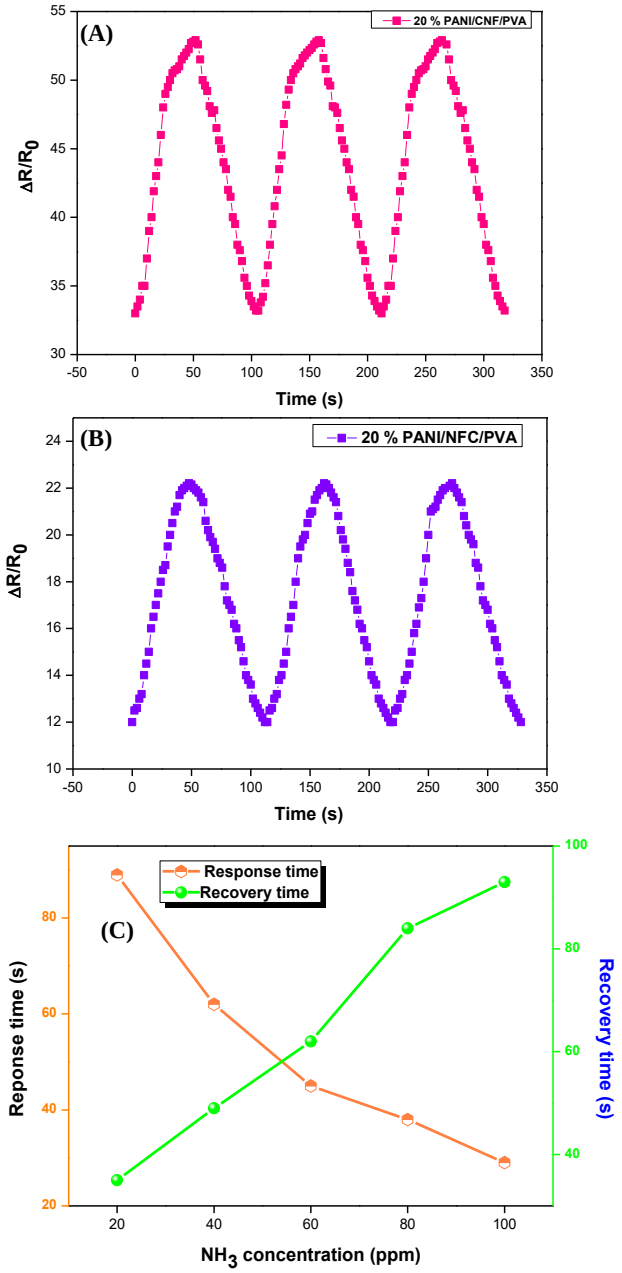

Figure 7.B.5: Reproducibility curves of A) PANI/CNF/PVA, B) PANI/NFC/PVA, C) response and recovery variation with NH_3 gas concentration

Short response time (46 s) and recovery time (62 s) are noted at 60 ppm of NH_3 gas concentration for PANI/CNF/PVA composites. A slight increase of response and recovery time is observed for PANI/NFC/PVA composites at the same NH_3 level. But at lower NH_3 concentrations of 20 ppm both composites take more time to respond (89 s) while the recovery time is reduced to 35 s. As NH_3 concentration increases both composites show lower response times and higher recovery times. At higher NH_3 concentration, the active sites of polyaniline are completely occupied with the NH_3 molecules, i.e. large number of H^+ ions are removed from the nitrogen atom of PANI. So, by the removal of NH_3 atmosphere, the composite is taking much time to restore their original energy level. So, from the response-recovery observation, it is clear that the response time increases with NH_3 gas concentration whereas the recovery time decreases. Complete recovery of the sensing material to its baseline value and the short response and recovery times make this composite a good sensor material.

7.B.4 Conclusion

PANI/CNF/PVA and PANI/NFC/PVA composites were prepared by ultrasonication-assisted mixing of PANI coated CNF/NFC fibers with poly(vinyl alcohol) solution. The composites performance as ammonia gas sensor was investigated at room temperature. The results revealed that the synergic effect of PANI/CNF and PVA led to high selectivity and fast response towards ammonia. When polyaniline is exposed to ammonia gas, protonation/deprotonation reactions cause the changes in the electrical resistance of the material. This was made use in the sensing of

ammonia gas. The influence of nanofibers on the sensing property was investigated. The response and recovery times, sensitivity and the stability of the sensing films were evaluated for both composites. Compared to PANI/NFC/PVA composite PANI/CNF/PVA composite exhibited higher sensitivity, faster response and recovery times and better stability towards ammonia gas sensing. This improvement in the sensing performance of CNF composite was attributed to the higher pores size and the interaction between PANI/CNF and PVA molecules. Thus, the prepared PANI/CNF/PVA composite offers great practical application as excellent ammonia sensor.

References

[1] G. Martinelli, M. C. Carotta, M. Ferroni, Y. Sadaoka, E. Traversa, Sens. Actuators B, 1999, 55, 99

[2] K. Arshak, V. Velusamy, O. Korostynska, K. Oliwa-Stasiak, C. Adley, IEEE Sens. J., 2009, 9, 1942

[3] J. Y. Lee, C. A. Bashur, A. S. Goldstein, C. E. Schmidt, Biomaterials, 2009, 30, 4325

[4] A. D. Wilson, Sensors, 2013,13, 2295

[5] S. Bhattacharya, S. Sridevi, R. Pitchiah, In Proceedings of the 2012 Sixth International Conference on Sensing Technology (ICST), Kolkata, India,18–21 December 2012, 422

[6] R. K. Yedavalli, R. K. Belapurkar, J. Control. Theory Appl., 2011, 9, 28

[7] C. Sanchez, P. Belleville, M. Popall, L. Nicole, Chem. Soc. Rev., 2011, 40, 696

[8] C. R. Young, N. Menegazzo, A. E. Riley, C. H. Brons, F. P. DiSanzo, J. L. Givens, J. L. Martin, [9] M. M. Disko, B. Mizaikoff, Anal. Chem., 2011, 83, 6141

[9] K. Arshak, E. Moore, G. Lyons, J. Harris, S. Clifford, Sens. Rev., 2004, 24, 181–198.

[10] B. Adhikari, S. Majumdar, Prog. Polym. Sci., 2004, 29, 699

[11] Z. Chen, C. Lu, Sensor Lett., 2005, 3, 274

[12] A. Oprea, N. Barsan, U. Weimar, M. L. Bauersfeld, D. Ebling, J. Wöllenstein, Sensors and Actuators B, 2008, 132, 404

[13] H. J. Sharma, D. V. Jamkar, S. B. Kondawar, Proc. Mater. Sci., 2015, 10, 186

[14] C. Steffens, M. L. Corazza, E. Franceschi, F. Castilhos, P. S. Herrmann, J. V. Oliveira, Sensors and Actuators B: Chemical, 2012, 171, 627

[15] H. Xu, D. Ju, W. Li, H. Gong, J. Zhang, J. Wang, B. Cao, Sens. Actuators B, 2016, 224, 654

[16] N. Elfström, R. Juhasz, I. Sychugov, T. Engfeldt, A. E. Karlström, J. Linnros, Nano Lett., 2007, 7, 2608

[17] A. Mekki, N. Joshi, A. Singh, Z. Salmi, P. Jha, P. Decorse, S. Lau-Truong, R. Mahmoud, M. M. Chehimi, D. K. Aswal, S.K. Gupta, Org. Elec., 2014, 15, 71

Part C

Thin film capacitor with PANI/CNF/PVA as dielectric layer

High K, Metal-Insulator-Metal (MIM) capacitor was fabricated using polymer thin film. The insulating material possessing high dielectric constant and low leakage current was developed using polyaniline, carbon nanofiber and poly(vinyl alcohol). The capacitance and dissipation factor were measured over a frequency range of 100 Hz to 20 MHz. At 100 Hz the thin film capacitor exhibited a capacitance of about 89.9 mF. Excellent charge storage was observed at lower frequency range with moderate dissipation factor. Embedded capacitor prototype using PANI/CNF/PVA composite achieved a capacitance density of about 89.9 mF/cm^2. Circuit application of the fabricated capacitor was also evaluated by measuring the charging and discharging times. This embedded capacitor technique improved the performance and reduced the cost of fabrication of traditional discrete capacitor technology.

7.C.1 Introduction

In recent years the introduction of high dielectric constant materials has boosted the development of high charge storage capacitors, gate dielectrics, electroactive materials etc. [1-3]. The materials possessing high dielectric constant and low dielectric loss are used as the insulating material in the parallel plate capacitors [4,5]. Variety of materials have been evaluated for the use in embedded capacitor applications.

Earlier, ferroelectric materials possessing permanent dipole moment and high dielectric constant were used for the fabrication of capacitors.

But these materials required very high processing temperatures of more than 600 ^{o}C which limited its wide use in high charge storage applications. Owing to the mild processing requirements polymeric materials are good alternatives. Nevertheless, the low dielectric constant of polymeric materials is a drawback. One of the ways to improve the dielectric properties of the polymeric materials is to couple it with high K materials.

Efforts have been made to prepare polymer composites that will meet the requirements of high charge storage capacitor [6-14]. Incorporation of nanomaterials as fillers is one of the preferred methods owing to the higher dielectric constant. Moreover, the nanocomposites possess good processability and better mechanical properties in addition to its excellent electrical, magnetic and dielectric properties. Due to the interfacial polarization in insulator-conductor systems ultra-high dielectric constant values can be obtained. Sometimes the effective dielectric constant of the metal-insulator composite could be three or four orders higher than that of the insulating polymer matrix.

Combination of conducting polymers with carbonaceous materials have developed as effective combination for the fabrication of efficient charge storage capacitors [15-22]. Though there are numerous reports on the high charge storing capacitors based on metal oxides and conducting polymers. The combination of the conducting polymer, carbon nanofiber and insulating polymer matrix is not much explored. In this chapter the fabrication of thin film capacitor with high dielectric constant and low dissipation factor using PANI/CNF/PVA as dielectric layer is discussed. Circuit application of the fabricated capacitor were also evaluated.

7.C.2 Theoretical background

Capacitance (C) is a measure of how much electric charge can be stored in a capacitor. The relationship between capacitance C and dielectric constant ε_r (k) is given by the following equation:

$$C = \frac{\varepsilon_0 \varepsilon_r A}{t} \quad \text{.....7.C.1}$$

where ε_0 is the dielectric constant of the vacuum, A is the area of the material, t is the thickness of the dielectric layer, and ε_r is the dielectric constant of the dielectric material. It is evident that the larger the dielectric constant, the larger the capacitance which can be realized in a given space. Therefore, materials of high dielectric constant are more favourable in practical use of embedded capacitors for miniaturization.

Due to the planar nature and the area dependency of the materials, the capacitance of the material can be described as the specific capacitance.

7.C.3 Experimental

7.C.3.1 Fabrication of capacitor

A detailed description of the methods employed for the preparation PANI/CNF/PVA composite is given in chapter 4B.

7.C.3.1.1 Thermal deposition of electrode

The glass substrate was cleaned chemically and was ultrasonicated for half an hour. After cleaning, the substrate was dried in air oven. Silver was used as electrode. It was coated on the glass plate which served as the bottom electrode. The metal was coated on the glass plate by vacuum deposition method to a thickness of about 0.05 mm. The vacuum

deposition technique was used at a vacuum level of 10-6 torr by thermal evaporation process. Silver was used for the deposition of the top electrode also. The electrode was deposited on the surface of the dielectric layer.

7.C.3.1.2 Deposition of dielectric material

The composite material was coated on the electrode by drop casting technique. The dielectric material was drop-casted by means of a micropipette and uniform thickness was assured by placing the glass electrode in an equilibrated surface. The thickness of the dielectric layer was determined by measuring the thickness of the glass plate before and after drop casting. The schematic representation of the process of the fabrication of the parallel plate metal-insulator-metal capacitor is shown in the figure 7.C.1.

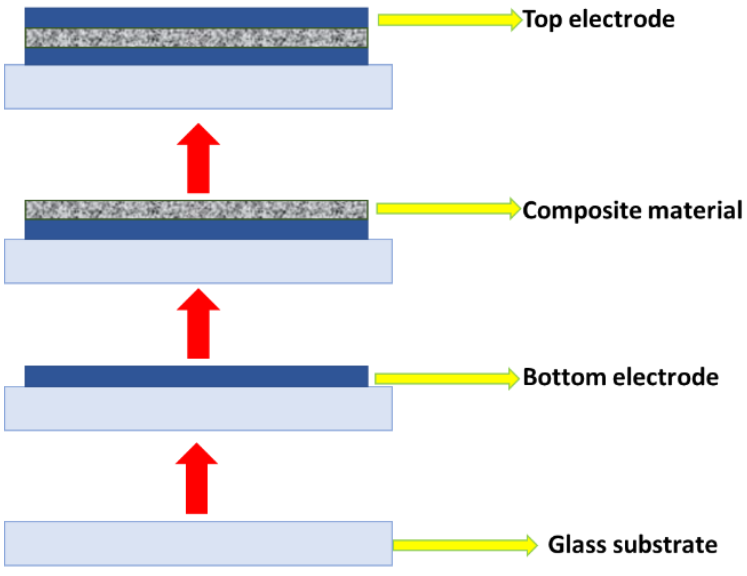

Figure 7.C.1: Fabrication of the MIM parallel plate capacitor

7.C.4 Results and discussion

7.C.4.1 Dielectric measurement of the capacitor

The capacitance and dissipation factor were measured by Wayne Kerr 6500 Impedance analyzer over a frequency range of 100 Hz to 20 MHz. The measurements were conducted at room temperature. Low frequency range was selected owing to the fact of Coulomb Blockade effect and interfacial polarization effect occurring in polymer nanocomposites. Moreover, the interfacial loss appears to be more in the high frequency region than the lower range [23].

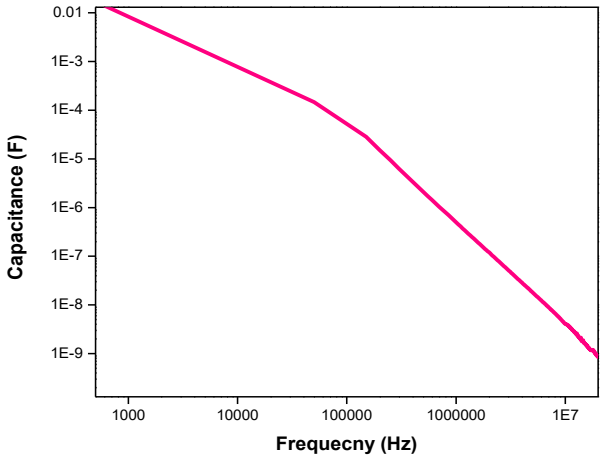

Figure 7.C.2: Variation of capacitance with the frequency

The capacitance variation of composite film with the alteration of frequency is given in the figure 7.C.2. At lower frequencies high capacitance is obtained. Excellent charge storage is observed at low frequency range. As the frequency increases the capacitance decreases. A capacitance of 89.9 mF is obtained at a frequency of 1000 Hz. This high value of capacitance strongly suggests use in high charge storage

applications. But the value reduces to about 1.3 nF when the frequency reaches 20 MHz. A capacitance density of 89.9 mF/cm^2 is achieved owing to the piling of charges at the interfaces of the composite. Due to the conductivity difference of PANI/CNF and PVA matrix interfacial polarization occurs. As a result, charges will be accumulated at the interface which in turn leads to the high dielectric constant.

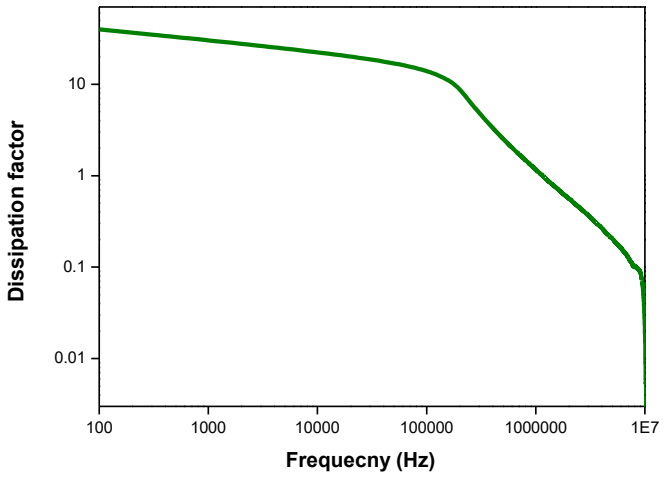

Figure 7.C.3: Dissipation factor of PANI/CNF/PVA composite with frequency

Table 7.C.1: Summarizing the capacitance, dissipation factor and capacitance density at different frequencies.

Frequency	Capacitance	Dissipation factor	Capacitance Density (mF/cm^2)
100 Hz	89.9 mF	38.7	89.9
50000 Hz	0.1 mF	18.7	0.1
500000 Hz	2.1 µF	2.5	0.0002
10 MHz	.049 µF	1.16	4.9*10^{-5}

Variation of dissipation factor with frequency is represented in figure 7.C.3. Dissipation factor is also following the same trend as capacitance variation. At lower frequencies, the composite exhibit very high dissipation factor which reduces when the frequency is increased. The high charge-storing efficiency also increases the dissipation factor. This means in higher storage conditions the composites dissipate more charge as heat. Generally, dissipation factor of a material depends on the distortional, interfacial, dipolar and conduction loss. Distortional loss is originated from the electronic and ionic polarization mechanism. The movement of atoms or rotation of filler particles cause the polarized interfaces in the composite. Interfacial loss occurs due to the movement or rotation of the molecules at the interface. Conduction loss is related to the DC conductivity of the composite. So the dissipation factor increases with the charge storing capacity of the capacitor.

7.C.4.2 Circuit application of the device

A capacitor can store charge due to the electrostatic attraction between the positive and negative charges. At some point the capacitor plates will be charged completely beyond which the charges cannot be added more. It represents the capacitance of the capacitor.

The circuit application of the fabricated capacitor was studied by designing a simple circuit using capacitor, resistor, switch and DC voltage source. In this circuit the battery is used to induce the electric potential across the capacitor. It causes equal and opposite charges to build on the plates of the capacitor. When the capacitor is not connected to battery there will not be any potential difference across the plates. That means the

capacitor is in the balanced condition. The capacitor was charged by closing the circuit. 9 V DC voltage source and 10 K resistor was used. So, the current will be of 0.9 A. At the beginning the voltage (Vc) across the capacitor will be zero and the current (Ic) will be maximum. As soon as the capacitor starts charging the voltage across the capacitor increases and the current reduces slowly. So, the capacitor is charged fully. The addition of the resistor in the circuit in series with the capacitor will not affect the potential difference across it, whereas it influences the charging time of the capacitor. After that the circuit is opened and the time taken for discharge was measured. Due to the internal leakage resistance the capacitor discharges slowly. The discharge current is maximum at the beginning of the discharge process and it reduces slowly until the charge becomes zero.

At any instance of charging process,

$$V = Vr + Vc \quad \text{.....7.C.2}$$
$$V = IcR + Vc \quad \text{.....7.C.3}$$

Where Vc is the potential difference across the capacitor, Ic is the charging current

The total voltage is the sum of the voltage drop across the resistor R and the voltage between the plates of the capacitor.

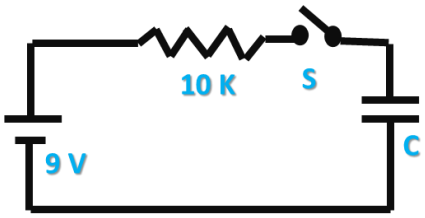

Figure 7.C.4: Circuit consisting of 9 V battery, 10 K resistor, switch and the fabricated capacitor

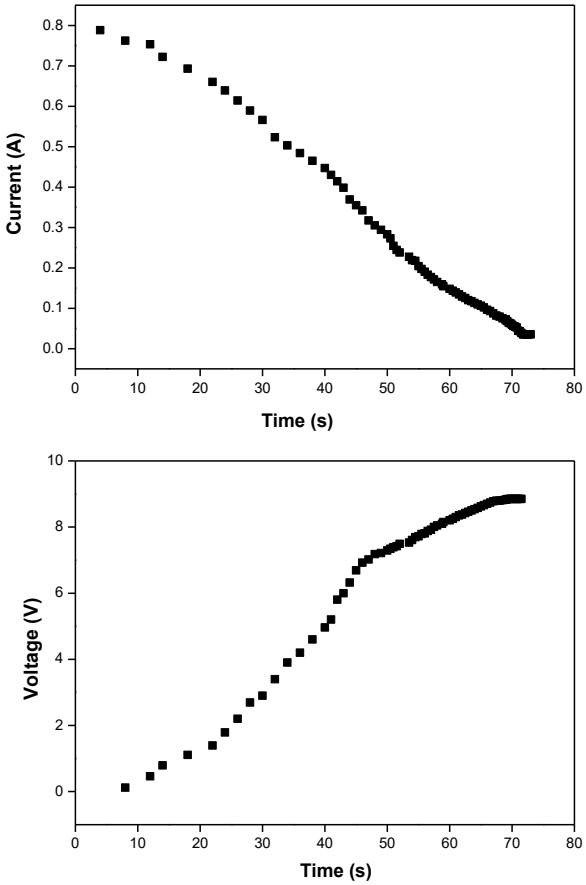

Figure 7.C.5: Variation of current and voltage with time

The variation of current and voltage with time during charging is plotted in the figure 7.C.5. When the capacitor is charged by closing the switch, the voltage across is the capacitor is zero and the current is maximum. The current reduces from 0.8 A to about 0.04 A within a time period of about 79 s. At the beginning the increase of voltage is very fast and reaches a constant value of about 8.6 V. The rate of increase is fast during the initial stages of the charging, then the rate decreases with time to a constant value.

The discharge time of the capacitor is measured when the circuit is open. The discharge time of the devise is about 93 s. During the discharging process the rate of decrease is more at the beginning and slows down as the time proceeds. It is evident from the figure 7.C.5 that the capacitor never fully charges or discharges

7.C.5 Conclusion

Metal insulator metal capacitor was fabricated using polymer composite material. This prototype achieved high capacitance with low dissipation factor. The variation of capacitance with frequency was studied for a range of frequency 100 Hz to 20 MHz. At low frequency the composite exhibited highest capacitance of about 89.9 mF with a dissipation factor of 38.7. Embedded capacitor prototype using PANI/CNF/PVA composite achieved a capacitance density of about 89.9 mF/cm^2. Both the capacitance and dissipation factor were reduced with the increase of frequency. The circuit applications of the developed capacitor were analyzed. The charging and discharging time of the developed capacitor was about 79 s and 93 s. Hence the developed composite material can be a good alternative choice for the development of embedded capacitors.

References

[1] A. Facchetti, M. H. Yoon, T. J. Marks, Adv. Mater., 2005, 17, 1705

[2] Q. M. Zhang, H. F. Li, M. Poh, F. Xia, Z. Y. Cheng, H. S. Xu, Nature, 2002, 419, 284

[3] Y. Bai, Z. Y. Cheng, V. Bharti, H. S. Xu, Q. M. Zhang, Appl. Phys. Lett., 2000, 76, 3804

[4] J. Prymark, S. Bhattacharya, K. Paik, R. R. Tummala, McGraw-Hill: New York, 2001

[5] R. K. Ulrich, L. W. Schaper, Integrated Passive Component Technology, IEEE Press, Wiley-Interscienc, 2003

[6] M. F. Frechette, M. L. Trudeau, H. D. Alamdari, S. Boily, IEEE Transactions on Dielectrics and Electrical Insulation, 2004, 11, 808

[7] Y. Yan, Q. Cheng, G. Wang, C. J. Li, Power Sources, 2011, 196, 7835

[8] J. Zhu, H. Gu, Z. Luo, N. Haldolaarachige, D. P. Young, S. Wei, Z. Guo, Langmuir, 2012, 28, 10246

[9] X. Yan, J. Chen, J. Yang, Q. Xue, P. Miele, ACS Appl. Mater. Interfaces, 2010, 2, 2521

[10] J. J. Xu, K. Wang, S. Z. Zu, B. H. Han, Z. X. Wei, ACS Nano, 2010, 4, 5019

[11] M. Ertas, R. M. Walczak, R. K. Das, A. G. Rinzler, J. R. Reynolds, Chem. Mater., 2012, 24, 433

[12] D. W. Wang, F. Li, J. P. Zhao, W. C. Ren, Z. G. Chen, J. Tan, Z. S. Wu, I. Gentle, G. Q. Lu, H. M. Cheng, ACS Nano, 2009, 3, 1745

[13] J. Lu, K. S. Moon, B.-K. Kim, C. P. Wong, Polymer, 2007, 48, 1510

[14] W. Fan, C. Zhang, W. W. Tjiu, K. P. Pramoda, C. He, T. Liu, ACS Appl. Mater. Interfaces, 2013, 5, 3382

[15] G. A. Snook, P. Kao, A. S. Best, J. Power Sources, 2011, 196, 1

[16] C.-M. Hung, Y.-C. Ho, I.-C. Wu, K. O, IEEEMTT-S Int. Microw. Symp. Dig., 1998, 505

[17] J. A. Babcock, S. G. Balster, A. Pinto, C. Dirnecker P. Steinmann, R. Jumpertz, B. El-Kareh, IEEE Electron Device Lett., 2001, 22, 230

[18] C. H. Ng, K. W. Chew, S. F. Chu, IEEE Electron Device Lett., 2003, 24, 506

[19] T. Ishikawa, D. Kodama, Y. Matsui, M. Hiratani, T. Furusawa, D. Hisamoto, IEDM Tech. Dig. ,2002, 940

[20] S. B. Chen, C. H. Lai, A. Chin, J. C. Hsieh, J. Liu, IEEE Electron Device Lett., 2002, 23, 185

[21] S. B. Chen, C. H. Lai, K. T. Chan, A. Chin, J. C. Hsieh, J. Liu, IEEE Electron Device Lett., 2002, 23, 203

[22] K. Zhang, L. L. Zhang, X. S. Zhao, J. Wu, Chem. Mater., 2010, 22, 1392.

[23] L. Jiongxin, K.-S. Moon, J. Xu, C. P. Wong, J. Mater. Chem., 2006, 16, 1543

…..ஜ۞ஜ…..

Chapter 8

SUMMARY AND CONCLUSIONS

Intrinsically conducting polymers find various applications in the field of electronics, electromechanical devices, electroluminescence and sensors. Novel devices based on conducting polymer composites possessing low percolation threshold, high conductivity, good dielectric properties and improved mechanical properties have been fabricated. The performance of the conducting polymer is improved by the modification with carbonaceous materials. Polyaniline/Carbon nanofiber composites facilitate the formation of extended charge transfer bands by introducing more conductive paths. PANI/CNF composites are prepared by the appropriate stoichiometric combination. Our strategy was to develop conducting polymer composites based on conducting fibers and non-conducting fibers. PANI/CNF and PANI/Cellulose composites were prepared by the in-situ polymerization of aniline in presence of carbon nanofibers and cellulose fibers separately.

The effect of dopant on the properties of PANI/CNF composite was studied using five different acid dopants. The dopants used were hydrochloric acid, sulfuric acid, phosphoric acid, camphor sulfonic acid

and toluene sulfonic acid. The electrical, dielectric and thermal properties were studied. High electrical conductivities and dielectric constant were observed for all PANI/CNF composites compared to pure PANI. However better conductivity and thermal stability of DC conductivity were observed for organic toluene sulfonic acid dopant, due to the better electron transfer in the system. Hydrochloric acid doped composites yielded good dielectric constant with lower loss tangent. Owing to the low cost and ease of processing HCl was selected as dopant for further studies.

Novel PANI/Cellulose/PVA composites were successfully fabricated by solution cast method. Cellulose was isolated from coir fibers by the repeated chemical and mechanical treatments. The isolated cellulose was refined in to three different sizes: macro, micro and nano sizes by employing appropriate processing techniques. The isolated fibers were characterized by different techniques all of which confirmed uniform fibrillation and the size distribution in the successive ranges. Three series of PANI/Cellulose/PVA composites containing fibers in three size ranges, i.e. macro, micro and nano were studied. The electrical, mechanical and dielectric characteristics were investigated. Compared to short cellulose fiber composite, nanocomposites exhibited higher dielectric permittivity together with lower loss factor in frequency range of 40 Hz to 30 MHz. PVA nanocomposite attained an AC conductivity of 3 S/m. For all the three composites, the real and imaginary electric moduli increased with conductivity. The addition of PANI coated cellulose fiber improved the tensile strength and storage modulus for micro and nanocomposites. But due to the poor compatibility of macro fiber the mechanical properties were decreased. TGA studies showed that the

thermal stability of all the composites increased with the addition of fibers. The addition of micro and nano cellulose fibers in to PVA molecules reduced the percentage of water absorption while it increased for the macro fibers.

Poly(vinyl alcohol) based conducting polymer composites were prepared using carbon nanofiber and poly(vinyl alcohol). PANI/CNF/PVA composite was prepared by the solution casting method. Compared to cellulose based composites, PANI/CNF/PVA composites exhibited improved electrical and mechanical properties. An electrical conductivity of 0.39 S/cm was achieved by 50 % PANI/CNF/PVA composite which is about times 10^{12} higher than that of pure PVA. Higher dielectric permittivity together with lower loss factor was achieved for CNF based nanocomposites in frequency range of 40 Hz to 30 MHz. The addition of PANI coated carbon nanofiber improved the tensile strength and storage modulus of the nanocomposites. But due to the poor compatibility at higher concentration the mechanical properties were decreased. Moreover, the addition of PANI/CNF into PVA matrix resulted in marked improvement in the thermal stability of poly(vinyl alcohol). The addition of PANI/CNF in to PVA molecules reduced the percentage of water absorption unlike PANI/Cellulose/PVA composite.

Cost effective, high performance dielectric composites based on poly(methyl methacrylate), cellulose fibers and polyaniline were prepared. The electrical, dielectric and mechanical properties were studied as a function of fiber content, fiber dimensions and polyaniline content. Among three different sizes of cellulose fibres excellent electric and

dielectric properties were obtained for nanocomposites with low percolation threshold. It can be due to the effective conductive network formed in case of nanocomposite. The composite exhibited almost similar properties as that of PANI/Cellulose/PVA composite. But, significant improvement in the properties was observed for PVA based composites than that of PMMA composites. Characterization of the composites suggest that this improvement is due to the extensive hydrogen bonding present in PVA composites. The properties of the composite were related to the even distribution of the fibrous fillers in the polymer matrix.

Polyaniline coated carbon nanofibers were incorporated into the PMMA matrix, yielded PANI/CNF/PMMA composite. Unlike PANI/CNF/ PVA composites hydrogen bonding interactions are absent in PMMA composites. Hence the property improvement is not up to that of PVA composites. The composite exhibited a dielectric constant of $1.4*10^8$at 40 Hz. In contrast to PANI/Cellulose/PMMA composites, higher dielectric permittivity together with lower loss factor was achieved for CNF based nanocomposites in frequency range of 40 Hz to 30 MHz. Mechanical properties of the composite were enhanced by the incorporation of polyaniline modified carbon nanofibers.

The relatively inferior properties of PMMA/Cellulose composite were thought to be due to the weak interaction between the hydrophilic cellulose and the hydrophobic PMMA. The compatibility of cellulose and PMMA was improved by the addition of Bis–(3-triethoxysilylpropyl)tetrasulphide (Si69). The composites were characterized and found that the interactions in PMMA/Cellulose/Si69 composite were mainly chemical in nature. The

presence of Si69 in the composite marginally increased the Tg of PMMA. The results proved that Si69 could be used for reinforcing PMMA/cellulose system very effectively. The Si69 remarkably improved the tensile strength, impact strength and flexural strength. The storage modulus of silane-coupled composites was much greater than that of pure PMMA. SEM images revealed well dispersion of cellulose in PMMA matrix in presence of Si69. This was in good agreement with the improved strength of the composite. But for higher filler weight percentage composites the properties were decreased due to the agglomeration of microcrystalline cellulose. The incorporation of cellulose into PMMA matrix increased the dielectric properties. The AC conductivity was reached a value of $1.4*10^{-4}$ S/m. In short, PMMA/Cellulose/Si69 composite can be used as high strength material with improved thermal properties, tensile strength, high impact energy and high storage modulus.

Excellent dielectric properties and electrical conductivity of the composites led to the exploration of EMI shielding property of the composites. The advancement in the communication technology leads increased radiation pollution. Consequently, there is a pressing need to protect the environment as well as the sensitive circuits from microwave radiations. The effect of conductivity of the two nanofibers on the EMI shielding was studied. Microwave characterizations of the composites were done in terms of permittivity, loss tangent, skin depth and absorption coefficient. High permittivity, absorption coefficient and low skin depth were obtained for carbon nanofiber based composites owing to its good electrical conductivity. The shielding effectiveness of two composites were measured in the 2-4 GHz (S-band) and 8-12 GHz (X-band) frequency range. Abrupt

increase of SE with increasing fiber concentration was observed for CNF based composite. An electromagnetic shielding effectiveness of about -31.5 dB in the S band region and of -32.2 dB in the X band was achieved at 0.12 mm thickness. The SE due to reflection and absorption were increased with increase of PANI/CNF content though the increase of SE_A was higher than SE_R. Additionally, CNF based composite film exhibited very low density of 0.21 g/cm^3. Higher permittivity with good EMI shielding efficiency was obtained for CNF composites compared to NFC based composites. It is due to the high conductivity of carbon nanofibers. Beside good electrical conductivity, high surface area of carbon nanofiber made PANI/CNF/PVA composite efficient for EMI shielding. The results clearly indicate how the conductivity of the filler is able to significantly affect the electromagnetic properties at the microwave frequencies. Compared to metals and other carbonaceous materials, this composite film resulted high specific EMI efficiency of -153.3 dB cm^3/g. Highly flexible polymer composite film with excellent absorption dominated electromagnetic interference shielding could serve as a promising EMI shielding material.

The redox properties of polyaniline have opened upnew avenues in biological field such as immobilization platform for tissue growth, biosensors, controlled drug delivery systems and neural probes etc. The hydrophilicity, molecular weight and the electrostatic attraction between PANI and bacteria have significant effects on antibacterial activity of polyaniline. The dopant molecule is one of the key factors that affects these properties. In view of growing importance to antibacterial drugs the effect of dopant on the antibacterial properties of PANI/CNF/PMMA nanocomposite

was studied. The antibacterial activity of the composites against *Escherichia coli*, *Klebsiella pneumoniae* and *Bacillus subtilis* was evaluated by agar well diffusion method. The activity was assessed by measuring the inhibition zone diameter and minimum inhibitory concentration. The composites showed variable toxicity indicating the dependence on doping agents. Positive zeta potential value of +39.60 mV obtained for H_3PO_4-PANI/CNF composites proved to be detrimental to bacteria. The highest antibacterial activity was observed for phosphoric acid doped composite. This was attributed to the high surface area, smallest size apart from the high positive zeta potential. The results revealed that the antimicrobial activity of polyaniline composites is tunable.

The flame retardant properties of polyaniline coated carbon nanofibers in PVA and PMMA matrices were studied. Large amounts of hydroxyl groups available in PVA make it a self-charring material and the charring can be improved further by proper compounding. Therefore, LOI values of PANI/CNF/PVA and PANI/CNF/PMMA nanocomposites were evaluated for investigating their flame retardant property. Both composites exhibited higher LOI values than pure polymers and increased with increasing PANI/CNF content. The flame retardant efficiency of PVA composite was significantly higher than that of PMMA composite. By the heat treatment PANI/CNF/PVA composite undergoes dehydrogenation and cyclization reaction resulting in the formation of polyconjugated ladder structures. This contributed to low flammability and high thermal stability of PVA composites.

Number of studies have indicated that poly(vinyl alcohol) is sensitive to moisture and can interact with water molecules through hydrogen bonding. Humidity sensing has become essential for weather prediction, historic preservation, environmental studies, mobile electronics etc. Sensor based on PVA composite was fabricated. The response of the sensor was evaluated from the change in capacitance with varying humidity levels. The analysis revealed that the sensors had a short response time (41 s) and good shelf life. The AC capacitance of the sensor film was measured over a relative humidity (RH) range of 30 % to 100 %. Compared to PANI/NFC/PVA composite, PANI/CNF/PVA composite exhibited higher sensitivity, shorter response time (41 s) and better recovery (46 s). The change of sensitivity for CNF based composite was from 290 to 6570 % at 100 Hz frequency.

At the same time, it is also crucial to detect and measure the accurate amount of the toxic pollutant gase like ammonia. The challenge was to develop humidity and gas sensor using the same material with good sensitivity, stability and response. When polyaniline is exposed to ammonia gas, protonation/deprotonation reactions take place resulting in changes in the electrical resistance.The difference in the sensing performance was studied by the incorporation of carbon nanofiber and nanofibrillated cellulose (NFC). The addition of CNF resulted better sensing properties. The response of the films to ammonia was investigated over a range of 0-100 ppm at room temperature. The observed sensitivity of the film was varied from 10 to 84. PANI/CNF/PVA composite was found to have much better response time (46 s) and sensitivity for ammonia sensing. This improvement in the sensing performance of CNF composite was attributed to the higher pores size and

the enhanced hydrogen bonding interaction with water molecules. Thus, the prepared PANI/CNF/PVA composite offers great practical application as excellent ammonia and humidity sensor.

The materials with high dielectric constant opened up many applications in the area of high charge storage capacitors, gate dielectrics, electroactive materials etc. Metal Insulator Metal (MIM) capacitor was fabricated using PANI/CNF/PVA composite. This prototype achieved high capacitance with low dissipation factor. The variation of capacitance with frequency was studied for a range of frequency 100 Hz to 20 MHz. At low frequency the composite exhibited highest capacitance of about 89.9 mF with a dissipation factor of 38.7. Embedded capacitor prototype using PANI/CNF/PVA composite achieved a capacitance density of about 89.9 mF/cm^2. Both the capacitance and dissipation factor were reduced with the increase of frequency. The circuit applications of the developed capacitor were analysed. The charging and discharging time of the developed capacitor was about 79 s and 93 s respectively.

Four different types of composites were developed based on PVA and PMMA thermoplastic polymers. Among them significant improvement in the mechanical, electrical and dielectric properties were obtained for PANI/CNF/PVA composite. Moreover, it could be used for flame retardant applications, exhibited excellent EMI shielding effectiveness. It could also be used for humidity and ammonia sensing. This composite has been found to be more efficient as a sensor in contrast to other polymeric composites as it can monitor both humidity and ammonia at room temperature.

Future Scope of the work

There are several lines of research arising from this work which should be pursued. Future work concerns

- The deeper analysis of the flame retardant mechanism of the PANI/CNF/PVA composite.
- Study the effect of thickness of the composite film on the EMI shielding efficiency.
- The use of PMMA based composites as dielectric material in the fabrication of capacitor.

…..ஜ۞ஜ…..

List of Publications

[1] Impact of Bis-(3-triethoxysilylpropyl)tetrasulphide on the properties of PMMA/Cellulose composite. V.P. Anju, Sunil K. Narayanankutty, *Polymer*, 119 (**2017**) 224-237.

[2] Polyaniline coated cellulose fiber / polyvinyl alcohol composites with high dielectric permittivity and low percolation threshold V.P. Anju, Sunil K. Narayanankutty, *AIP Advances*, **6**, (**2016**) 015109.

[3] Effect of Dopants on the Antimicrobial activity of PANI/CNF/PMMA Composites, V.P. Anju, Sunil K. Narayanankutty (communicated)

[4] Novel Humidity and Ammonia Sensor Based on Nanofibers/ Polyaniline/Polyvinyl alcohol composite. V.P. Anju, P.R. Jithesh, Sunil K. Narayanankutty (communicated)

[5] Development of flexible Carbon Nanofiber and Nanofibrillated cellulose Based Composite sheet as Excellent Electromagnetic Shielding Material, V.P. Anju, Sunil K. Narayanankutty (communicated)

Conferences Attended and Paper Presented

[1] Humidity and Ammonia Sensor Based on Nanofibers/Polyaniline/ Polyvinyl alcohol, V.P. Anju and Sunil K. Narayanankutty, Emerging Trends in Nanocomposites, KSCS, October, 2017, Kerala, India

[2] Synthesis, Characterization and Properties of PVA/PANI/Cellulose fiber Conductive Composites. V.P. Anju and Sunil K. Narayanankutty, 4th *ISCA*, December, **2014,** Pacific University, Udaipur, Rajasthan, India.

[3] Synthesis, Characterization and Properties of PVA/PANI/Cellulose fiber Conductive Composites. V.P. Anju and Sunil K. Narayanankutty, December, 2014, KKTM College, Kerala.

[4] Synthesis and conductivity studies of Poly vinyl alcohol/Poly Aniline/Cellulose Fiber. V.P. Anju and Sunil K. Narayanankutty, *SSC*, November, 2016, Kerala, India.

[5] The effect of Bis –(3-triethoxysilylpropyl)tetrasulphide as a coupling agent on the properties of PMMA/Cellulose composite. V.P. Anju and Sunil K. Narayanankutty, *NTAC*, November, 2016, Kerala, India.

.....ꕥ.....

Curriculum Vitae

Anju V P

Department of Polymer Science & Rubber Technology
Cochin University of Science and Technology
Kerala, India

Email: *anjuvp09@gmail.com*
Tel: +91-9847660211

Education

- **M. Sc. in Chemistry** [2010-2012], Calicut University, Kerala
- **B. Sc. in Chemistry** [2007-2010], Calicut University, Kerala
- **Ancillaries:** Mathematics and Physics.

List of Publications

[1] Impact of Bis-(3-triethoxysilylpropyl)tetrasulphide on the properties of PMMA/Cellulose composite. V.P. Anju, Sunil K. Narayanankutty, *Polymer*, 119 (2017) 224-237.

[2] Polyaniline coated cellulose fiber / polyvinyl alcohol composites with high dielectric permittivity and low percolation threshold V.P. Anju, Sunil K. Narayanankutty, *AIP Advances*, 6, (2016) 015109.

[3] Effect of Dopants on the Antimicrobial activity of PANI/CNF/PMMA Composites, V.P. Anju, Sunil K. Narayanankutty (communicated)

[4] Novel Humidity and Ammonia Sensor Based on Nanofibers/ Polyaniline/Polyvinyl alcohol composite. V.P. Anju, P.R. Jithesh, Sunil K. Narayanankutty (communicated)

[5] Development of flexible Carbon Nanofiber and Nanofibrillated cellulose Based Composite sheet as Excellent Electromagnetic Shielding Material, V.P. Anju, Sunil K. Narayanankutty (communicated)

[6] Metallaboranes from Metal Carbonyl Compounds and Their Utilization as Catalysts for Alkyne Cyclotrimerization. V. P. Anju, Subrat Kumar Barik, Bijnaneswar Mondal, V. Ramkumar, and Sundargopal Ghosh, *ChemPlusChem* (2014), 79, 546 – 551.

[7] Mixed-Metal Chalcogenide Tetrahedral Clusters with an Exo-polyhedral Metal Fragment: K. Yuvaraj, D. K. Roy, V. P. Anju, B. Mondal, B. Varghese and S. Ghosh, *Dalton Trans.* (2014), *43*, 17184.

[8] Chemistry of Homo- and Heterometallic Bridged-Borylene Complexes. K. Yuvaraj, D. K. Roy, K. Geetharani, B. Mondal, V. P. Anju, P. Shankhari, V. Ramkumar and S. Ghosh, *Organometallics (*2013), *32*, 2705.

[9] B-H bond iodination of polyhedral dimolybdaborane and dimolybdathiaborane clusters. Kiran Kumarvarma Chakrahari, Arunabha Thakur, V.P. Anju, Sundargopal Ghosh, *Journal of Organometallic Chemistry* (2013) 1-5.

[10] Transition-metal variation as a probe into the catalytic activity of metallaboranes.

[11] V.P. Anju, Dipak Kumar Roy, R.S. Anju, Sundargopal Ghosh, Journal of *Organometallic Chemistry* (2013), 733, 79-81

Conferences Attended and Paper Presented

[1] Humidity and Ammonia Sensor Based on Nanofibers/Polyaniline/ Polyvinyl alcohol, V.P. Anju and Sunil K. Narayanankutty, Emerging Trends in Nanocomposites, KSCS, October, 2017, Kerala, India

[2] Synthesis, Characterization and Properties of PVA/PANI/Cellulose fiber Conductive Composites. V.P. Anju and Sunil K. Narayanankutty, 4th *ISCA*, December, 2014, Pacific University, Udaipur, Rajasthan, India.

[3] Synthesis, Characterization and Properties of PVA/PANI/Cellulose fiber Conductive Composites. V.P. Anju and Sunil K. Narayanankutty, December, 2014, KKTM College, Kerala.

[4] Synthesis and conductivity studies of Poly vinyl alcohol/Poly Aniline/Cellulose Fiber. V.P. Anju and Sunil K. Narayanankutty, *SSC*, November, 2016, Kerala, India.

[5] The effect of Bis –(3-triethoxysilylpropyl)tetrasulphide as a coupling agent on the properties of PMMA/Cellulose composite. V.P. Anju and Sunil K. Narayanankutty, *NTAC*, November, 2016, Kerala, India.

[6] A Highly Active Catalyst for the Cyclotrimerization of Alkynes to Substituted Benzenes. V.P.Anju and S. Ghosh, *NDCS*, 7-9 December, 2012, IIT Delhi, New Delhi, India.

[7] A Highly Active Catalyst for the Cyclotrimerization of Alkynes to Substituted Benzenes.. V.P.Anju, and S. Ghosh , *CCC*, 8-10 February, 2013, CLRI, Chennai, India.

Awards/Fellowships Received

- Junior Research Fellowship (JRF-CSIR), CSIR-UGC, India
- Graduate Aptitude Test in Engineering (GATE), India 2012.
- Suvarna Jubilee Award in M.Sc. Chemistry during the year 2010-2012

Personal Profile

Date of Birth	:	21.03.1990
Permanent Address	:	Poothapilly House, Eloor North, Udyogamanadal P O Pin: 683501 Ernakulam, Kerala, India

…..ஜ۞ஜ…..